A Quantitative Weld Sizing Criterion for Welded Connections in Lightweight Shipboard Structures: Modeling, Validation, and Structural Applications

by

Hanqing Lu

A dissertation submitted in partial fulfillment
of the requirements for the degree of
Doctor of Philosophy
(Naval Architecture and Marine Engineering)
in the University of Michigan
2021

Doctoral Committee:

Professor Pingsha Dong, Chair
Associate Professor Matthew D. Collette
Associate Professor Jason P. McCormick
Associate Professor David J. Singer

Hanqing Lu

hqlu@umich.edu

ORCID iD: 0000-0001-7710-1764

Dedication

This dissertation is dedicated to my parents, my wife and all my family members, who have always believed in me and supported me throughout my journey.

I am also infinitely grateful to my mentor, Prof. Pingsha Dong, who has gone beyond his ways to help me both in my academic and personal life over the last 10 years.

Acknowledgements

First and foremost, I would like to express my infinite gratitude to my advisor and mentor, Prof. Pingsha Dong, for his continuous support and guidance throughout my Ph.D. program. His knowledge helps me, and his work ethic motivates me every time when I have a hard time in research.

In addition, I would like to sincerely appreciate the rest of my doctoral committee: Prof. David J. Singer, Prof. Matthew D. Collette, and Prof. Jason P. McCormick. Their guidance and advice help the completeness of this thesis.

Finally, I want to thank all my colleagues, including but limited to Shaopin Song, Shizhu Xing, Xianjun Pei, Jifa Mei, Alina Shrestha, and Sandipp Ravi. I truly cherish all the testing, modeling, and theory discussions that we have done and accomplished together.

Table of Contents

Dedication ii

Acknowledgements iii

List of Tables viii

List of Figures ix

List of Appendices xv

List of Symbols xvi

Abstract xxi

Chapter 1 Introduction 1

1.1 Research Background 1

1.1.1 Challenges in Construction of Lightweight Structures 1

1.1.2 Limitations in Traditional Weld Sizing Criteria 3

1.2 Representative Research Efforts on Quantitative Weld Sizing 6

1.2.1 Past Experimental Findings 7

1.2.2 Past Theoretical Developments 9

1.2.3 “Directional Strength-Increase Factor” 11

1.3 Research Objectives 13

1.4 Dissertation Structure 14

Chapter 2 Strength Analysis of Fillet Welds under Longitudinal and Transverse Shear Conditions 17

Abstract 17

2.1 Introduction 18

2.2 Weld Throat Stress Characterization 22
2.2.1 Traction Stress Method 22
2.2.2 Calculation Procedure 23
2.2.3 Analysis of Test Specimens 27
2.3 Testing Procedure 39
2.4 Analysis of Test Results 43
2.4.1 Using Conventional Method 44
2.4.2 Using Traction Stress Method 46
2.5 Conclusions 49
Acknowledgments 50
Chapter 3 An Analytical Shear Strength Model for Load-Carrying Fillet-Welded Connections Incorporating Nonlinear Effects 51
Abstract 51
3.1 Introduction 52
3.2 Analytical Weld Throat Stress Model 57
3.2.1 Shear Failure Criterion 57
3.2.2 Treatment of Plate-to-Plate Contact 61
3.2.3 Limit State Definition 64
3.3 Nonlinear Finite Element Analysis 66
3.3.1 FE Model Details 67
3.3.2 FE Results 69
3.4 Analysis of Test Data 73
3.4.1 Shear Strength Correlation 74
3.4.2 Critical Weld Throat Plane Angle Estimation 75
3.4.3 Applications for Combined Loading Conditions 76
3.5 Conclusions 77

Acknowledgments 78

Chapter 4 A Quantitative Weld Sizing Criterion and Applications in Load Capacity Evaluation of Hollow Structural Section Joints 79

Abstract 79

4.1 Introduction 80

4.2 Assessment of Traditional Weld Sizing Approaches 82

4.2.1 Engineering Shear Stress 82

4.2.2 Directional Strength-Increase Factor 84

4.3 Traction Stress based Weld Strength Criterion 87

4.4 Analysis of Fillet-Welded HSS Connections 90

4.4.1 Finite Element Analysis using TSM 92

4.4.2 Weld Effective Length in HSS-to-HSS Joints 105

4.4.3 Ultimate Load Capacity Estimation 106

4.4.4 Weld Sizing Criterion 114

4.5 Conclusions 115

Chapter 5 Discussion 116

5.1 Aluminum Alloys 117

5.2 Titanium Alloys 120

5.3 Weld Size Effects 127

5.4 Generalized Quantitative Weld Sizing Criterion 132

Chapter 6 Conclusions and Future Work 138

6.1 Major Contributions 138

6.2 Areas of Future Study 140

Appendix A Shear Strength Correlation between Longitudinal and Transverse Shear Specimens using Conventional Method 142

Appendix B Shear Strength Correlation between Longitudinal and Transverse Shear Specimens using Traction Stress Method 151

Appendix C Shear Strength Correlations by Traction Stress Method with and without Plate Contact Effects 160

Appendix D Shear Strength Correlations between Longitudinal and Transverse Specimens Made of Aluminum Alloys 165

Appendix E Shear Strength Correlations between Longitudinal and Transverse Specimens Made of Titanium Alloys 170

References 176

List of Tables

Table 2.1: Shear specimens tested in this study 39

Table 4.1: Geometric properties of HSS-to-plate and HSS-to-HSS connections 106

Table 4.2: Mechanical properties of HSS-to-plate and HSS-to-HSS connections 107

Table 4.3: Weld size reduction from Eq. (4.2) by Eq. (4.22) 114

Table 5.1: Aluminum alloys shear specimens tested in this study 117

Table 5.2: Titanium alloys shear specimens tested in this study 121

Table 5.3: Weld size reduction from traditional approach (Eq. (1.2))by proposed weld sizing criterion (Eq. (5.7) for longitudinal shear specimens 135

Table 5.4: Weld size reduction from traditional approach (Eq. (1.2))by proposed weld sizing criterion Eq. (5.7) for transverse shear specimens 136

Table 5.5: Weld size reduction from traditional approach (Eq. (1.2))by proposed weld sizing criterion Eq. (5.7) for HSS connections from literature 137

List of Figures

Figure 1.1: Welding-induced distortion observed on a ship panel 2

Figure 1.2: Standard fillet weld shear strength specimen: (a) longitudinal shear loaded; (b) transverse shear loaded 3

Figure 1.3: Theoretical weld throat a_{45} as failure plane for standard fillet welded shear testing specimens 4

Figure 1.4: Typical weld throat failure plane observed on transverse shear specimen 5

Figure 1.5: Shear strength discrepancy between longitudinal and transverse shear specimens by Eq. (1.1) 6

Figure 1.6: Fillet weld under remote load P with loading angle α 7

Figure 1.7: Classical wedge solution used by Kato and Morita (1974) 10

Figure 1.8: Assumed force system in the study of Kamtekar (1982) 10

Figure 2.1: AWS standard shear strength test specimens: (a) longitudinal shear; (b) transverse shear 19

Figure 2.2: Fillet weld leg and weld throat definition in AWS B4.0 20

Figure 2.3: Traction stress components acting on a weld throat plane at an angle of θ 24

Figure 2.4: Linear representation and decomposition of weld throat traction stress components 24

Figure 2.5: Global coordinate system versus local coordinate system 26

Figure 2.6: Transformation of nodal forces on a weld throat cut plane in 3D solid element model into statically equivalent forces and moments with respect to weld throat mid-section along weld line 27

Figure 2.7: A representative 3D solid finite element model used for longitudinal shear specimens ($1" = 25.4$ mm) 29

Figure 2.8: Three cut planes through weld for calculating longitudinal shear stress along weld line 29

Figure 2.9: Normalized longitudinal shear stress distribution on three cut planes along weld line 30

Figure 2.10: Demonstration of mesh-insensitivity of traction stress method – longitudinal shear specimen: (a) FE models with different element sizes; (b) comparison of normalized shear stress along weld line obtained from each model shown in Figure 2.10a 31

Figure 2.11: SCF for longitudinal shear specimens as a function of relative fillet weld leg size (s/T_1) 33

Figure 2.12: A representative plane-strain finite element model for transverse shear specimen . 35

Figure 2.13: Comparison of analytical and finite element results for transverse shear stress and normal stress as a function of cut angle θ 36

Figure 2.14: Free-body diagram for transverse shear specimen with equal weld leg size s 37

Figure 2.15: Shear strength test specimens prior to testing: (a) longitudinal shear; (b) transverse shear 41

Figure 2.16: Laser scan device for weld profile and weld size determination 41

Figure 2.17: Typical load-displacement curves: (a) longitudinal shear (b) transverse shear 42

Figure 2.18: Shear failure angles: (a) longitudinal shear, about 45°; (b) transverse shear, about 22.5° 43

Figure 2.19: Comparison of shear strengths between longitudinal and transverse shear specimens using Eq. (2.1): (a) DH36 with FCAW; (b) HSLA80 with FCAW; (c) HSLA80 with GMAW.. 46

Figure 2.20: Comparison of shear strengths between longitudinal and transverse shear specimens using traction stress method: (a) DH36 with FCAW; (b) HSLA80 with FCAW; (c) HSLA80 with GMAW 48

Figure 3.1: Fillet-welded specimen under transverse shear loading condition..... 52

Figure 3.2: Typical weld throat failure plane observed on transverse shear specimens, noticeably smaller than 45° as assumed in Eq. (3.1) 54

Figure 3.3: Shear strength correlations between transverse and longitudinal shear specimens: traditional method Eq. (3.1) versus traction stress method: (a) DH36, FCAW, and 71T1-C weld wire; (b) HSLA80, FCAW, and 101T-C weld wire..... 55

Figure 3.4: Failure angles measured in transverse shear specimens after fracture 56

Figure 3.5: Traction stress components acting on a weld throat plane at an angle of θ: (a) Fillet weld between base and attachment plate; (b) Traction stress definition on weld throat plane at angle θ 58

Figure 3.6: Linear representation and decomposition of weld throat traction stress components 59

Figure 3.7: Illustration of combined loading on a load-carrying fillet weld..... 59

Figure 3.8: Critical weld throat failure plane angle θ_{max} as a function of loading angle α: analytical versus experimental results 61

Figure 3.9: Analytical weld throat model incorporating resultant contact force C..... 62

Figure 3.10: Effect of contact ratio on critical weld throat plane angle and maximum shear stress reduction 63

Figure 3.11: FE model and stress-strain relationship used for modeling transverse shear specimen: (a) A representative FE model of transverse shear specimen; (b) Stress-strain curve representing elastic-perfect-plastic material used in FEA calculations..... 68

Figure 3.12: FE results without contact effects: (a) Shear force on critical weld throat plane; (b) Shear stress ratio τ_b/τ_m on critical weld throat plane; (c) Membrane shear stress τ_m at $D_{FEA}/D_U = 1$: analytical vs FE results..... 71

Figure 3.13: Computed contact ratio K as a function of relative load point displacement D_{FEA}/D_U 72

Figure 3.14: Critical weld throat plane as a function of contact ratio: analytical versus FE results 73

Figure 3.15: Shear strength correlations by traction stress method with and without contact effects: (a) DH36, FCAW, and 71T1-C weld wire; (b) HSLA80, FCAW, and 101T-C weld wire..... 75

Figure 3.16: Predicted failure angle versus measured failure angle 75

Figure 4.1: Hollow structural sections: circular hollow sections and rectangular hollow sections 80

Figure 4.2: Standard fillet-welded shear testing specimens: (a) longitudinal shear loaded; (b) transverse shear loaded 83

Figure 4.3: Theoretical weld throat a_{45} as failure plane for standard fillet-welded shear testing specimens..... 84

Figure 4.4: Combined shear loaded fillet weld with loading angle α..... 85

Figure 4.5: Traction stress components acting on a weld throat plane at an angle of θ 87

Figure 4.6: Linear representation and decompostion of weld throat traction stress components. 88

Figure 4.7: Fillet weld strength correlation comparison between traction stress method and traditional approach 89

Figure 4.8: Fillet weld strength correlation comparison between TSM and TSM with nonlinearity 89

Figure 4.9: Critical weld failure angle correlation between traction stress method and test data measurement 90

Figure 4.10: Fillet-welded HSS connections: (a) HSS to rigid plate; (b) HSS to HSS 91

Figure 4.11: Cross section A-A of branch member in Figure 4.10: (a) CHS; (b) RHS..... 92

Figure 4.12: FE models for fillet-welded HSS connections: (a) CHS; (b) RHS 93

Figure 4.13: Normalized traction stress distribution along weld circumference on CHS connection under 90° loading..... 95

Figure 4.14: 2D axisymmetrci FE modeling for CHS connections..... 95

Figure 4.15: Ratio K vs R_b/t_b for CHS connections with different t_b..... 96

Figure 4.16: Normalized traction stress and ratio K distribution along weld circumference for RHS connections 98

Figure 4.17: Ratio K vs B_b/t_b for RHS connections 100

Figure 4.18: Correlation of ratio K vs λ_1 for both CHS and RHS connections by Eq. (4.10) ... 101

Figure 4.19: Normalized shear stress at 0° weld throat plane vs local radius effect for RHS.... 102

Figure 4.20: Normalized shear stress at 0° weld throat plane vs $C_{b,max}/t_b$ for RHS..... 103

Figure 4.21: Normalized shear stress at 0° weld throat plane vs λ_2 for RHS..... 104

Figure 4.22: Load capacity correlations between test results and AISC 109

Figure 4.23: Load capacity correlations between test results and AISC with directional strength-increase factor..... 110

Figure 4.24: Load capacity correlations between test results and CSA with directional strength-increase factor..... 110

Figure 4.25: Load capacity correlations between test results and Eurocode 3..... 111

Figure 4.26: Load capacity correlations between test results and TSM: (a) Nominal weld shear strength is set to 60% of its tested ultimate tensile strength; (b) Nominal weld shear strength is set to 67% of its tested ultimate tensile strength 113

Figure 5.1: Comparison of shear strengths between longitudinal and transverse shear specimens of AL 5456 with GMAW and 5556 weld wire: (a) AWS traditional equation; (b) traction stress method; (c) traction stress method with nonlinear effects..... 119

Figure 5.2: Comparison of shear strengths between longitudinal and transverse shear specimens of AL 6082 with GMAW and 5183 weld wire: (a) AWS traditional equation; (b) traction stress method; (c) traction stress method with nonlinear effects 120

Figure 5.3: Comparison of shear strengths between longitudinal and transverse shear specimens of Ti 6-4 with GTAW: (a) AWS traditional equation; (b) traction stress method; (c) traction stress method with nonlinear effects 123

Figure 5.4: Comparison of shear strengths between longitudinal and transverse shear specimens of Ti CP with GMAW: (a) AWS traditional equation; (b) traction stress method; (c) traction stress method with nonlinear effects 125

Figure 5.5: Comparison of shear strengths between longitudinal and transverse shear specimens of Ti 425 with GMAW: (a) AWS traditional equation; (b) traction stress method; (c) traction stress method with nonlinear effects 126

Figure 5.6: Weld penetration in load-carrying fillet weld 127

Figure 5.7: Weld penetration vs weld size 128

Figure 5.8: Shear strength vs weld size 129

Figure 5.9: Hardness test for weld with different size: (a) hardness test procedure; (b) hardness test results for DH36 with FCAW & 71T1-C; (c) hardness test results for HSLA80 with FCAW & 101T-C 131

Figure A.1: Shear strength correlation between longitudinal and transverse shear specimens using conventional method for DH36 with FCAW and 71T1-C weld wire 145

Figure A.2: Shear strength correlation between longitudinal and transverse shear specimens using conventional method for HSLA-80 with FCAW and 101T-C weld wire 148

Figure A.3: Shear strength correlation between longitudinal and transverse shear specimens using conventional method for HSLA-80 with GMAW and MIL-100S weld wire 150

Figure B.1: Shear strength correlation between longitudinal and transverse shear specimens using traction stress method for DH36 with FCAW and 71T1-C weld wire 154

Figure B.2: Shear strength correlation between longitudinal and transverse shear specimens using traction stress method for HSLA-80 with FCAW and 101T-C weld wire 157

Figure B.3: Shear strength correlation between longitudinal and transverse shear specimens using traction stress method for HSLA-80 with GMAW and MIL-100S weld wire 159

Figure C.1: Shear strength correlations by traction stress method with and without contact effects for DH36 with FCAW, and 71T1-C weld wire 161

Figure C.2: Shear strength correlations by traction stress method with and without contact effects for HSLA-80 with FCAW, and 101T-C weld wire 163

Figure C.3: Shear strength correlations by traction stress method with and without contact effects for HSLA-80 with GMAW, and MIL-100S weld wire 164

Figure D.1: Shear strength correlations between longitudinal and transverse specimens made of AL 5456 with GMAW and 5556 weld wire: a comparison between AWS traditional equation and traction stress method with/without nonlinear effects 167

Figure D.2: Shear strength correlations between longitudinal and transverse specimens made of AL 6082 with GMAW and 5183 weld wire: a comparison between AWS traditional equation and traction stress method with/without nonlinear effects 169

Figure E.1: Shear strength correlations between longitudinal and transverse specimens made of Ti 6-4 with GMAW: a comparison between AWS traditional equation and traction stress method with/without nonlinear effects 170

Figure E.2: Shear strength correlations between longitudinal and transverse specimens made of Ti 6-4 with GTAW: a comparison between AWS traditional equation and traction stress method with/without nonlinear effects 171

Figure E.3: Shear strength correlations between longitudinal and transverse specimens made of Ti CP with GMAW: a comparison between AWS traditional equation and traction stress method with/without nonlinear effects 172

Figure E.4: Shear strength correlations between longitudinal and transverse specimens made of Ti CP with GTAW: a comparison between AWS traditional equation and traction stress method with/without nonlinear effects 173

Figure E.5: Shear strength correlations between longitudinal and transverse specimens made of Ti 425 with GMAW: a comparison between AWS traditional equation and traction stress method with/without nonlinear effects 174

Figure E.6: Shear strength correlations between longitudinal and transverse specimens made of Ti 425 with GTAW: a comparison between AWS traditional equation and traction stress method with/without nonlinear effects 175

List of Appendices

Appendix A Shear Strength Correlation between Longitudinal and Transverse Shear Specimens using Conventional Method 142

Appendix B Shear Strength Correlation between Longitudinal and Transverse Shear Specimens using Traction Stress Method 151

Appendix C Shear Strength Correlations by Traction Stress Method with and without Plate Contact Effects 160

Appendix D Shear Strength Correlations between Longitudinal and Transverse Specimens Made of Aluminum Alloys 165

Appendix E Shear Strength Correlations between Longitudinal and Transverse Specimens Made of Titanium Alloys 170

List of Symbols

a_{45}	Weld throat size along 45° angle from base plate
a_θ	Weld throat size along θ angle from base plate
B	Nominal chord section width on RHS connections
B_b	Nominal branch section width on RHS connections
C	Contact force generated from plate-to-plate contact in transverse shear specimens
C_b	Distance between weld toe and centroid of cross section
$C_{b,max}$	Max distance between weld toe and centroid of cross section along weld direction
$C_{b,min}$	Min distance between weld toe and centroid of cross section along weld direction
D	Chord section width on CHS connections
D_b	Branch section width on CHS connections
D_{FEA}	Load point displacement obtained from finite element model
$F_{n,x'}$	Nodal force at the nth node along weld line with respect to local x' direction
$F_{n,y'}$	Nodal force at the nth node along weld line with respect to local y' direction
$F_{n,z'}$	Nodal force at the nth node along weld line with respect to local z' direction
F_x	Nodal force with respect to global x axis
F_y	Nodal force with respect to global y axis
F_z	Nodal force with respect to global z axis
$F_{x'}$	Nodal force with respect to global x' axis
$F_{y'}$	Nodal force with respect to global y' axis
$F_{z'}$	Nodal force with respect to global z' axis

$f_{n,x'}$	Line force at the nth node along weld line with respect to local x' direction
$f_{n,y'}$	Line force at the nth node along weld line with respect to local y' direction
$f_{n,z'}$	Line force at the nth node along weld line with respect to local z' direction
f_{uts}	UTS of test coupon from rigid endplate or chord on HSS connections
$f_{uts,b}$	UTS of test coupon from hollow section plate on HSS connections
$f_{uts,w}$	UTS of test coupon from as-laid weld on HSS connections
$f_{x'}$	Line force with respect to local x' axis
f_{ys}	Yield strength of test coupon from rigid endplate or chord on HSS connections
$f_{ys,b}$	Yield strength of test coupon from hollow section plate on HSS connections
$f_{ys,w}$	Yield strength of test coupon from as-laid weld on HSS connections
$f_{y'}$	Line force with respect to local y' axis
$f_{z'}$	Line force with respect to local z' axis
K	Ratio of normal stress to shear stress on 0° weld throat plane
L	Total measured weld length carrying load
L_e	Effective weld length carrying load
l_{n-1}	Element edge length along weld line at the nth node
$M_{n,x'}$	Nodal moment at the nth node along weld line with respect to local x' direction
$M_{n,y'}$	Nodal moment at the nth node along weld line with respect to local y' direction
$M_{n,z'}$	Nodal moment at the nth node along weld line with respect to local z' direction
$m_{n,x'}$	Line moment at the nth node along weld line with respect to local x' direction
$m_{n,y'}$	Line moment at the nth node along weld line with respect to local y' direction
$m_{n,z'}$	Line moment at the nth node along weld line with respect to local z' direction
$m_{y'}$	Line moment with respect to local y' axis
$m_{z'}$	Line moment with respect to local z' axis

n	Total number of nodes defining weld line in finite element model
P	Remotely applied load in shear specimen testing
P_L	Remotely applied longitudinal force parallel to weld axis
$P_{n,w}$	Estimated ultimate load capacity of fillet welds on HSS connections
P_T	Remotely applied transverse force perpendicular to weld axis
P_u	Peak load obtained in load-displacement curve from a shear strength test
R_b	Branch section radius on CHS connections
r_c	Local radius at the RHS corner
S	Shear force acting on a weld throat plane
s	Fillet weld leg size
s_p	Weld penetration
T_1	Base plate thickness of longitudinal or transverse shear specimen in a test program
T_2	Lap plate thickness of longitudinal or transverse shear specimen in a test program
T_b	Base plate thickness of standard longitudinal or transverse shear specimen
t	Base plate or chord plate thickness
t_b	Branch plate thickness on HSS connections
α	Loading angle between remotely applied load P and weld axis
β_w	Correlation factor for fillet welds in EN1993-1-8
$\varepsilon_{rup,b}$	Elongation of test coupon at rupture from hollow section plate on HSS connections
ε_{rup}	Elong. of test coupon at rupture from rigid endplate or chord on HSS connections
$\varepsilon_{rup,w}$	Elongation of test coupon at rupture from as-laid weld on HSS connections
θ	Angle between weld throat plane and base plate
θ_{max}	Angle of critical weld throat plane
λ_1	Parameter for ratio K correlation
λ_2	Parameter for $\tau_{Tm}(0)$ correlation

λ_3	Parameter for P_u estimation with different loading direction
σ	Normal stress
σ_b	Bending part of normal stress
σ_m	Membrane part of normal stress
σ_R	Resultant stress, i.e., $\sigma_R = \sqrt{\sigma_m^2 + \tau_{Tm}^2}$
τ_e	Effective shear stress for characterizing shear strength of fillet welds
$\tau_{e,max}$	Maximum effective shear stress for defining shear strength of fillet welds
τ_L	Longitudinal shear stress
τ_{Lb}	Bending part of longitudinal shear stress
τ_{Lm}	Membrane part of longitudinal shear stress
$\tau_{Lm,max}$	Maximum membrane part of longitudinal shear stress occurring at weld end
τ_n	Nominal shear traction stress at 0° weld throat plane
τ_T	Transverse shear stress
τ_{Tb}	Bending part of transverse shear stress
τ_{Tm}	Membrane part of transverse shear stress
$\tau_{Tm,max}$	Maximum membrane part of transverse shear stress
$\sigma_{u,b}$	Ultimate tensile strength of base plate material
$\tau_{u,b}$	Shear strength of base plate material
$\tau_{u,w}$	Weld shear strength determined from a test
τ_{u,w_0}	Weld shear strength determined from a longitudinal shear test (0° loading angle)
τ_{u,w_α}	Weld shear strength determined from a shear test with loading angle α
τ_{u,w_L}	Weld shear strength determined from longitudinally loaded fillet weld
τ_{u,w_T}	Weld shear strength determined from transversely loaded fillet weld
$\tau_{\%}$	Normalized weld shear strength by averaged value from the same test group

ϕ	Design safety factor

Abstract

Rampant welding-induced distortions in construction of modern lightweight shipboard structures not only increase production cost, but also cause structural integrity concerns in service. Numerous recent studies have shown that overwelding in complying with the existing empirical-based fillet weld sizing criteria is the key contributor. Fillet-welded connections are widely used in the construction of marine structures. However, due to the complex stress state in fillet-welded connections and the lack of an effective means to relate the stress state at a joint to failure conditions observed in standardized component tests, existing weld sizing criteria in Codes and Standards used today were largely based on design experiences and observations from limited test data, dating back to decades ago. Therefore, a more quantitative mechanics-based weld sizing criterion must be developed for not only enabling the cost-effective construction of lightweight ship structures, but also ensuring structural safety in service.

In this study, a traction stress based mesh-insensitive method is introduced for characterizing the complex stress state and its relationship to weld failure conditions in fillet-welded components. The insights gained enable the development of a closed-form solution for relating weld throat shear stress state to remotely applied loading conditions, which in turn leads to an effective traction stress based failure criterion serving as a mechanics basis for achieving quantitative weld sizing.

To support and validate the analytical developments, a comprehensive testing program using over 200 standard longitudinal and transverse shear joint specimens was carried out. The test

results have proven the effectiveness of the closed-form failure criterion in predicting both failure angle and correlating joint strength test data. A careful observation of the test data obtained in this study suggests that certain nonlinear effects such as plate-to-plate contact can be important in certain type of test configurations. This leads to the development of a new analytical formulation for incorporating the nonlinear effects to further generalize the effective traction stress based weld sizing failure criterion for a broader range of structural applications.

To further validate the effectiveness of the developed quantitative weld sizing failure criterion, a large number of well-known full-scale test data available from past and recent literature on hollow structural section (HSS) joints have been analyzed in detail. The results show that the correlations between the predicted failure loads with the proposed failure criterion and the measured loads offer as much as 60% improvement over those predicted by the existing Codes and Standards, confirming the validity of the proposed failure criterion resulted from this study.

Finally, within the context of these standard shear test specimens and full-scale HSS connections, it can be shown that the quantitative weld sizing criterion proposed in this study can result in a weld size reduction as much as 40%, compared with the existing empirical-based weld sizing criteria used today, which can be very beneficial for welding-induced distortion control in the construction of lightweight shipboard structures.

Chapter 1 Introduction

1.1 Research Background

1.1.1 Challenges in Construction of Lightweight Structures

Fillet welded connections are widely used in the construction of modern ship and civil structures for connecting secondary structures to main structures and transmitting loads from one member to another. Therefore, one of the most important design considerations for these structures is to ensure that load-carrying fillet welds possess a strength equal to or higher than those of connected members, as described in various existing weld sizing criteria, such as MIL-STD-1628 (Department of Defense, 1974) for ship structures and AISC 360 (AISC, 2010) for civil structures. It is well known that the stress state at fillet-welded connections can be very complex and difficult for quantitative determination, even using today's finite element computational tools. This is mainly because of stress or strain singularity (or sharp notch effects) at weld locations, i.e., at weld toe and weld root (Dong et al., 2010a). In addition, the difference in flexibility or compliance between the connected members can make the stress determination more difficult (Packer & Cassidy, 1995). As a result of lacking an effective means of quantitatively determining the weld stress state, existing weld sizing criteria in current Codes and Standards are empirical and tend to be excessively conservative in nature, which often result in significantly oversizing of fillet welds (Packer et al., 2016; Nie & Dong, 2012).

In the past, some level of overwelding was not a major concern when dealing with traditional shipboard structures mostly made of relatively thick plates. Things are much different in recent years as there is an increasing demand for structural lightweighting in marine structures.

Thin and high-strength plates have been more and more used in modern ship structures to improve fuel economy and operational performance. For example, from 1990 to 2000s, the usage ratio of thin steel (10 mm or less) to thick plate structures for naval vessels built at Northrop Grumman Ship Systems (NGSS) has risen from less than 10% to over 90% (Huang et al., 2004; Huang et al., 2007). In addition to thin steel, other materials with high strength-to-weight ratio, such as aluminum alloys (Paik et al., 2006) and titanium alloys (Dong et al., 2013) are also being considered for achieving effective lightweighting in marine structures to meet the tightened lightweight requirements. However, due to the fact that thin plates possess less ability to resist welding-induced residual stress, the use of oversized fillet welds in lightweight structures not only increases unnecessary structural weight and construction cost, but also, more importantly, introduces significant welding-induced distortions during construction, and incurs correction cost, as shown in Figure 1.1. In fact, as the structural lightweight demands intensify over the last decade or so, overwelding has been identified as the most significant contributor to widespread distortions in ship and offshore constructions (Huang et al., 2014; Huang et al., 2016) and one of the major obstacles to overcome to achieve the lightweighting goal.

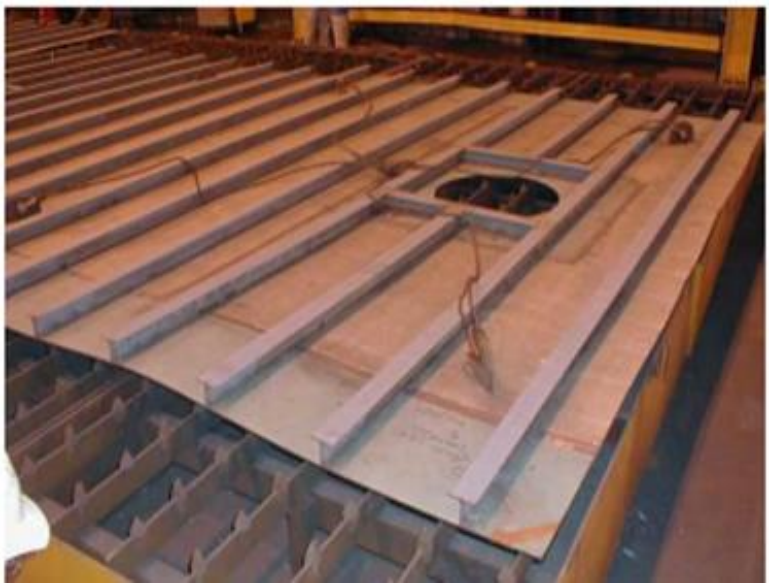

Figure 1.1: Welding-induced distortion observed on a ship panel

1.1.2 Limitations in Traditional Weld Sizing Criteria

As discussed above, due to lack an effective means of quantitatively determining the complex stress state in weld, existing traditional weld sizing criteria in current Codes and Standards, such as MIT-STD-1628 (Department of Defense, 1974), ABS 96 (ABS, 2000), AWS D1.1 (AWS, 2015), and other design specifications, such as Eurocode 3 (CEN, 2005), AISC 360 (AISC, 2010) and CSA S16 (CSA, 2014), have been empirical in nature since 1970s and they were developed based on static shear strength testing of standard longitudinal and transverse shear specimens, of which fillet welds are parallel (0°) and perpendicular (90°) to the remote loading direction (P) respectively, as depicted in AWS B4.0 (AWS, 2007) in Figure 1.2.

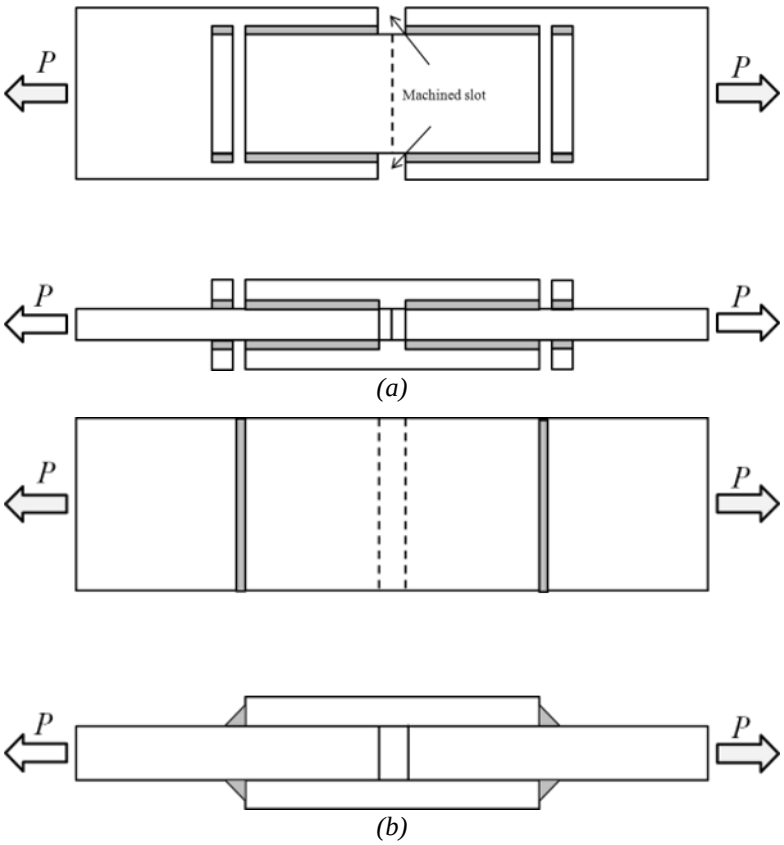

Figure 1.2: Standard fillet weld shear strength specimen: (a) longitudinal shear loaded; (b) transverse shear loaded

A nominal weld throat stress defined by Eq. (1.1), also referred to as an "engineering shear stress" in DNV-RP-C203 (DNV, 2012), has been used as the mechanics basis in these weld sizing

criteria since 1950s (AWS B4.0, 2007) for determining fillet weld strengths from both standard longitudinal and transverse shear specimens, i.e., $\tau_{u,wL}$ and $\tau_{u,wT}$ respectively.

$$\tau_{u,w} = \frac{P_u}{a_{45} \times L} \tag{1.1}$$

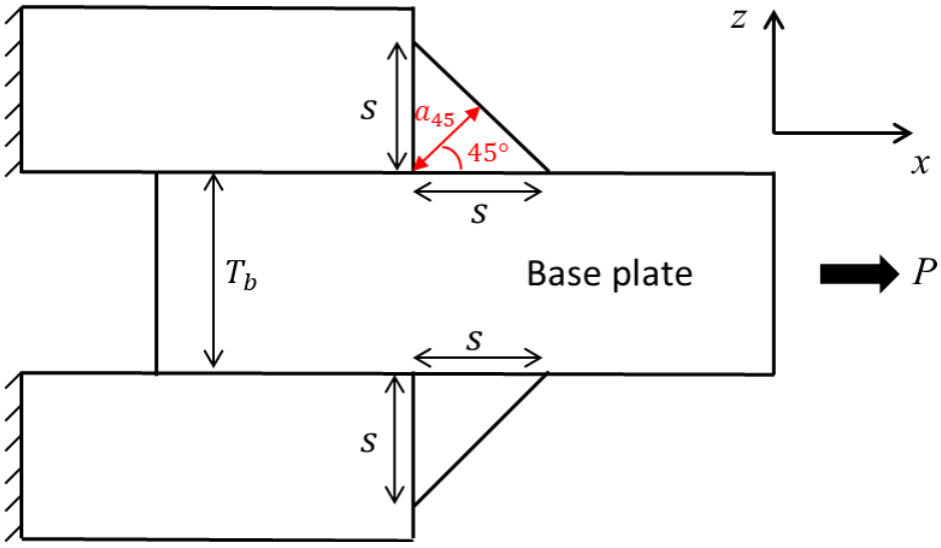

Figure 1.3: Theoretical weld throat a_{45} as failure plane for standard fillet welded shear testing specimens

As illustrated in Figure 1.3, the major assumptions in Eq. (1.1) are: (1) weld failure plane is assumed along the shortest weld throat size a_{45}, i.e., with a weld failure angle of 45°; (2) weld throat stress distribution along weld length (*Y*-axis) is uniform. Although these assumptions make Eq. (1.1) simple to use for processing test data, it has been shown to exhibit some serious limitations in correlating test data as demonstrated by investigations both in the past and recent years. Firstly, it has been well established that failure angle of transver shear specimens tends to occur at an angle much smaller than 45°, but more close to 22.5°, as illustrated in Figure 1.4, for various weldment made of mild steel (Kato & Morita, 1974; McClellan, 1990; Lu et al., 2015), high strength steel (Björk et al., 2012; Khurshid et al., 2012), aluminum alloys (Krumpen & Jordan, 1984; Marsh, 1985 & 1988), as well as titanium alloys (Dong et al., 2013; Nie & Dong, 2012). It should be noted that any effective stress definition used in a failure criterion should have the ability

to predict the correct failure path. Clearly, the engineering shear stress defined by Eq. (1.1) fails in this regard. Secondly, under longitudinal shear loading conditions, although weld failure angle of about 45° has been observed, weld throat stress distribution along weld length is far from being uniform in this type of test specimens, unlike the conditions assumed in arriving at Eq. (1.1). The test results from McClellan (1990) and Dong et al. (2013) showed that longitudinal shear specimens tend to exhibit weld failure initiated at weld ends (near the machined slot locations in Figure 1.2a). Finite element analysis (FEA) performed by Nie and Dong (2012), as well as by Lu et al. (2015) also demonstrated that severe stress concentration at weld ends of longitudinal shear specimens must be properly taken into account in analyzing the test data. As a result, it can be concluded that Eq. (1.1) produces significant discrepancies in analyzing weld strengths from the standard fillet-welded shear test specimens, resulting in a shear strength in longitudinal shear specimens, which can be 30% to 80% lower than that in transverse shear specimens. Such discrepancies in shear strength interpretation are illustrated in Figure 1.5 for the case with a fillet weld size of 6 mm, conducted in this study.

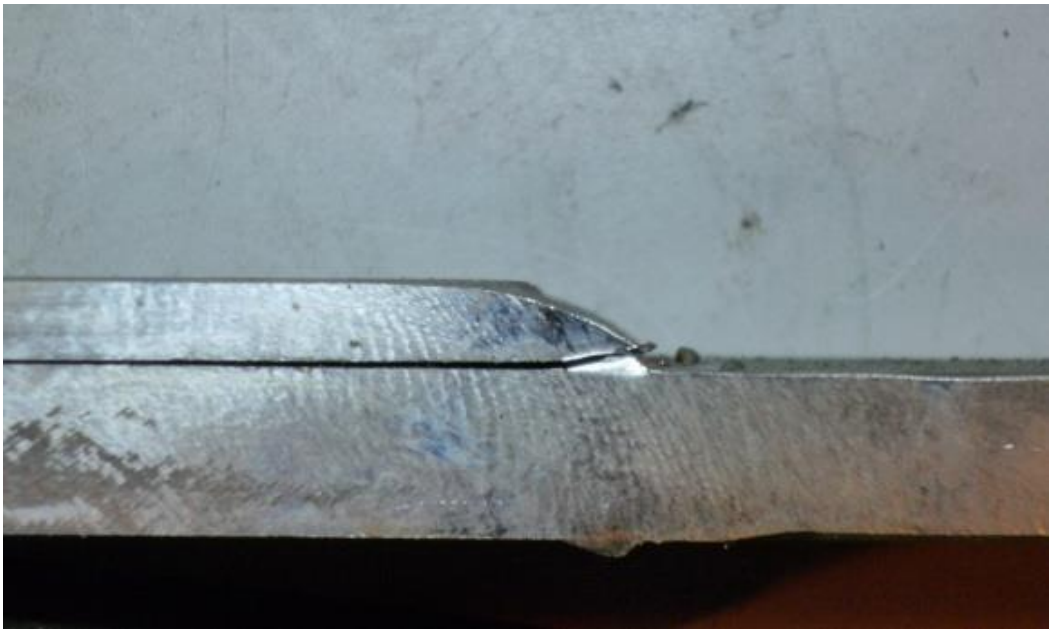

Figure 1.4: Typical weld throat failure plane observed on transverse shear specimen

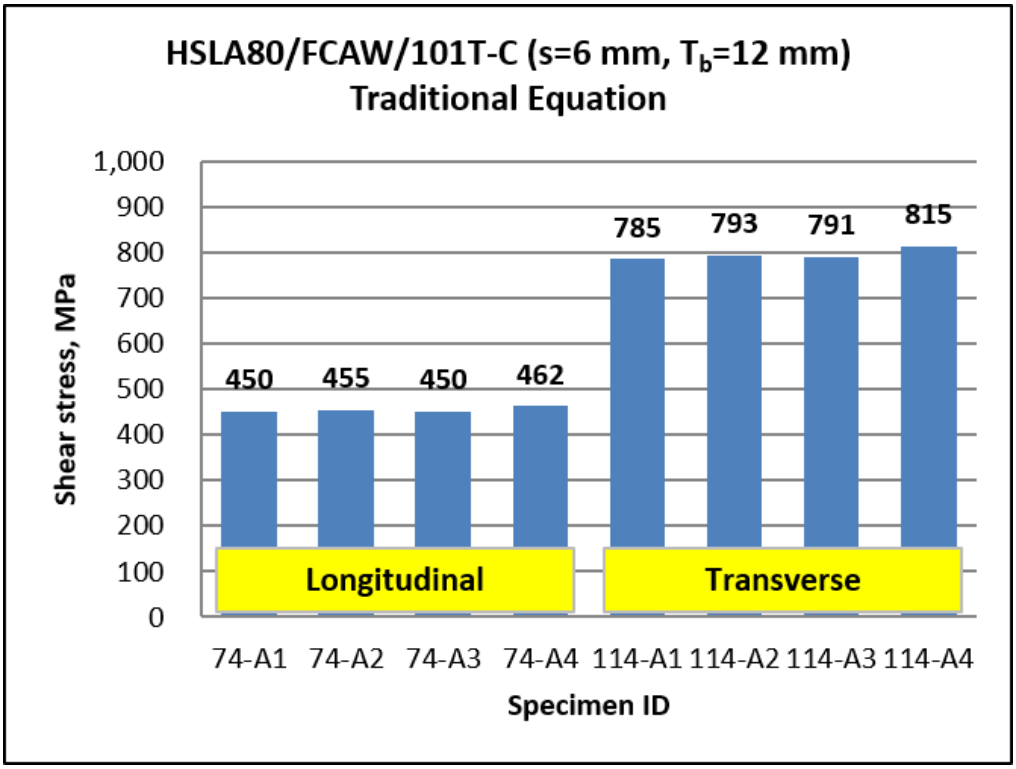

Figure 1.5: Shear strength discrepancy between longitudinal and transverse shear specimens by Eq. (1.1)

Due to its inability in reconciling the significant differences between the longitudinal and transverse shear strengths, the weld sizing equation according to Eq. (1.1) has been used in practice by factoring in a conservative margin based on experience to avoid weld failures in structural connections. In doing so, the longitudinal shear strength $\tau_{u,wL}$ is typically used for sizing fillet welds in various existing traditional criteria, as expressed by Eq. (1.2), often leading to significantly oversized fillet welds, as pointed out by various researchers recently (Lu et al., 2015; Nie & Dong, 2012).

$$\frac{s}{T_b} = 0.7071 \times \frac{\sigma_{u,b}}{\tau_{u,w_L}} \tag{1.2}$$

1.2 Representative Research Efforts on Quantitative Weld Sizing

In pursuing an improved weld sizing criterion that can eliminate the excessive conservatism in the existing empirical-based weld sizing criteria, numerous research efforts have

been carried out both experimentally and theoretically in the past and recent years. One of the major findings was that load-carrying capacity of fillet weld is a function of loading angle, i.e., angle α between the applied remote load P and the weld direction, as shown in Figure 1.6. This is consistent with the discrepancies in the shear strengths obtained from the longitudinal ($\alpha = 0°$) versus transverse ($\alpha = 90°$) shear test specimens when Eq. (1.1) is used, as discussed in Sec. 1.1.

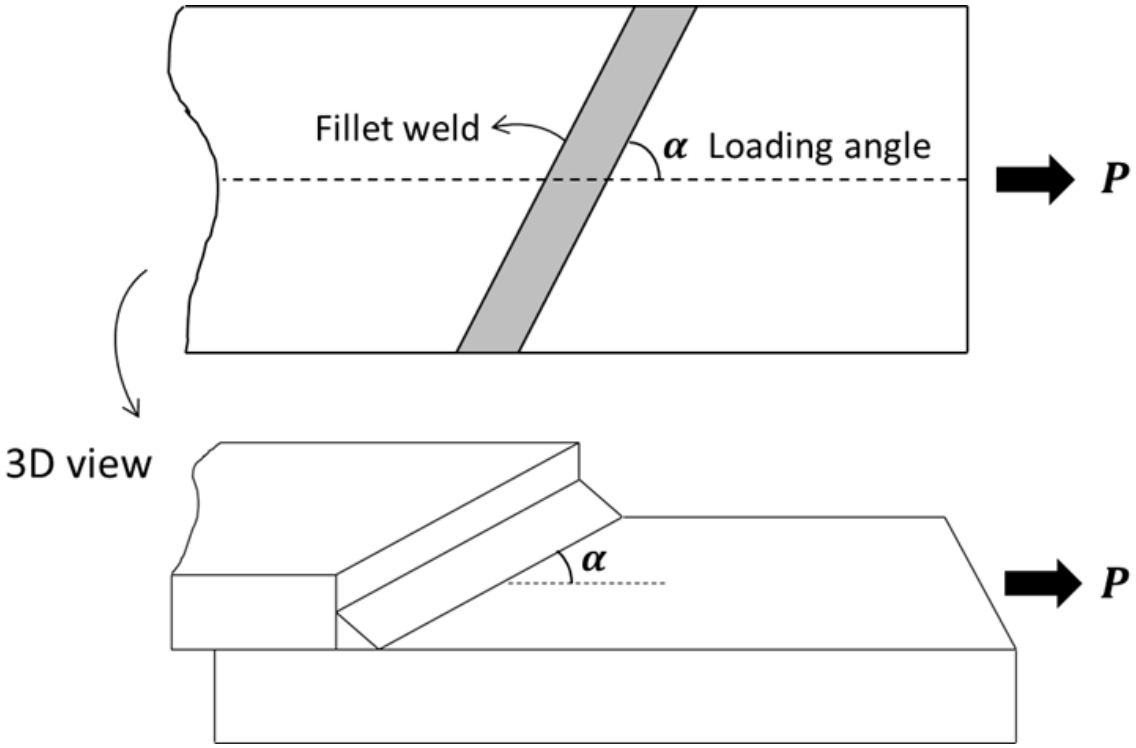

Figure 1.6: Fillet weld under remote load P with loading angle α

1.2.1 Past Experimental Findings

The needs for resolving the discrepancies in shear strengths obtained from longitudinal and transverse shear tests were discussed as early as 1930s, by Spraragen and Claussen (1942) in a literature review of 423 fillet weld static tests conducted during 1932 to 1940. They found: (1) the fracture loads obtained from standard longitudinal shear specimens were about 60% to 100% of those obtained from standard transverse shear specimens; (2) shear strength data were more scattered in transverse shear specimens. In 1959, Archer et al. (1959) performed a series of fillet

weld tests and reported that transverse-to-longitudinal shear strength ratior was 1.59 and the failure angle of transverse shear specimens were far smaller than 45°. Similarly, Ligtenberg (1968) did a statistical analysis over a large series of weldment tests (conducted by an international research program) with tensile strength from 450 to 580 MPa and obtained a transverse-to-longitudinal shear strength ratio of 1.59. In addition, Higgins and Preece (1968) conducted 168 tests to determine fillet weld strength of standard longitudinal and transverse shear specimens and reported that the transverse loaded fillet welds were about 1.41 to 1.54 times stronger than the longitudinal loaded fillet welds. The test data published by IIW (1980) suggested that transverse-to-longitudinal shear strength ratio was equal to 1.22 and the observed higher strength ratio in their testing efforts was caused by the friction and supporting effects between the connected plates. McClellan (1990) focused on testing 96 shear specimens with flux cored arc (FCAW) welding electrodes for both mild and high strength steel and showed that transverse shear strength was about 1.3 to 1.5 times stronger than longitudinal shear strength. More recent studies done by Nie and Dong (2012), as well as by Lu et al. (2015) demonstraed almost doubled transverse shear strength compared to longitudinal shear strength when Eq. (1.1) was used.

In addition, Butler and Kulak (1971 & 1972) conducted testing of 23 fillet-welded specimens with loading angle α varying from 0° to 90° (see Figure 1.6) and empirically determined weld strength as a function of loading angle, showing a 44% load-carrying capacity increase in transverse shear speciments compared over longitudinal shear specimens. Later, Krumpen and Jordan (1984) utilized the findings from Butler and Kulak (1971 & 1972), i.e., transverse-to-longitudinal shear strength ratio of 1.44, and proposed a series of equations for reducing fillet weld size. Their equations later have been adopted by AWS (AWS, 2007). A similar experimental study by Miazga and Kennedy (1989), including 42 fillet-welded specimens loaded

from 0° to 90°, demonstrated a weld sizing effect that load-carrying capacity ratios between the transverse and longitudinal shear specimens were 1.28 and 1.60 corresponding to 5 mm and 9 mm weld sizes, respectively. In their study, Miazga and Kennedy (1989) also developed a simplified semi-analytical solution based on the maximum shear stress theory with an empirical coefficient, showing weld strength increased up to 50% when the loading angle increased from 0° to 90°.

1.2.2 Past Theoretical Developments

In the area of theoretical developments for supporting quantitative weld sizing, an in-depth study done by Kato and Morita (1974) should be noted, in which they adopted a classical wedge solution from theory of elasticity (Timoshenko, 1951). They derived an analytical solution, yielding a weld throat failure angle of 22.5° for transverse shear specimens and a transverse-to-longitudinal shear strength ratio of 1.46. Although the predicted failure angle seemed in an agreement with their test retuls, there were some limitations in their study: (1) the shear strength definition was based on a local stress definition, which is not suited for design engineer in practice; (2) the maximum shear stress value used in their proposed failure criterion was not the actual maximum but the minimum value along the 22.5° plane, as shown in Figure 1.7; (3) the inherent assumption of uniform stress distribution along the edge of the wedge geometry is not consistent with the stress distribution in fillet-welded specimens. Therefore, the effective stress definition proposed by Kato and Morita has not attracted much attention in the literature since.

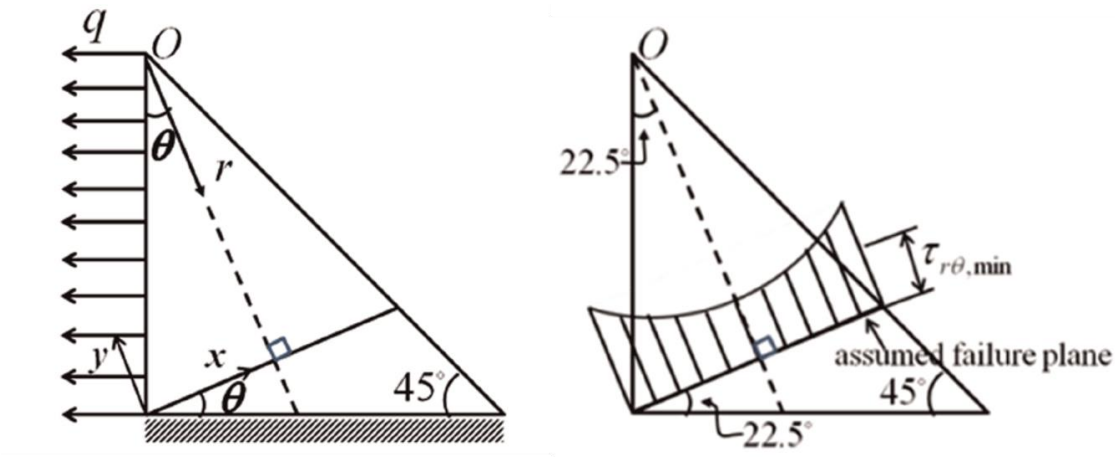

Figure 1.7: Classical wedge solution used by Kato and Morita (1974)

Furthermore, Kamtekar (1982 & 1987) developed a theoretical model using principal stress approach and von Mises yield criterion and proposed load-carrying capacity of transverse loaded fillet welds was 1.41 and 1.22 times that of longitudinal loaded fillet welds with and without considering residual stress, respectively. However, the force systems in his study subjectively added a vertical shear force (P') and a normal force (P') on the weld legs, and treated them equal to the applied force P, as shown in Figure 1.8, leading to a weld failure angle of 0° or 90°, which was clearly not consistent with the testing results documented in the literature discussed above.

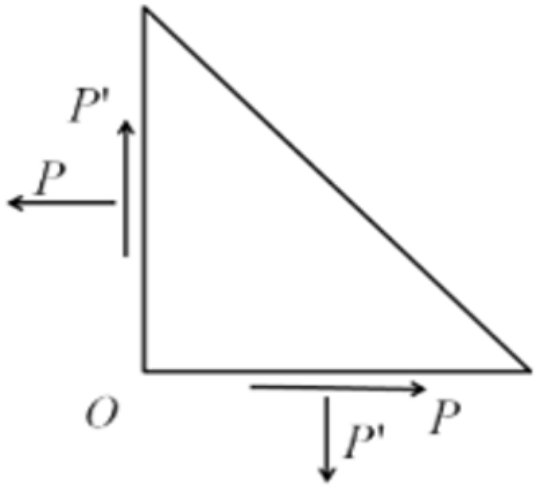

Figure 1.8: Assumed force system in the study of Kamtekar (1982)

The loading angle dependency was also observed when limit state analysis theorems were applied for analysis of failure load of a fillet weld. For example, using von Mises yield criterion by assuming elastic perfectly plastic material behavior, Jensen (1988) developed lower and upper bounds of load-carrying capacity of fillet weld in the state of yielding and their dependency to the direction of loading. In addition, using static and kinematic theorems of limit analysis, Picón and Cañas (2009) developed lower and upper bounds of failure load and rapture angle of fillet weld with Tresca and von Mises criteria and found they were functions of loading angle.

Last but not least, using the results of De Bruyne (1944), Swannell (1967 & 1972) developed an analytical solution showing that stress non-uniformly distributed along weld length in longitudinal fillet-welded specimen with the highest stress concentration at both weld ends. However, his analytical expression suggested that shear stress distribution was symmetircal with regard to weld length, which is not consistent with the results of finite element analysis (FEA) recently done by Nie and Dong (2012) and Lu et al. (2015).

1.2.3 "Directional Strength-Increase Factor"

Both the experimental and theoretical results described above on the load-carrying capacity variation in the fillet welded components as a function of loading angles have led to the development of a "directional strength-increase factor" (Kennedy et al., 1985), which was empirically formulated in the form of Eq. (1.3) by Lesik and Kennedy (1988 & 1990). It has been adopted by major design standards or specifications, such as AISC (AISC, 2010) and CSA (CSA, 2014). Note that τ_{u,w_0} in Eq. (1.3) is the same as the longitudinal shear strength τ_{u,w_L} in Eq. (1.2).

$$\frac{\tau_{u,w_\alpha}}{\tau_{u,w_0}} = 1.00 + 0.50\sin^{1.5}\alpha \tag{1.3}$$

However, major limitations exist in this empirical approach when dealing with structural applications. Firstly, it has been shown that the directional strength-increase factors determined from Eq. (1.3) produce a significant scatter in interpreting the experimental test data available in literature. For example, transverse-to-longitudinal shear strength ratio varied from 1.0 to 2.0 among different testing programs discussed in the previous section, which suggests that there might be other factors at play, such as the weld size effects that were clearly present in the study of Miazga and Kennedy (1989). Secondly, in the previous studies, the assumption of uniform weld throat stress distribution along the weld direction was only appropriate for the standard simple transverse shear specimens but not at all for the standard longitudinal shear specimens. As demonstrated by Nie and Dong (2012) as well as by Lu et al. (2015), severe weld throat stress concentration occurs at the ends of longitudinal weld and cannot be ignored for weld strength determination. In addition, the stress distribution along a weld can be much more complex than being uniform in the structural applications even if the fillet welds are only transversely loaded, which will be investigated in the context of hollow structural section (HSS) connections. Furthermore, a limit state approach by Lu and Dong (2020) demonstrated contact force between the overlapped plates has a significant effect on the weld throat stress state, which had been ignored or inadequately considered in the force systems from the previous theoretical models. Lastly, a correct failure criterion used for weld strength determination should be consistent for fillet-welded components regardless of loading angle, as discussed by Nie and Dong (2012) and Lu et al. (2015). However, this was clearly not the case with the approach incorporating a directional strength-increase factor, e.g., in the form of Eq. (1.3).

Based on the above discussions, it seems reasonable to state that an effective stress definition used for both determining weld strength and developing weld failure criterion has not

resolved to date. Both the engineering shear stress (Eq. (1.1)) and the directional strength-increase factor (Eq. (1.3)) lack of a rigorous mechanics underpinning for supporting the development of a more generalized weld sizing criterion for lightweight ship structures.

1.3 Research Objectives

The main objective of this research is to establish quantitative weld sizing criteria that are built upon sound structural mechanics principles through an in-depth understanding of weld throat stress state and its relationship with joint configurations and loading conditions. As such, the premise of this research is that the shear strength derived from a fillet-welded component should serve as a joint strength property which should not be dependent upon test specimen configurations and loading conditions. In doing so, a new effective stress parameter must be formulated through an improved understanding of weld throat stress state and its effects on joint failure and validated through comprehensive experimental testing at both simple joint specimen and large-scale structural connection levels. To achieve this overarching goal, the following specific objectives and associated research areas are planned:

- Establish a new effective stress formulation for characterizing weld throat stress state in fillet-welded test specimens.
- Develop a new failure criterion based on the effective stress formulation so that a unified fillet weld shear strength can be extracted consistently from standard test specimens of welded conditions.
- Validate the effectiveness of the proposed failure criterion by conducting shear strength tests using standard longitudinal and transverse shear specimens, covering various combinations of plate thicknesses, base metal types, welding processes, and filler metals.

- Further refine the failure criterion incorporating geometric nonlinear effects, which may exist both in simple joint specimen testing and complex structural applications.
- Extend the findings obtained from small-scale joint specimens to large-scale structural connections and prove the effectiveness by correlating the predicted and actual failure loads of fillet-welded connections.
- Propose a quantitative fillet weld sizing criterion that can lead to a significant weld size reduction from those determined using the traditional empirical-based weld sizing criteria used today for supporting a cost-effective construction of lightweight ship structures while ensuring structures' safe operation.

1.4 Dissertation Structure

This dissertation is structured in a multi-manuscript format. After an integrated introduction (Chapter 1), three manuscripts (two published and one submitted) are presented in Chapters 2 through 4. Chapter 5 provides an integrated discussion, which is then followed by an integrated conclusion in Chapter 6.

In Chapter 1, the needs in quantitative weld sizing criteria are presented, based on a detailed critical assessment of the relevant publications in the literature. Representative experimental investigations and theoretical developments, as well as numerical approaches are highlighted, with an emphasis on their key findings and limitations. Then, the main research objectives are stated along with an outline of the specific areas of investigation to be performed in this study.

In Chapter 2, a mesh-insensitive traction stress method is introduced to define an effective stress for characterizing weld throat stress state in fillet weld. Both numerical calculation procedure and closed-form analytical solution of the proposed effective stress are demonstrated in detail. Then, a failure criterion is proposed for determination of fillet weld shear strength. The

effectiveness of the failure criterion is verified by carrying out a comprehensive static strength test program using standard longitudinal and transverse shear specimens relevant to ship structure applications.

In Chapter 3, a limit state based analytical formulation of weld throat stress model incorporating nonlinear effects is presented for load-carrying fillet-welded connections. The validity of the resulting analytical solution is verified by finite element computation incorporating nonlinear material, nonlinear geometry, and nonlinear boundary condition effects. In addition, its effectiveness in correlating shear strengths obtained from standard longitudinal and transverse shear specimens has been proven through the re-analysis of over 100 shear tests performed earlier by Lu et al. (2015).

In Chapter 4, to verify the generality of the proposed effective stress and failure criterion, traction stress method is introduced to evaluate the strength of large-scale structural level fillet-welded connections, i.e., HSS joints. The results are then generalized into a closed-form expression with a clearly defined mechanics basis. This expression relates weld throat stress to fillet weld size and remote load, with its dimensional geometric parameters being determined through a detailed parametric finite element analysis (FEA). The effectiveness of the closed-form expression is demonstrated by comparing the predicted failure loads with those measured from HSS test data available from literature.

In Chapter 5, the generality of the results developed in Chapter 2 and 3 for weldment made of mild and high strength steel are verified by correlating the test data of weldment made of different materials, such as aluminum alloys and titanium alloys. As a result, in conjunction with all the developments presented in Chapter 2, 3 and 4, a quantitative weld sizing criterion is proposed for eliminating overwelding in the construction of lightweight ship structures. The

effectiveness of the weld sizing criterion is proven by providing significant weld size reduction from those determined using traditional existing empirical-based weld sizing criteria for both standard test lab specimens and actual structural applications. In the end, the weld penetration effect is also integrated into the proposed weld sizing criterion for further weld size reduction.

Chapter 2 Strength Analysis of Fillet Welds under Longitudinal and Transverse Shear Conditions

Abstract

In support of the development of improved fillet weld sizing criteria for lightweight ship structures, a comprehensive static strength test program using longitudinal and transverse shear specimens according to AWS B4.0 Standards has been conducted. This test program covers base material with strength ranging from 71 ksi (490 MPa) to 96 ksi (660 MPa) and weld size ranging from 1/8" (3 mm) to 3/8" (10 mm). This chapter focuses on a traction stress based analysis of the test data as an effort to establish a unified shear strength definition for load-carrying fillet welded specimens regardless of shear loading conditions. The proposed shear strength definition proves to be effective in correlating fillet weld strength test data of the longitudinal and transverse shear specimens. The results of this investigation demonstrate that existing shear strength definitions used by various weld sizing criteria such as those given by Class Societies have two major limitations: (1) it cannot be related to a critical stress state on experimentally observed failure plane in transverse shear specimens; (2) it underestimates shear stress at failure due to severe stress concentration at weld end in typical longitudinal shear specimens. These two limitations have been shown to be the major cause for having two significantly different shear strength values: one is transverse shear strength obtained from transverse shear specimens and the other is longitudinal shear strength obtained from longitudinal shear specimens.

Keywords: load carrying fillet welds, shear strength, strength testing, traction stress method, finite element analysis, failure criterion

2.1 Introduction

In ship and offshore structures, fillet welds are commonly used for transmitting loads from one part to another. In fact, most structural connections in ship structures are fillet welded. Therefore, one of the most important design considerations for ship and offshore structures is to ensure that load-carrying fillet welds possess a strength equal to or higher than that of nearby base plates, as described in US Navy's weld sizing criteria, such as MIL-STD-1628 (Department of Defense, 1974) and further refined by Krumpen (1984) for meeting weld sizing needs as high strength steels and modern welding processes were being introduced. Today, there are numerous fillet weld design guidance documents available, such as ABS 96 (ABS, 2000) for naval vessel applications, Eurocode 3 (CEN, 2005) and IIW (IIW, 1976) for general structural applications, as recently discussed by Picón and Cañas (2009) in which a limit analysis based strength evaluation procedure was also presented in the context of elastic-plastic finite element analysis. However, the basic assumptions in calculating fillet weld throat stress for strength characterization purpose remain the same as those given in AWS B4.0 (AWS, 2007), i.e., by assuming a failure angle of 45° from base plate and a uniform throat stress distribution along weld line. Such assumptions often lead to the use of much lower fillet weld strengths seen in longitudinal shear specimens than those in transverse shear specimens for fillet weld sizing purpose in order to be conservative, resulting in oversized welds. The use of oversized welds had been attributed, at least in part, to the development of severe welding-induced distortions in lightweight shipboard structures during construction of some naval surface combatants, as recently discussed by Huang et al (2014). Therefore, there is a growing interest in developing an improved weld sizing method for both

satisfying weld strength requirements and eliminating overwelding for facilitating distortion control during construction.

Almost all existing weld sizing criteria are based on either an averaged shear stress or averaged stress resultant across fillet weld throat plane at 45° from base plate under given loading conditions and compare it with fillet weld strengths obtained using standard longitudinal and transverse shear specimens.

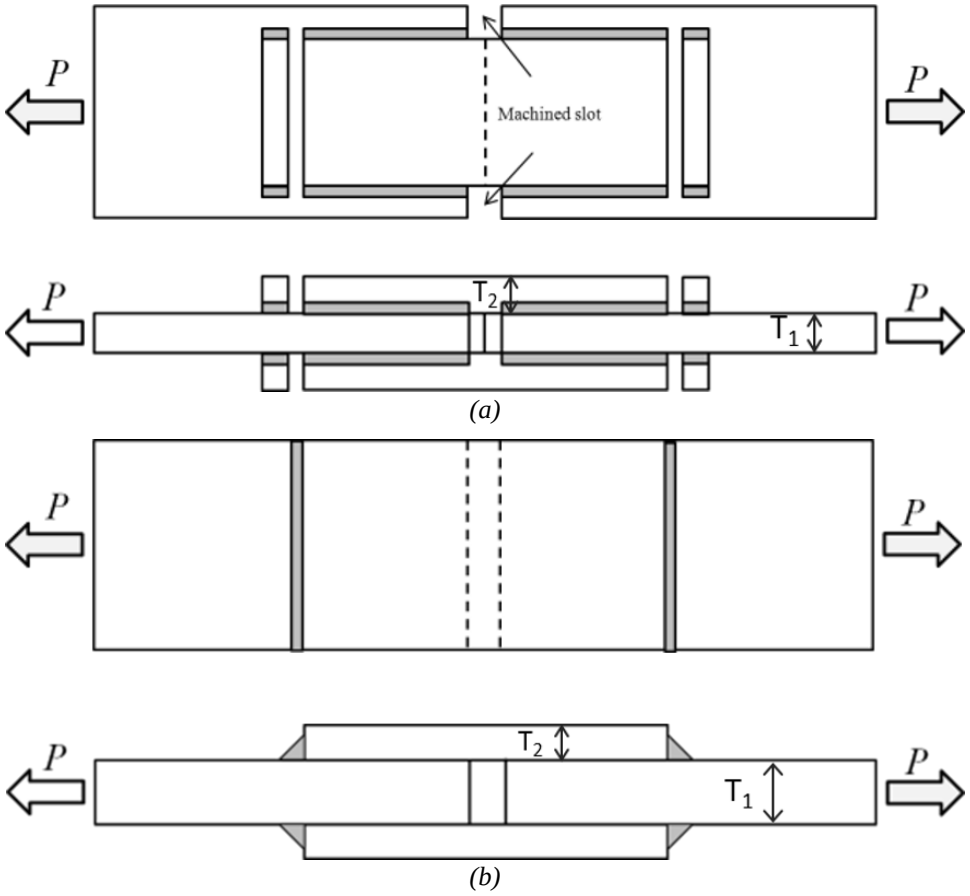

Figure 2.1: AWS standard shear strength test specimens: (a) longitudinal shear; (b) transverse shear

Commonly used standard longitudinal and transverse shear specimens in fillet weld strength testing are typical of those stipulated in AWS B4.0 (AWS, 2007), as illustrated in Figure 2.1. The resulting shear strength is calculated by using the following formula given in AWS B4.0 (2007) for both the longitudinal and transverse shear specimens:

$$\tau_{u,w} = \frac{P_u}{a_{45} \times L} \tag{2.1}$$

In Eq. (2.1), P_u represents the peak load prior to failure obtained from strength test, L the total load-carrying weld length, and $\tau_{u,w}$ the resulting shear strength; in addition, as shown in Figure 2.2, s is the fillet weld leg size, and a_{45} is the shortest length across weld, i.e., $a_{45} = s \times \cos\theta$ where $\theta = 45°$ is assumed in AWS B4.0 (AWS, 2007), also known as weld throat size.

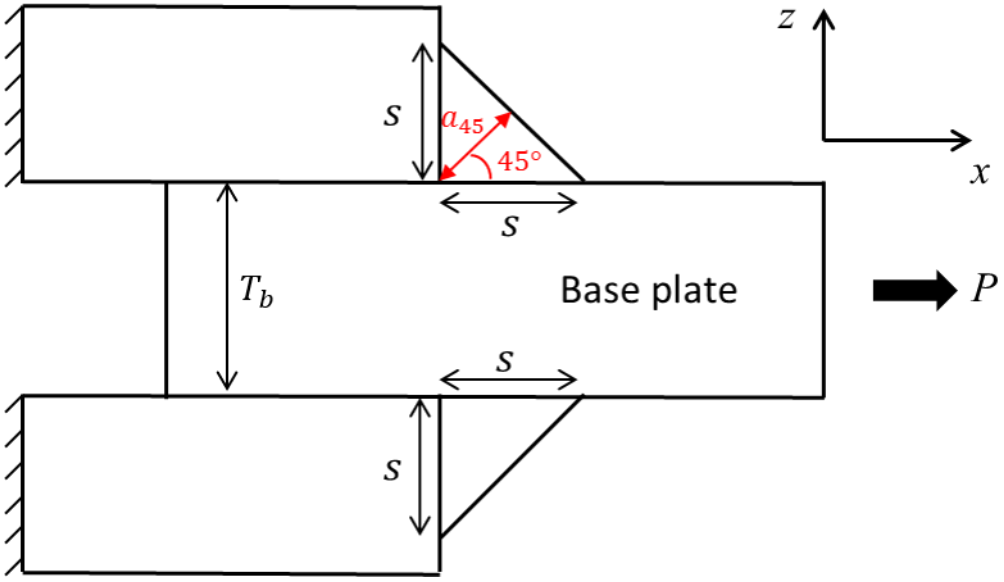

Figure 2.2: Fillet weld leg and weld throat definition in AWS B4.0

Eq. (2.1) is used as a basis in developing various fillet weld sizing criteria, such as in MIL-STD-1628 (Department of Defense, 1974), Krumpen (1984), and others (ABS, 2000; CEN, 2005). Although it is simple to use for processing test data, Eq. (2.1) has been shown to exhibit some serious limitations in correlating test data as demonstrated by investigations both in the past and recent years. Firstly, it has been well established in literature that failure angle of transver shear specimens tends to occur at about 22.5° rather than at 45° as assumed in Eq. (2.1); Secondly, shear stress distribution along weld line direction in longitudinal shear specimens is far from being uniform as assumed in Eq. (2.1). The former was repeatedly confirmed experimentally on transverse shear specimens by various researchers for weldment made of mild steel (Kato &

Morita, 1974; McClellan, 1990), high strength steel (Björk et al., 2012; Khurshid et al., 2012), aluminum alloys (Krumpen & Jordan, 1984; Marsh, 1985 & 1988), as well as titanium alloys (Dong et al., 2013; Nie & Dong, 2012). The latter has recently been illustrated by using a finite element based traction stress method by Nie and Dong (2012) in their re-evaluation of some existing test data reported in literature. Their results showed that significant shear stress concentration exists at weld ends (at the "machined slot" positions in longitudinal shear specimens as shown in Figure 2.1a), which can be attributed to typically lower shear strengths in longitudinal shear specimens compared with those in transverse shear specimens, as reported in the literature (Nie & Dong, 2012). However, more test data are needed in order to both validate the findings given by Nie and Dong and develop correction schemes for using Eq. (2.1) for fillet weld strength determination.

In this chapter, we first outline the traction stress approach for shear strength analysis proposed by Nie and Dong (2012) with a focus upon its specific implementation in analyzing specimens of interest in this study. After demonstrating its finite element mesh-insensitivity, the traction stress method is used to compute peak shear stresses on specimens under longitudinal and transverse shear conditions involved in a companion strength test program as outlined in Huang et al. (2014 & 2016). The analysis results are then presented in a form that can be used as a correction coefficient to Eq. (2.1) for performing test data analyzing, depending upon if longitudinal or transverse shear specimens are involved. After that, a large amount of shear strength test data obtained as a part of this study is analyzed using the proposed correction scheme with respect to Eq. (2.1). For comparison purpose, data interpretation using the conventional method represented by Eq. (2.1) is also presented. To facilitate the data correlation process, some of the experimental details such as fillet weld leg size measurement procedure are also discussed. Finally, the

implication of the analysis results from this study for achieving a quantitative weld sizing criterion is discussed.

2.2 Weld Throat Stress Characterization

Encouraged by an earlier investigation by Nie and Dong (2012), this study further extends the traction stress method for investigating its ability for correlating a large amount of fillet weld shear strength test data recently completed in a companion experimental testing program outlined by Huang et al. (2014 &2016). For completeness, a brief discussion is provided here on the relevant elements of the traction stress method to the current investigation. For more detailed discussions on traction stress method, readers can consult some recent publications, e.g., by Dong (2001) for weld fatigue related applications and by Nie and Dong (2012) for shear strength correlations.

2.2.1 Traction Stress Method

Traction-based structural stress method and its basic concept for fatigue evaluation of welded joints were first introduced by Dong (2001) and was then shown to enable the formulation of a master S-N curve method given by Dong (2005), which since has been adopted by the 2007 ASME Div 2 Code (Dong et al., 2010). As demonstrated by Nie and Dong (2012), the traction stress method has several advantages for applications in fillet weld shear strength evaluations:

(1) Traction stress method is a nodal force based method in which equilibrium conditions are enforced in stress calculation process with respect to a hypothetical cut plane, resulting in good mesh-insensitivity at stress concentration locations.

(2) In fatigue applications (Dong, 2001 & 2005), the method is implemented for extracting through-thickness membrane and bending parts of three traction stress components. For static shear strength analysis in a fillet-welded component, it is only the membrane parts of shear traction

stress components that need to be considered, which offers a remarkable simplicity for general 3D applications in complex structures.

(3) Additionally, it has been shown that membrane parts of traction stress components obtained from linear elastic analysis provide a reasonable representation of traction stress components when the plane is subjected to elastic-plastic deformation, in which bending part tends to rapidly diminish as a result of local yielding, as discussed by Nie and Dong (2012), and Dong et al. (2014). Therefore, such a traction stress method potentially offers an efficient (although approximate in nature) elastic solution to static shear strength characterization problems without resorting to nonlinear finite element computation for which elastic-plastic material property would have to be considered.

Furthermore, it should be noted that traction stress method based on elastic analysis procedure can be further justified in view of the fact that conventional shear strength calculation procedures (e.g., Eq. (2.1)) and weld sizing criteria (e.g., Krumpen's method (1984)) are all based on statically-equilibrium conditions without considering material nonlinearity prior to final failure.

2.2.2 Calculation Procedure

Along any given weld throat plane of fillet-welded specimens, say an angle of θ from base plate, a hypothetical cut exposes three traction stress components with respect to the local coordinate system (x'-y'-z'), termed as normal stress $\sigma(x')$, transverse shear stress $\tau_T(x')$ and longitudinal shear stress $\tau_L(x')$, as shown in Figure 2.3. All three components may exist in general under arbitrary loading conditions and may exhibit a complex distribution along the plane. These stresses are singular at weld root, causing severe mesh-sensitivity in peak stress determination when using conventional finite element methods. The singularity in stresses at weld root can be effectively suppressed by introducing the nodal force based traction stress method.

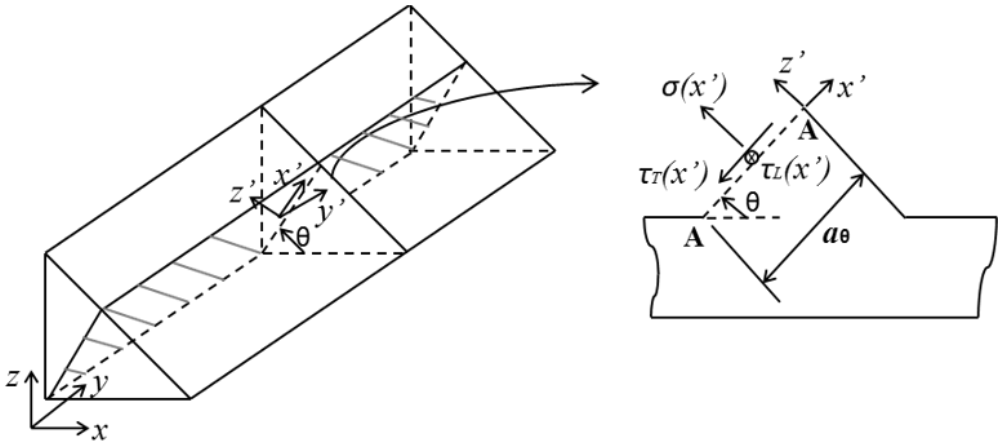

Figure 2.3: Traction stress components acting on a weld throat plane at an angle of θ

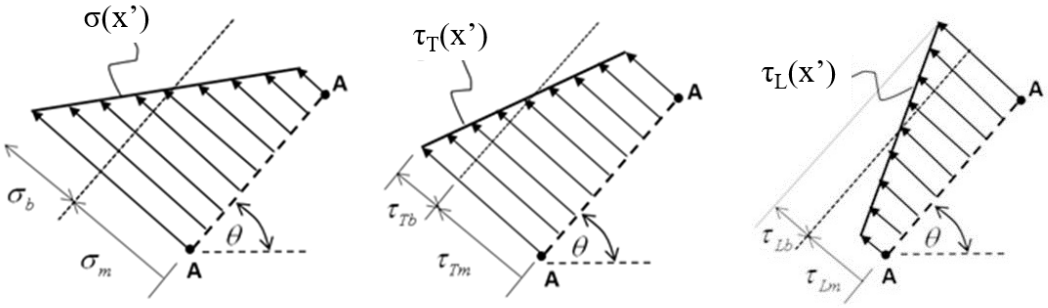

Figure 2.4: Linear representation and decomposition of weld throat traction stress components

With this traction stress method, the linear forms of the three traction stress components ($\sigma(x')$, $\tau_T(x')$, $\tau_L(x')$) with respect to the local coordinate system (i.e., (x'-y'-z') in Figure 2.3) can be decomposed, in a statically equivalent manner, into their membrane and bending parts as seen in Figure 2.4 and expressed in terms of line forces and line moments with respect to the mid-distance of the weld throat cut cross-section A-A along a_θ:

$$\sigma = \sigma_m + \sigma_b = \frac{f_{z'}}{a_\theta} + \frac{6m_{y'}}{a_\theta^2}$$

$$\tau_L = \tau_{Lm} + \tau_{Lb} = \frac{f_{y'}}{a_\theta} + \frac{6m_{z'}}{a_\theta^2} \qquad (2.2)$$

$$\tau_T = \tau_{Tm} = \frac{f_{x'}}{a_\theta}$$

Where a_θ is weld throat dimension at an angle of θ from base plate and $f_{x'}$, $f_{y'}$, $f_{z'}$ and $m_{y'}$, $m_{z'}$ are line forces and line moments with respect to the local coordinate system. Note that the transverse shear traction stress in Eq. (2.2) is represented by its membrane component, consistent with transverse shear stress definition in plate and shell theory, in which transverse shear stress exhibits a parabolic distribution through plate thickness direction.

The line forces/moments in Eq. (2.2) can be related to nodal forces/moments that are available from finite element calculations after being rotated into the same local coordinate system (x'-y'-z') through a system of simultaneous equations, as expressed by Eq. (2.3) (Dong, 2005). For example, with the hypothetical cut "A-A" along the weld line (i.e., along y axis) as shown in Figure 2.3, line forces in z' direction (normal to cut plane) can be directly obtained by solving the following system of simultaneous linear equations (Dong, 2005 & 2010):

$$\begin{Bmatrix} F_1 \\ F_2 \\ F_3 \\ \vdots \\ F_{n-1} \\ F_n \end{Bmatrix}_{z'} = \begin{bmatrix} \frac{l_1}{3} & \frac{l_1}{6} & 0 & 0 & \cdots & 0 \\ \frac{l_1}{6} & \frac{(l_1+l_2)}{3} & \frac{l_2}{6} & 0 & \cdots & 0 \\ 0 & \frac{l_2}{6} & \frac{(l_2+l_3)}{3} & \frac{l_3}{6} & 0 & 0 \\ 0 & 0 & \ddots & \ddots & \ddots & 0 \\ \vdots & \ddots & \ddots & \ddots & \frac{(l_{n-2}+l_{n-1})}{3} & \frac{l_{n-1}}{6} \\ 0 & \cdots & \cdots & 0 & \frac{l_{n-1}}{6} & \frac{l_{n-1}}{3} \end{bmatrix} \begin{Bmatrix} f_1 \\ f_2 \\ f_3 \\ \vdots \\ f_{n-1} \\ f_n \end{Bmatrix}_{z'} \quad (2.3)$$

In the above equation, n is the total number of the nodes ($n-1$ is the total number of the element edges if linear elements are considered) defining the weld line in y direction in Figure 2.3. In Eq. (2.3), F_1, F_2, …, F_n represent nodal forces at Node 1, 2, …, n on the weld line for each node with respect to the z' direction after being rotated from the global coordinate system (x-y-z) into the local coordinate system (x'-y'-z'), as shown in Figure 2.5.

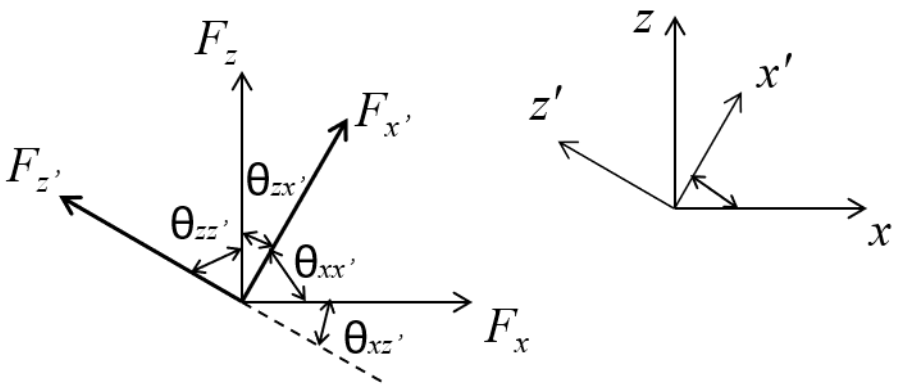

Figure 2.5: Global coordinate system versus local coordinate system

This transformation process is illustrated by Eq. (2.4), where F_x, F_z, M_x, M_z are nodal forces and nodal moments with respect to the global coordinate system. By inverting Eq. (2.3), line forces f_1, f_2, …, f_n can be calculated for insertion into Eq. (2.2) so that membrane part of normal traction stress component can be calculated at each position along weld line. In the same manner, submitting nodal moments (M_1, M_2, …, M_n) with respect to y' axis into Eq. (2.3), the corresponding line moments (m_1, m_2, …, m_n) can be calculated for insertion into Eq. (2.2) for computing bending part of normal traction stress component.

$$\begin{aligned} F_{x'} &= F_x \cos\theta_{xx'} + F_z \cos\theta_{zx'} \\ F_{z'} &= F_x \cos\theta_{xz'} + F_z \cos\theta_{zz'} \\ M_{x'} &= M_x \cos\theta_{xx'} + M_z \cos\theta_{zx'} \\ M_{z'} &= M_x \cos\theta_{xz'} + M_z \cos\theta_{zz'} \end{aligned} \tag{2.4}$$

The calculation procedure above is directly applicable if plate and shell element models are used since relevant nodal forces and nodal moments are directly available from finite element calculations. When using three dimensional (3D) solid element models such as those used in this study, the following pre-processing procedure is needed to transform nodal forces at nodes situated on the cross-section cut A-A into equivalent nodal forces and nodal moments acting on its mid-section (i.e., at half of distance a_θ from weld root), as shown in Figure 2.6:

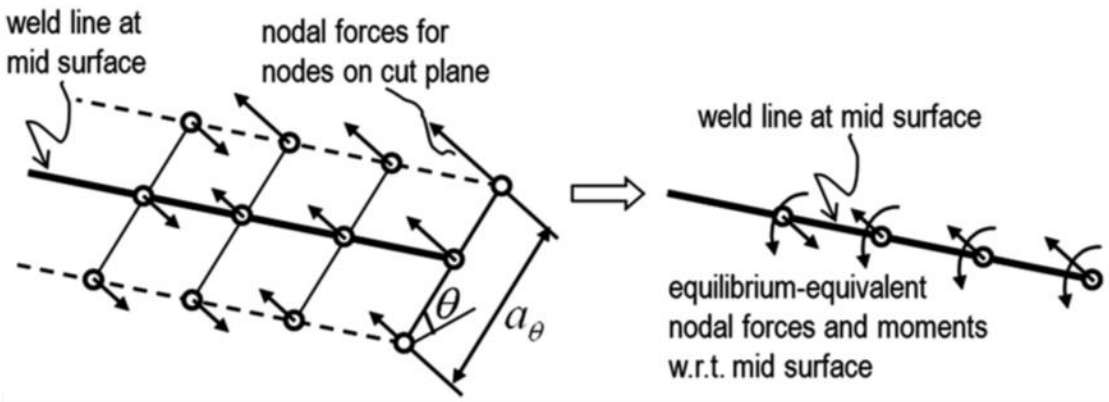

Figure 2.6: Transformation of nodal forces on a weld throat cut plane in 3D solid element model into statically equivalent forces and moments with respect to weld throat mid-section along weld line

2.2.3 Analysis of Test Specimens

After examining various effective strength failure criteria, Nie and Dong (2012) have shown that an effective stress expressed in terms of membrane parts of shear traction stress components (Figure 2.3 & Figure 2.4) can be used for characterizing shear strength of fillet-welded specimens under either longitudinal or transverse shear loading conditions. In this study, an effective shear stress definition postulated for specimens of interest under general loading conditions can be expressed as:

$$\tau_e = \sqrt{\tau_{Lm}^2 + \tau_{Tm}^2} \tag{2.5}$$

Note that Eq. (2.5) makes use of stress resultant definition in terms of membrane parts of the two orthogonal shear traction stress components on a hypothetical cut plane. For shear strength characterization of the specimens in Figure 2.1, the critical values of τ_{Lm} and τ_{Tm} are to be calculated at ultimate failure load obtained from shear strength test. If there is only one shear stress component dominating (either longitudinal or transverse shear stress), Eq. (2.5) reduces to the one proposed by Nie and Dong (2012). In what follows, both the specific procedure for calculating the effective shear stress given in Eq. (2.5) and calculation results of the shear specimens tested in this study are presented.

2.2.3.1 Longitudinal Shear Specimen

For longitudinal shear specimens, as shown in Figure 2.1a, only the membrane part of the longitudinal shear stress needs to be considered since the transverse shear stress proves to be negligible. Therefore, according to Eq. (2.5), the effective shear stress definition simply becomes:

$$\tau_e = \tau_{Lm} \tag{2.6}$$

For calculating the longitudinal shear stress distribution along a weld throat plane, 3D solid finite element model like the one shown in Figure 2.7 is used. Based on the specimen geometry given in AWS B4.0 (2007) (also shown in Figure 2.1a), three symmetry planes are considered, resulting in a one-eighth of the longitudinal shear specimen being modeled. Both the symmetry conditions and applied load (force *P* representing a uniform stress acting on the base plate end cross section) are illustrated in Figure 2.7. Parabolic solid elements ("C3D20R": 20 node solid element with reduced integration scheme in ABAQUS (Dassault Systemes, 2018)) are used and linear elastic behavior is assumed. By following the procedure of the traction stress method described in Sec. 2.2.2, weld throat membrane shear stress along the weld line (local y' direction in Figure 2.8) can be calculated.

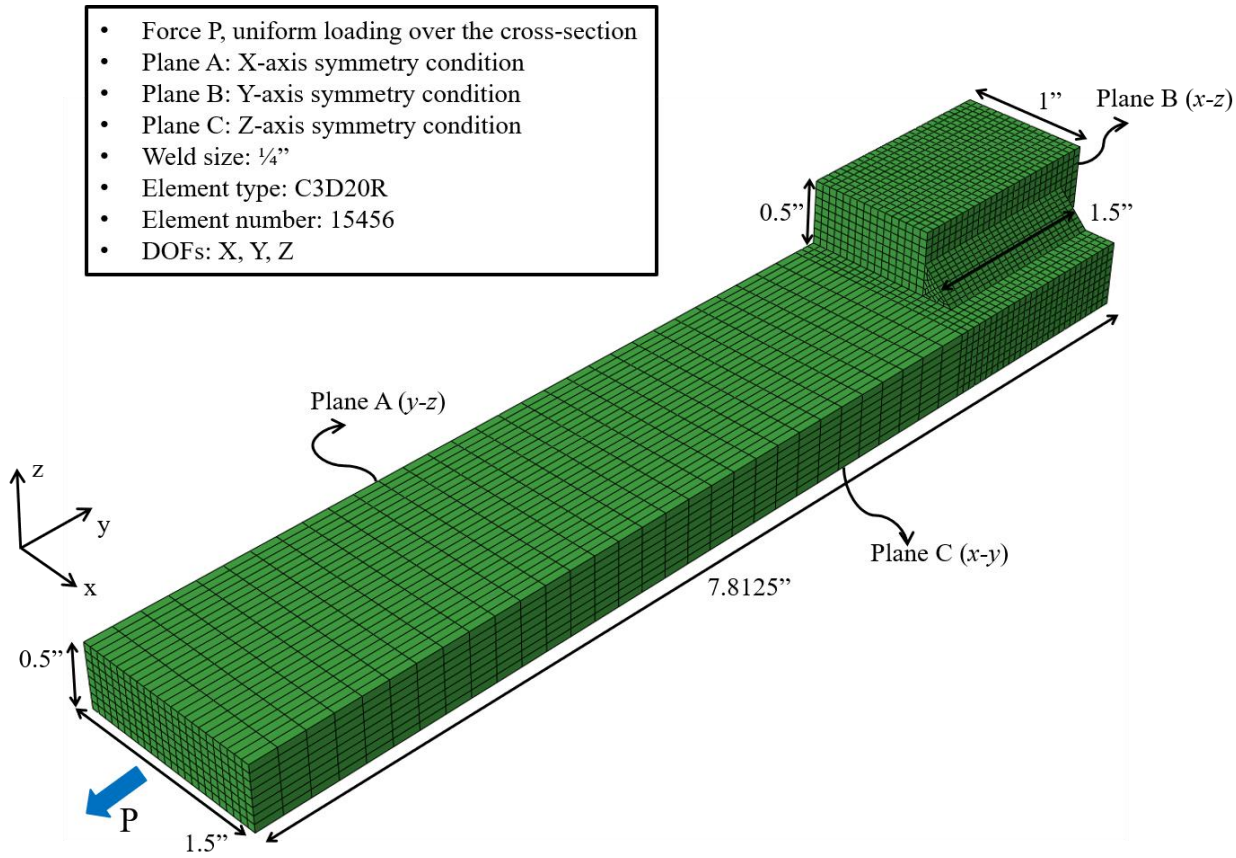

Figure 2.7: A representative 3D solid finite element model used for longitudinal shear specimens (1" = 25.4 mm)

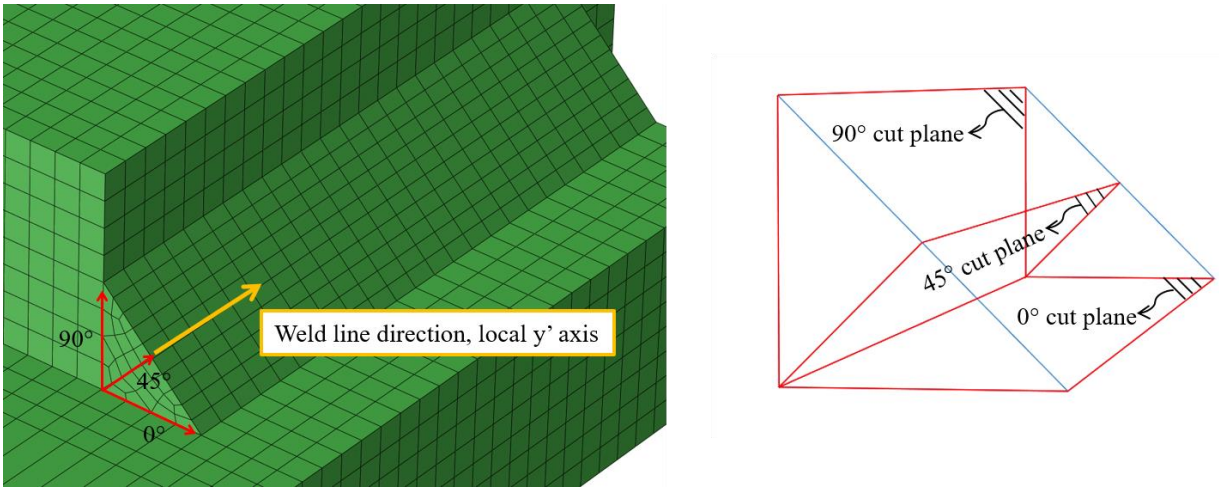

Figure 2.8: Three cut planes through weld for calculating longitudinal shear stress along weld line

The calculated longitudinal shear stress distributions (normalized by $P/(a \times L)$) corresponding to the three cut planes (see Figure 2.8) along weld line are plotted in Figure 2.9. The following can be observed:

(1) Longitudinal shear stress along 45° cut plane has the maximum stress value along the entire weld line, comparing with planes at 0° and 90°, confirming that the weld throat plane at 45° is the weakest plane. This agrees with both the experimental findings of this study (to be discussed in the next section) and what was demonstrated by Nie and Dong (2012).

(2) Unlike stress in transverse shear specimens, longitudinal shear stress is non-uniformly distributed along the 45° weld throat cut plane and its largest value occurs at the weld end near the machined slot (indicated in Figure 2.1a). At this position (see Figure 2.9), the maximum normalized shear stress value is about 1.2, indicating that shear stress value is 20% higher than that calculated by the conventional shear stress equation (Eq. (2.1)) where no stress concentration effect is considered. It is important to note that an averaged shear stress of unity at the 45° cut plane can be identified in Figure 2.9, which is the basic assumption of Eq. (2.1).

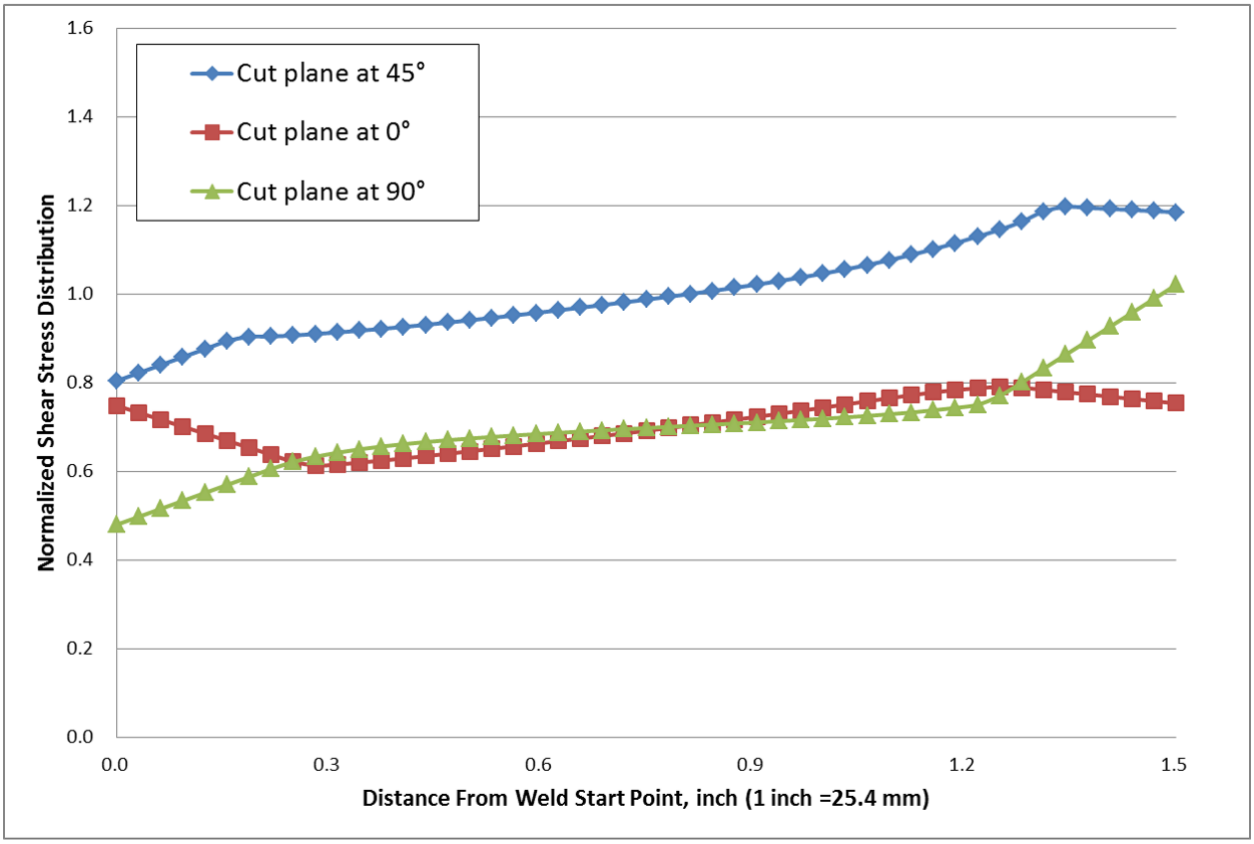

Figure 2.9: Normalized longitudinal shear stress distribution on three cut planes along weld line

To demonstrate that the traction stress components calculated are indeed reasonably mesh-insensitive for shear stress concentration characterization for longitudinal shear specimens shown in Figure 2.1a, several finite element models with different element sizes (see Figure 2.10a) were considered here for examining the maximum shear stress along the weld line. As shown in Figure 2.10b, a good mesh-insensitivity in stress calculation results can be obtained with less than 5% variation at weld end, as element size varies in terms of fillet weld leg size (s) from $s/8$ to $s/2$.

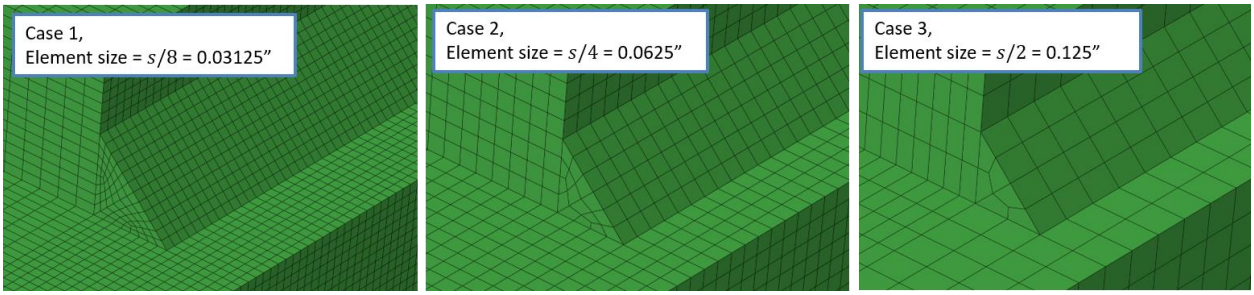

(a)

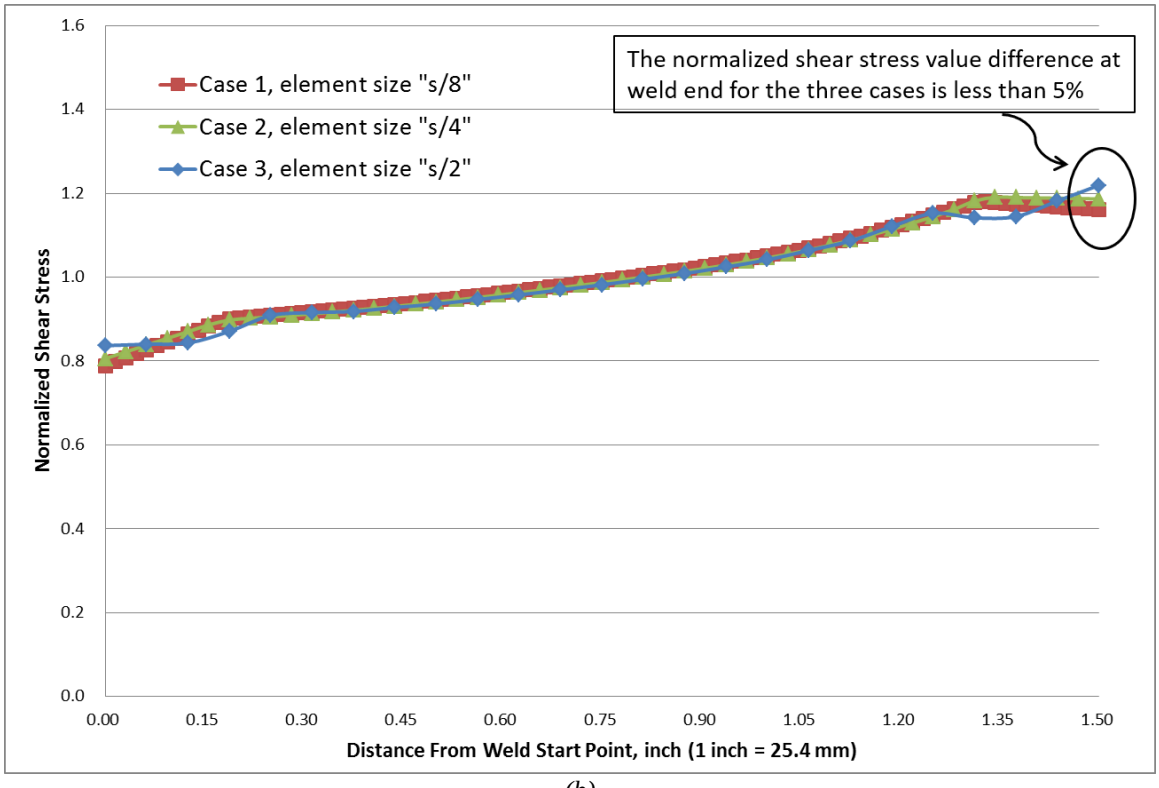

(b)

Figure 2.10: Demonstration of mesh-insensitivity of traction stress method – longitudinal shear specimen: (a) FE models with different element sizes; (b) comparison of normalized shear stress along weld line obtained from each model shown in Figure 2.10a

With the confirmation of its good mesh-insensitivity, the traction stress method is then used to determine stress concentration factor (*SCF*), defined as the peak longitudinal shear stress at weld end normalized by $P/(a \times L)$ given in Eq. (2.1), for longitudinal shear specimen configurations tested in the experimental study. The final *SCF* results are presented in Figure 2.11 as a function of normalized fillet weld leg size (s/T_1) for two base plate thicknesses (T_1 = 12 mm and 25 mm) considered in this study. It can be seen that *SCF* decreases as relative weld leg size (s/T_1) increases and *SCF* results also show a strong dependency on base plate thickness (T_1), which cannot be taken into account in traditional shear stress calculation procedure, such as Eq. (2.1) given in AWS B4.0.

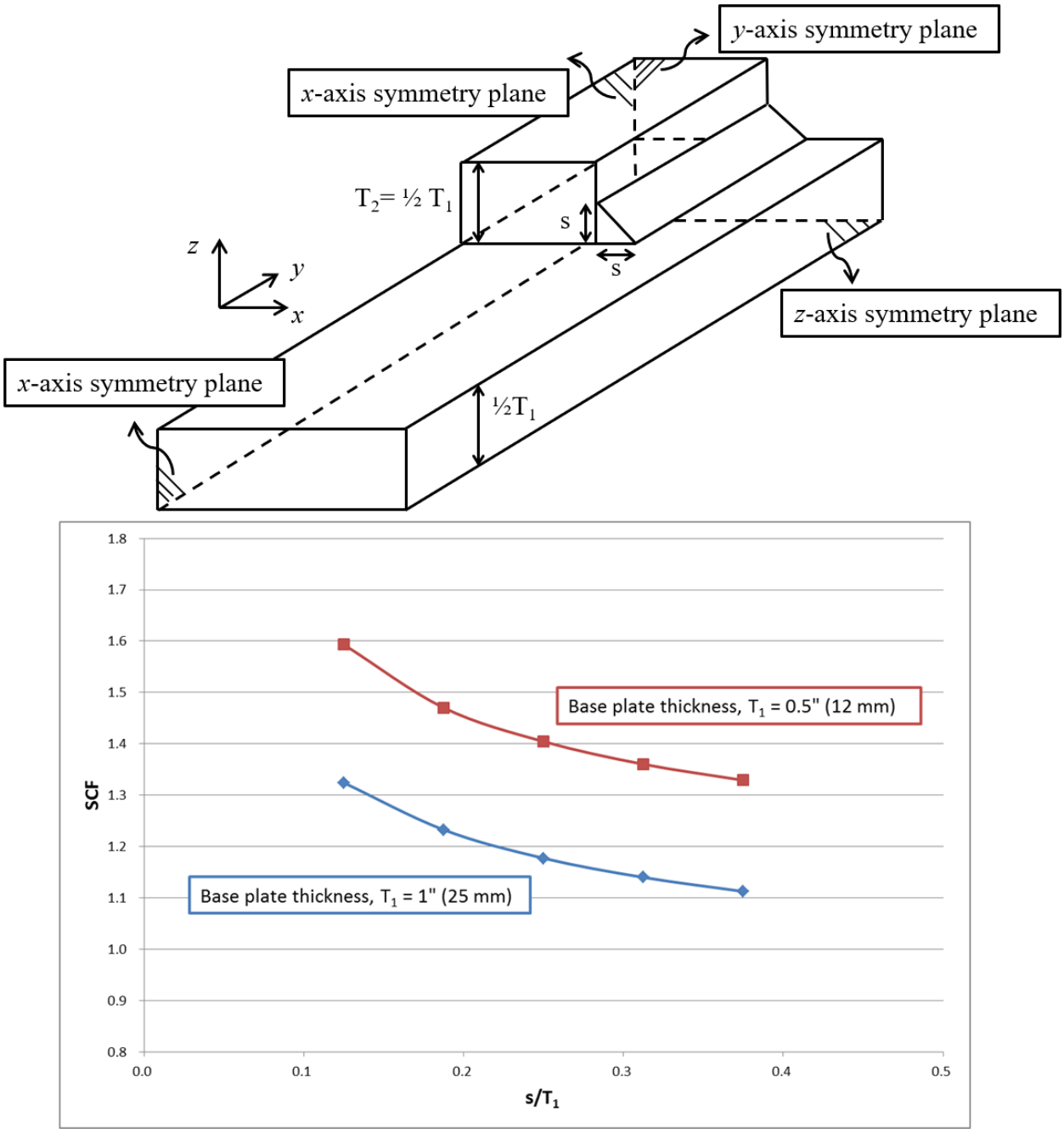

Figure 2.11: SCF for longitudinal shear specimens as a function of relative fillet weld leg size (s/T_1)

With the *SCF* results in Figure 2.11, the maximum longitudinal shear stress occurring at weld end corresponding to failure load, i.e., peak load measured during a test, can be expressed as:

$$\tau_{Lm,\max} = \tau_{u,w_L} = SCF \times \left(\frac{P_u}{a_{45} \times L}\right) \tag{2.7}$$

in which the term within the parenthesis represents the AWS shear strength determination formula given in Eq. (2.1). Note that Eq. (2.7) assumes that elastically calculated maximum membrane stress concentration factor (*SCF*) continues to serve as a characteristic stress scaling parameter in nonlinear regime leading up to final failure. This assumption will be validated in Section 2.4 when test data are analyzed. Since all *SCF* values in Figure 2.11 are larger than unity, the traction stress based shear strength (τ_{u,w_L}) is larger than that determined by AWS formula, suggesting that the shear stress definition given in Eq. (2.1) of AWS B4.0 (2007) underestimates actual shear stress acting on the weld throat plane for longitudinal shear specimens, e.g., by as much as 60% if a base plate thickness T_1 of 0.5" (12 mm) is considered.

2.2.3.2 Transverse Shear Specimen

Transverse shear specimen can be analyzed in the same manner as demonstrated in the previous section of longitudinal shear specimen. Due to the two-dimensional nature of stress state involved (see Figure 2.1b), 2D cross-section model under plane strain conditions (element type: "CPE8R" in ABAQUS (Dassault Systemes, 2018)) are used in this study for simplicity. From Eq. (2.5), the corresponding effective shear stress simply becomes:

$$\tau_e = \tau_{Tm} \tag{2.8}$$

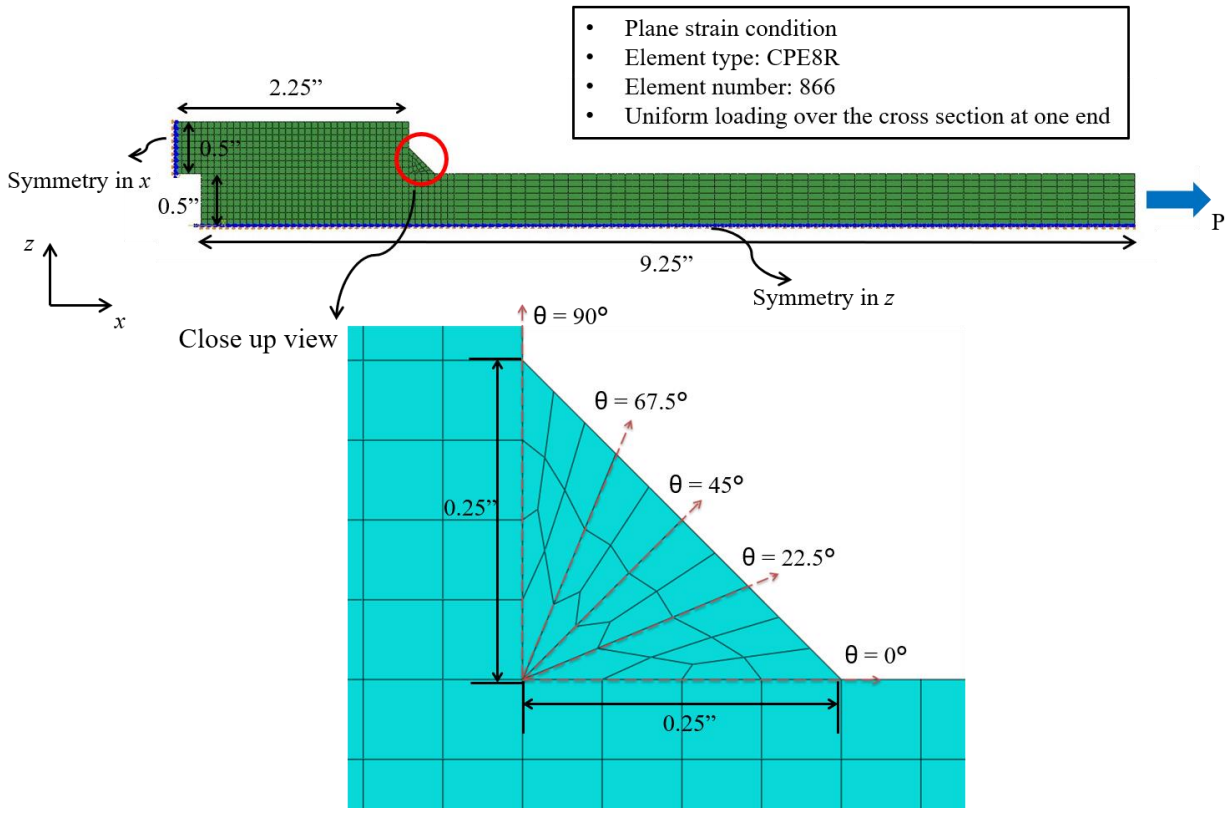

Figure 2.12: A representative plane-strain finite element model for transverse shear specimen

A representative plane-strain finite element model with quarter symmetry conditions is shown in Figure 2.12. Similar to the calculations performed for longitudinal shear specimen, a theoretical failure plane is postulated as the plane on which transverse shear traction stress reaches its maximum value among all planes searched. A total of five planes (from angle of 0° to 90° shown in Figure 2.12) are searched by calculating traction stresses on all cut planes. The FE-based traction stress results are shown as symbols in Figure 2.13. It is important to note that the maximum transverse shear stress occurs at 22.5° cut plane in Figure 2.13, rather than at 45°, as assumed in traditional shear stress calculation method as described by Eq. (2.1).

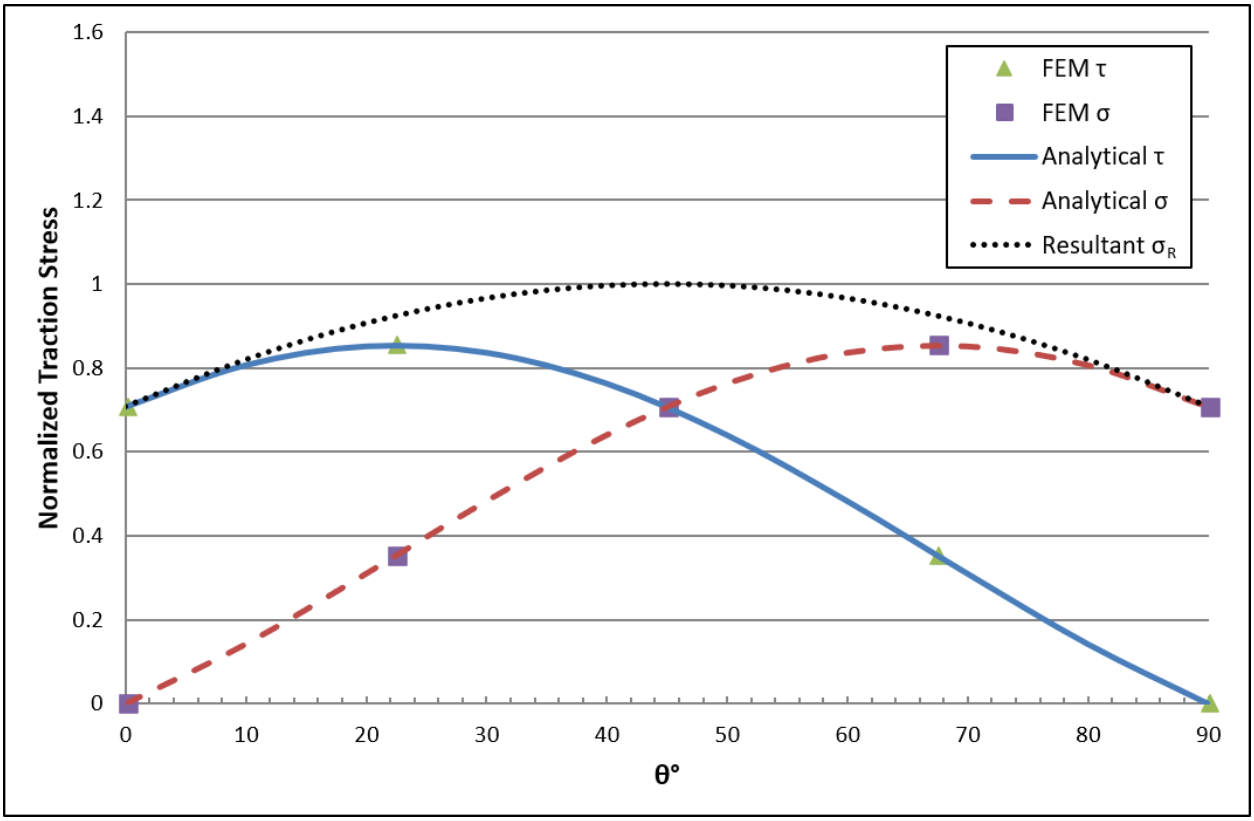

Figure 2.13: Comparison of analytical and finite element results for transverse shear stress and normal stress as a function of cut angle θ

To facilitate the interpretation of the FE results in Figure 2.13, it should be useful to introduce the closed-form analytical solution developed by Nie and Dong (2012) for transverse shear specimen by considering a problem definition shown in Figure 2.14. For fillet weld with equal leg size (s), weld throat dimension a_θ with any given angle θ can be obtained as:

$$a_\theta = \frac{s}{\sin\theta + \cos\theta} \tag{2.9}$$

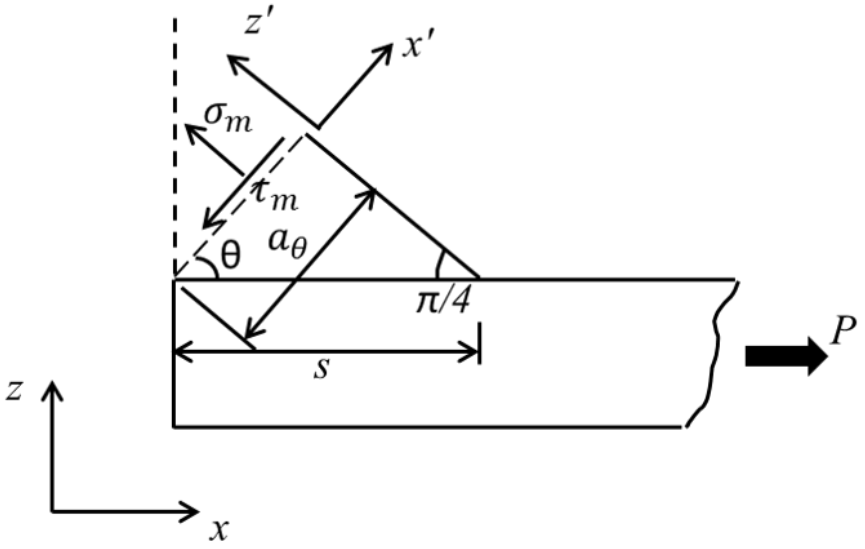

Figure 2.14: Free-body diagram for transverse shear specimen with equal weld leg size s

Then, the membrane parts of normal stress (σ_m) and transverse shear stress (τ_{Tm}) on the cut plane become:

$$\tau_{Tm}(\theta) = \frac{P \times \cos\theta}{a_\theta \times L} = \left(\frac{\sqrt{2}(\sin 2\theta + \cos 2\theta + 1)}{4}\right) \times \left(\frac{P}{a_{45} \times L}\right) \tag{2.10}$$

$$\sigma_m(\theta) = \frac{P \times \sin\theta}{a_\theta \times L} = \left(\frac{\sqrt{2}(\sin 2\theta - \cos 2\theta + 1)}{4}\right) \times \left(\frac{P}{a_{45} \times L}\right) \tag{2.11}$$

The analytical results given in Eqs. (2.10) and (2.11) are also plotted in Figure 2.13 as lines. The results from both analytical and finite element solutions coincide exactly with each other, proving the validity of the finite element traction stress method used in this study. This is as expected since both FE based traction stress method and the analytical solution deal with the same stress definitions, and both satisfy equilibrium conditions. Additionally, Figure 2.13 clearly indicates that transverse shear stress (τ_{Tm}) reaches its maximum value at exactly $\theta = 22.5°$. This is consistent with the experimental observations discussed both in an earlier publication (McClellan, 1990) and recent experimental investigation (Huang et al., 2014) in which typical failure plane was consistently found at about 22.5° in transverse shear specimens.

The exact angle of plane that yields the maximum transverse shear stress can be readily demonstrated by equating the first derivative of Eq. (2.10) with respect to angle θ to zero, i.e.,

$$\left(\frac{\cos 2\theta - \sin 2\theta}{\sqrt{2}}\right) \times \left(\frac{P}{a_{45} \times L}\right) = 0 \tag{2.12}$$

which leads to $\theta = \pi/8$ (or 22.5°) exactly. This maximum transverse shear traction stress at angle of $\theta = \pi/8$ can now be expressed in terms of the shear stress definition in AWS B4.0 (i.e., Eq. (2.1)) by substituting $\theta = \pi/8$ into Eq. (2.10), yielding:

$$\tau_{Tm,\max} = \tau_{u,w_T} = \left(\frac{2+\sqrt{2}}{4}\right) \times \left(\frac{P_u}{a_{45} \times L}\right) \tag{2.13}$$

Eq. (2.13) can be used to calculate the traction stress based shear strength (τ_{u,w_T}) for transverse shear specimens if failure load P_u is known from transverse shear specimen testing. Note that the term $(2+\sqrt{2})/4$ in Eq. (2.13) becomes a multiplier of about 0.854 against the conventional shear stress definition in Eq. (2.1) for conversion to the present traction stress based shear strength definition, suggesting an overestimation of about 15% in shear strength for transverse shear specimens if the conventional AWS B4.0 (AWS, 2007) procedure is used.

Furthermore, it is worth noting that the conventional shear strength definition given in Eq. (2.1) can be recovered as the maximum value of stress resultant by taking advantage of the closed-form analytical solutions given by Eqs. (2.10) and (2.11) at $\theta = 45°$, i.e.,

$$\sigma_{R,\theta=45^\circ} = \sqrt{\left(\sigma_{m,\theta=45^\circ}\right)^2 + \left(\tau_{Tm,\theta=45^\circ}\right)^2} = \frac{P}{a \times L} \tag{2.14}$$

as shown in Figure 2.13 (dotted line at the top). As demonstrated both in literature (McClellan, 1990; Björk et al., 2012; Dong et al., 2013) and the next section, a failure angle of about 22.5° has been consistently observed in test data from transverse shear specimens. As a

result, the stress resultant based shear stress definition in Eq. (2.14) (also Eq. (2.1)) is inadequate for characterizing shear strength in this type of specimens.

With the above developments, Eq. (2.7) along with the *SCF* results in Figure 2.11 for longitudinal shear specimens and Eq. (2.13) for transverse shear specimens can now be directly used for analyzing fillet weld shear strength test data from standard specimens, such as those performed in this study, as discussed in the next section.

2.3 Testing Procedure

Both longitudinal and transverse shear specimens in this study were designed according to AWS B4.0 (AWS, 2007). Major ship hull steel grades with matching filler materials and associated welding processes were considered. Nominal or design fillet weld leg size varied from 1/8" (3 mm) to 3/8" (10 mm). A summary of test specimens used in this study is given in Table 2.1. Further details of the test specimens and justifications can be found in Huang et al. (2014 & 2016).

Table 2.1: Shear specimens tested in this study

Specimen Type	Base Material	Base Material UTS	Welding Process	Filler Material	Base Plate Thickness T_1	Nominal Weld Size s	Number
Longitudinal Shear	DH36	71 ksi (490 MPa)	FCAW	71T1-C	0.5" (12 mm) 1" (25 mm)	1/8" (3 mm) – 3/8" (10 mm)	24
	HSLA80	96 ksi (660 MPa)	FCAW	101T-C	0.5" (12 mm) 1" (25 mm)	1/8" (3 mm) – 3/8" (10 mm)	24
			GMAW	MIL-100S	1" (25 mm)	3/16" (5mm) – 3/8" (10 mm)	16
Transverse Shear	DH36	71 ksi (490 MPa)	FCAW	71T1-C	0.5" (12 mm) 1" (25 mm)	1/8" (3 mm) – 3/8" (10 mm)	24
	HSLA80	96 ksi (660 MPa)	FCAW	101T-C	0.5" (12 mm) 1" (25 mm)	1/8" (3 mm) – 3/8" (10 mm)	24
			GMAW	MIL-100S	1" (25 mm)	3/16" (5mm) – 3/8" (10 mm)	16

Representative longitudinal and transverse shear specimens prior to strength test are shown in Figure 2.15 for illustration purpose. Fillet weld leg size was measured using a laser scan device

(known as Wiki-Scan[1]) before test, as illustrated in Figure 2.16, which provides a consistent determination of fillet weld leg size. In addition, weld leg size was also measured by a digital caliper after test by examining fracture surfaces and failure paths, referred here as post-fracture measurement. These laser and post-fracture measurements are used to facilitate shear strength test data correlations in addition to the use of nominal weld leg sizes. Furthermore, both types of weld leg size measurements are also used to establish typical variation in weld size in shop floor practice. As found during the strength test, actual measured weld sizes can be as much as 30% to 50% different from the nominal weld sizes specified by design, which would have significant effects on shear strength characterization in view of Eq. (2.7) and Eq. (2.13). Therefore, to better fillet weld shear strength, all strength calculation results reported from this point on in this study are based on post-fracture measurements rather than the nominal ones. Note that these post-fracture weld size measurements take into account of weld penetration status. Detailed fillet weld leg size and weld quality effects on shear strength characterization will be discussed in a separate publication due to the space limitation here.

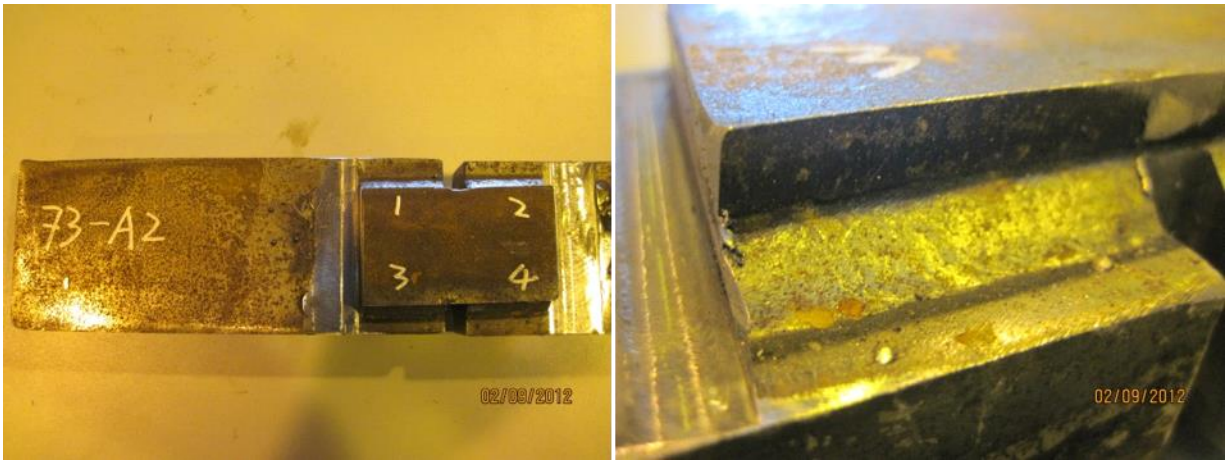

(a)

[1] Wiki-Scan™: Welding Inspection System, a product of SERVO ROBOT INC.

(b)

Figure 2.15: Shear strength test specimens prior to testing: (a) longitudinal shear; (b) transverse shear

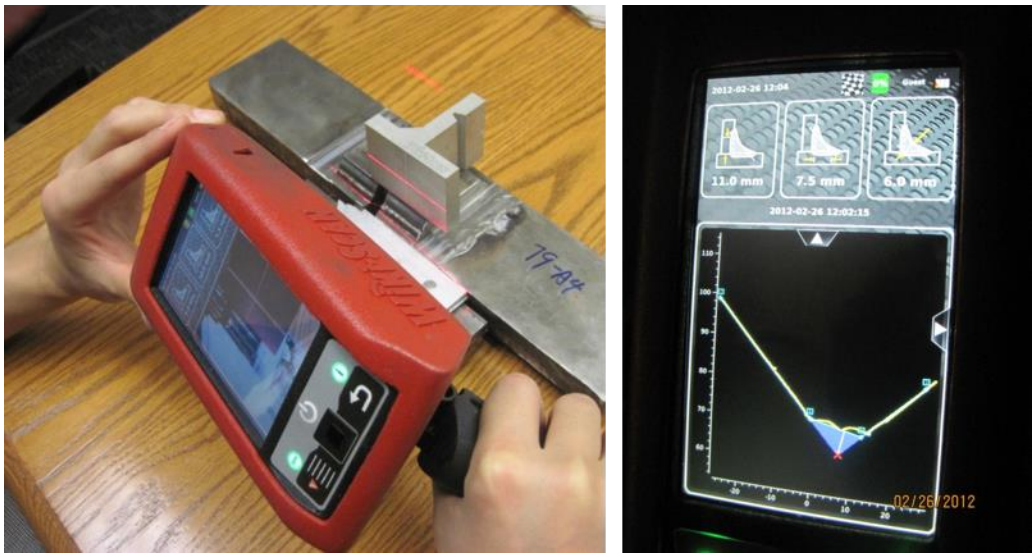

Figure 2.16: Laser scan device for weld profile and weld size determination

All specimens were tested using MTS 200-kip machine. Load and crosshead displacement curves were documented for identifying peak load at failure, i.e., P_u. Representative load-displacement curves for the two types of shear specimens are shown in Figure 2.17, in which peak load P_u at failure for each specimen is also indicated. In addition, fracture surfaces after strength test were carefully examined, such as failure angles and any anomalies involved. As shown in Figure 2.18, failure angles are indeed consistent with the traction stress based shear strength

analysis results discussed in the previous sections, i.e., at 45° in longitudinal shear specimens (Figure 2.9) and at 22.5° in transverse shear specimens (Figure 2.13).

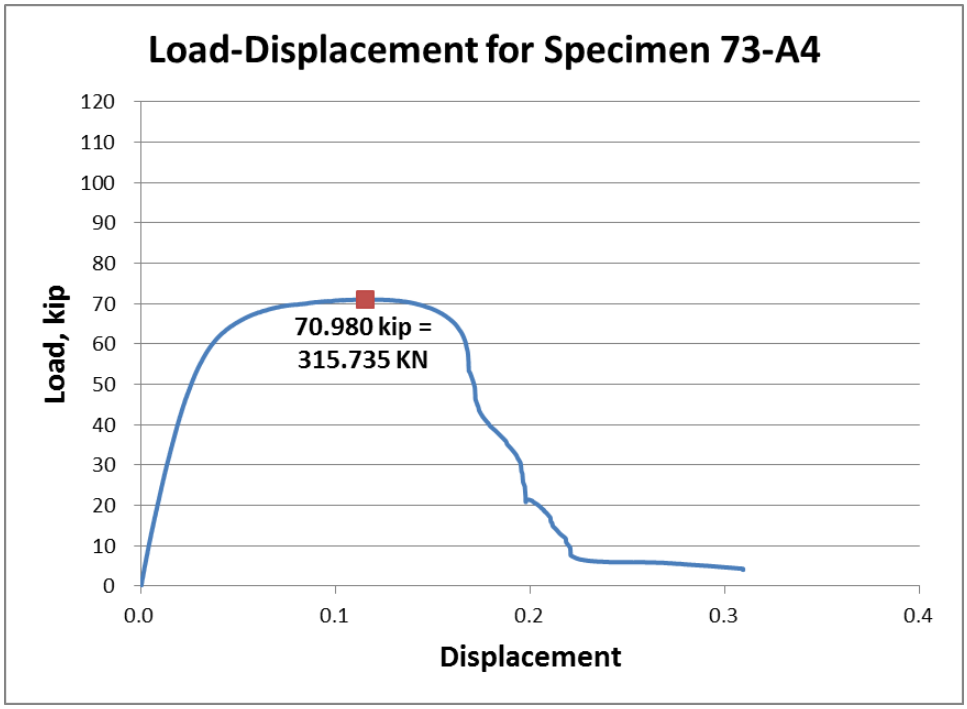

(a)

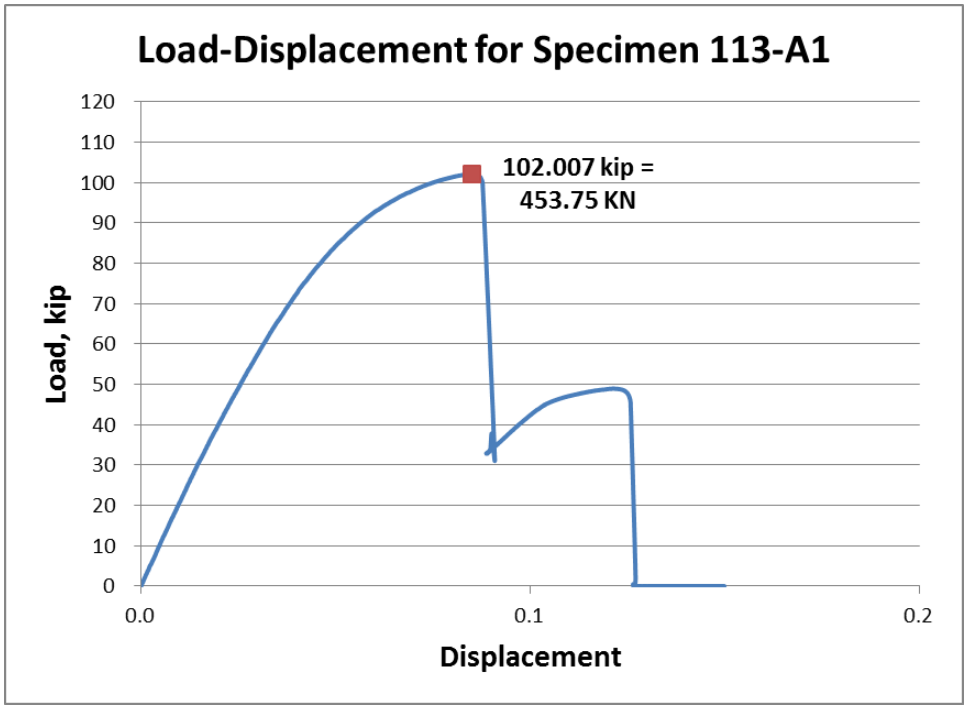

(b)

Figure 2.17: Typical load-displacement curves: (a) longitudinal shear (b) transverse shear

(a)

(b)

Figure 2.18: Shear failure angles: (a) longitudinal shear, about 45°; (b) transverse shear, about 22.5°

2.4 Analysis of Test Results

In the following sections, shear strength test data are first analyzed using the conventional method such as the one given in Eq. (2.1) by AWS B4.0 (2007). Then, the traction stress based

shear strength characterization method (Eq. (2.7) & Eq. (2.13)) are used to correlate the test data collected from both longitudinal and transverse shear specimens conducted in this study.

2.4.1 Using Conventional Method

Consistent with the general trend observed by Nie and Dong (2012), Figure 2.19 clearly shows that shear strengths from longitudinal shear specimens are significantly lower than those from transverse shear specimens in each of the three test groups when Eq. (2.1) is used. Figure 2.19a shows the results from specimens made of DH36 steel welded with FCAW process, 71T1-C weld wire, and a nominal weld leg size of 3/16" (5 mm); while Figure 2.19b shows the results from specimens made of HSLA80 steel welded with FCAW process, 101T-C weld wire, and a nominal weld leg size of 1/4" (6 mm); Figure 2.19c summarizes test results from specimens made of HSLA80 steel welded with GMAW process, MIL-100S weld wire, and a nominal weld leg size of 3/8" (10 mm). In all cases shown in Figure 2.19, the averaged discrepancy in shear strengths between longitudinal and transverse shear specimens is as large as about 44 ksi (303 MPa) for DH36 (FCAW) specimens with a nominal weld leg size of 3/16" (5 mm), about 44 ksi (303 MPa) for HSLA80 (FCAW) with a nominal weld leg size of 1/4" (6 mm), and 33 ksi (228 MPa) for HSLA80 (GMAW) with a nominal weld leg size of 3/8" (10 mm), respectively. A similar trend is consistently observed for other test groups in Table 2.1 and will be demonstrated in Appendix A.

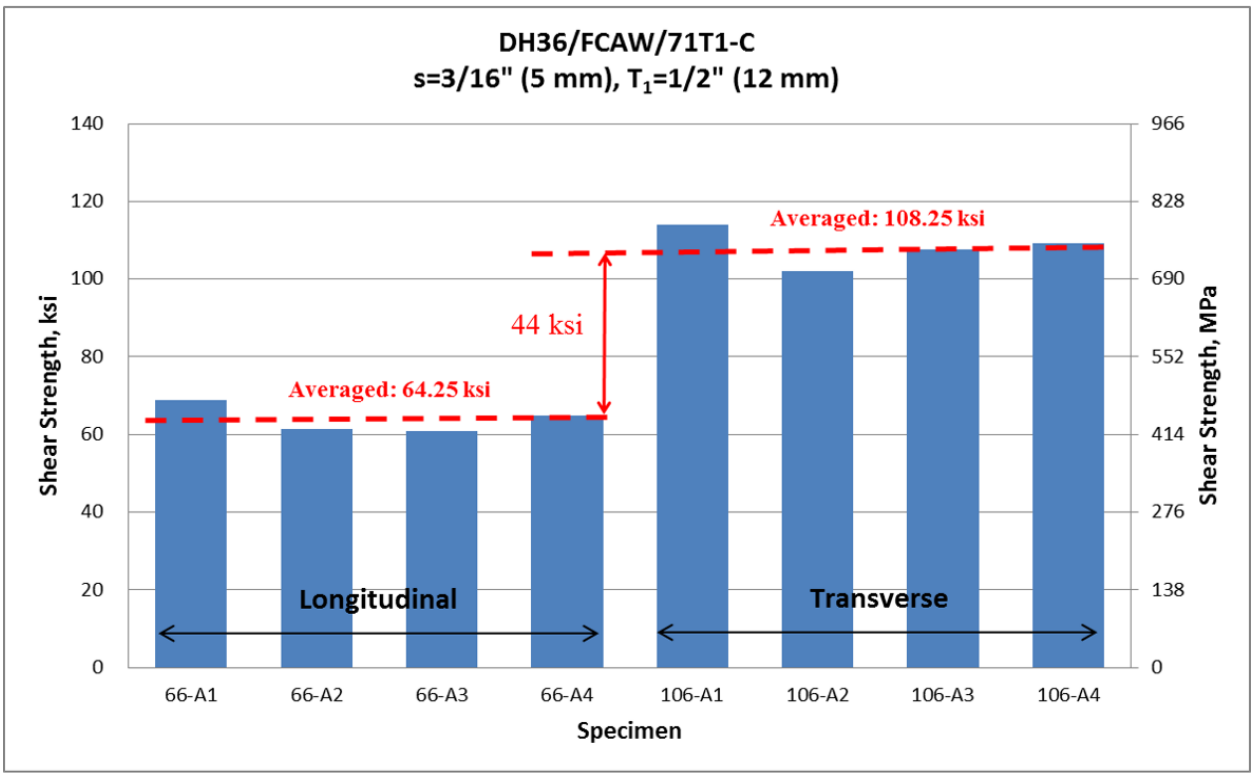
DH36/FCAW/71T1-C
s=3/16" (5 mm), T1=1/2" (12 mm)
Shear Strength, ksi
Shear Strength, MPa
140
120
100
80
60
40
20
0
966
828
690
552
414
276
138
0
Averaged: 108.25 ksi
44 ksi
Averaged: 64.25 ksi
Longitudinal
Transverse
66-A1
66-A2
66-A3
66-A4
106-A1
106-A2
106-A3
106-A4
Specimen

(a)

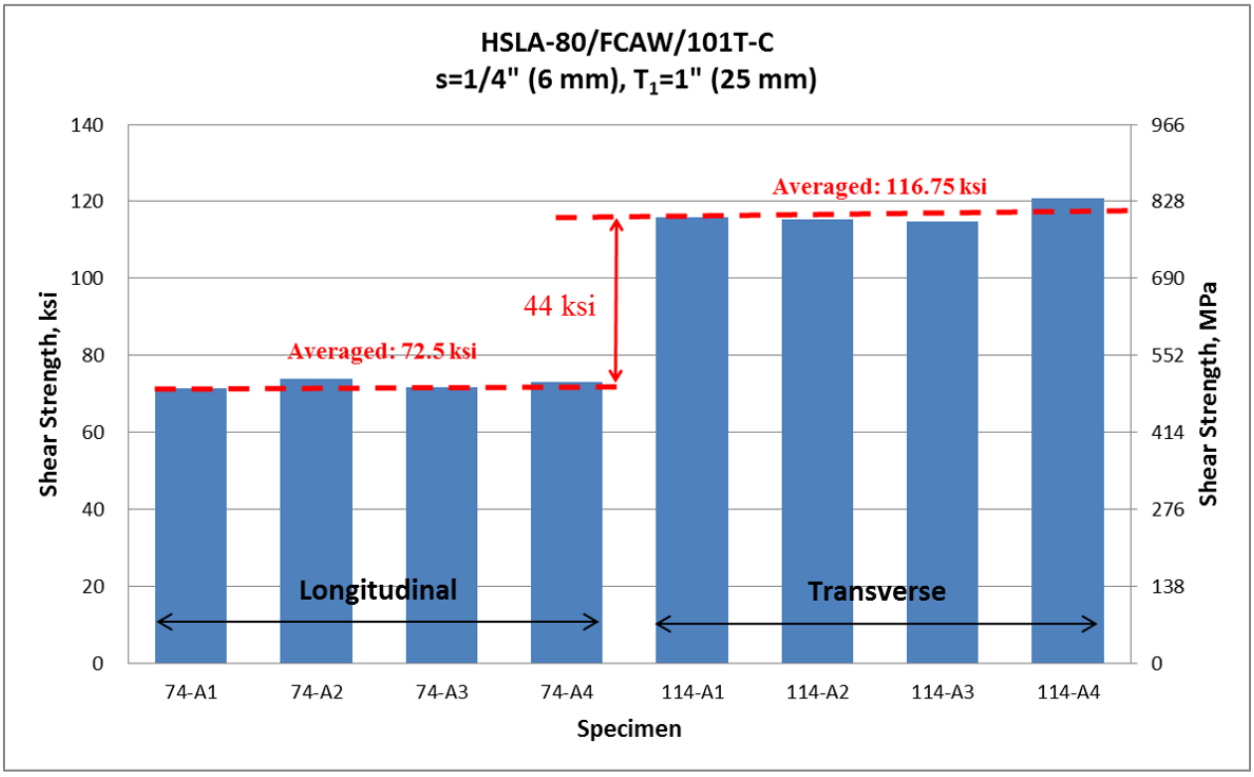
HSLA-80/FCAW/101T-C
s=1/4" (6 mm), T1=1" (25 mm)
Shear Strength, ksi
Shear Strength, MPa
140
120
100
80
60
40
20
0
966
828
690
552
414
276
138
0
Averaged: 116.75 ksi
44 ksi
Averaged: 72.5 ksi
Longitudinal
Transverse
74-A1
74-A2
74-A3
74-A4
114-A1
114-A2
114-A3
114-A4
Specimen

(b)

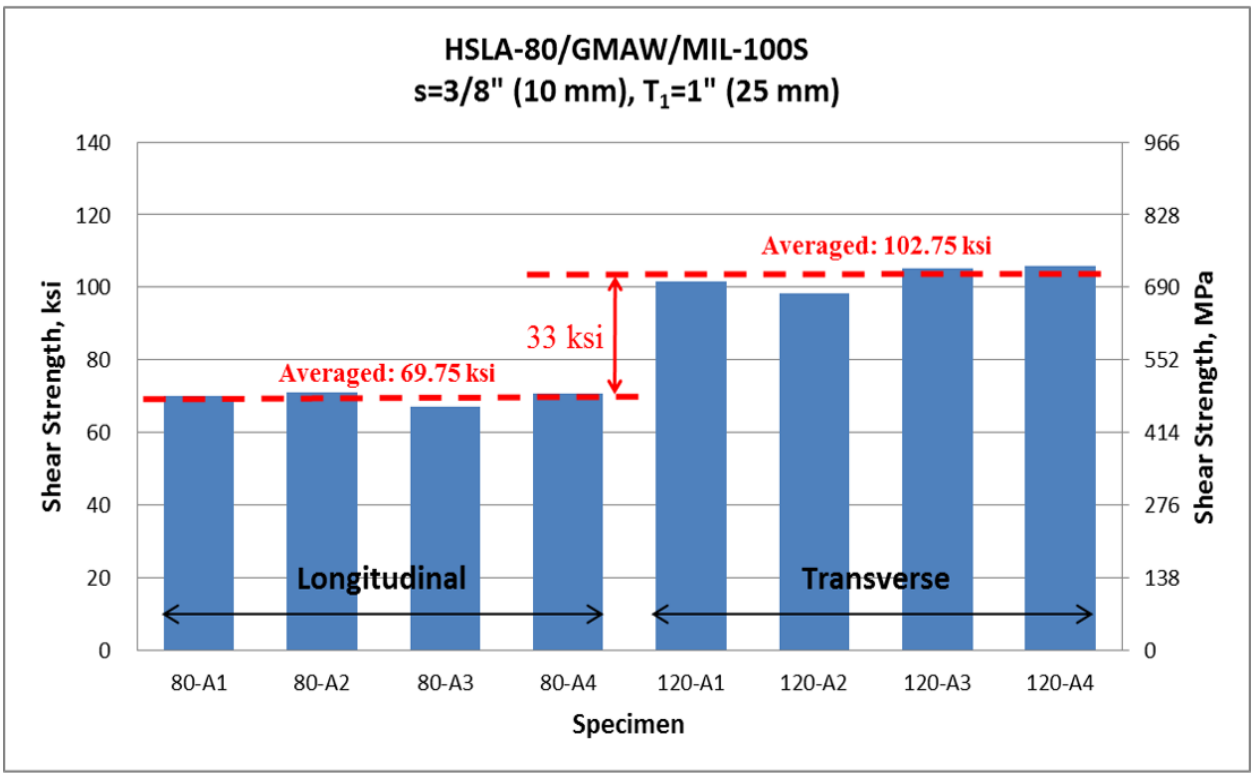

(c)

Figure 2.19: Comparison of shear strengths between longitudinal and transverse shear specimens using Eq. (2.1): (a) DH36 with FCAW; (b) HSLA80 with FCAW; (c) HSLA80 with GMAW

2.4.2 Using Traction Stress Method

As discussed in the previous sections, traction stress method can be used to analyze the same shear strength test data shown in Figure 2.19 by applying correction coefficients against Eq. (2.1) for longitudinal shear specimens according to Eq. (2.7), in which *SCF* as a function of s/T_1 is given Figure 2.11, and for transverse shear specimens according to Eq. (2.13). The results are shown in Figure 2.20. In contrast to the significant discrepancies in shear strengths between longitudinal and transverse shear specimens observed in Figure 2.19, Figure 2.20 shows a significantly improved correlation in shear strengths between longitudinal and transverse shear specimens. With the traction stress method, the averaged discrepancy is reduced from 44 ksi (303 MPa) to 7 ksi (48 MPa) for DH36 (FCAW) (see Figure 2.20a), from 44 ksi (303 MPa) to 13 ksi (90 MPa) for HSLA80 (FCAW) (see Figure 2.20b), and from 33 ksi (228 MPa) to 9 ksi (62 MPa)

for HSLA80 (GMAW) (see Figure 2.20c). A similar trend is also observed for the rest of test groups listed in Table 2.1 and will be presented in Appendix B.

It is important to note that shear strength of fillet-welded specimens should not be dependent upon shear loading conditions or specimen types. In this regard, the general agreement between shear strengths tested using longitudinal and transverse shear specimens clearly shows the effectiveness of the traction stress method in extracting a unified shear strength regardless of loading conditions or specimen types. Note that there still exist some noticeable differences between the two testing type specimens in Figure 2.20, in which longitudinal shear specimens tend to give a lower averaged shear strength than that from transverse shear specimens. This may be attributed to the non-uniformity in shear stress distribution along weld line in longitudinal shear specimens, which can introduce localized damage initially at weld end leading to final shear failure. This is an area of further study in the near future.

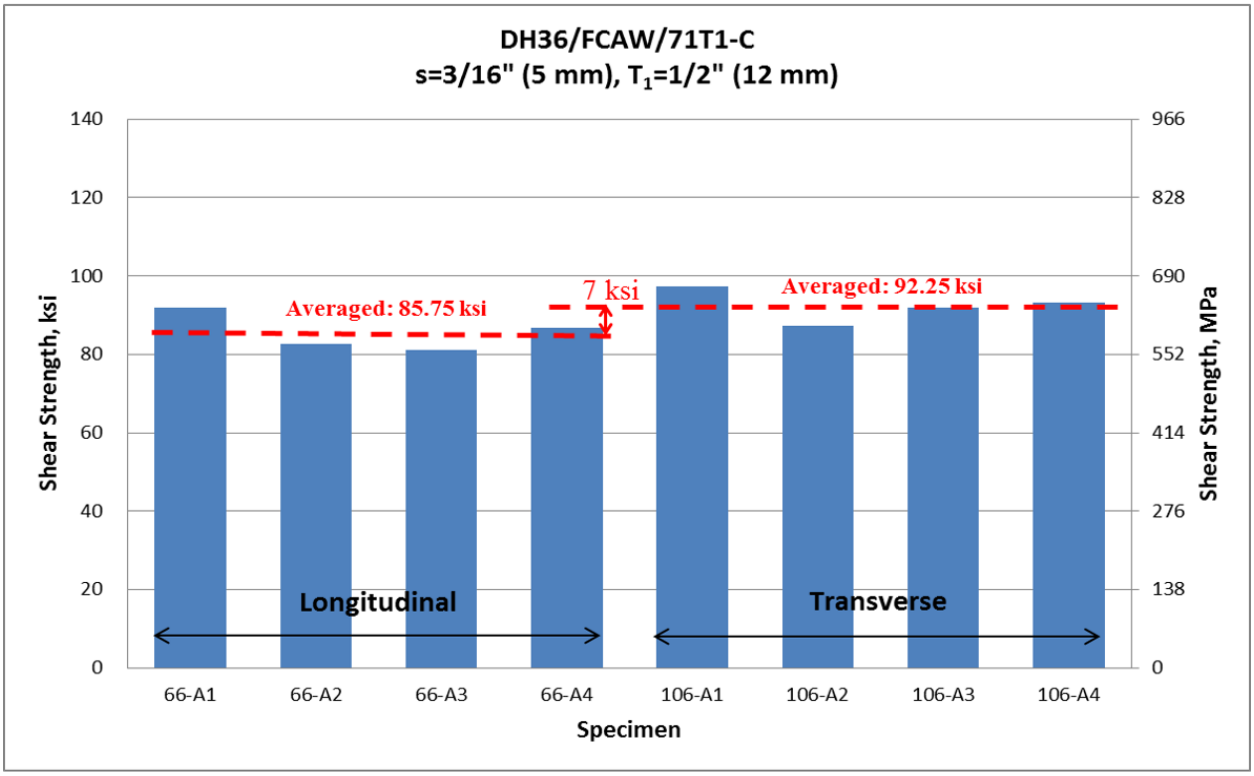

(a)

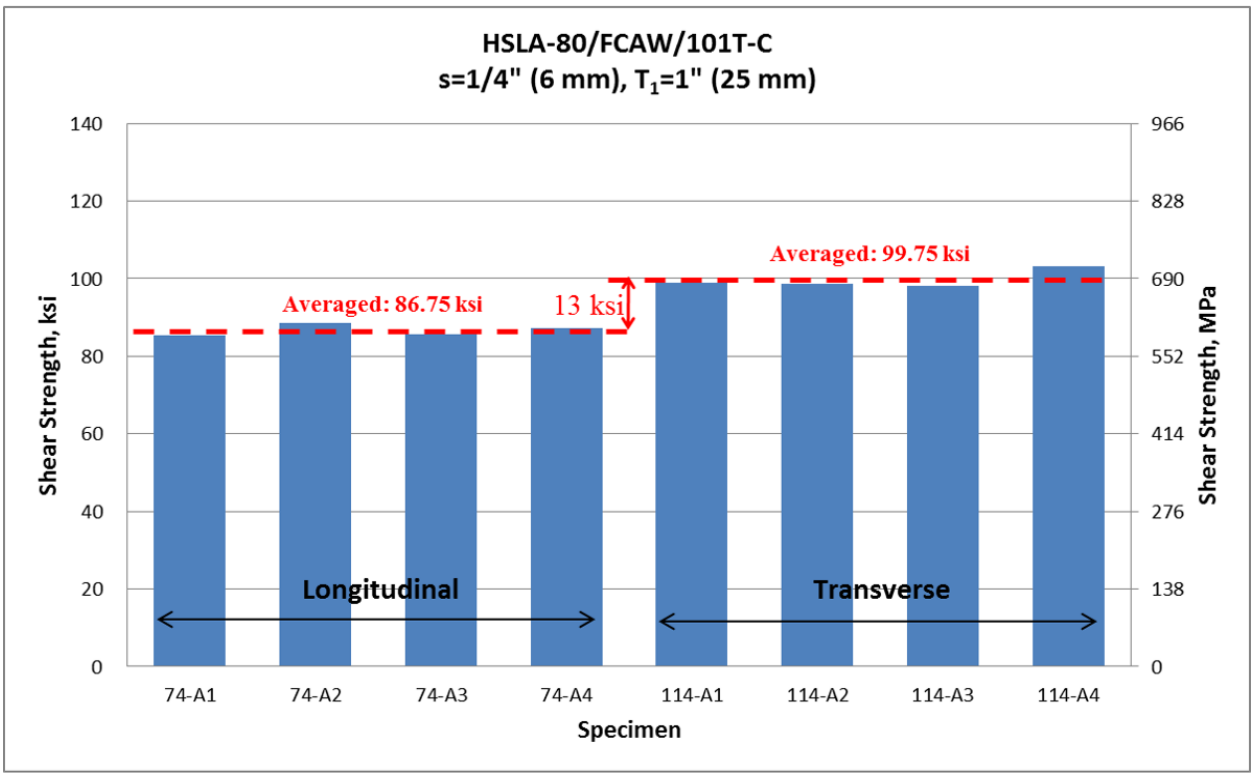

(b)

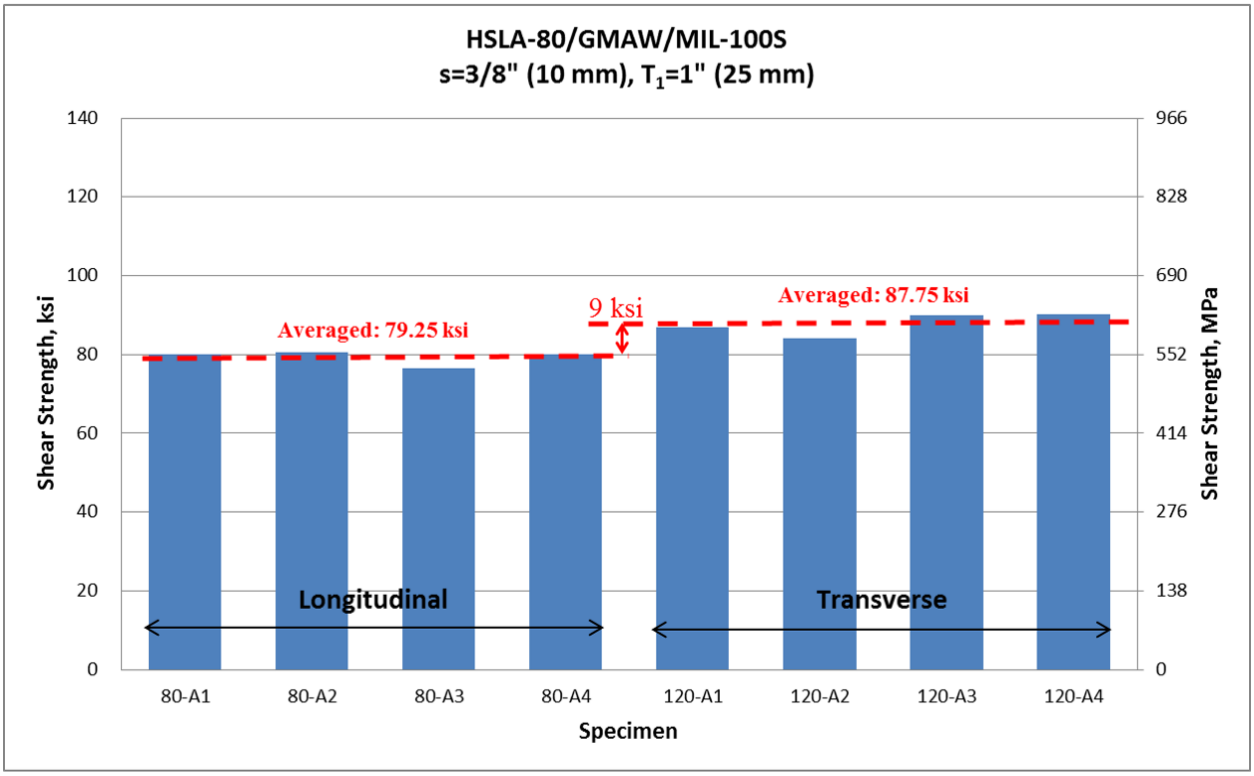

(c)

Figure 2.20: Comparison of shear strengths between longitudinal and transverse shear specimens using traction stress method: (a) DH36 with FCAW; (b) HSLA80 with FCAW; (c) HSLA80 with GMAW

2.5 Conclusions

After carrying out a comprehensive static strength test program on standard longitudinal and transverse shear specimens relevant to shipboard structure applications, a traction stress based shear strength definition has been proven effective for correlating shear strength test data. The following major conclusions can be drawn:

1. Weld strengths of standard longitudinal and transverse shear specimens, such as those stipulated in AWS B4.0, can be reliably determined by calculating the critical membrane shear stress at failure on critical weld throat plane. The critical weld throat failure plane for longitudinal shear specimens is at 45° ($\pi/4$) from base plate while for transverse shear specimens at 22.5° ($\pi/8$), as determined by the traction stress method presented and validated by the large amount of tests performed in this study.
2. Conventional shear stress formula (Eq. (2.1)), shown as a form of stress resultant definition in this chapter, has two major limitations: (1) incorrectly predicting the failure plane at 45° in transverse shear specimens; (2) incapable of capturing shear stress concentration (Figure 2.9) near weld end in longitudinal shear specimens. These limitations have been shown to have contributed to the presence of two types of shear strengths (one from transverse shear specimen testing and the other from longitudinal shear specimen testing), of which one allowable shear strength value must be chosen for fillet weld sizing purpose.
3. With the traction stress based shear strength definition, both the maximum shear stress plane (i.e., failure plane) and shear stress concentration at weld end can be correctly captured, resulting in a unified shear strength definition regardless of shear loading conditions or specimen types. A correction scheme has been proposed with respect to

the conventional shear stress formula (Eq. (2.1)) for analyzing test data collected from standard longitudinal and transverse shear specimens, such as those given in AWS B4.0 as shown in Figure 2.1. Furthermore, since both longitudinal and transverse shear specimens yield approximately the same shear strength value with the proposed traction stress method, the use of transverse shear specimens is highly recommended for determining in-situ fillet weld shear strength. Therefore, the analytical equation given in Eq. (2.10) can be conveniently used in practice for achieving a quantitative fillet weld sizing in design for lightweight ship structures.

Acknowledgments

The publication is made possible by the financial support by the National Research Foundation of Korea (NRF) Gant funded by the Korea government (MEST) through GCRC-SOP at University of Michigan under Project 2-1: Reliability and Strength Assessment of Core Parts and Material System. The authors are grateful to the encouragement and oversight by Project PI Professor M. H. Kim during the preparation of this report.

Chapter 3 An Analytical Shear Strength Model for Load-Carrying Fillet-Welded Connections Incorporating Nonlinear Effects

Abstract

In this chapter, an analytical formulation of weld throat stress model is presented for defining limit state condition of fillet-welded connections incorporating plate-to-plate contact conditions. The validity of the resulting analytical solution is verified by finite element computation incorporating nonlinear material and nonlinear geometry effects. In addition, its effectiveness in correlating shear strengths obtained from transverse and longitudinal shear specimens has been demonstrated through the re-analysis of over 100 shear tests performed by the same authors as an early part of the same study. As a result, a unified fillet weld shear strength can be demonstrated regardless of test specimen configurations and shear loading conditions, while conventional shear strength equation is incapable of reconciling the differences in shear strengths between those obtained from transverse and longitudinal shear specimens. Furthermore, the present developments provide a basis for achieving a quantitative fillet weld sizing criterion for design and construction of fillet-welded structures under complex loading conditions, for which a unified shear strength and robust weld throat stress calculation procedure are prerequisites.

Keywords: fillet welds, shear strength, weld sizing, traction stress method, finite element method, contact force, limit state, stress concentration, weld throat stress

3.1 Introduction

Existing fillet weld sizing criteria for design and construction of fillet-welded structures have been empirical, e.g. the MIL-STD-1628 (Department of Defense, 1974), AISC 360 (AISC 2010), Eurocode 3 (CEN 2005), and others (AWS 2015 & CSA 2014). Due to their inherent conservatisms built in, these weld sizing criteria often lead to oversized welds, which tend to cause significant distortions in modern lightweight structures (Huang et al., 2004 & 2007). The empirical nature of these weld sizing criteria can be attributed to the fact that weld throat stress determination is difficult due to stress/strain singularity at weld root. As a result, a nominal weld throat shear stress definition, often referred to as an "engineering shear stress" in DNV-RP-C203 (DNV, 2012), is widely adopted for calculating weld shear strengths from standard fillet weld specimen tests (see Figure 3.1), e.g. by AWS B4.0 (AWS, 2007), as shown in Eq. (3.1) below:

$$\tau_{u,w} = \frac{P_u}{a_{45} \times L} \tag{3.1}$$

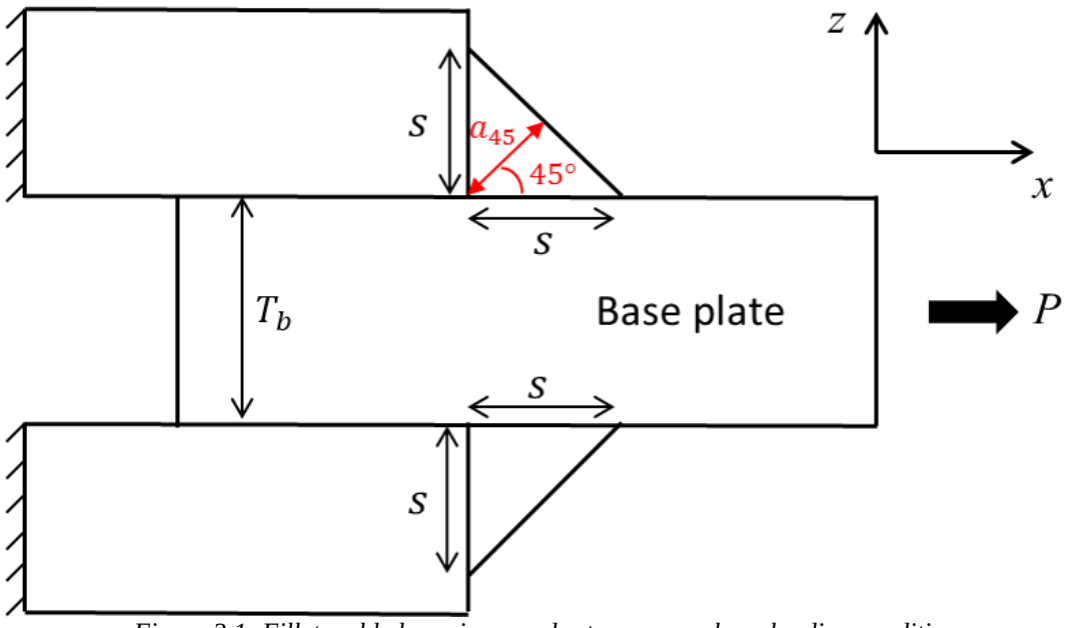

Figure 3.1: Fillet-welded specimen under transverse shear loading condition

As shown analytically by Nie and Dong (2012), even under simple transverse shear conditions shown in Figure 3.1, the critical weld throat plane on which shear stress attains its maximum is in fact not at 45° (or $\pi/4$) as assumed in Eq. (3.1), but at 22.5° (or $\pi/8$) instead. The analytical solution was also further confirmed by their mesh-insensitive traction structural stress results (Nie & Dong, 2012), which were formulated based on a working-equivalent argument in terms of nodal forces available from finite element (FE) analysis results. The mesh-insensitive method can be used for more general loading conditions and complex connection geometries, e.g. standard longitudinal shear specimens stipulated by AWS B4.0 (AWS, 2007), in which shear stress tends to exhibit stress concentration at weld ends in addition to stress singularity at weld root and weld toe locations. Furthermore, the predicted failure angle of 22.5° is, to a large extent, consistent with the experimental observations by numerous researchers decades ago, such as Butler and Kulak (1971), Kato and Morita (1974), Kennedy et al. (1985), and by the same authors of this study more recently (Lu et al., 2015) for structural steel, as illustrated in Figure 3.2. It is worth noting that a recent study (Yang et al., 2019) regarding to stainless steel fillet weld has also showed a much smaller failure angle than 45° in transverse shear specimens.

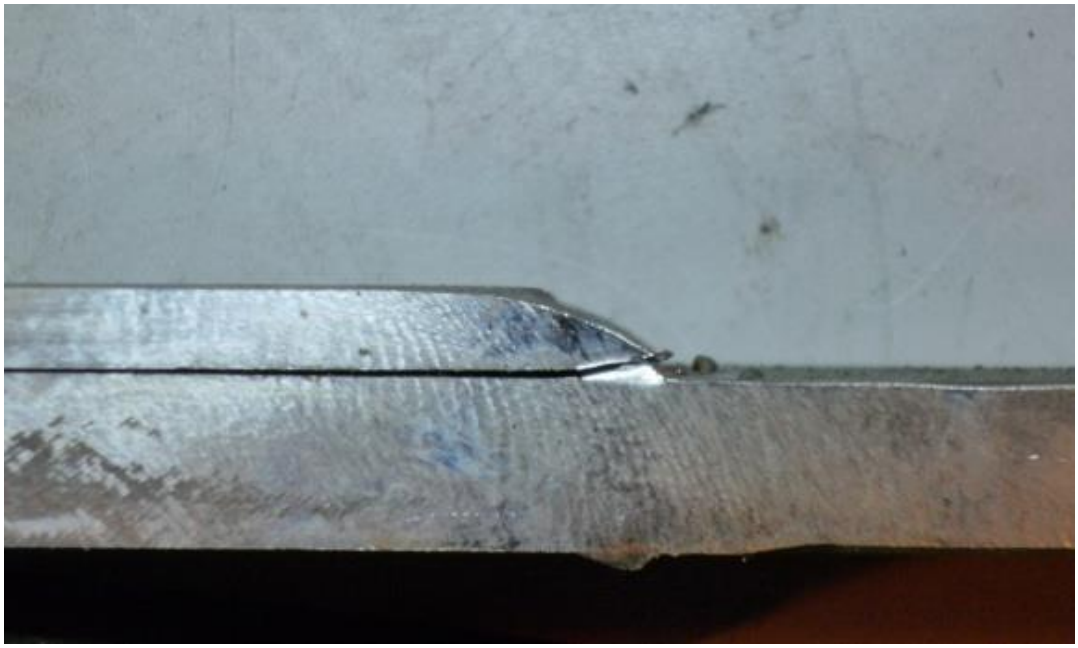

Figure 3.2: Typical weld throat failure plane observed on transverse shear specimens, noticeably smaller than 45° as assumed in Eq. (3.1)

By considering a large amount of test results from a comprehensive experimental testing program, Lu et al. (2015) have demonstrated that an improved correlation of fillet weld shear strengths between transverse and longitudinal shear specimens can be achieved when the traction stress method was used, as shown in Figure 3.3. In contrast, the conventional shear stress definition in Eq. (3.1) results in significant discrepancies in fillet weld shear strengths. In fact, the inability of Eq. (3.1) in correlating shear strength test data between transverse and longitudinal shear specimens has been long established, as discussed by numerous previous studies (Miazga & Kennedy, 1989; Kamtekar, 1982; Kato & Morita, 1974) for structural steel. Most recently, a 1.5 transverse-to-longitudinal weld shear strength ratio has been found by Yang et al. (2019) for stainless steel weldments when Eq. (3.1) was used. Two major factors can be attributed to the improved shear strength correlations when using the traction stress method: one is the use of the correct weld throat plane of 22.5° on which maximum shear stress is calculated for transverse shear specimens; the other is a consistent determination of the maximum shear stress at weld end in longitudinal shear specimens by means of the mesh-insensitive traction stress method.

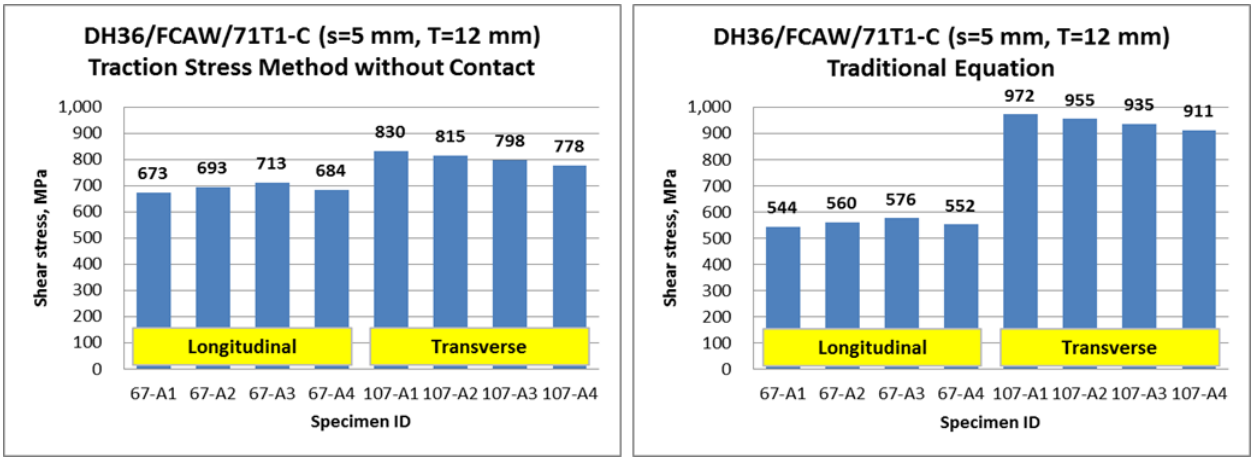

(a)

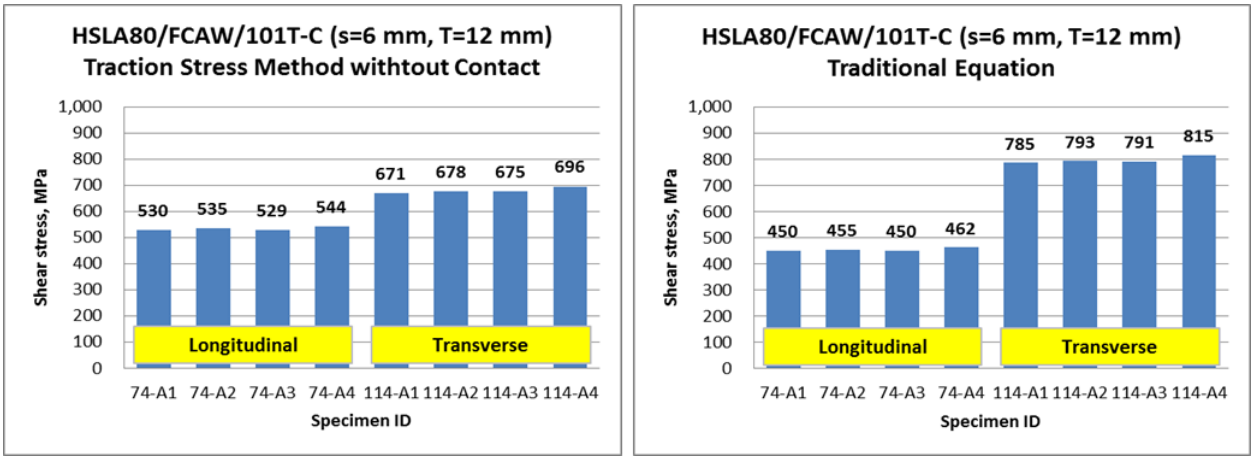

(b)

Figure 3.3: Shear strength correlations between transverse and longitudinal shear specimens: traditional method Eq. (3.1) versus traction stress method: (a) DH36, FCAW, and 71T1-C weld wire; (b) HSLA80, FCAW, and 101T-C weld wire

However, some of the test data (Lu et al., 2015) still exhibit some noticeable discrepancies in weld shear strengths between transverse and longitudinal shear specimens, as shown on the left-hand side of Figure 3.3, which warrants further investigation. Upon a further examination of measurement data of over 100 tests (Lu et al., 2015) conducted as a part of the same study, one possible reason may be attributed to the fact that actual weld throat failure planes measured in transverse shear specimens are consistently lower than 22.5° which was analytically determined by Nie and Dong (2012) under statically determinate conditions, as shown in Figure 3.4. The reduced weld throat failure angles seen from the tests (see Figure 3.4) could be attributed to the

presence of plate-to-plate contact in these transverse shear specimens, although some earlier studies such as those (Nie & Dong, 2012; Lu et al., 2015) have stated such contact effects should be negligible. However, a more recent study in load-carrying cruciform fillet-welded by Xing et al. (2016) showed that the presence of any resultant force in z axis (see Figure 3.1) would cause a reduction in critical weld throat plane angle in fatigue.

Another aspect that requires further investigation is if material nonlinearity has effects on the maximum shear stress development on the critical weld throat plane. In the aforementioned investigations, it was assumed that shear stress distribution should attain essentially a uniform state along critical weld throat plane, when a peak load capacity is reached. This assumption stems from the hypothesis that any local plastic deformation caused by stress concentration at weld root tend to reduce stress gradient to such an extent that an approximately uniform shear stress distribution along the critical weld throat plane can be assumed when failure load is reached, as demonstrated in an elastic-plastic structural stress analysis of a tubular joint by Dong and Hong (2004), and in weld low-cycle fatigue evaluations by a structural strain method by Pei et al. (2019 & 2020).

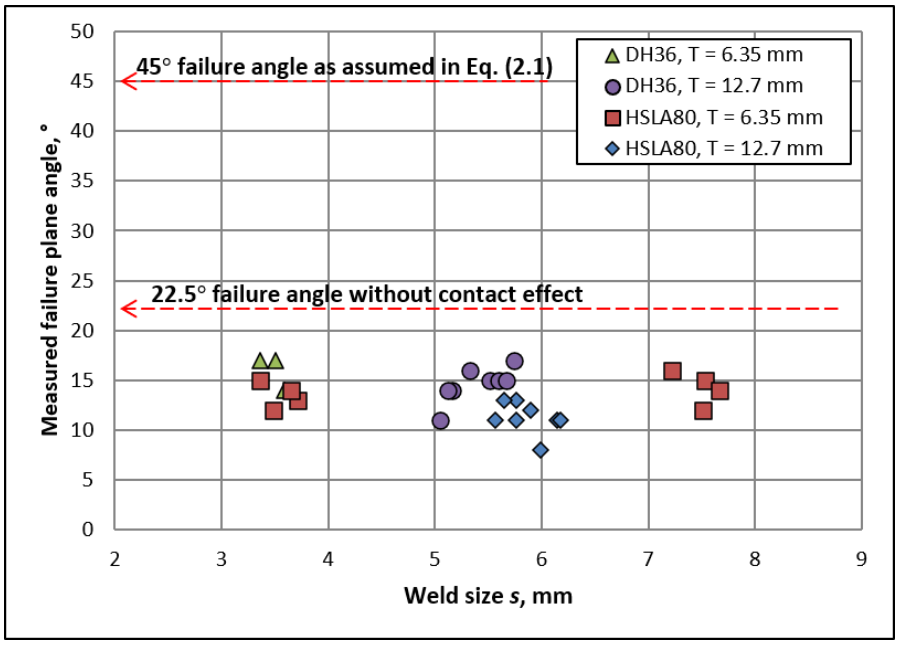

Figure 3.4: Failure angles measured in transverse shear specimens after fracture

With above considerations in mind, this chapter starts with an analytical fillet weld throat stress model construct by incorporating a contact-induced resultant force. As a result, it is found that the presence of such a resultant force significantly reduces the critical weld throat plane angle. Then, a limit state based approach is introduced for determining critical contact ratio expressed as a ratio of resultant contact force over remotely applied force. With this critical contact ratio, critical weld throat plane angle can be determined, along which the maximum shear stress can be related to peak load measured in shear specimen tests for determining shear strength of fillet welds. Nonlinear finite element analyses (FEA) incorporating both plate-to-plate contact and material nonlinearity are also presented for validating the findings from the analytical fillet weld throat stress model. Finally, shear strength test data obtained from a large number of transverse and longitudinal fillet-welded specimens as a part of the same study (Lu et al., 2015) are re-evaluated by using the refined weld throat stress model incorporating contact effects. The results show that a significantly improved correlation in shear strengths can now be achieved between transverse and longitudinal shear specimens, implying that unified shear strength exists regardless of test specimen configurations or shear loading conditions.

3.2 Analytical Weld Throat Stress Model

3.2.1 Shear Failure Criterion

As previously discussed by Nie and Dong (2012), Lu et al. (2015) and Xing et al. (2016), a hypothetical cut along any weld throat plane of a fillet weld, say at an angle of θ from base plate, exposes three traction stress components with respect to the local coordinate system (x'-y'-z') as illustrated in Figure 3.5. These traction stresses are referred to as normal stress $\sigma(x')$, transverse shear stress $\tau_T(x')$, and longitudinal shear stress $\tau_L(x')$, respectively.

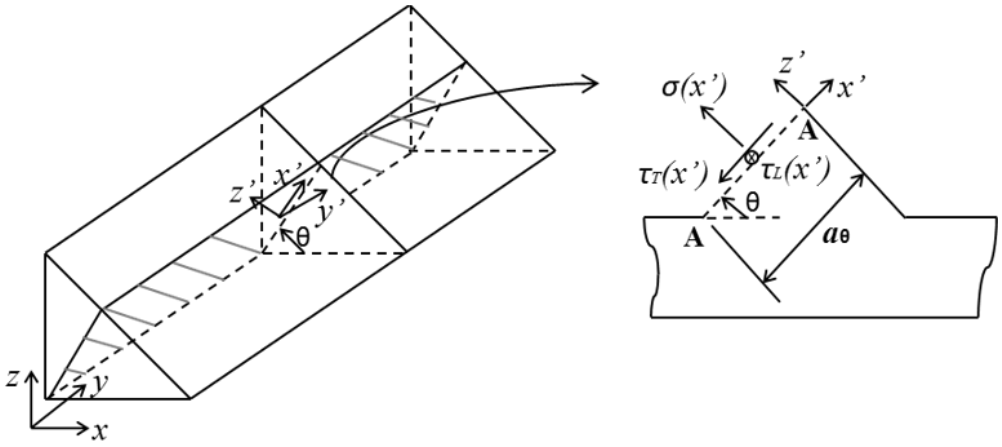

Figure 3.5: Traction stress components acting on a weld throat plane at an angle of θ: (a) Fillet weld between base and attachment plate; (b) Traction stress definition on weld throat plane at angle θ

By following the nodal force based traction stress method (Dong et al, 2010a), the three weld throat traction stresses can be presented in a statically equivalent linear forms, each of which consists its membrane and bending parts with respect to the mid-distance of the weld throat cut cross-section A-A along a_θ, as shown in Figure 3.6. The linear forms of the three traction stress components are expressed by Eq. (3.2):

$$\sigma = \sigma_m + \sigma_b$$

$$\tau_L = \tau_{Lm} + \tau_{Lb} \tag{3.2}$$

$$\tau_T = \tau_{Tm}$$

Detailed derivations on how to calculate the membrane and bending parts of the weld throat traction stresses in a mesh-insensitive manner can be found in Chapter 2, Nie and Dong (2012), as well as Lu et al. (2015), which will not be repeated here. The use of the three traction stress components for multiaxial fatigue evaluation can be found by Dong and Hong (2006), Wei and Dong (2010), as well as Dong et al. (2010b) under proportional loading conditions, and by Mei and Dong (2017a & 2017b) for arbitrary non-proportional loading conditions.

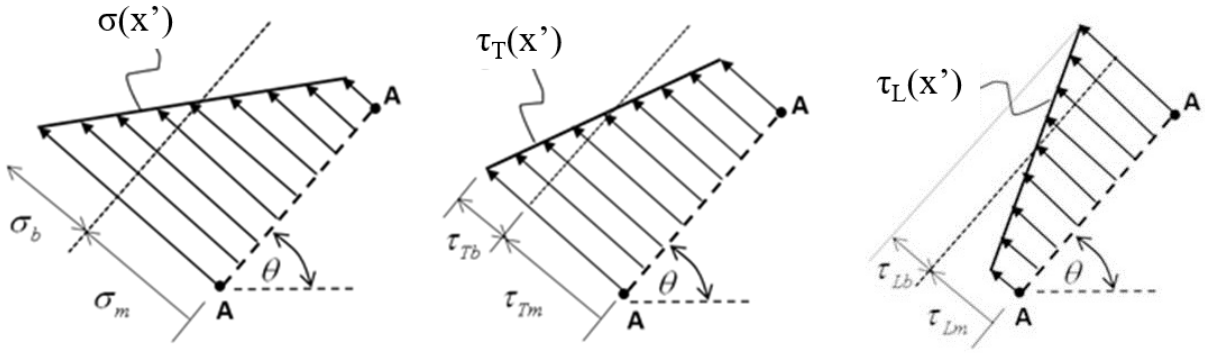

Figure 3.6: Linear representation and decomposition of weld throat traction stress components

For static shear strength analysis of load-carrying fillet welds, only membrane shear traction stresses need to be considered (Nie & Dong, 2012; Lu et al., 2015). Then, as previously discussed by Lu et al. (2015), the maximum resultant membrane shear traction stress can be used as a shear failure criterion for fillet welds under combined transverse and longitudinal shear loading conditions (see Figure 3.7), i.e.,

$$\tau_{e,max} = \text{Max}\left\{\sqrt{\tau_{Lm}(\theta)^2 + \tau_{Tm}(\theta)^2}\right\} \leq \tau_{u,w} \tag{3.3}$$

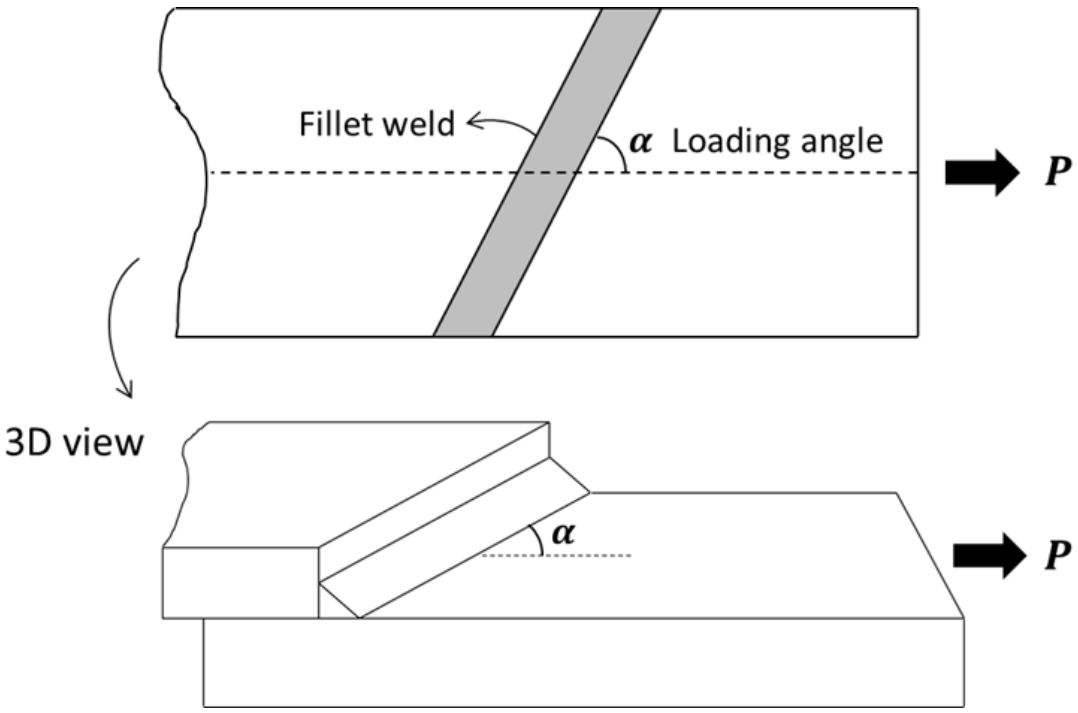

Figure 3.7: Illustration of combined loading on a load-carrying fillet weld

Both components in Eq. (3.3) can be computed by means of the mesh-insensitive traction stress method for a given structural component using a system of simultaneous equations given in Chapter 2 (also in Nie & Dong, 2012; Lu et al., 2015). When dealing with simple lab test specimens such as those discussed in the preceding section for which applied transverse and longitudinal forces (P_T and P_L) are directly available from shear specimen testing, $\tau_{Tm}(\theta)$ and $\tau_{Lm}(\theta)$ can be analytically expressed as:

$$\tau_{Tm}(\theta) = \frac{P_T \times \cos\theta \times (\cos\theta + \sin\theta)}{s \times L}$$
$$\tau_{Lm}(\theta) = \frac{P_L \times (\cos\theta + \sin\theta)}{s \times L} \tag{3.4}$$

Then, $\tau_{e,max}$ under combined loading conditions can be written as:

$$\tau_{e,max} = \frac{P}{s \times L} \times (\cos\theta_{max} + \sin\theta_{max}) \times \sqrt{(\sin\alpha \times \cos\theta_{max})^2 + (\cos\alpha)^2} \tag{3.5}$$

where $\alpha = \tan^{-1}(P_T/P_L)$ as shown in Figure 3.7. Then the critical weld throat plane angle θ_{max} on which $\tau_{e,max}$ attains its maximum can be calculated by setting the first derivative of Eq. (3.5) with respect to θ to 0, i.e.,

$$\begin{aligned}&(\cos\theta_{max} - \sin\theta_{max}) \times \sqrt{(\sin\alpha \times \cos\theta_{max})^2 + (\cos\alpha)^2} \\ &= (\cos\theta_{max} + \sin\theta_{max}) \times \frac{\sin\alpha^2 \times \cos\theta_{max} \times \sin\theta_{max}}{\sqrt{(\sin\alpha \times \cos\theta_{max})^2 + (\cos\alpha)^2}}\end{aligned} \tag{3.6}$$

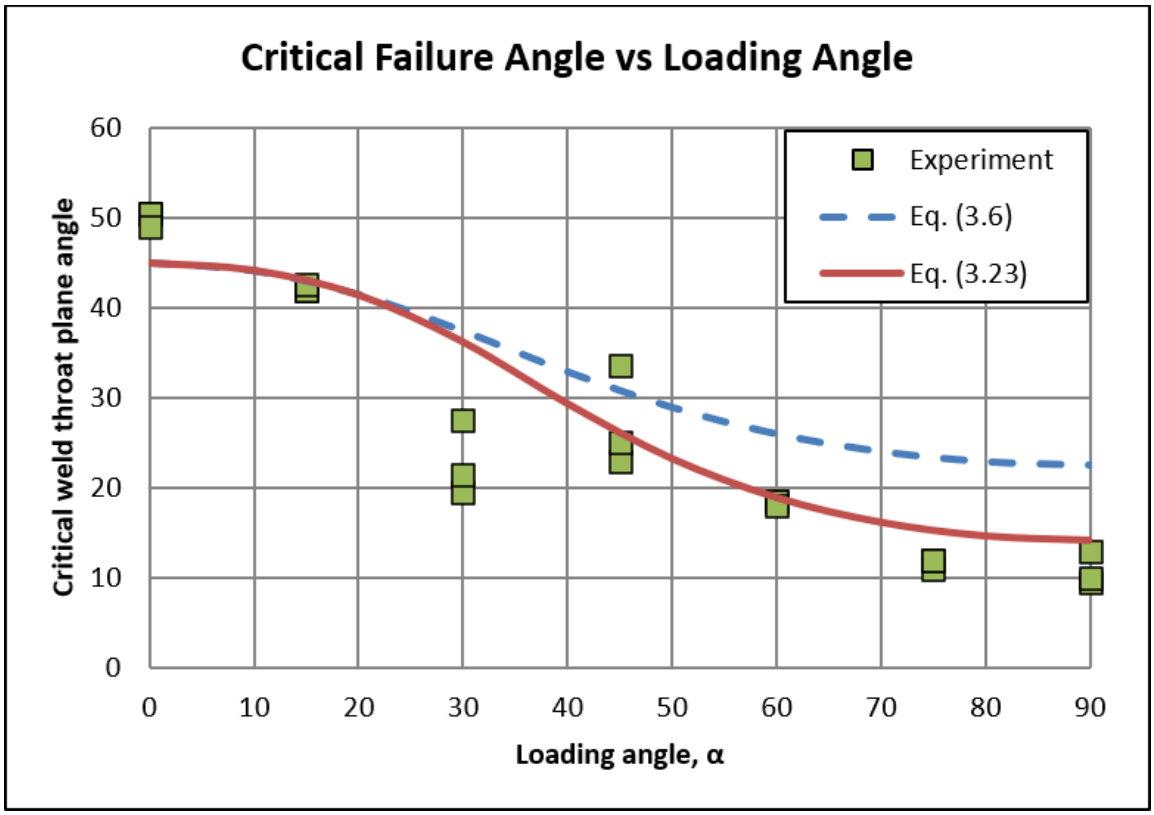

Figure 3.8: Critical weld throat failure plane angle θ_{max} as a function of loading angle α: analytical versus experimental results

As shown in Eq. (3.6), critical weld throat plane angle θ_{max} is now a function of loading angle α. For example, under pure longitudinal shear condition (i.e., $\alpha = 0$), $\tau_{e,max}$ occurs at $\theta_{max} = \pi/4$; and under pure transverse shear condition (i.e., $\alpha = \pi/2$), $\tau_{e,max}$ occurs at $\theta_{max} = \pi/8$ without considering any contact effects. As α varies from 0 to $\pi/2$, the curve of θ_{max} analytically satisfying Eq. (3.6) is shown in Figure 3.8 as a dash line, which seems to provide a reasonable upper bound estimate of failure angles observed in experiments (Miazga, & Kennedy, 1989) (shown as symbols). A further improvement in formulating Eq. (3.6) will be discussed in the next section.

3.2.2 Treatment of Plate-to-Plate Contact

Based on findings from past investigations (Kato & Morita, 1974; IIW, 1980; Picón & Cañas, 2009), including those using the traction stress method (Nie & Dong, 2012; Lu et al., 2015),

any potential plate-to-plate contact is more likely to occur in transverse shear specimens than in longitudinal shear specimens. This can be attributed to the fact that shear deformation mechanism involved in transverse shear specimens is different from that in longitudinal shear specimens. In the former, any plastic slip along weld throat plane would result in a movement which has a directional component potentially leading to plate-to-plate contact, while in the latter there exists no such a component. This indeed has been confirmed by finite element analysis performed as a part of this study. Therefore, only transverse shear conditions are considered hereafter.

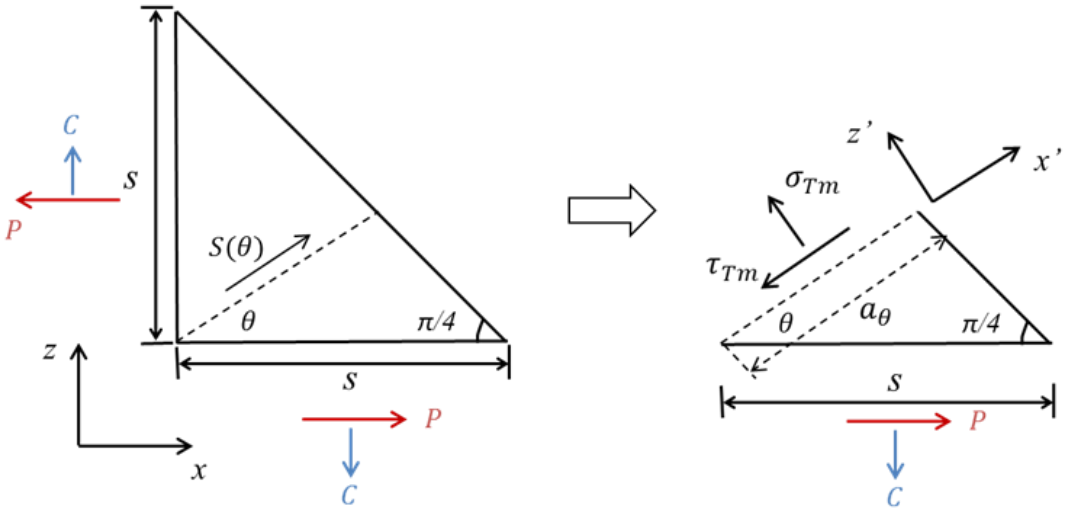

Figure 3.9: Analytical weld throat model incorporating resultant contact force C

Consider a loading system shown Figure 3.9, in which P and C represent remotely applied load and resultant contact force generated from plate-to-plate contact in transverse shear specimens, respectively. Then a closed-form solution of $\tau_{Tm}(\theta)$ acting on a weld throat plane at any angle θ can be expressed be Eq. (3.7):

$$\tau_{Tm}(\theta) = \frac{P \times \cos\theta - C \times \sin\theta}{a_\theta \times L} = \frac{(P \times \cos\theta - C \times \sin\theta) \times (\cos\theta + \sin\theta)}{s \times L} \quad (3.7)$$

where the first derivative with respect to θ gives the maximum shear plane angle θ_{max} as

$$\theta_{max} = \frac{1}{2} \times \tan^{-1}\left(\frac{1-K}{1+K}\right), \qquad K = \frac{C}{P} \quad (3.8)$$

Eq. (3.8) indicates that θ_{max} is a function of contact ratio K, which is not known at this stage. It should be noted that if setting $C = 0$ as a special case, Eq. (3.7) becomes:

$$\tau_{Tm}(\theta) = \frac{P \times \cos\theta}{a_\theta \times L} = \left(\frac{\sqrt{2}(\sin 2\theta + \cos 2\theta + 1)}{4}\right) \times \left(\frac{P}{a_{45} \times L}\right) \tag{3.9}$$

leading to $\theta_{max} = \pi/8$ or 22.5°, as expected when plate-to-plate contact force C is not considered (Nie & Dong, 2012; Lu et al., 2015).

The relationship between θ_{max} and K is plotted in Figure 3.10. It can be seen that θ_{max} decreases monotonically to 0 as K reaches unity. This suggests that any presence of plate-to-plate contact in a transverse shear specimen reduces θ_{max} to a value less than 22.5°. For instance, at a contact ratio K of 0.4, the maximum shear stress plane occurs at about 12°, resulting in about 12% reduction in maximum shear stress, as shown in Figure 3.10. Note that the ordinate on the right in Figure 3.10 represents the ratio of the maximum weld throat shear stresses between with and without considering contact ratio K described by Eq. (3.7) and Eq. (3.9), respectively.

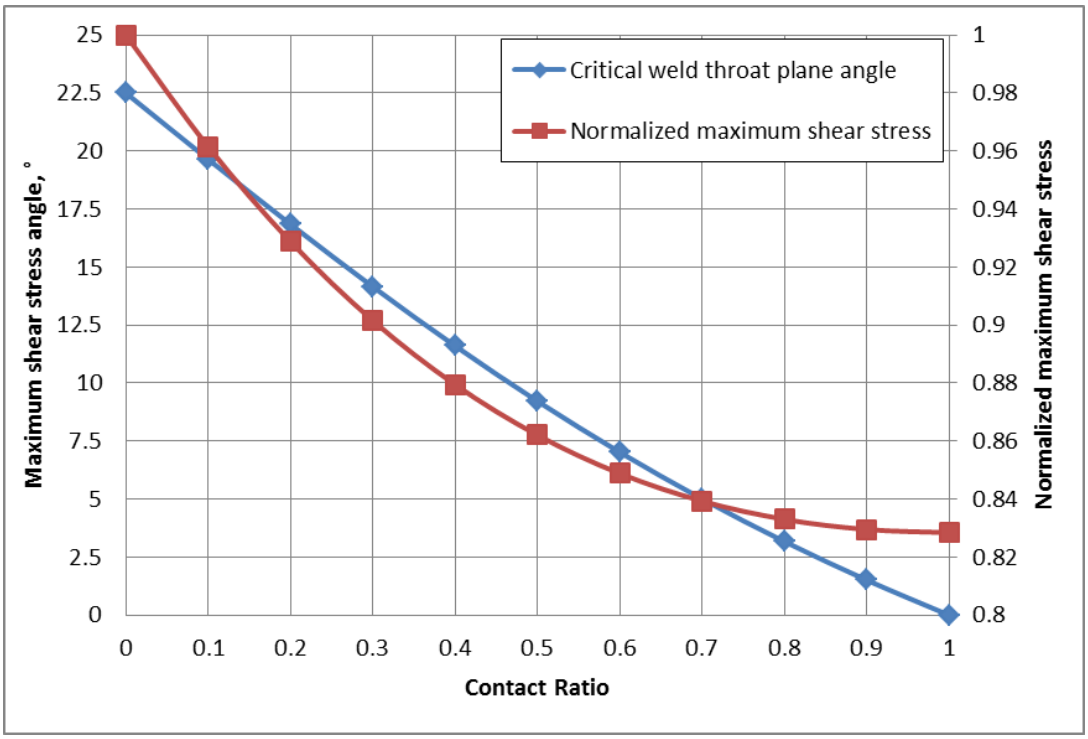

Figure 3.10: Effect of contact ratio on critical weld throat plane angle and maximum shear stress reduction

Furthermore, Figure 3.10 implies that a limit load definition corresponding to large plastic deformation effects, i.e., local necking along a fillet weld throat plane, could only occur when θ_{max} reaches to 0 (i.e., contact ratio K monotonically increases from 0 to 1), which contradicts the experimental findings as shown in Figure 3.4. Indeed, finite element analysis incorporating nonlinear geometry and nonlinear material property effects performed in this study is only able to produce a well-defined limit load through weld necking mechanism when $\theta_{max} = 0$, not relevant for interpreting the experimental data involved in this study. This also means that maximum shear stress reaches its strength limit long before weld necking develops at $\theta_{max} = 0$ due to the presence of the contact force C. As a result, an analytical approach for defining limit state for incorporating the resultant contact force C will be examined next.

3.2.3 Limit State Definition

As is well known, a simple smooth bar specimen subjected to a remote tension load P develops maximum normal stress (or UTS) as P reaches to its maximum, i.e., $\Delta P = 0$, at which point cross-section necking begins. Within the context of shear dominated deformation process, it can be postulated that a load-carrying fillet-welded specimen subjected to transverse shear loading conditions develops maximum shear stress (i.e., at shear strength) along critical weld throat plane (θ_{max}) when resultant shear force reaches to maximum, i.e., $\Delta S = 0$ on the same plane, at which point a shear force limit state is realized.

Considering a simple case with $C = 0$ in Figure 3.9, shear force $S(\theta)$ on any weld throat plane at angle θ can be simply expressed as

$$S(\theta) = P \times \cos\theta \tag{3.10}$$

The corresponding critical weld throat plane angle is shown to be a constant value 22.5° or $\pi/8$, as derived in Section 3.2.2, leading to shear force increment ΔS expressed as

$$\Delta S\left(\frac{\pi}{8}\right) = \Delta P \times \cos\frac{\pi}{8} \tag{3.11}$$

Therefore, the corresponding limit state in terms of shear force S, defined as $\Delta S = 0$ also occurs at 22.5° weld throat plane on which $\Delta P = 0$ is also satisfied.

For the case of fillet weld with contact force ($C \neq 0$ in Figure 3.9), shear force S and shear force increment ΔS on any weld throat plane at angle θ can be expressed as:

$$S(\theta) = P \times \cos\theta - C \times \sin\theta \tag{3.12}$$

$$\Delta S(\theta) = \Delta P \times \cos\theta - \Delta C \times \sin\theta - P \times \sin\theta \times \Delta\theta - C \times \cos\theta \times \Delta\theta \tag{3.13}$$

Because the limit state in shear force is defined as $\Delta S = 0$ on the maximum shear stress plane, Eq. (3.13) can be re-written as:

$$\begin{aligned}\Delta S(\theta) = {} & \Delta P \times \cos\left(\frac{1}{2} \times \tan^{-1}\left(\frac{1-K}{1+K}\right)\right) - \Delta C \times \sin\left(\frac{1}{2} \times \tan^{-1}\left(\frac{1-K}{1+K}\right)\right) \\ & -P \times \sin\left(\frac{1}{2} \times \tan^{-1}\left(\frac{1-K}{1+K}\right)\right) \times \left(\frac{-(P \times \Delta C - C \times \Delta P)}{(2K^2+2) \times P^2}\right) \\ & -C \times \cos\left(\frac{1}{2} \times \tan^{-1}\left(\frac{1-K}{1+K}\right)\right) \times \left(\frac{-(P * \Delta C - C * \Delta P)}{(2K^2+2) \times P^2}\right)\end{aligned} \tag{3.14}$$

by substituting θ with the maximum shear stress angle θ_{max} (Eq. (3.8)) and $\Delta\theta$ with $\Delta\theta_{max}$ which can be expressed as, according to Eq. (3.8):

$$\Delta\theta_{max} = \frac{-\Delta K}{2K^2+2} \tag{3.15}$$

$$\Delta K = \frac{P \times \Delta C - C \times \Delta P}{P^2} \tag{3.16}$$

In seeking the limit state conditions corresponding to both $\Delta S = 0$ and $\Delta P = 0$, Eq. (3.14) becomes:

$$\Delta C \times \left\{ -\sin\left(\frac{1}{2} \times \tan^{-1}\left(\frac{1-K}{1+K}\right)\right) + \sin\left(\frac{1}{2} \times \tan^{-1}\left(\frac{1-K}{1+K}\right)\right) \times \left(\frac{1}{2K^2+2}\right) + \cos\left(\frac{1}{2} \times \tan^{-1}\left(\frac{1-K}{1+K}\right)\right) \times \left(\frac{K}{2K^2+2}\right) \right\} = 0 \tag{3.17}$$

Note that $\Delta C = 0$ is a trivial solution to Eq. (3.17). The non-trivial solution to Eq. (3.17) can be obtained by setting the term within "{}" being 0, i.e.,

$$-\sin\left(\frac{1}{2} \times \tan^{-1}\left(\frac{1-K}{1+K}\right)\right) + \sin\left(\frac{1}{2} \times \tan^{-1}\left(\frac{1-K}{1+K}\right)\right) \times \left(\frac{1}{2K^2+2}\right) + \cos\left(\frac{1}{2} \times \tan^{-1}\left(\frac{1-K}{1+K}\right)\right) \times \left(\frac{K}{2K^2+2}\right) = 0 \tag{3.18}$$

It can be shown that $K \approx 0.3$ is the solution to Eq. (3.18), which leads to a weld throat failure plane angle $\theta_{max} = 14°$, according to Eq. (3.8). It is important to note that a critical weld throat plane angle of 14° estimated here is in a reasonable agreement with the measurements of weld throat failure angle from test specimens, as shown in Figure 3.4. As presented in a later section, shear strengths calculated using such a K value lead to an improved agreement between transverse and longitudinal shear specimens.

3.3 Nonlinear Finite Element Analysis

Nonlinear finite element analyses reported here were performed for two purposes: (1) to verify the early assumption made in Eq. (3.3) that as plastic deformation becomes increasingly dominant, $\tau_m + \tau_b$ on the critical weld throat plane (i.e., $\theta = \theta_{max}$) approaches to τ_m, i.e., $\tau_b \rightarrow 0$, as assumed in some recent studies (Nie & Dong, 2012; Lu et al., 2015; Pei et al., 2019); (2) to verify the analytical limit state formulation presented in the previous section, particularly the validity of the maximum shear stress plane angle as a function of K, as shown in Figure 3.10.

3.3.1 FE Model Details

A representative FE model for transverse shear specimen depicted in Figure 3.1 is shown in Figure 3.11a by taking advantage of the quarter symmetry conditions in the transverse shear specimens with displacement control at one end. Refined elements (with element size in order of 0.008 t) were used for representing the fillet weld and its surrounding area, as shown in the zoomed view. Second order plane strain elements with reduced integration, i.e., CPE8R, have been used since the weld is relatively long compared to its leg size that out-of-plane normal and shear strains are considered to be zero. The same model was used to examine nonlinear deformation behaviors with and without plate-to-plate contact including nonlinear geometry effects through ABAQUS "NLGEOM" (Dassault Systemes, 2018) for dealing with large displacements and large distortions. Newton's method and ABAQUS default automatic increment size control algorithm are used in this study for efficiently solving the nonlinear problems. In addition, nonlinear material behavior for both base plate and weld metal is assumed to follow elastic-perfect-plastic stress-strain curve (see Figure 3.11b), in which Young's modulus (224769 MPa) and yield strength (550 MPa) are based upon stress-strain curve obtained from weldment material's tensile tests. The use of elastic-perfect-plastic material model eliminates the difference between true stress-strain curve and engineering stress-strain curve, and most importantly it stems from the following principle considerations: (1) providing an upper bound estimation of any plate-to-plate contact effects as plastic deformation develops within fillet weld; (2) being consistent with the lower bound definition of the limit state conditions discussed in the previous section; (3) tested yield strength 550 MPa and ultimate tensile strength 610 MPa (Huang et al., 2014 & 2016) showed that strain hardening effects were not significant.

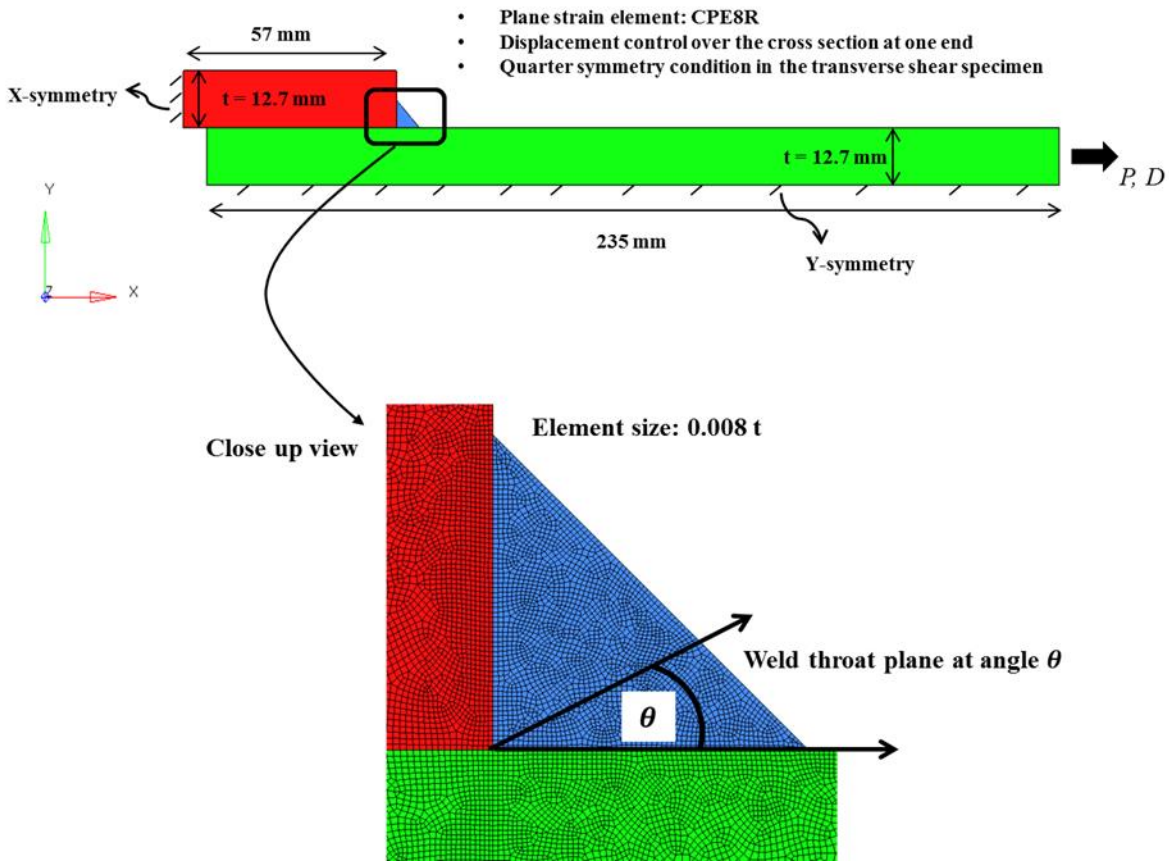

(a)

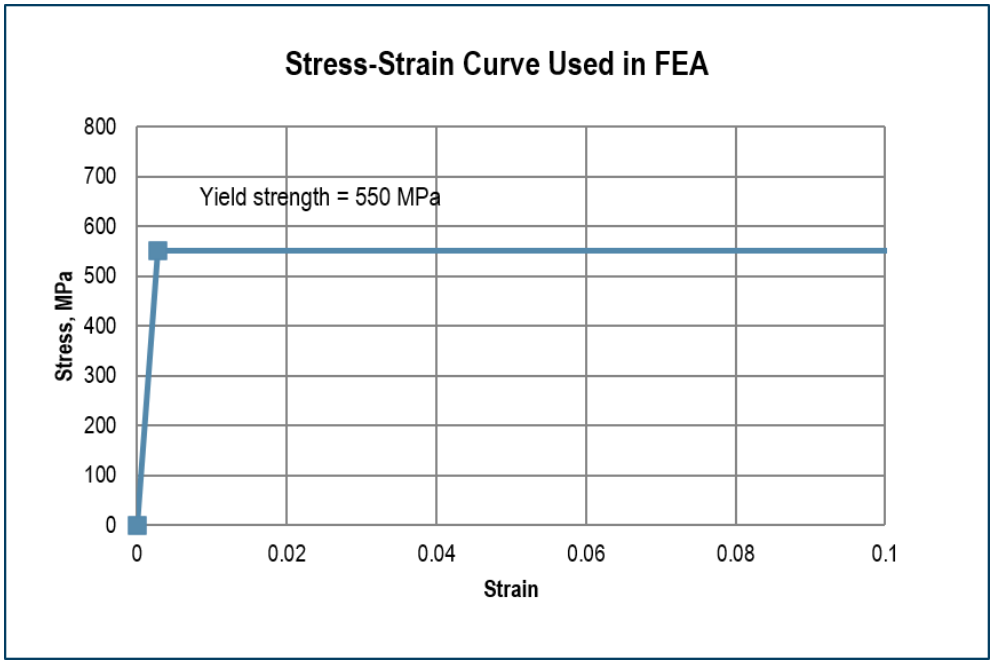

(b)

Figure 3.11: FE model and stress-strain relationship used for modeling transverse shear specimen: (a) A representative FE model of transverse shear specimen; (b) Stress-strain curve representing elastic-perfect-plastic material used in FEA calculations

As shown in Figure 3.11a, the use of fine mesh allows a detailed search of maximum shear stress plane for validating the analytical solutions discussed in Sec. 3.2. For convenience, τ_m and τ_b acting on any weld throat plane at an arbitrary angle θ are calculated using the following equations:

$$\tau_m(\theta) = \frac{1}{a_\theta}\int_0^{a_\theta} \tau(x') \times dx' \tag{3.19}$$

$$\tau_b(\theta) = \frac{6}{{a_\theta}^2}\int_0^{a_\theta} \tau(x') \times \left(\frac{a_\theta}{2} - x'\right) \times dx' \tag{3.20}$$

which are equivalent to nodal force based traction stress method for 2D problems as demonstrated by Dong et al. (2010a). In addition, the equations above are more convenient for the present case since τ_m and τ_b on a weld throat plane can be calculated without needing to place nodal positions along each plane to be searched.

Given weld throat plane shear stress $\tau_m(\theta)$ from Eq. (3.19), shear force S acting on the same weld throat can be obtained as:

$$S(\theta) = \tau_m(\theta) \times a_\theta \tag{3.21}$$

which can then be plotted against load point displacement for identifying limit load position according to the limit state definition derived in the previous section.

3.3.2 FE Results

3.3.2.1 Results without Considering Contact Effects

Without considering plate-to-plate contact (i.e., $C = 0$ in Figure 3.9), the computed shear force acting on the critical weld throat plane, i.e., $S(\theta_{max}) = \tau_m(\theta_{max}) \times a_{\theta_{max}}$ according to Eq. (3.19), is plotted against load point displacement D_{FEA} in Figure 3.12a, which shows that the shear force S reaches its maximum S_U at $D_{FEA} = D_U$. In a similar manner, shear traction stress

components τ_m and τ_b on the critical weld throat plane according to Eq. (3.19) and Eq. (3.20) are plotted in Figure 3.12b in terms of τ_b/τ_m ratio as a function of relative load point displacement D_{FEA}/D_U. As can be seen, during the initial stage of loading or elastic deformation stage, τ_b is significant due to the severe stress concentration at weld root. As remote load increases and plastic deformation develops, τ_b diminishes rapidly and becomes negligible as $D_{FEA}/D_U \approx 0.8$. Upon further loading, τ_m becomes the only dominant shear stress component, i.e., $\tau_m + \tau_b \rightarrow \tau_m$, agreed with the results from Pei and Dong (2019). Therefore, the validity of the analytical fillet weld throat stress model depicted in Figure 3.9 can now be quantitatively justified when both nonlinear material behavior and nonlinear geometry effects are taken into account. Furthermore, at $D_{FEA}/D_U = 1$, $\tau_m(\theta)$ predicted by the analytical model in Sec. 3.2 and by the nonlinear finite element model in Figure 3.11 are compared in Figure 3.12c, which demonstrates an excellent agreement, representing the first such validation to the authors' best knowledge.

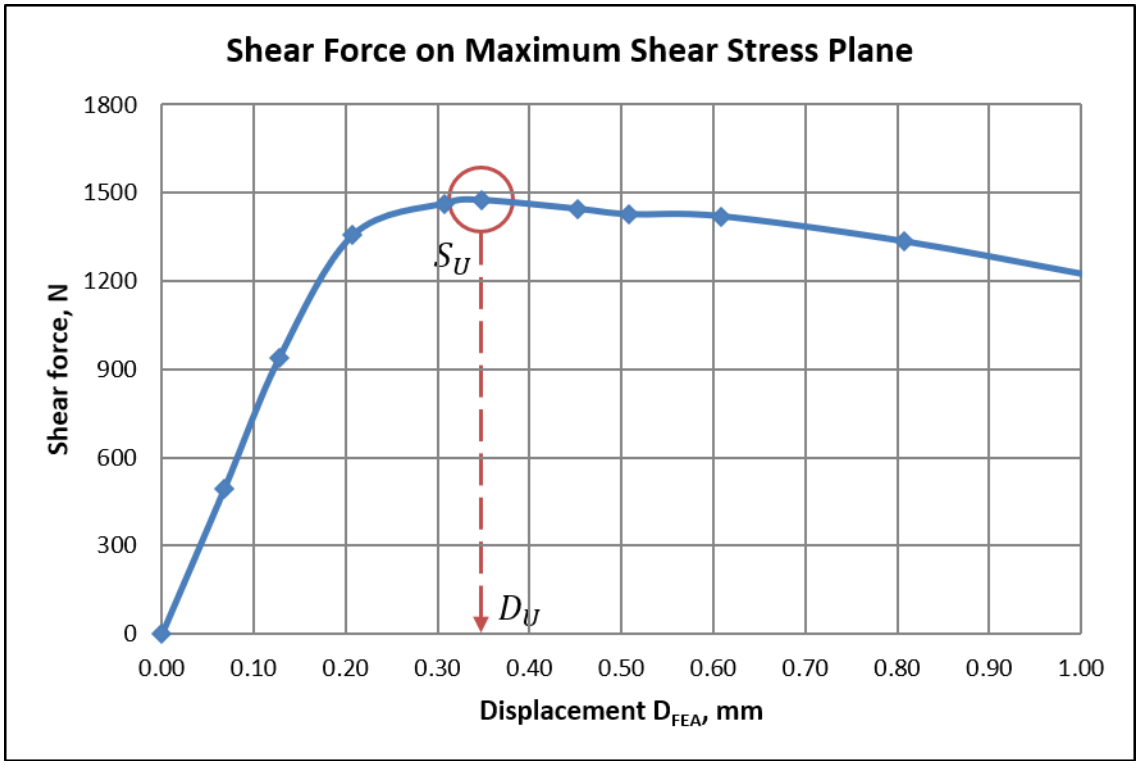

(a)

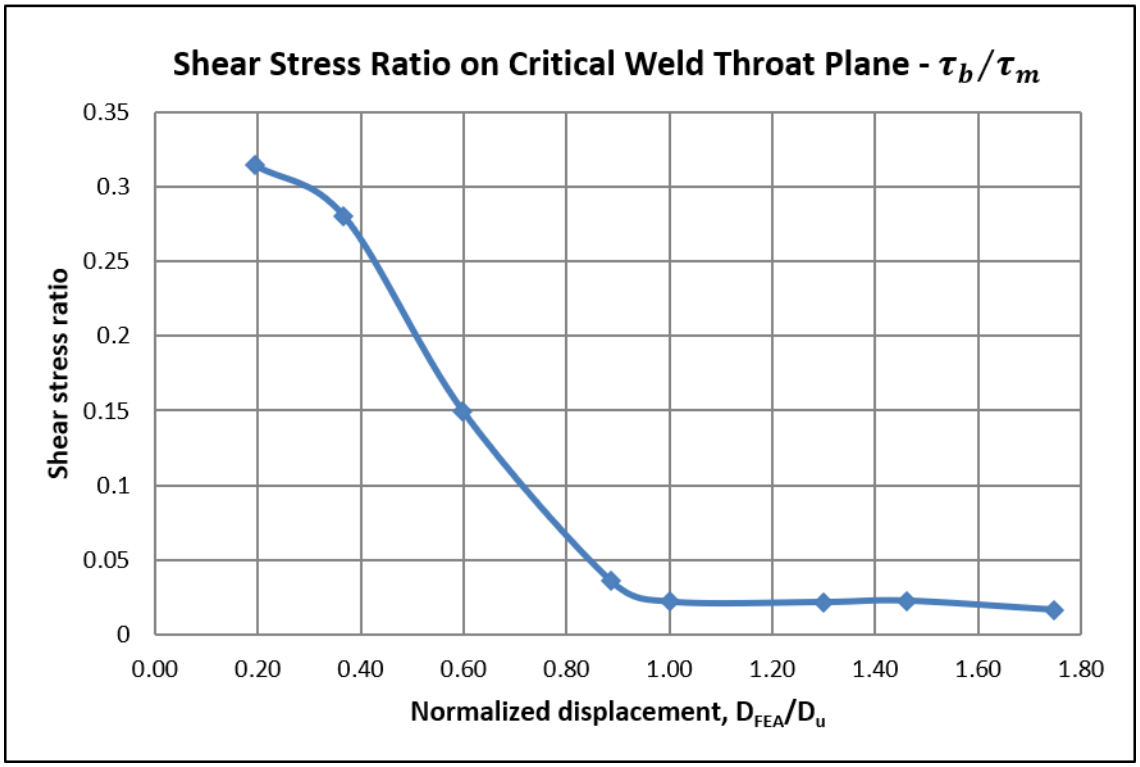

(b)

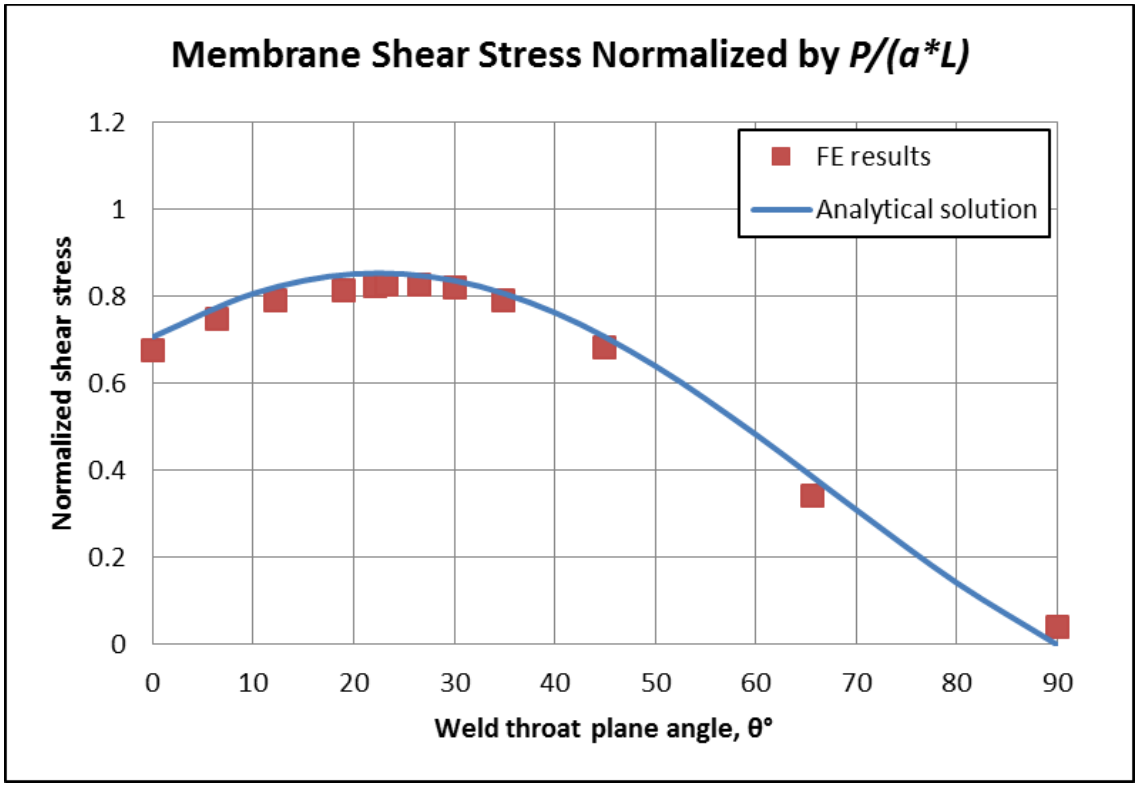

(c)

Figure 3.12: FE results without contact effects: (a) Shear force on critical weld throat plane; (b) Shear stress ratio τ_b/τ_m on critical weld throat plane; (c) Membrane shear stress τ_m at $D_{FEA}/D_U = 1$: analytical vs FE results

3.3.2.2 Results with Considering Contact Effects

When considering plate-to-plate contact, nodal forces at the contact interface between the lap and base plates in Figure 3.11a are collected and summed for calculating the resultant contact force C. The resulting contact ratio $K = C/P$ as a function of normalized load point displacement D_{FEA}/D_U is shown in Figure 3.13.

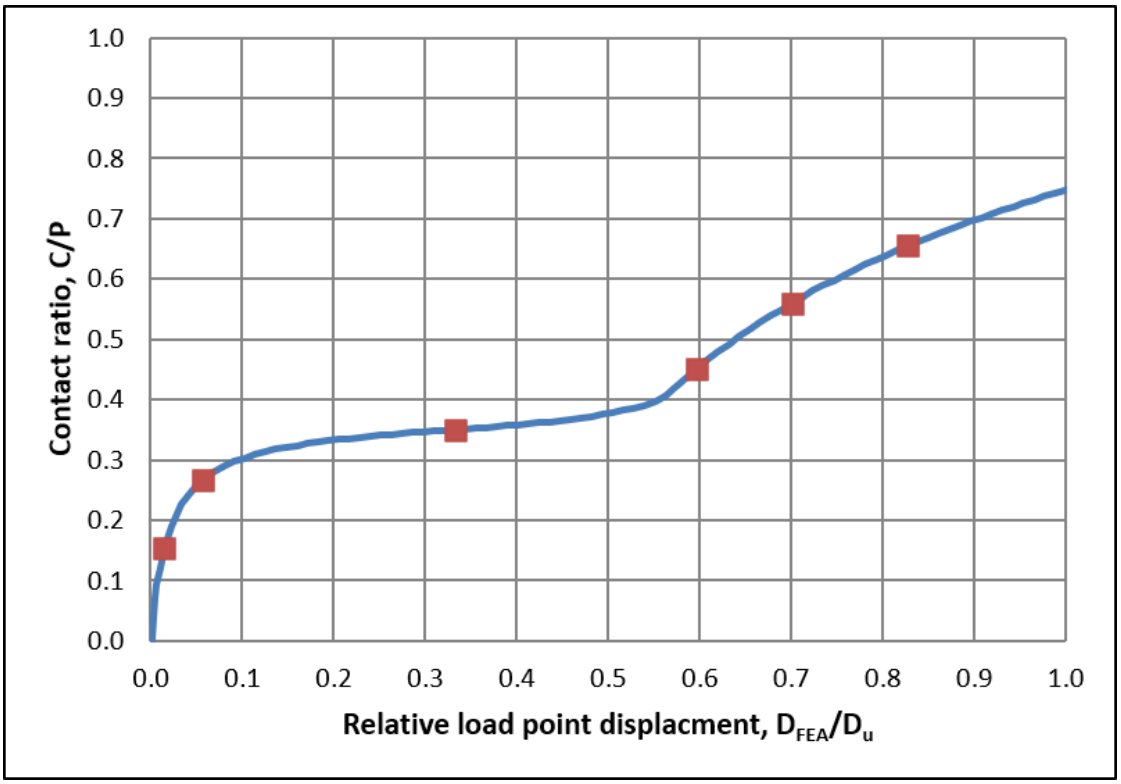

Figure 3.13: Computed contact ratio K as a function of relative load point displacement D_{FEA}/D_U

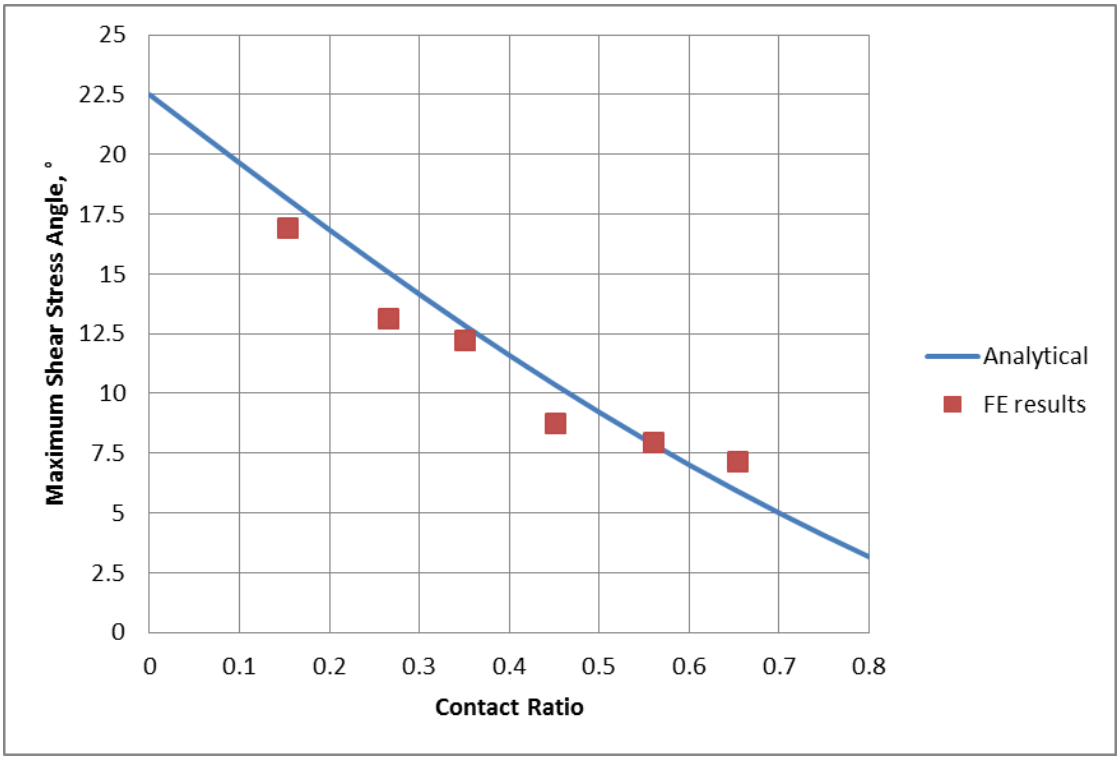

Figure 3.14: Critical weld throat plane as a function of contact ratio: analytical versus FE results

To examine the validity of Eq. (3.8) for determining critical weld throat plane, on which maximum transverse shear stress acts, a total of six positions (indicated by symbols) spanning the entire contact ratio curve shown in Figure 3.13 are considered for determining the critical weld throat plane angle as a function of contact ratio C/P from the nonlinear FE results. The critical weld throat plane results are shown in Figure 3.14 and compared with the analytical solution taken from Figure 3.10. A good agreement can be seen in Figure 3.14, proving the validity of the analytical developments presented in Sec 3.2.3 for determining the limit state of interest in this study.

3.4 Analysis of Test Data

With the new developments discussed in Sec. 3.2, particularly on the effect of plate-to-plate contact on critical weld throat plane angle, as confirmed by nonlinear FE results in Sec. 3.3, the shear strength test data reported by the authors recently (Lu et al., 2015) can now be re-analyzed

for demonstrating an improved correlation in shear strengths of fillet welds between transverse and longitudinal shear conditions. Note that all the transverse and longitudinal shear specimens analyzed in this chapter were manufactured and delivered according to MIL-STD-1689A (Department of Defense, 1990).

3.4.1 Shear Strength Correlation

By taking $K = 0.3$, i.e., assuming that plate-to-plate contact existed in all transverse shear specimens in the testing program (Lu et al., 2015), transverse shear test results can be re-calculated according to Eq. (3.7) and Eq. (3.8) and then compared with longitudinal shear test results. As can be seen in Figure 3.15, for both combinations of base metal and weld wire, the improvement in shear strength correlations between the transverse and longitudinal shear tests is evident once contact effects are considered. It should be noted that such an improvement in shear strength data correlation can be observed in all test groups in Lu et al. (2015), which are given in Appendix C for completeness.

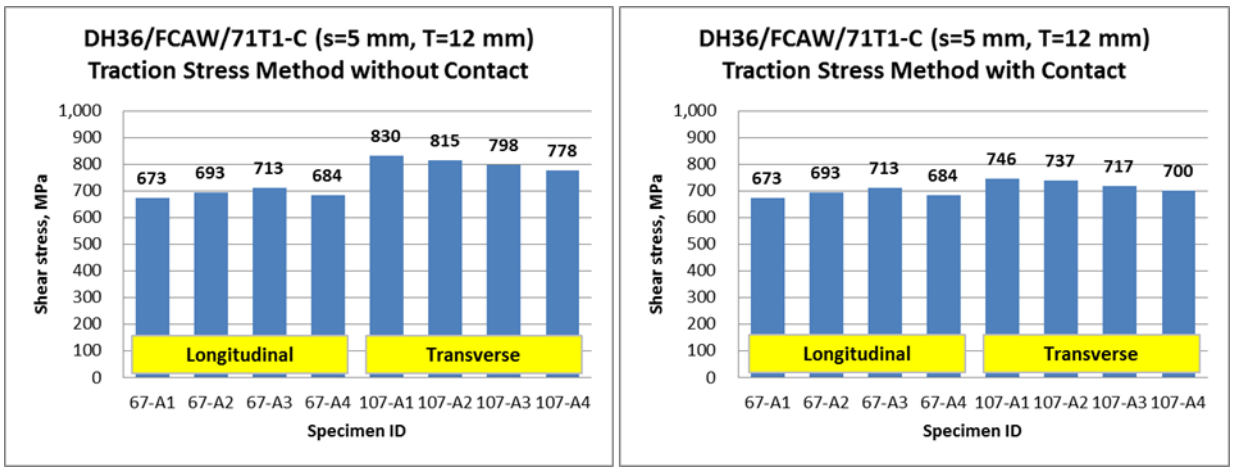

(a)

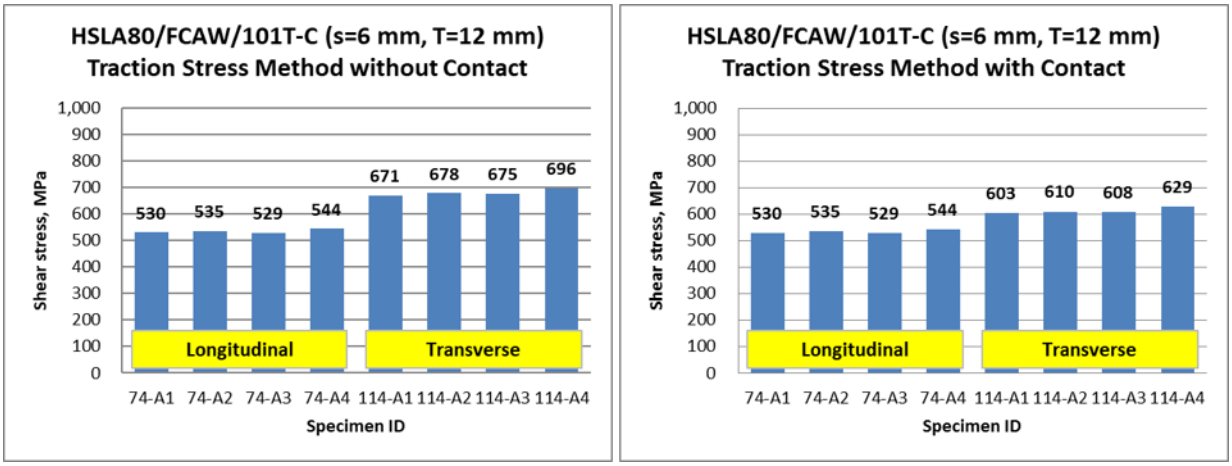

(b)

Figure 3.15: Shear strength correlations by traction stress method with and without contact effects: (a) DH36, FCAW, and 71T1-C weld wire; (b) HSLA80, FCAW, and 101T-C weld wire

3.4.2 Critical Weld Throat Plane Angle Estimation

In addition, critical weld throat plane angle of transverse shear specimens can now be more reasonably estimated by Eq. (3.8) by setting $K = 0.3$, which yields $\theta_{max} \approx 14°$. A significantly improved agreement with the experimental measurements can be clearly seen in Figure 3.16.

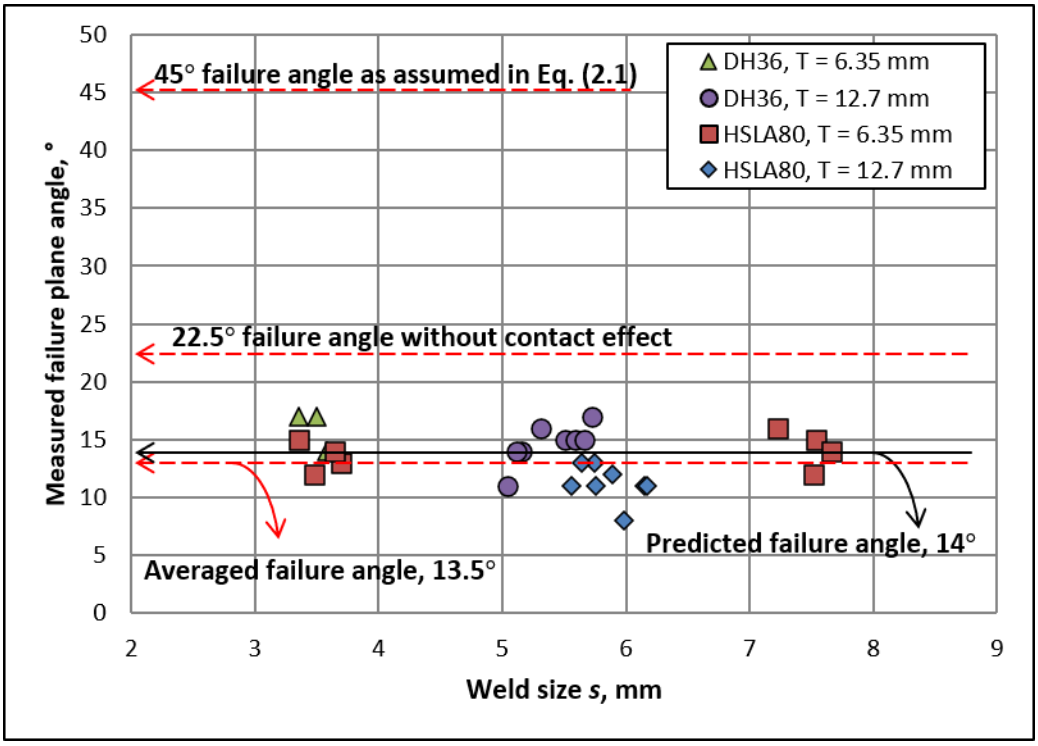

Figure 3.16: Predicted failure angle versus measured failure angle

3.4.3 Applications for Combined Loading Conditions

As a further validation for the new analytical development regarding treatment of contact effects, the test results obtained under various combined loading conditions shown in Figure 3.8 can now be re-analyzed by introducing $K = 0.3$ into Eq. (3.5), which can be re-written as:

$$\tau_{e,max} = \frac{P}{s \times L} \times (\cos\theta_{max} + \sin\theta_{max}) \times \sqrt{\{\sin\alpha \times (\cos\theta_{max} - 0.3\sin\theta_{max})\}^2 + (\cos\alpha)^2} \tag{3.22}$$

By setting the first derivative of Eq. (3.22) with respect to θ equal to 0, the critical weld throat plane angle θ_{max} can be obtained by solving the equation below iteratively:

$$\frac{\cos\theta_{max} - \sin\theta_{max}}{\cos\theta_{max} + \sin\theta_{max}} \times \sqrt{\{\sin\alpha \times (\cos\theta_{max} - 0.3\sin\theta_{max})\}^2 + (\cos\alpha)^2} = \frac{2\sin\alpha^2 \times (\cos\theta_{max} - 0.3\sin\theta_{max}) \times (\sin\theta_{max} + 0.3\cos\theta_{max})}{\sqrt{\{\sin\alpha \times (\cos\theta_{max} - 0.3\sin\theta_{max})\}^2 + (\cos\alpha)^2}} \tag{3.23}$$

The theoretically estimated critical weld throat plane angle (Eq. (3.23)) is plotted as a function of loading angle α (see the solid line in Figure 3.8). Again, the present approach shows a marked improvement, particularly for the test data from the study of Miazga and Kennedy (1989) when the loading angle $\alpha \geq 45°$, for which transverse shear conditions become more dominant, so does the contact effects.

Note that some discrepancies between analytical and test results can still be observed, especially for loading angle at about 30°. The reasons are not clear at this point. Some possible contributors to the discrepancies could be variations in fillet weld sizes, weld quality, and test conditions. More controlled test data would be needed for understanding the causes of these discrepancies, which will be reported at a later date when results become available. Nevertheless,

the correlation between the analytical results of this study and the test results shown in Figure 3.8 still represents the best correlation to date, to the authors' best knowledge.

3.5 Conclusions

In this chapter, an analytical formulation is presented for defining limit state condition in fillet-welded connections incorporating plate-to-plate contact effects. The analytical solution is then validated by finite element computation incorporating nonlinear material and nonlinear geometry conditions. In addition, its effectiveness in correlating shear strengths obtained from transverse and longitudinal shear specimens has been proven through the re-analysis of over 100 shear tests obtained by the same authors in an early part of the same study (Lu et al., 2015). As a result, a unified fillet weld shear strength can be established regardless of test specimen configurations and shear loading conditions, while conventional shear strength equation is incapable of reconciling the differences in shear strengths by as much as 50% as seen in this study and in the literature (Butler & Kulak, 1971; Kato & Morita, 1974; Yang et al., 2019) between transverse and longitudinal shear specimens.

Additional specific findings include:

1. Membrane shear stress is shown dominating the shear strength behavior in fillet-welded test specimens stipulated by widely used Codes and Standards, proving the validity of the analytical weld throat stress model adopted here and presented earlier in Chapter 2.
2. The presence of plate-to-plate contact causes a noticeable reduction of weld throat failure angle in transverse shear specimen from the theoretical value of 22.5°, which must be considered in order to avoid an over-estimation of shear strength from tests.

3. The unified fillet weld shear strength can be used to predict load capacity of complex fillet-welded connections under combined shear loading conditions, as demonstrated in Figure 3.8.
4. The present developments provide a basis for achieving a quantitative fillet weld sizing criterion for design and construction of fillet-welded structures, for which unified shear strength and robust weld throat stress calculation procedure are prerequisites.

Acknowledgments

The authors acknowledge the support of this work through a grant from CRRC Qiqihar Rolling Stock Co., Ltd.

Chapter 4 A Quantitative Weld Sizing Criterion and Applications in Load Capacity Evaluation of Hollow Structural Section Joints

Abstract

Existing weld sizing procedures for hollow structural section (HSS) joints in Codes and Standards are empirical in nature, often resulting in oversized welds. There is a growing interest in quantitative weld sizing for ensuring both structural safety and cost-effective construction of lightweight hollow section structures. In this chapter, a mesh-insensitive traction stress method is introduced for evaluating strength of fillet-welded HSS joints. The results are then generalized into a closed-form expression with a clearly defined mechanics basis. This expression relates weld throat shear stress to fillet weld size and remote load, with its dimensional geometric parameters being determined through a detailed parametric finite element analysis (FEA) of circular hollow section (CHS) and rectangular hollow section (RHS) joints with various dimensions. The effectiveness of the closed-form expression is demonstrated by comparing the predicted failure loads with those measured from a large number of HSS test data available from literature. Furthermore, the proposed quantitative weld sizing criterion can lead to as much as 20% weld size reduction from those determined using existing empirical-based weld sizing criteria, which can be very beneficial for welding-induced distortion control in construction of lightweight thin-walled structures.

Keywords: fillet weld, shear strength, traction stress method, hollow structural section, weld sizing, finite element analysis, lightweight

4.1 Introduction

Hollow structural sections (HSS) are widely used in civil and marine structures due to their high section stiffness, load-bearing ability and lightweight attributes. The most common HSS forms are circular hollow sections (CHS) and rectangular hollow sections (RHS), as illustrated in Figure 4.1. Both their lightweight and friendliness for field construction increasingly make the hollow structural sections a desirable choice (Wardenier et al., 2002).

Figure 4.1: Hollow structural sections: circular hollow sections and rectangular hollow sections

Various forms of frame structures can be readily constructed by performing fillet welding between HSS intersections, which serve as load transfer joints from one member to another. However, although overall frame structure can be designed in such a way that each HSS is subjected to relatively simple loading conditions, the stress state at joints can be very complex and difficult for quantitative determination. This is mainly because of stress or strain singularity (notch effects) at weld locations, i.e., at weld toe and weld root (Dong et al., 2010a). In addition, the difference in flexibility between the HSS and transition plates which are often used as fillet weld landing surfaces, makes the weld stress singularity even more severe (Packer & Cassidy, 1995). As a result of lacking an effective means for quantitatively determining the weld stress state,

engineers have been relying on empirical design rules in current codes and standards, which often oversize the fillet welds for preventing premature failures under anticipated loading conditions (Packer et al., 2016). However, the use of oversized fillet welds in modern lightweight structures not only increases structural weight and construction cost, but also introduces severe welding-induced distortions during construction (Huang et al., 2004 & 2007). As structural lightweight demands intensify, over-welding has been identified as the major contributor to widespread distortions in shipbuilding and offshore construction over the last decade or so (Huang et al., 2014 & 2016). Therefore, a quantitative weld sizing criterion is needed for both ensuring structural safety and reducing construction cost for taking advantage of HSS in modern lightweight ship structures.

In this chapter, after briefly examining traditional weld sizing criteria (e.g., empirical based "engineering shear stress" definition and "directional strength-increase factor") in Sec. 4.2, authors then introduce the mesh-insensitive traction stress method (TSM), which has been used for determining weld strength in load-carrying fillet-welded plate joints, as a means of quantitatively determining fillet weld shear strength in HSS connections in Sec 4.3. It should be noted that TSM has shown effective both in fatigue evaluation of welded joints (Dong et al., 2010a; Xing et al., 2016; Mei & Dong, 2017a & 2017b) and static weld strength characterization at simple specimen level (Nie & Dong, 2012; Lu et al., 2015; Lu & Dong, 2020). In Sec. 4.4, detailed traction stress states at typical CHS and RHS joints will be examined for establishing transferability between the shear strength determined in simple plate joints and load capacity in HSS connections. Through a careful examination of detailed finite element analysis (FEA) results, a set of key parameters have been identified for determining critical locations governing the load capacity in HSS connections, leading to a much-improved load capacity correlation compared to the existing traditional weld

sizing approaches. Finally, those parameters are incorporated into a proposed TSM based weld sizing criterion, which gives a significant weld size reduction without compromising joint load capacity.

4.2 Assessment of Traditional Weld Sizing Approaches

4.2.1 Engineering Shear Stress

Due to the failure of capturing the weld stress singularity, existing traditional fillet weld sizing criteria, such as MIT-STD-1628 (Department of Defense, 1974), ABS 96 (ABS, 2000), AWS D1.1 (AWS, 2015), and other design specifications, such as Eurocode 3 (CEN, 2005), AISC 360 (AISC, 2010) and CSA S16 (CSA, 2014), have been taking a conservative approach to ensure the fillet welds possessing higher strength than those of the connected branch members. A nominal weld throat stress defined by Eq. (4.1), also referred to as an "engineering shear stress" in DNV-RP-C203 (DNV, 2012), has been used in these criteria for calculating fillet weld strengths from both standard longitudinal and transverse shear specimens, of which fillet welds are parallel (0°) and perpendicular (90°) to the remote loading direction (P) respectively, as depicted by AWS B4.0 (AWS, 2007) in Figure 4.2.

$$\tau_{u,w} = \frac{P_u}{a_{45} \times L} \tag{4.1}$$

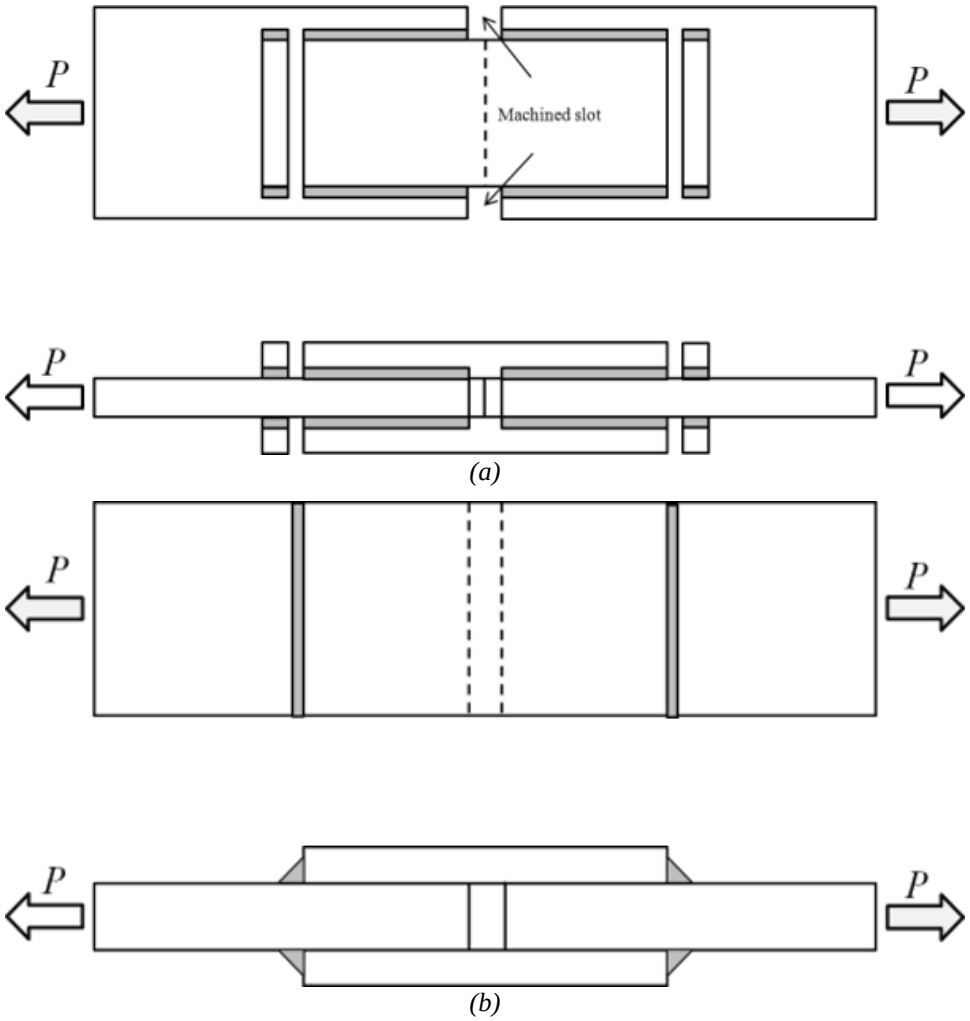

Figure 4.2: Standard fillet-welded shear testing specimens: (a) longitudinal shear loaded; (b) transverse shear loaded

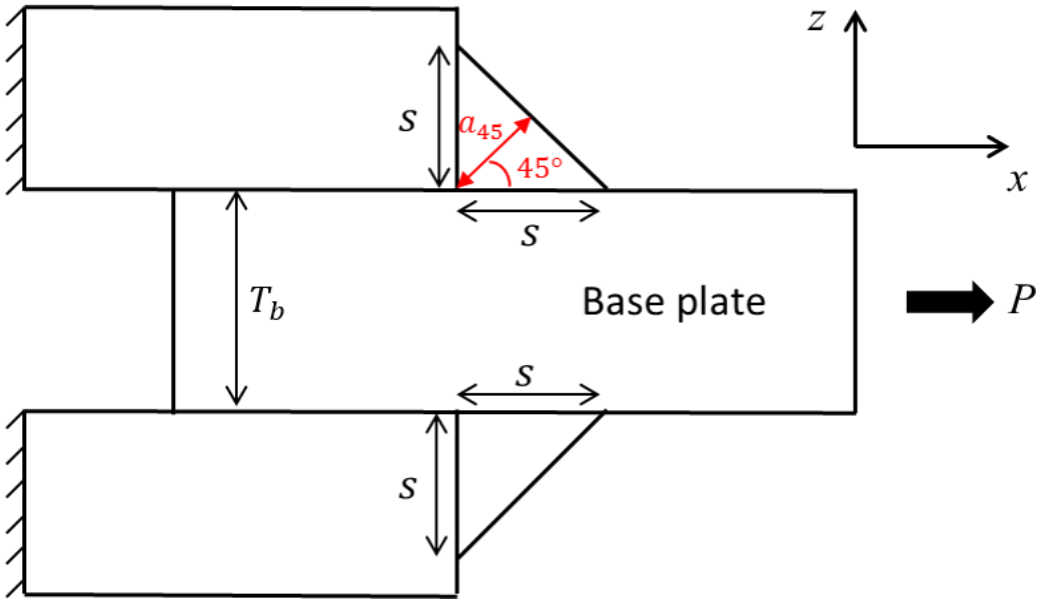

Figure 4.3: Theoretical weld throat a_{45} as failure plane for standard fillet-welded shear testing specimens

As illustrated in Figure 4.3, by assuming: (1) 45° failure angle measured from base plate and; (2) uniform weld throat stress distribution along weld line (y-axis), Eq. (4.1) has been used for determining longitudinal and transverse shear strength (τ_{u,w_L} and τ_{u,w_T}) from the standard longitudinal and transverse shear specimens (see Figure 4.2), respectively. Due to the lack of means to reconcile the significant differences between τ_{u,w_L} and τ_{u,w_T}, the longitudinal shear strength τ_{u,w_L}, which can be 30 to 80% lower, is typically used for sizing fillet welds in various existing traditional criteria, as expressed by Eq. (4.2), which can be excessively conservative (Lu et al., 2015), leading to significantly oversized fillet welds.

$$\frac{s}{T_b} = 0.7071 \times \frac{\sigma_{u,b}}{\tau_{u,w_L}} \tag{4.2}$$

4.2.2 Directional Strength-Increase Factor

Due to the increasing demand in structural lightweighting, there is a growing interest in eliminating weld oversizing for distortion control and cost reduction purposes. Along this line, some of the representative studies (Spraragen & Claussen, 1942; Higgins & Preece, 1968; Butler

& Kulak, 1971; Kato & Morita, 1974; Kamtekar, 1982 & 1987; Miazga & Kennedy, 1989) have shown that the load-carrying capacity of fillet welds is a function of loading angle, i.e., the angle α between the remotely applied load P and the weld axis as shown in Figure 4.4. For instance, an experimental study by Miazga and Kennedy (1989), including 42 fillet-welded shear specimens loaded from 0° to 90°, showed that load-carrying capacity ratios between the transverse and longitudinal shear specimens were 1.28 and 1.60 for 5 mm and 9 mm weld sizes, respectively. In the same study, Miazga and Kennedy (1989) also developed an analytical model based on the maximum shear stress theory with parameters empirically obtained from the experimental results, showing load-carrying capacity of fillet weld increased up to 50% when the loading angle α increased from 0° to 90°.

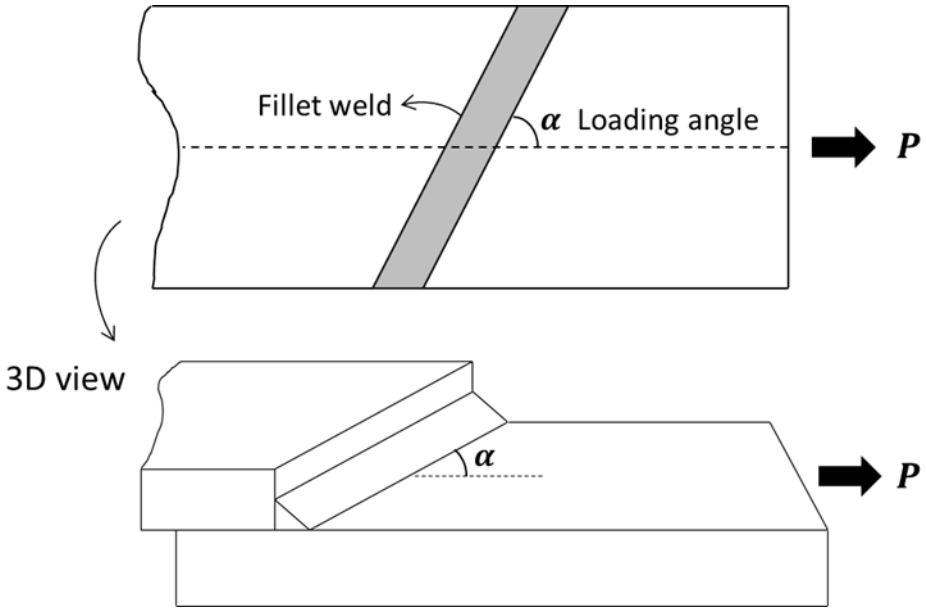

Figure 4.4: Combined shear loaded fillet weld with loading angle α

These observations on the load-carrying capacity variation in the fillet welded components subjected to different loading angles have led to the development of a directional strength-increase factor, as empirically formulated in the form of Eq. (4.3) by Lesik and Kennedy (1990), which has been adopted by some design specifications such as CSA S16 (CSA, 2014) and AISC 360 (AISC,

2010) for reducing fillet weld sizes. Note that τ_{u,w_0} in Eq. (4.3) is the same as the longitudinal shear strength τ_{u,w_L} in Eq. (4.2).

$$\frac{\tau_{u,w_\alpha}}{\tau_{u,w_0}} = 1.00 + 0.50\sin^{1.5}\alpha \tag{4.3}$$

However, there exist some major limitations in the empirical approach described by Eq. (4.3) for structural applications. First, it has been shown that the directional strength-increase factors determined from Eq. (4.3) have shown a significant scatter in interpreting the experimental test data available in literature, which suggests that there might be other factors at play. For example, the weld size effect was clearly present in the study of Miazga and Kennedy (1989). Secondly, in the previous studies, the assumption of uniform weld throat stress distribution along weld direction was only appropriate for the standard simple transverse shear specimens but not at all for the standard longitudinal shear specimens. As demonstrated by Nie and Dong (2012) as well as by Lu et al. (2015), severe weld throat stress concentration occurs at the end of longitudinal weld axis and should not be ignored for weld strength determination. In addition, the stress distribution along weld direction could be much more complex than being uniform in the structural applications even if the fillet welds are transversely loaded, which will be demonstrated for the HSS connections in the later part of this study. Furthermore, a limit state approach by Lu and Dong (2020) demonstrated contact force between the overlapped plates has a significant effect on the weld throat stress state, which had been ignored or inadequately considered in the force systems from the previous theoretical models. Lastly, the failure criterion used for weld strength determination should be consistent for a fillet welded component regardless of loading angle as discussed by Nie and Dong (2012) and Lu et al. (2015). However, this was not the case as implied by introducing a directional strength-increase factor, e.g., in the form of Eq. (4.3).

Based on the above discussions, it seems reasonable to state that both the engineering shear stress and directional strength-increase factor lack of a rigorous mechanics underpinning for supporting the development of a more generalized weld sizing criterion.

4.3 Traction Stress based Weld Strength Criterion

To address the inconsistencies in fillet weld strength characterizations discussed in the previous section, the mesh-insensitive traction stress method has been shown effective (Nie & Dong, 2012; Lu et al., 2015). For completeness, a brief description of the method is given below, with an emphasis on applications in analyzing HSS joints for facilitating the discussions in the later sections of this chapter.

To deal with the weld throat failure, three traction stress components with respect to the local coordinate system (x'-y'-z'), referred to as normal stress $\sigma(x')$, transverse shear stress $\tau_T(x')$, and longitudinal shear stress $\tau_L(x')$ as seen in Figure 4.5, are exposed on any fillet weld throat plane at an angle of θ from base plate and are presented in a work-equivalent linear form as in Eq. (4.4), each of which consists of its membrane and bending parts with respect to the mid-distance of the weld throat cut cross section A-A along a_θ, as shown in Figure 4.6.

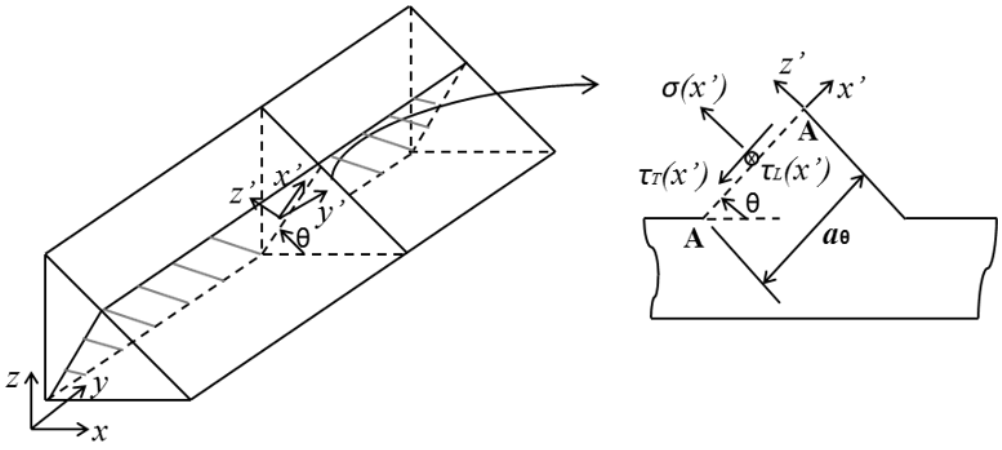

Figure 4.5: Traction stress components acting on a weld throat plane at an angle of θ

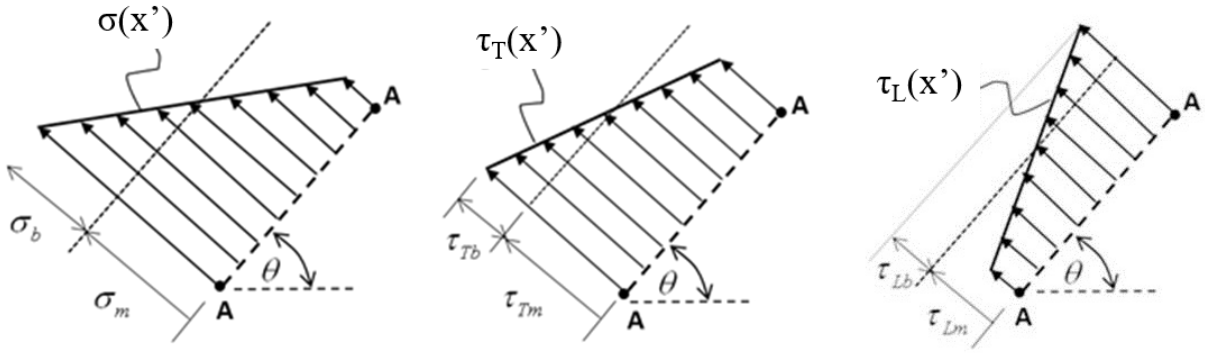

Figure 4.6: Linear representation and decompostion of weld throat traction stress components

$$\sigma = \sigma_m + \sigma_b$$

$$\tau_T = \tau_{Tm} + \tau_{Tb} \tag{4.4}$$

$$\tau_L = \tau_{Lm} + \tau_{Lb}$$

Through the experimental and analytical studies (Nie & Dong, 2012; Lu et al., 2015), the TSM based weld failure criterion, for fillet welds under combined longitudinal and transverse shear loading conditions, has been defined as the maximum resultant membrane shear stress on the critical weld throat plane as expressed by Eq. (4.5), following which great weld strength correlations improvement compared to using the traditional approach (Eq. (4.1)) have been achieved for over 200 pieces of testing specimens configured with the most commonly used base and weld filler materials (steel, titanium alloy, and aluminum alloy, etc.), welding processes (GTAW, FCAW, and GMAW, etc.), and dimensions (plate thickness, weld length, and weld size, etc.), such as the example shown in Figure 4.7.

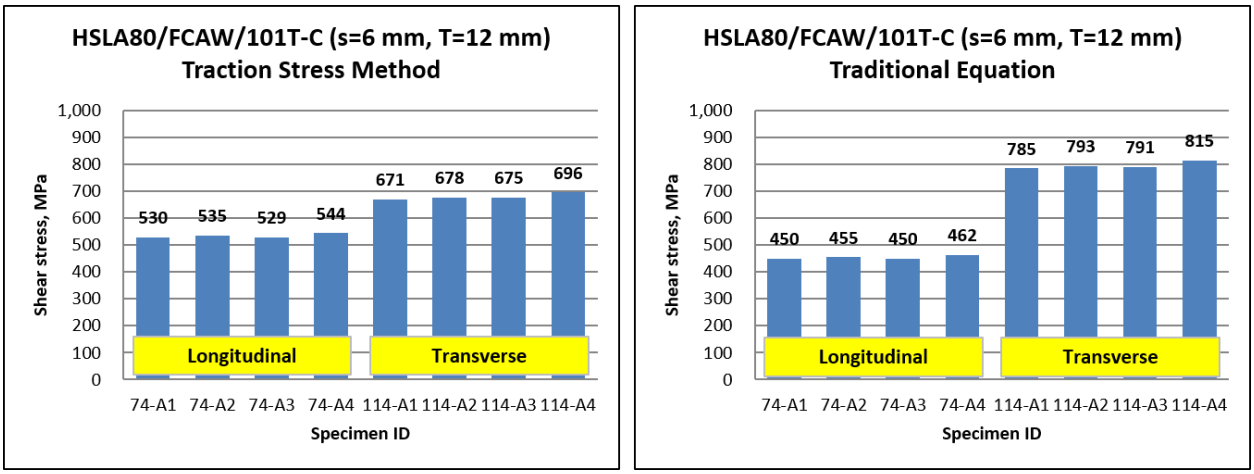

Figure 4.7: Fillet weld strength correlation comparison between traction stress method and traditional approach

$$\tau_{e,max} = \text{Max}\left\{\sqrt{\tau_{Lm}(\theta)^2 + \tau_{Tm}(\theta)^2}\right\} \leq \tau_{u,w} \tag{4.5}$$

An additional important improvement to the TSM failure criterion has been developed to include the effects of nonlinear mechanical properties and contact conditions on the weld throat stress state (Lu & Dong, 2020). As a result, the new procedure not only provides more effective data correlation between longitudinal and transverse shear tests as shown in Figure 4.8, but also enables a significantly improved failure angle prediction for the fillet-welded specimens subjected to loading direction varying from 0° to 90° with respect to weld line direction as shown Figure 4.9. Detailed formulation and calculation procedures can be found in Lu and Dong (2020), which will not be repeated here due to space limit.

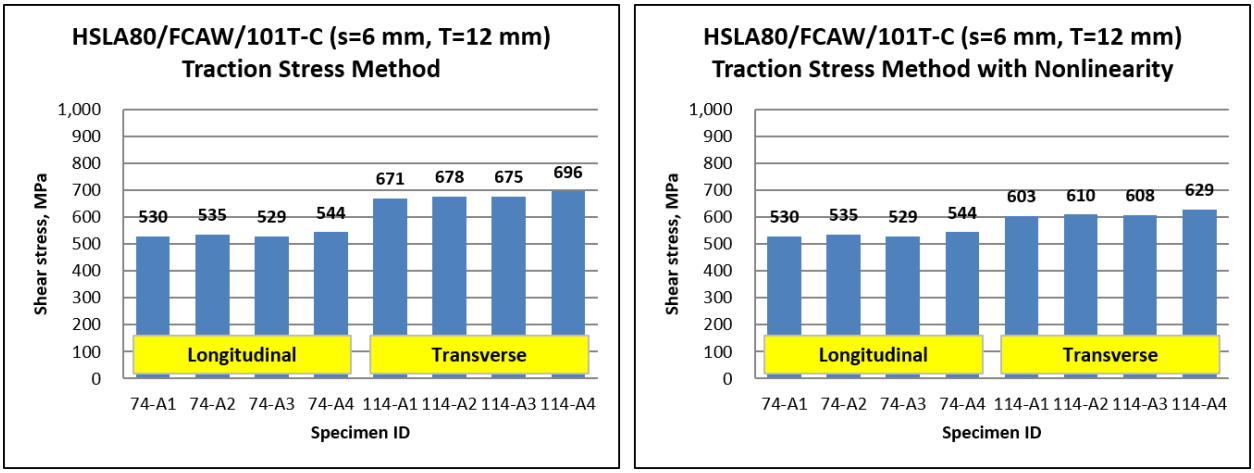

Figure 4.8: Fillet weld strength correlation comparison between TSM and TSM with nonlinearity

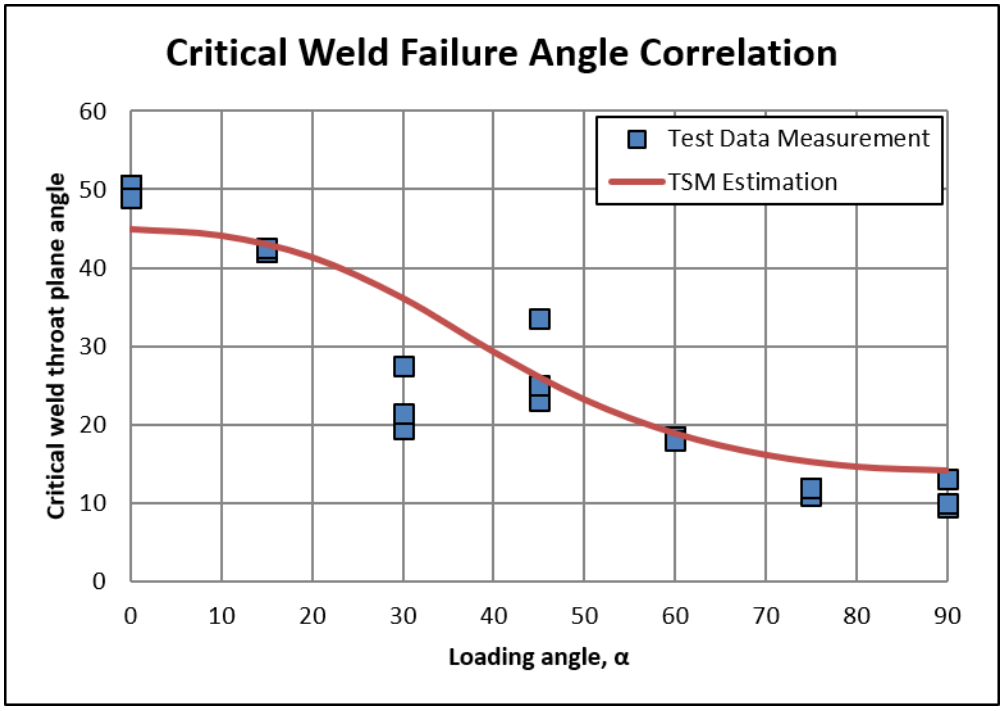

Figure 4.9: Critical weld failure angle correlation between traction stress method and test data measurement

Then, the question becomes how the quantitative failure criterion given in Eq. (4.5), proven effective as seen in Figure 4.9, can be implemented for determining critical fillet weld sizing or estimating load capacity of a HSS joint. The following section provides the detailed developments in this regard.

4.4 Analysis of Fillet-Welded HSS Connections

Without losing generality, we consider two representative HSS joint configurations as shown in Figure 4.10, on which there exist an sufficient amount of test data for a validation purpose (Packer & Cassidy, 1995; Tousignant, 2017). These are HSS joint with an inset rigid plate (see Figure 4.10a) and HSS to HSS cruciform joint (see Figure 4.10b). Two most common cross-section geometries (section A-A) of branch member, i.e., circular and rectangular hollow section, are considered in this study, as shown in Figure 4.11.

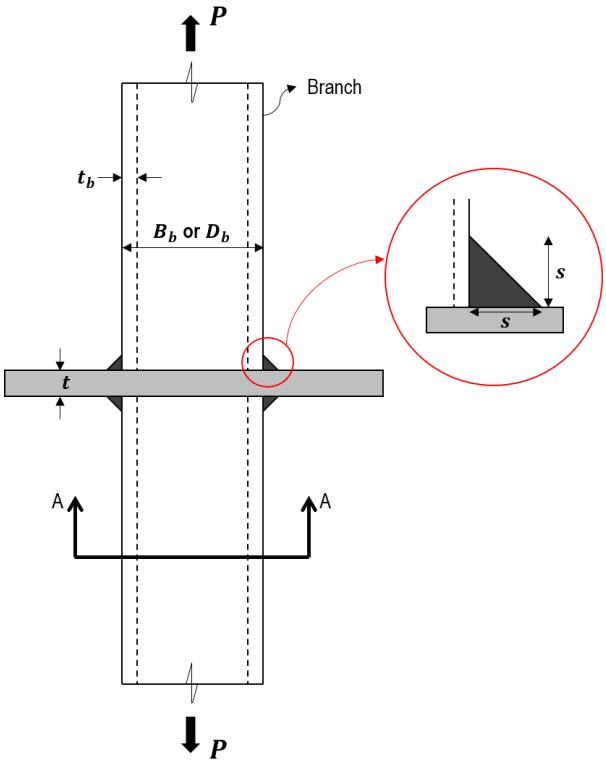

(a)

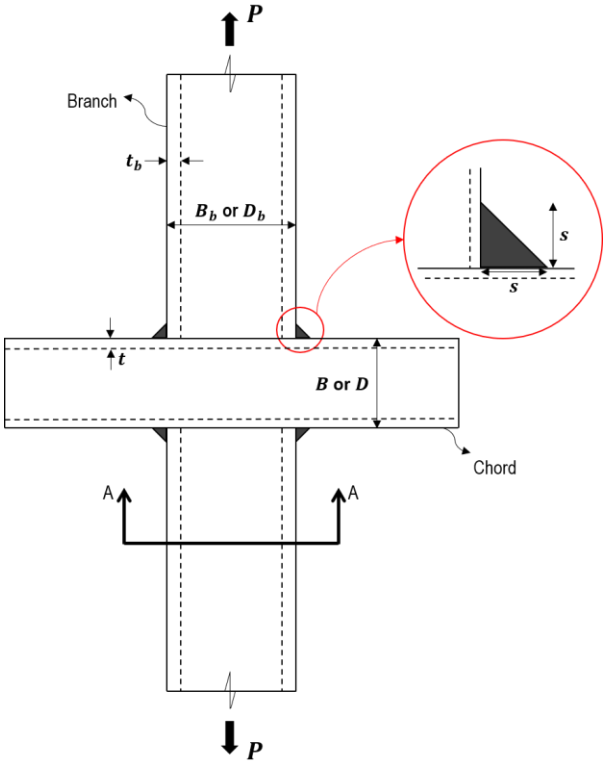

(b)

Figure 4.10: Fillet-welded HSS connections: (a) HSS to rigid plate; (b) HSS to HSS

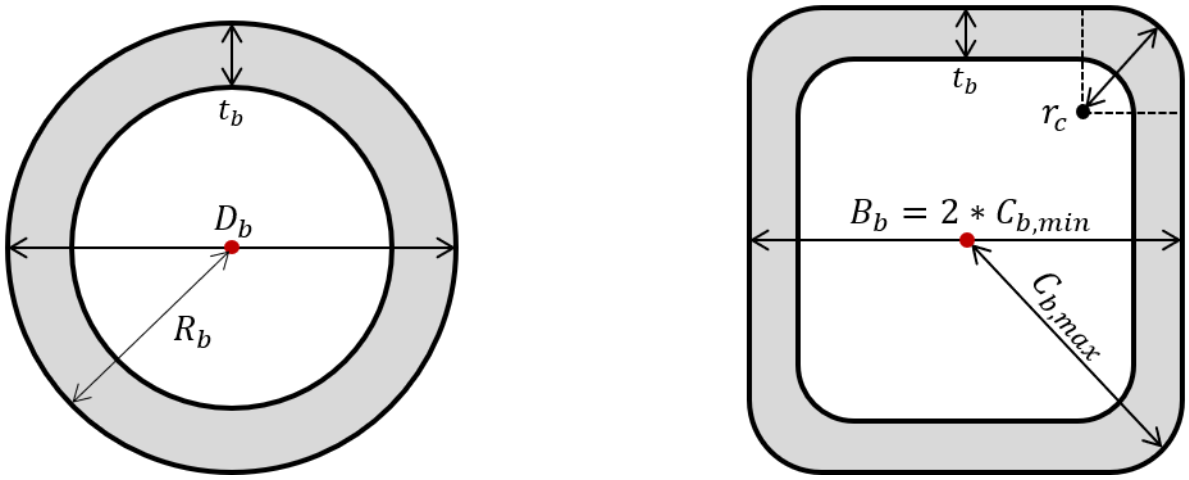

Figure 4.11: Cross section A-A of branch member in Figure 4.10: (a) CHS; (b) RHS

4.4.1 Finite Element Analysis using TSM

Three-dimensional (3D) solid element models were developed using ABAQUS (Dassault Systemes, 2018), with various geometric parameters, such as branch member width D_b or B_b varying from 40 to 200 mm, branch member thickness t_b from 2 to 80 mm, and fillet weld size s from 4 to 12 mm. Both CHS and RHS are modeled being welded to the fixed rigid endplate to remove the landing surface flexibility effect for the time being, as depicted in Figure 4.10a. Sufficiently fine linear 3D brick elements (2 mm and C3D8) are chosen to mesh the fillet weld and its surrounding area for both the CHS and RHS connections. Nominal structural steel elastic material properties are assigned, and nonlinear material and geometric (large deformation) behaviors are not considered according to the results from the previous studies (Lu et al., 2015; Lu & Dong, 2020). Remote tension load P perpendicular to the weld toe surface is incrementally applied at the far end of the branch member. Representative FE models for CHS and RHS joints are shown in Figure 4.12. The mesh-insensitive traction stresses acting on the selected weld throat cut plane (angle θ plane in Figure 4.12) are then computed using the nodal force based procedure for 3D solid element models given in Nie and Dong (2012) and Lu et al. (2015), which will not be repeated here due to space limit.

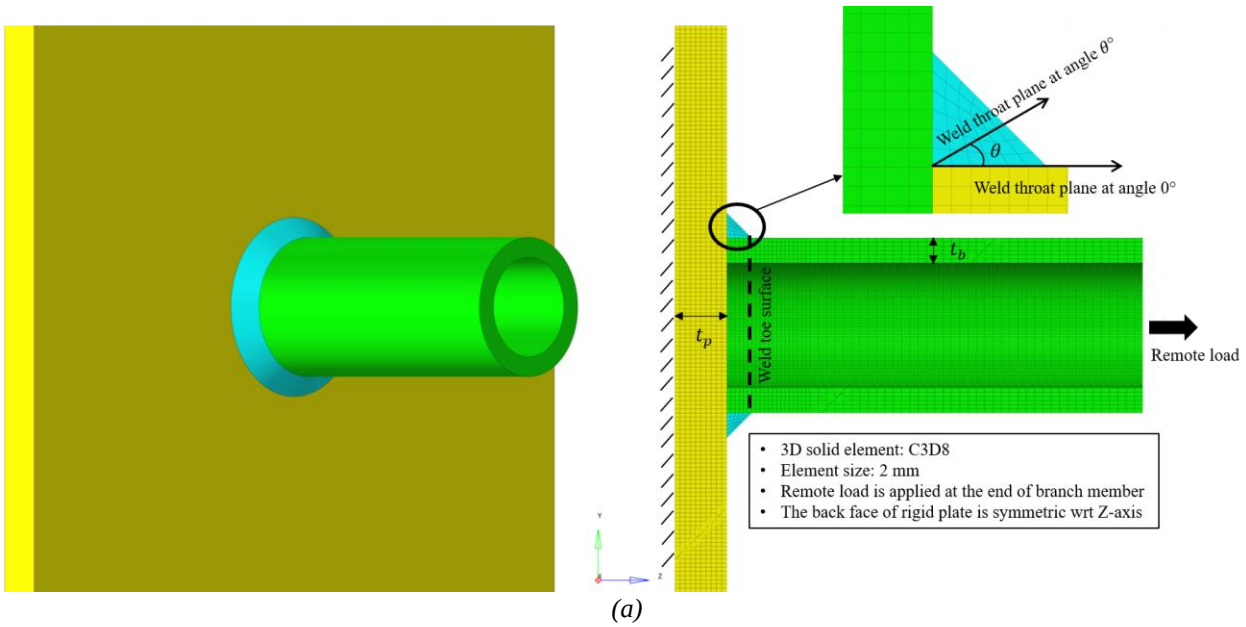

(a)

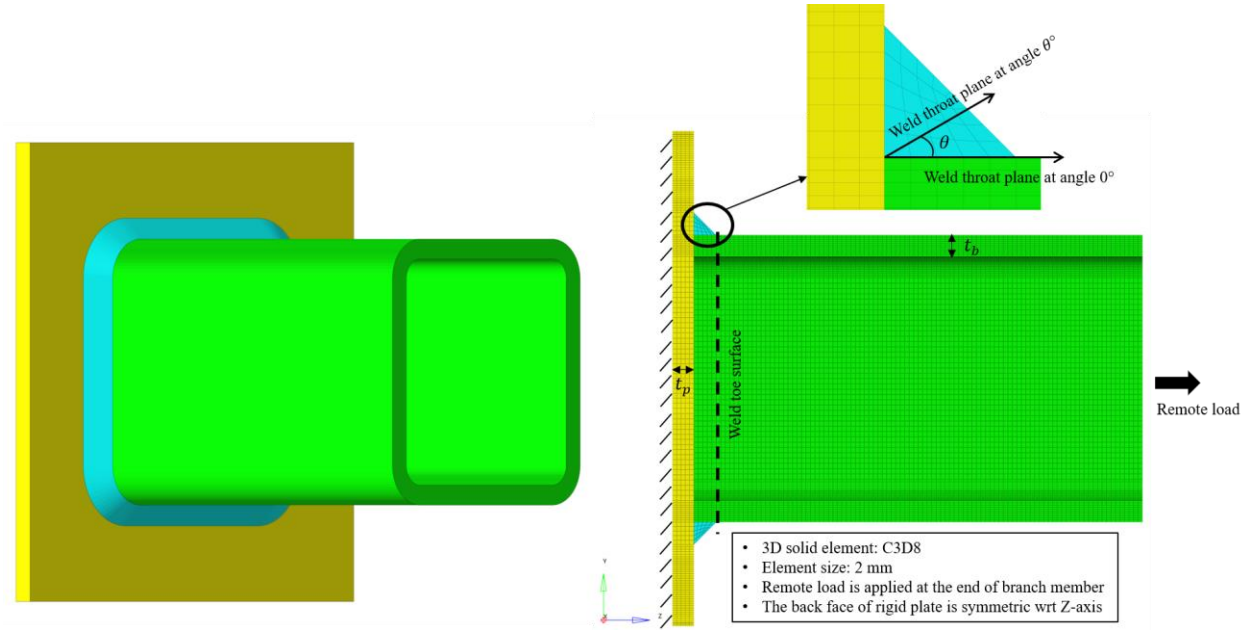

(b)

Figure 4.12: FE models for fillet-welded HSS connections: (a) CHS; (b) RHS

Since the weld is transversely loaded, i.e., remote load direction is at 90° to the fillet weld line, the resulting longitudinal shear stress is found to be negligible and only transverse shear stress is attributed to the weld failure. Therefore, Eq. (4.5) can be simplified to Eq. (4.6), in which transverse shear stress ($\tau_{Tm}(\theta)$) on any weld throat plane with angle θ can be calculated following the study of Lu and Dong (2020).

$$\tau_{e,max} = \max\{\tau_{Tm}(\theta)\} = \max\{\tau_{Tm}(0) \times (\cos\theta - K\sin\theta) \times (\cos\theta + \sin\theta)\}$$
$$K = \frac{\sigma_m(0)}{\tau_{Tm}(0)} \tag{4.6}$$

However, unlike the transversely loaded open fillet welds on the standard plate specimens, of which both $\tau_{Tm}(0)$ and K can be analytically derived following a traction stress based limit state approach, it is expected that $\tau_{Tm}(0)$ and K are not uniform along the weld line, particularly at the corner locations in RHS, and vary for different sized HSS connections. Therefore, the main objective of the FE base parametric study here is to elucidate the behaviors of $\tau_{Tm}(0)$ and K and their governing parameters so that $\tau_{e,max}$ can be analytically obtained.

4.4.1.1 Results – CHS Connections

Starting with CHS connections, shear stress $\tau_{Tm}(0)$ and normal stress $\sigma_m(0)$ at the 0° weld throat plane along the circumference from a 3D CHS FE model, normalized by nominal shear stress defined as $\tau_n = P/(s \times L)$, are plotted in Figure 4.13, from which a few findings can be summarized: (1) both the shear and normal stresses uniformly distribute along the weld, i.e., the structural constraint on the weld is uniform for CHS connections; (2) shear stress $\tau_{Tm}(0)$ is equal to the nominal shear stress $\tau_n = P/(s \times L)$, meaning there is no stress concentration caused by geometric singularity; (3) significant self-equilibrium normal stress acts on the 0° face due to the structural constraint even though no external load parallel to the weld toe surface is applied.

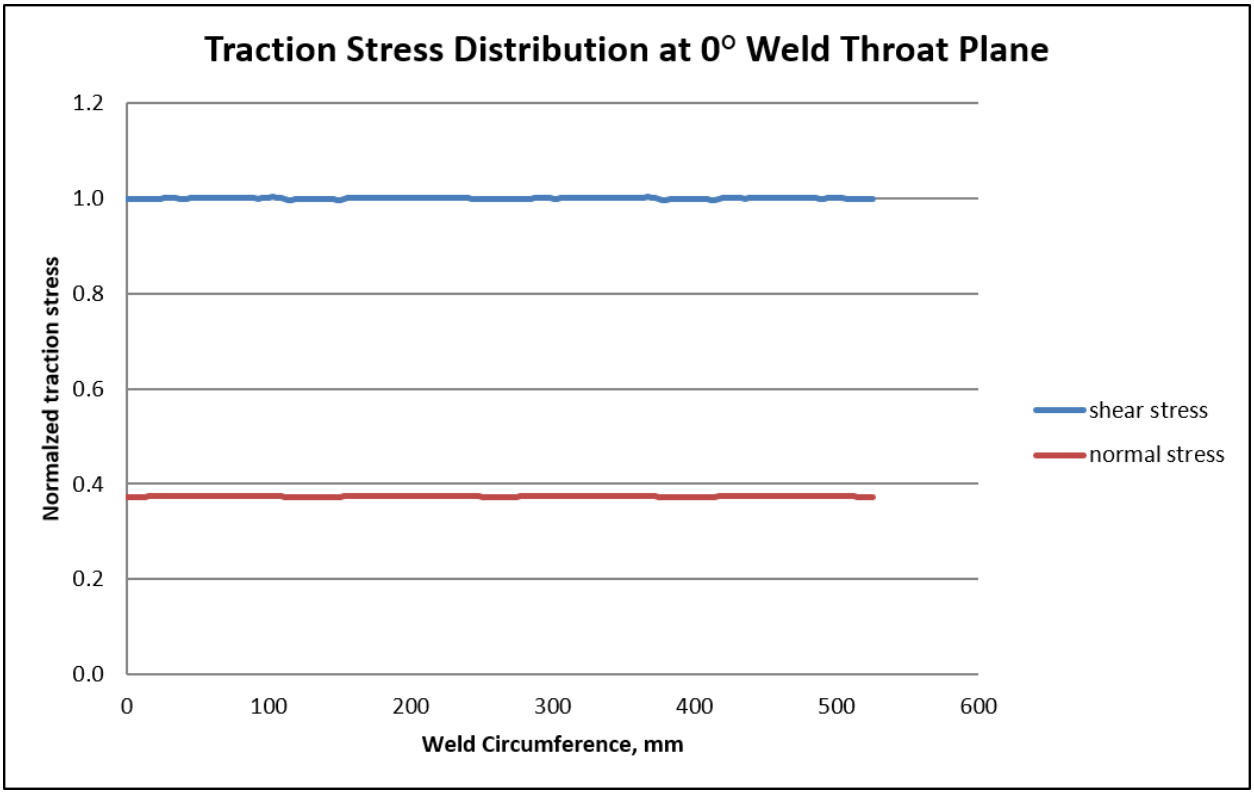

Figure 4.13: Normalized traction stress distribution along weld circumference on CHS connection under 90° loading

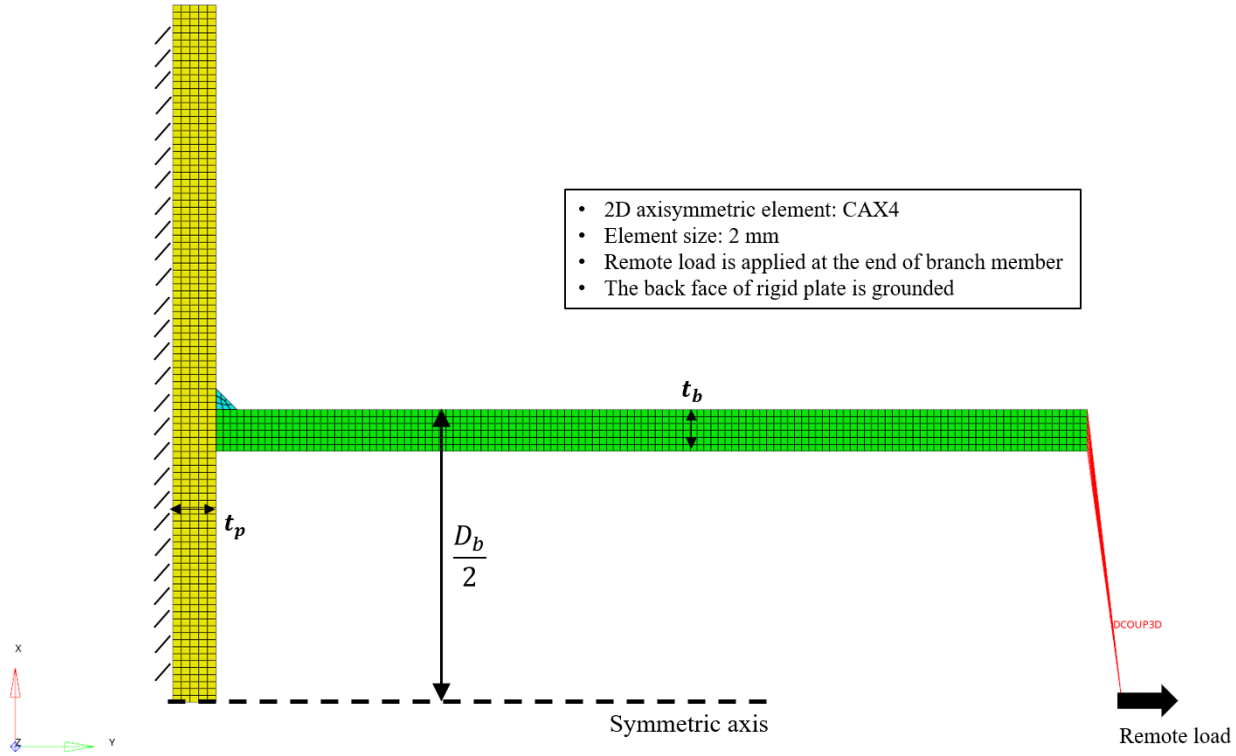

Figure 4.14: 2D axisymmetrci FE modeling for CHS connections

The 3D FE model results shown in Figure 4.13 confirm that axisymmetric model, as illustrated in Figure 4.14, can be directly used to represent the CHS connections, although the base plate is square-shaped. As such, with the axisymmetric traction stress results obtained from various CHS connections with combinations of geometric parameters (R_b, t_b, s, etc.), ratio K are shown to be a function of branch member radius R_b (i.e., $D_b/2$) and thickness t_b, as shown in Figure 4.15. It can be summarized that: (1) the ratio K decreases when R_b/t_b increases; (2) when R_b/t_b equal to 1, the ratio K data scatters a bit, i.e., thicker t_b having larger K value; (3) however, the ratio K ($R_b/t_b = 1$) reaches to 0.5 and becomes stable when t_b is thick enough, i.e., upper bound of ratio K being 0.5. (4) noting that the ratio K variance between different weld sizes for the same R_b/t_b is minimum, it is considered negligible in this study.

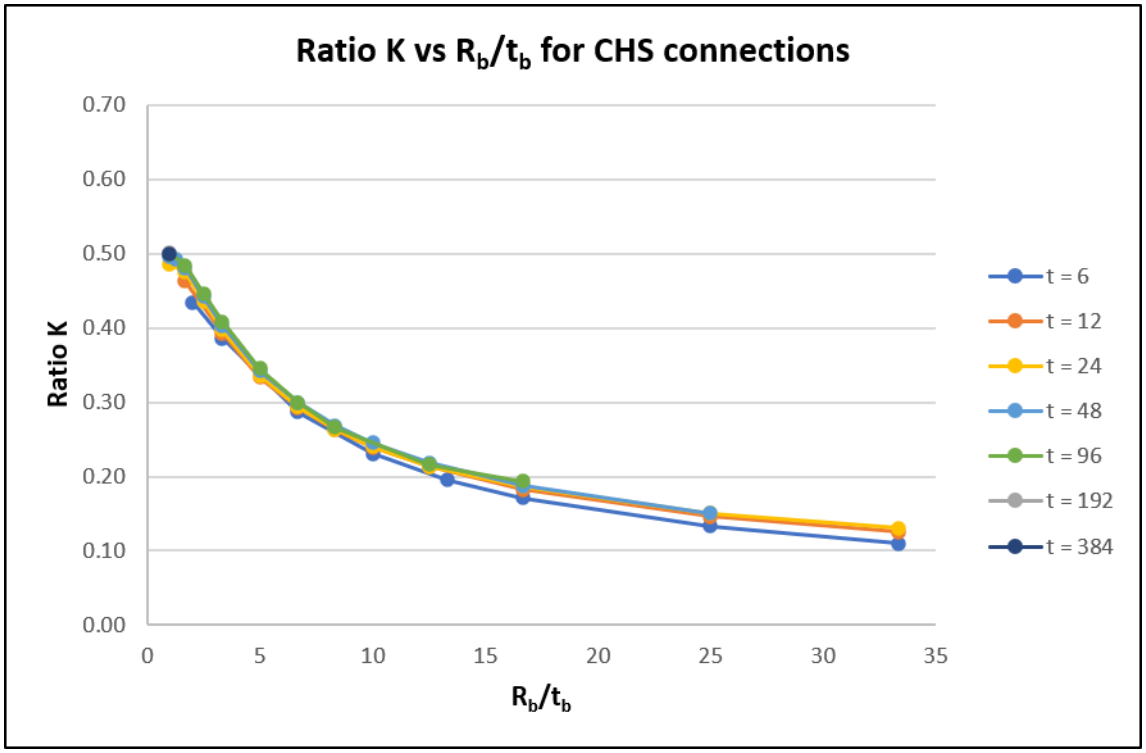

Figure 4.15: Ratio K vs R_b/t_b for CHS connections with different t_b

A careful examination of Figure 4.15 indicates that a logarithmic equation can be used to provide the best fit of the correlation between K and R_b/t_b, as expressed by Eq. (4.7), of which

the upper bound represent solid circular section (i.e., $R_b/t_b = 1$ and $K_{upper} = 0.5$). In addition, Eq. (4.7) indicates that normal stress effect can be negligible when R_b/t_b is large enough. By substituting Eq. (4.7) into Eq. (4.6), both shear strength and failure angle of fillet welds on the 90° loaded CHS connections can be obtained by the closed-form expression as shown in Eq. (4.8):

$$K = -0.1089 \ln \frac{R_b}{t_b} + 0.5 \tag{4.7}$$

$$\tau_{u,w} = \frac{P_u}{s \times L} \times (\cos \theta_{max} - K \times \sin \theta_{max}) \times (\cos \theta_{max} + \sin \theta_{max})$$

$$\theta_{max} = \frac{1}{2} \times \tan^{-1}\left(\frac{0.5 + 0.1089 \ln \frac{R_b}{t_b}}{1.5 - 0.1089 \ln \frac{R_b}{t_b}}\right) \tag{4.8}$$

4.4.1.2 Results – RHS Connections

Unlike the CHS connections, shear stress $\tau_{Tm}(0)$, normal stress $\sigma_m(0)$ and ratio K from the 3D RHS FE models are non-uniformly distributed along the weld circumference, as shown in Figure 4.16. It can be observed that: (1) both stress and ratio K distributions are concentrated at the corners of the section, i.e., the weld toe locations with the max distance to the cross-section centroid ($C_b = C_{b,max}$ in Figure 4.11b) along weld; (2) the value of normal stress or ratio K hits the valley at the locations of $C_b = C_{b,min}$ along weld.

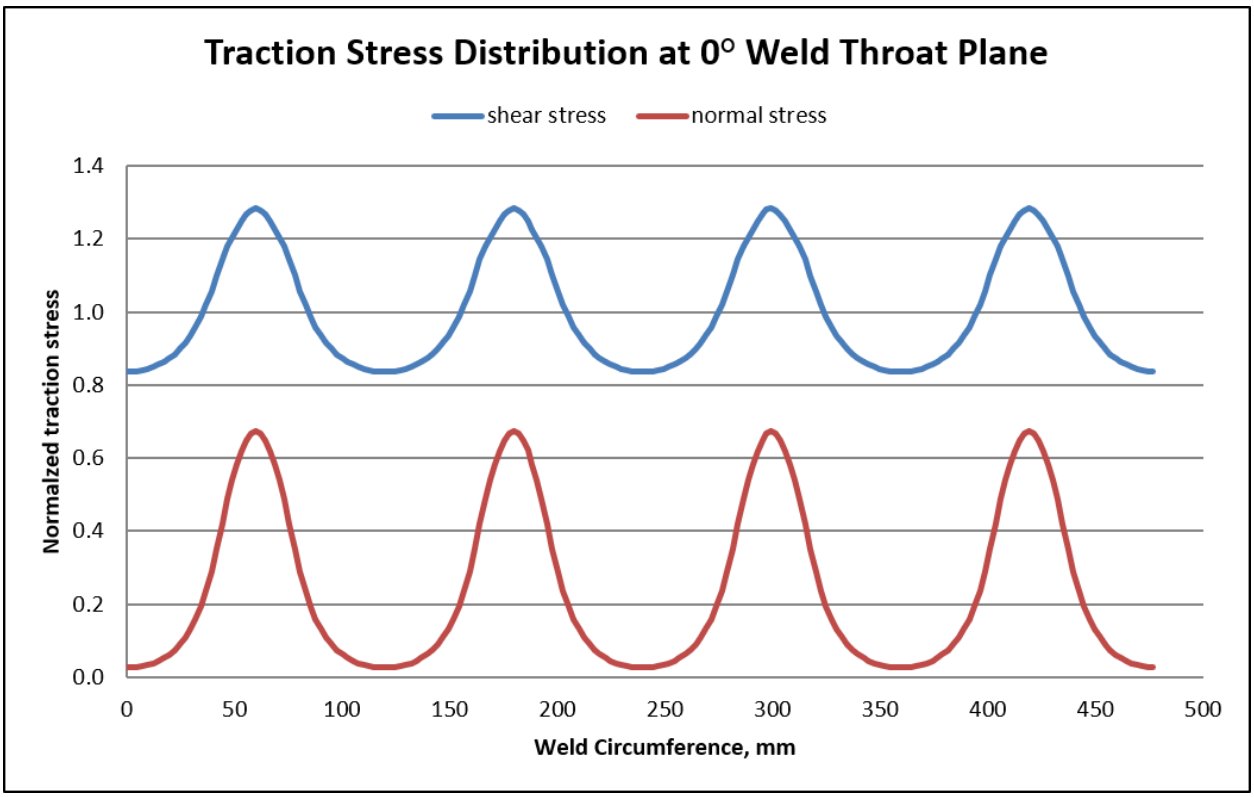

(a)

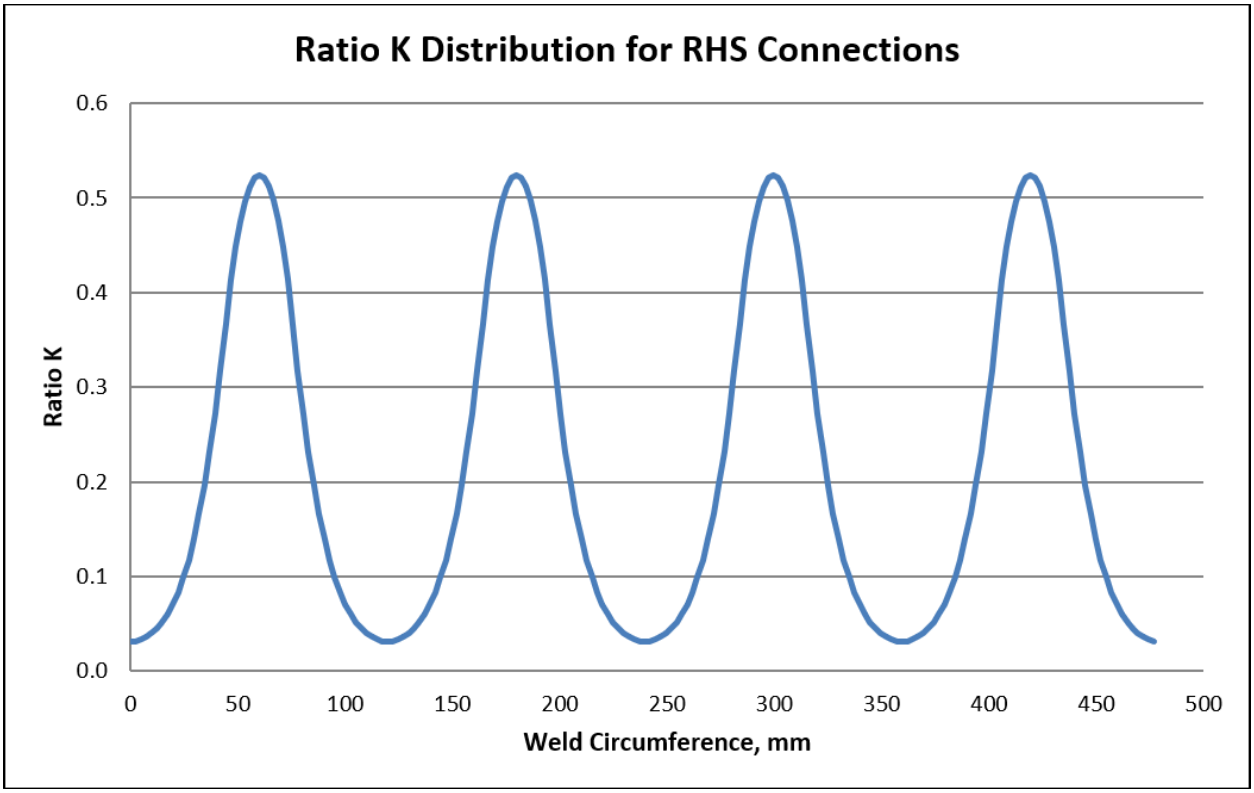

(b)

Figure 4.16: Normalized traction stress and ratio K distribution along weld circumference for RHS connections

The non-uniform variations in Figure 4.16 along weld axis exhibit a quarter symmetry, consistent with the component geometry and loading condition given in Figure 4.12b, as expected. The reason for using a full 3D FE model is for consideration of other non-symmetrical loading conditions in a future study. Note that the weld strength evaluation requires the determination of weld throat stress at the critical failure locations, which are situated at the RHS corners in this case. Therefore, in order to use Eq. (4.6) to compute the maximum weld throat shear stress in the RHS connections, a closed-form expression is needed to relate the ratio K to the traction stresses at the locations of $C_b = C_{b,max}$.

To do so, one possible scenario is to simply substitute the size ratio parameter R_b/t_b from the CHS connections with B_b/t_b from the RHS connections into Eq. (4.7), by assuming that the parameters D_b $(= 2R_b)$ and B_b serve as the same size parameter for the HSS. Then, the K parameter obtained from the RHS FE models should have a similar relationship to that observed in the CHS connections. However, this is not the case, as shown in Figure 4.17. There seems no clear correlation between the K ratio and B_b/t_b as a size ratio parameter for the RHS connections.

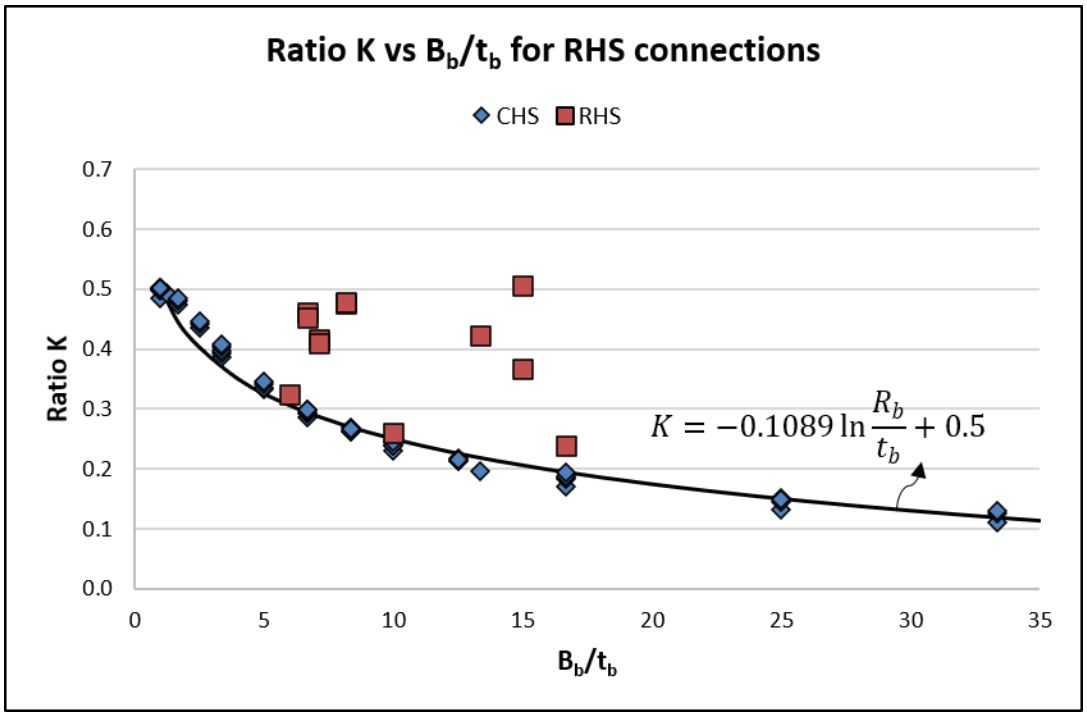

Figure 4.17: Ratio K vs B_b/t_b for RHS connections

Upon further examination on the detailed behavior of K ratio at the RHS corner locations, it is found that the local radius r_c at $C_b = C_{b,max}$ (see Figure 4.11b) must be considered in a dimensionless size ratio parameter (λ_1) defined as:

$$\lambda_1 = \frac{r_c}{t_b} \times \frac{C_{b,min}}{C_{b,max}} \tag{4.9}$$

Note that the CHS connections have constant r_c and C_b (both equal to R_b). Then, Eq. (4.9) becomes simply $\lambda_1 = R_b/t_b$, which is the same parameter used in Eq. (4.7) for CHS connections. Therefore, a generalized closed-form logarithmic equation can be developed in terms of the parameter λ_1 for ratio K calculation for both CHS and RHS connections, as expressed in Eq. (4.10), by which an excellent correlation of FEA results can be demonstrated in Figure 4.18. It is certainly plausible that other parameters such as weld size s may also have some effects on ratio K, which can be argued as higher order effects and assumed negligible in this study.

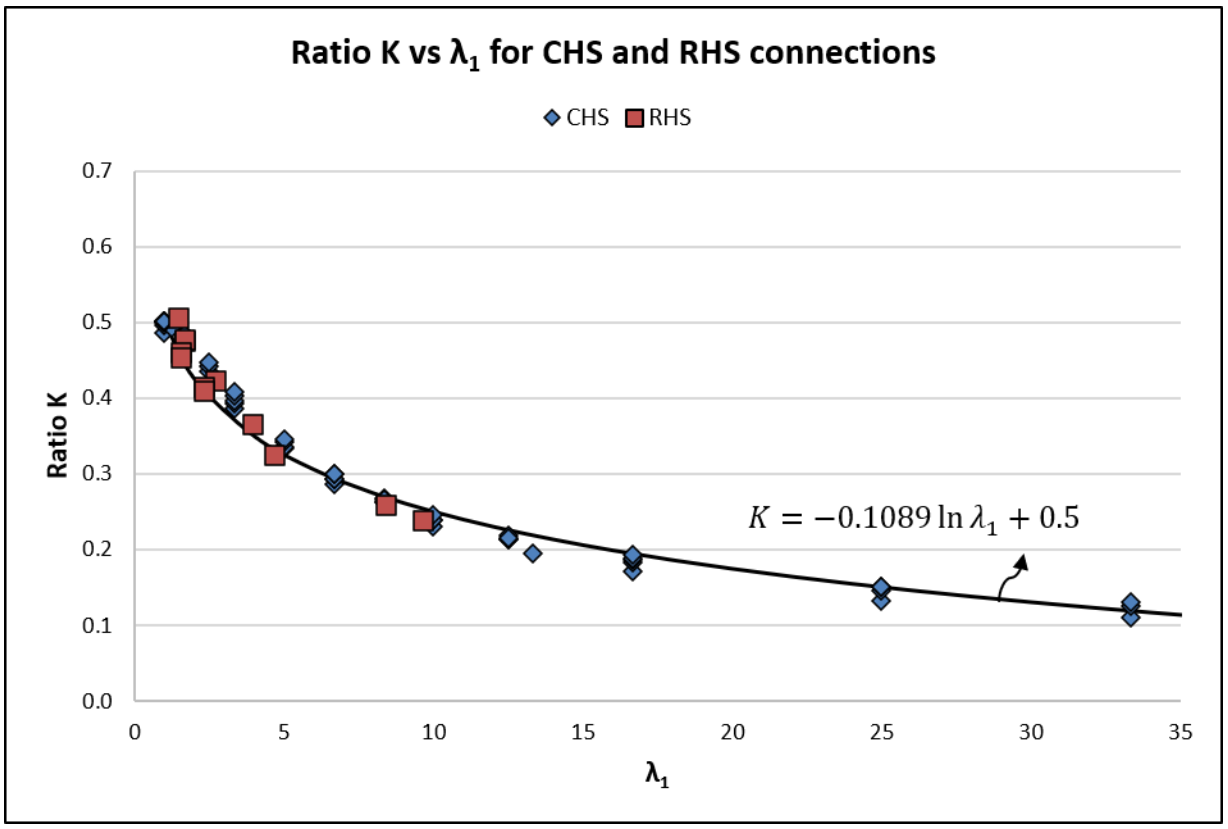

Figure 4.18: Correlation of ratio K vs λ_1 for both CHS and RHS connections by Eq. (4.10)

$$K = -0.1089 \ln \lambda_1 + 0.5 \tag{4.10}$$

Encouraged by the development shown in Figure 4.18, a similar parametric study is performed to examine the shear traction stress at the 0° weld throat plane, i.e., $\tau_{Tm}(0)$, to complete the development of the closed-form expression for weld shear strength calculation. Again, only the critical failure locations (RHS corners) are of interest here. Taken from the ratio K calculations, the first parameter investigated is the local radius at the RHS corners, i.e., r_c/t_b. It can be seen that the normalized shear stress $\tau_{Tm}(0)\ /\tau_n$ reduces when r_c/t_b increases, but exhibits a significant scatter as shown in Figure 4.19. The results in Figure 4.19 suggest that other dimensional parameters need to be considered.

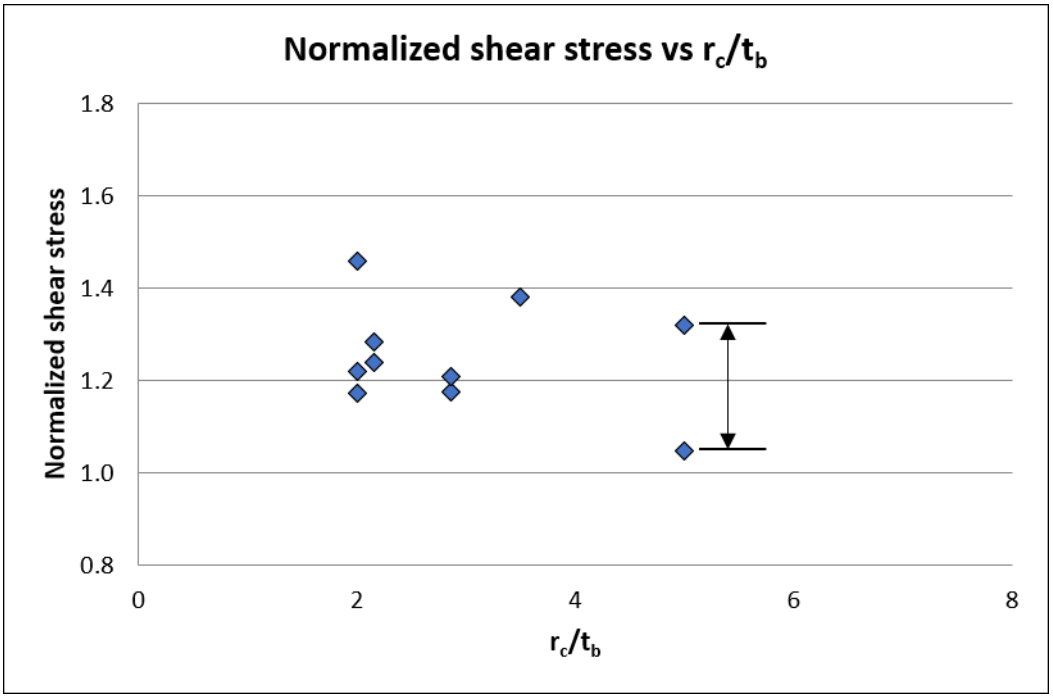

Figure 4.19: Normalized shear stress at 0° weld throat plane vs local radius effect for RHS

One such a parameter can be defined as the ratio of the maximum distance from the fillet weld toe to the cross-section centroid and the cross-section plate thickness, i.e., $C_{b,max}/t_b$, as shown in Figure 4.11. The normalized shear stress $\tau_{Tm}(0)\ /\tau_n$ has higher values when the RHS connection has larger $C_{b,max}/t_b$ at the section corner, as shown in Figure 4.20.

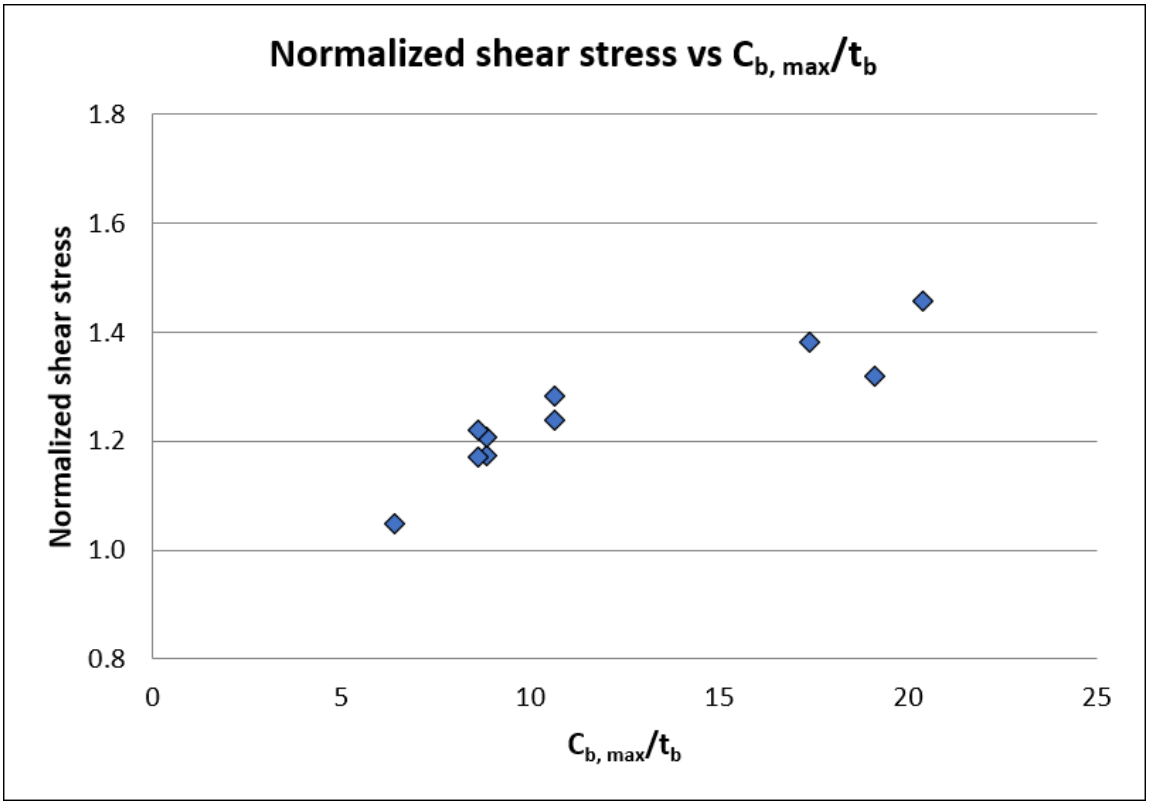

Figure 4.20: Normalized shear stress at 0° weld throat plane vs $C_{b,max}/t_b$ for RHS

The two parameters, r_c/t_b and $C_{b,max}/t_b$, have the opposite effect on $\tau_{Tm}(0)$ at the RHS corners. Therefore, a combination of the two could potentially provide a further improved correlation. Indeed, an excellent correlation of $\tau_{Tm}(0)$ can be obtained, as demonstrated in Figure 4.21, where the dimensionless parameter λ_2 as expressed in Eq. (4.11) is used. The corresponding linear relationship between $\tau_{Tm}(0)\ /\tau_n$ and λ_2 can be expressed in Eq. (4.12).

$$\lambda_2 = \frac{C_{b,max} - r_c}{t_b} \tag{4.11}$$

$$\frac{\tau_{Tm}(0)}{\tau_n} = 0.0225 \times \lambda_2 + 1.0 \tag{4.12}$$

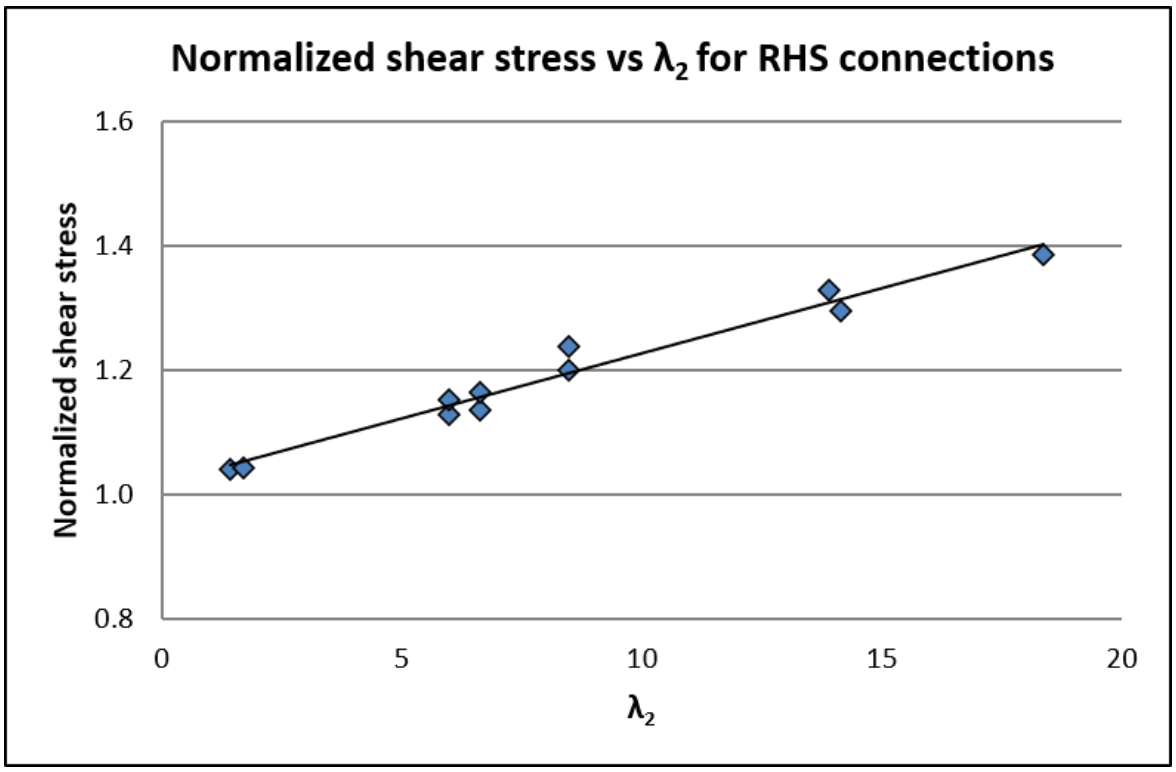

Figure 4.21: Normalized shear stress at 0° weld throat plane vs λ_2 for RHS

A number of points are worth noting: (1) other parameters besides λ_2 such as weld size effect are considered to be higher order and negligible in the above development; (2) parameter λ_2 is equal to 0 for the CHS connections ($C_{b,max} = r_c$), leading to $\tau_{Tm}(0)/\tau_n = 1.0$ according to Eq. (4.12) as its lower bound, meaning that traction stress is uniformly distributed along weld in CHS, which is in a good agreement with both the testing observations and FEA results (see Figure 4.13). Therefore, similar to λ_1 and Eq. (4.10), both the parameter λ_2 and the closed-form expression given by Eq. (4.12) possess a sufficient degree of generality and are applicable to both CHS and RHS connections.

Finally, by placing Eqs. (4.10) and (4.12) into Eq. (4.6), the resulting closed-form expression is given in Eq. (4.13), which can be used to calculate the maximum weld throat shear stress ($\tau_{u,w}$) at the critical locations in either CHS-to-plate or RHS-to-plate structural joints under

remote load P_u or to determine the minimum weld size s required if weld shear strength $\tau_{u,w}$ is given.

$$\tau_{u,w} = \frac{P_u}{s \times L} \times (0.0225 \times \lambda_2 + 1.0) \times \{\cos\theta_{max} - (-0.1089 \ln \lambda_1 + 0.5) \times \sin\theta_{max}\} \times (\cos\theta_{max} + \sin\theta_{max}) \quad (4.13)$$

$$\theta_{max} = \frac{1}{2} \times \tan^{-1}\left(\frac{0.5 + 0.1089 \ln \lambda_1}{1.5 - 0.1089 \ln \lambda_1}\right)$$

in which L represents the total weld length carrying load.

4.4.2 Weld Effective Length in HSS-to-HSS Joints

To take full advantages of the analytical expression given in Eq. (4.13), weld length L needs to be estimated for HSS-to-HSS welded joints, in which weld landing surface flexibility of the chord member (see Figure 4.10b) has been shown to have a major effect on weld stress state (Packer & Cassidy, 1995). Based on our evaluations of available methods, the authors of this study propose to adopt "Weld Effective Lengths Method" used in AISC 360 (2010) for HSS-to-HSS joints. The weld effective lengths method (WELM), which had been first recommended by Frater & Packer (1992a, 1992b) and Packer & Cassidy (1995), is adopted by AISC 360 (2010) for taking account of the weld landing surface flexibility effect in weld design for various HSS-to-HSS connections. According to Packer and Henderson (1997), the effective load-carrying weld length, L_e, can be calculated by Eq. (4.14) for the HSS-to-HSS joints:

$$L_e = \frac{2B_b}{\sin\alpha} \quad (4.14)$$

Replacing the measured weld length L in Eq. (4.13) by the effective weld length L_e in Eq. (4.14), Eq. (4.15) can be derived to calculate the maximum weld throat stress at the critical locations for HSS-to-HSS joints.

$$\tau_{u,w} = \frac{P_u}{s \times L_e} \times (0.0225 \times \lambda_2 + 1.0) \times \{\cos\theta_{max} - (-0.1089 \ln \lambda_1 + 0.5) \times \sin\theta_{max}\} \times (\cos\theta_{max} + \sin\theta_{max}) \quad (4.15)$$

$$\theta_{max} = \frac{1}{2} \times \tan^{-1}\left(\frac{0.5 + 0.1089 \ln \lambda_1}{1.5 - 0.1089 \ln \lambda_1}\right)$$

4.4.3 Ultimate Load Capacity Estimation

To validate the FEA results from the above sections, the estimated ultimate load capacity ($P_{n,w}$) of the fillet welded HSS connections obtained from the generalized closed-form equations, i.e., Eq. (4.13) for HSS-to-rigid-plate joints and Eq. (4.15) for HSS-to-HSS joints, are compared to the actual failure loads (P_u) obtained from the weld strength tests. In addition, Eqs. (4.13) and (4.15) are compared to the traditional weld strength equations from the existing design specifications, such as AISC 360 (AISC, 2010), CSA S16 (CSA, 2014), and Eurocode 3 (CEN, 2005), to demonstrate how much improvement they can provide. Note that the derivations of the traditional weld strength equations can be found in the corresponding design specifications, thus will not be demonstrated in this section due to space limit.

The test results of the CHS and RHS connections evaluated in this section are obtained from the studies of Frater (1986), Packer and Cassidy (1995), Oatway (2014), and Tousignant (2017), which attain various combinations of geometric properties (such as plate thickness and cross section profile) and material properties (such as yield strength f_{ys} and ultimate strength f_{uts}) designed specifically for weld connection failure, as summarized in Table 4.1 and Table 4.2, respectively.

Table 4.1: Geometric properties of HSS-to-plate and HSS-to-HSS connections

No.	**Type**	D **or** B **mm**	D_b **or** B_b **mm**	t **mm**	t_b **mm**	s **mm**	$C_{b,max}$ **mm**	r_c **mm**	P_u **kN**

1	RHS to Plate	N/A	127.0	25.0	7.78	5.12	83.22	15.88	831
2	RHS to Plate	N/A	127.0	25.0	7.78	8.37	83.22	15.88	1166
3	RHS to Plate	N/A	127.0	25.0	7.78	7.49	83.22	15.88	1235
4	RHS to Plate	N/A	127.0	25.0	7.78	8.28	83.22	15.88	1311
5	RHS to Plate	N/A	177.8	25.0	12.53	9.03	111.23	35.00	2433
6	RHS to Plate	N/A	177.8	25.0	12.53	12.29	111.23	35.00	2574
7	RHS to Plate	N/A	177.8	25.0	12.53	9.96	111.23	35.00	2525
8	RHS to Plate	N/A	177.8	25.0	12.53	10.27	111.23	35.00	2302
9	RHS to Plate	N/A	127.6	19.0	9.54	6.10	82.32	19.08	1020
10	RHS to Plate	N/A	127.6	19.0	9.54	5.25	82.32	19.08	960
11	RHS to Plate	N/A	127.6	19.0	9.54	4.85	82.32	19.08	840
12	RHS to Plate	N/A	127.6	19.0	9.54	6.75	82.32	19.08	1140
13	CHS to Plate	N/A	167.9	25.0	6.70	6.82	83.95	83.95	1261
14	CHS to Plate	N/A	167.9	25.0	6.70	9.39	83.95	83.95	1279
15	CHS to Plate	N/A	127.4	25.0	11.55	9.72	63.70	63.70	1459
16	CHS to Plate	N/A	127.4	25.0	11.55	11.29	63.70	63.70	1597
17	CHS to Plate	N/A	101.0	25.0	7.34	9.04	50.50	50.50	841
18	CHS to Plate	N/A	101.0	25.0	7.34	8.76	50.50	50.50	864
19	RHS to RHS	253.8	126.9	12.08	12.20	5.96	80.66	21.90	527
20	RHS to RHS	253.8	126.9	12.08	12.20	7.04	80.66	21.90	687
21	RHS to RHS	253.8	203.0	12.08	12.05	5.28	134.13	22.72	907
22	RHS to RHS	253.8	203.0	12.08	12.05	6.86	134.13	22.72	868

Table 4.2: Mechanical properties of HSS-to-plate and HSS-to-HSS connections

No.	**Type**	**Plate or HSS Chord**			**HSS Branch**			**As-laid Weld**		
		f_{ys} **MPa**	f_{uts} **MPa**	ε_{rup} **-**	$f_{ys,b}$ **MPa**	$f_{uts,b}$ **MPa**	$\varepsilon_{rup,b}$ **-**	$f_{ys,w}$ **MPa**	$f_{uts,w}$ **MPa**	$\varepsilon_{rup,w}$ **-**
1	RHS to Plate	383	563	0.24	412	478	0.33	563	619	0.28
2	RHS to Plate	383	563	0.24	412	478	0.33	563	619	0.28
3	RHS to Plate	383	563	0.24	412	478	0.33	563	619	0.28
4	RHS to Plate	383	563	0.24	412	478	0.33	563	619	0.28

5	RHS to Plate	383	563	0.24	380	489	0.33	563	619	0.28
6	RHS to Plate	383	563	0.24	380	489	0.33	563	619	0.28
7	RHS to Plate	383	563	0.24	380	489	0.33	563	619	0.28
8	RHS to Plate	383	563	0.24	380	489	0.33	563	619	0.28
9	RHS to Plate	351	558	0.36	426	500	N/A	634	687	0.24
10	RHS to Plate	351	558	0.36	426	500	N/A	634	687	0.24
11	RHS to Plate	351	558	0.36	426	500	N/A	634	687	0.24
12	RHS to Plate	351	558	0.36	426	500	N/A	641	739	0.24
13	CHS to Plate	409	566	0.24	421	501	0.31	501	571	0.26
14	CHS to Plate	409	566	0.24	421	501	0.31	501	571	0.26
15	CHS to Plate	409	566	0.24	431	488	0.35	501	571	0.26
16	CHS to Plate	409	566	0.24	431	488	0.35	501	571	0.26
17	CHS to Plate	409	566	0.24	385	450	0.35	501	571	0.26
18	CHS to Plate	409	566	0.24	385	450	0.35	501	571	0.26
19	RHS to RHS	410	-	-	545	-	-	471	574	0.30
20	RHS to RHS	410	-	-	545	-	-	471	574	0.30
21	RHS to RHS	410	-	-	445	-	-	471	574	0.30
22	RHS to RHS	410	-	-	445	-	-	471	574	0.30

4.4.3.1 AISC without Directional Strength-Increase Factor

Eq. (4.16), derived based on engineering shear stress (Eq. (4.1)), is used in AISC 360 (AISC, 2010) for calculating nominal load capacity ($P_{n,w}$) of fillet welds, in which the weld shear strength is set as $\tau_{u,w} = 0.60 \times f_{uts,w}$.

$$P_{n,w} = 0.60 \times f_{uts,w} \times (0.7071 \times s \times L), \text{ for HSS-to-plate}$$
$$P_{n,w} = 0.60 \times f_{uts,w} \times (0.7071 \times s \times L_e), \text{ for HSS-to-HSS} \quad (4.16)$$

The load capacity correlations between the AISC 360 (AISC, 2010) nominal value and test results are summarized in Figure 4.22. It clearly shows that the predicted nominal loads poorly fit the test data with coefficient of determination $R^2 = 0.58$ and they are consistently under-predicted

by as much as 47% without even adding the design safety factor ($\phi = 0.75$) into consideration. Therefore, following AISC (AISC, 2010) will cause the HSS connections severely over-welded.

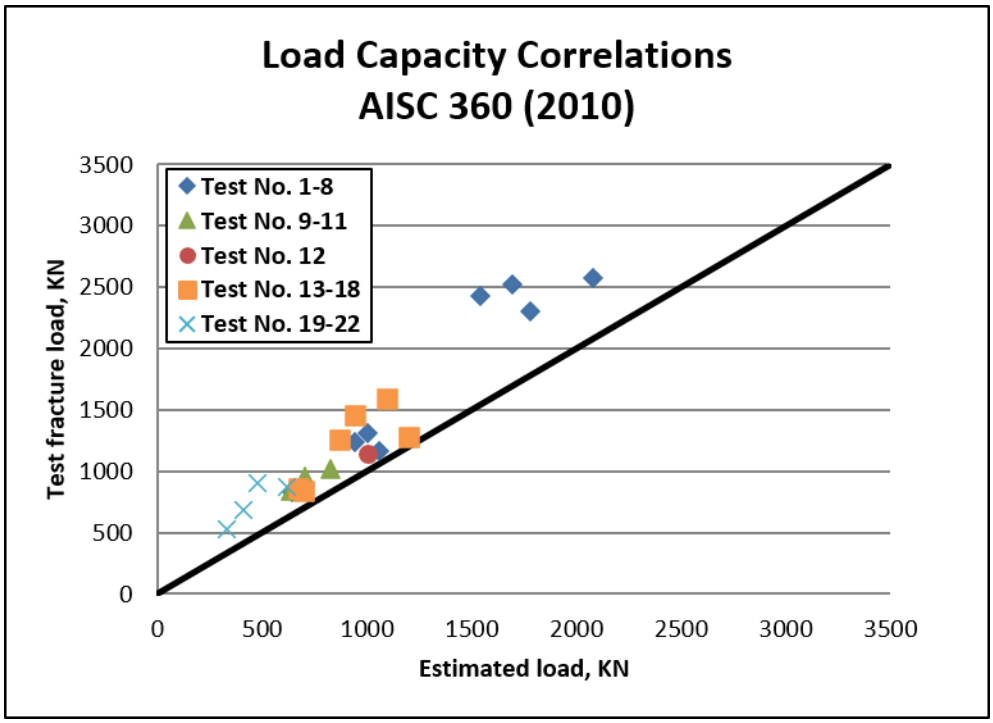

Figure 4.22: Load capacity correlations between test results and AISC

4.4.3.2 CSA and AISC with Directional Strength-Increase Factor

Alternatively, both AISC 360 (AISC, 2010) and CSA S16 (CSA, 2014) permits the use of directional strength-increase factor for the calculation of the nominal load capacity, as shown in Eq. (4.17) and Eq. (4.18), respectively. Note that the weld shear strength is assumed as $\tau_{u,w} = 0.67 \times f_{uts,w}$ in CSA S16 (CSA, 2014).

$$\begin{aligned} P_{n,w} &= 0.60 f_{uts,w}(0.7071 \times s \times L) \times (1.0 + 0.50 \sin^{1.5} \alpha), \text{ for HSS-to-plate} \\ P_{n,w} &= 0.60 f_{uts,w}(0.7071 \times s \times L_e) \times (1.0 + 0.50 \sin^{1.5} \alpha), \text{ for HSS-to-HSS} \end{aligned} \quad (4.17)$$

$$\begin{aligned} P_{n,w} &= 0.67 f_{uts,w}(0.7071 \times s \times L) \times (1.0 + 0.50 \sin^{1.5} \alpha), \text{ for HSS-to-plate} \\ P_{n,w} &= 0.67 f_{uts,w}(0.7071 \times s \times L_e) \times (1.0 + 0.50 \sin^{1.5} \alpha), \text{ for HSS-to-HSS} \end{aligned} \quad (4.18)$$

The correlation results of the equations above are shown in Figure 4.23 and Figure 4.24, respectively, where load capacities are consistently over-estimated. The over-estimation will lead

to insufficient weld size causing immature connection fracture, and therefore should not be accepted for design safety perspective.

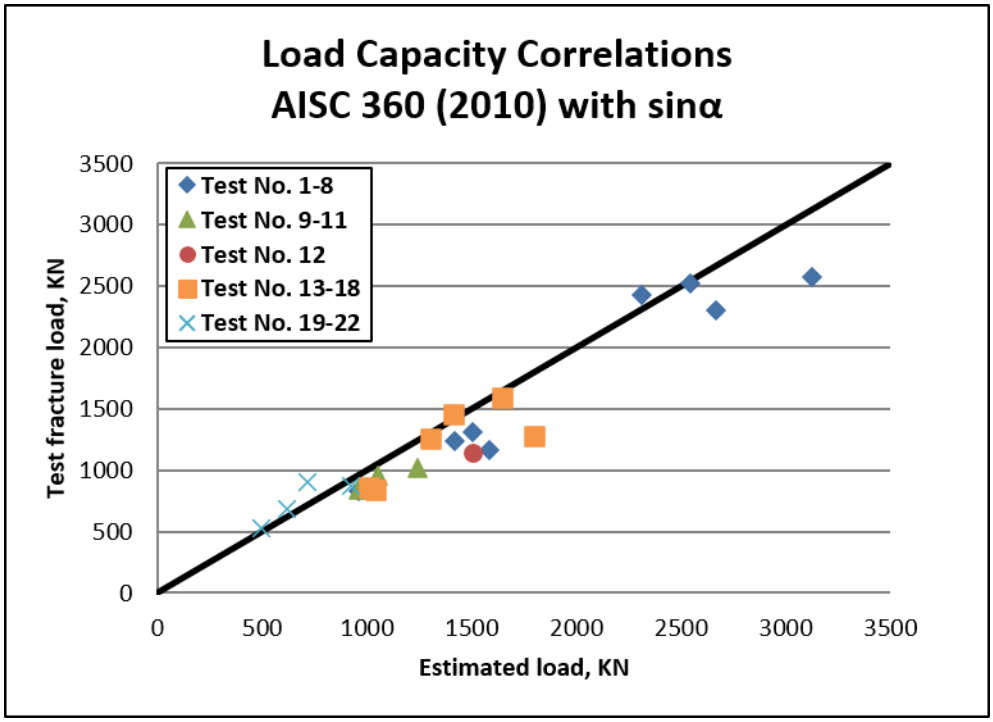

Figure 4.23: Load capacity correlations between test results and AISC with directional strength-increase factor

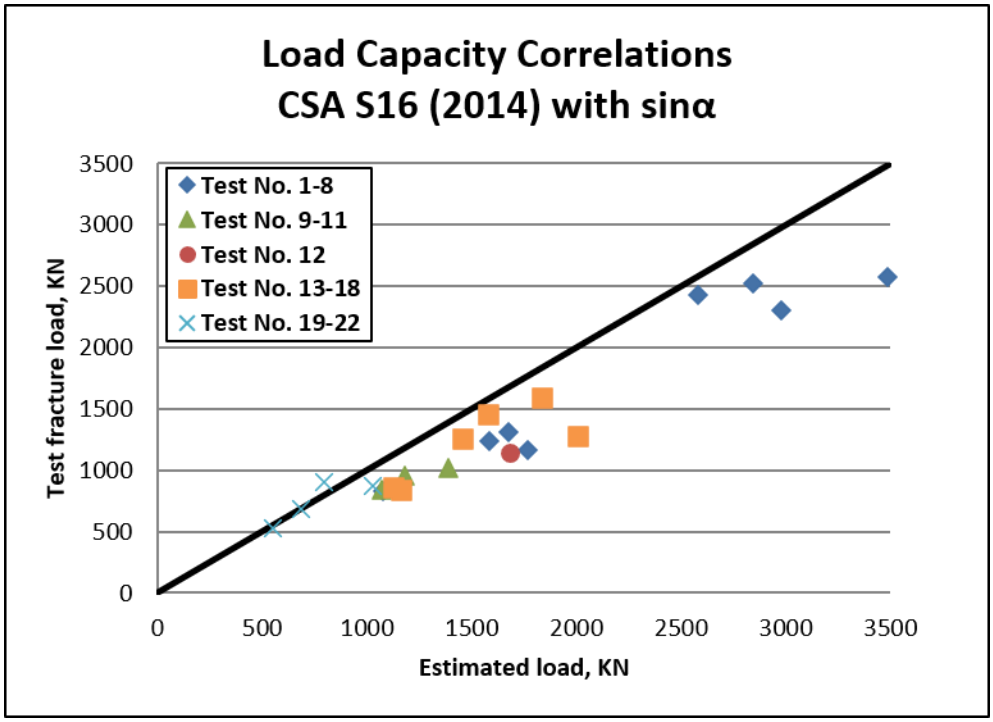

Figure 4.24: Load capacity correlations between test results and CSA with directional strength-increase factor

4.4.3.3 Eurocode 3 CEN 1993-1-8

Following Eurocode 3 (CEN, 2005), the nominal load capacity can be calculated by Eq. (4.19), in which the correlation factor for fillet welds, β_w, is taken as 0.9 according to Eurocode 3 (CEN, 2005).

$$P_{n,w} = \frac{f_{uts,b}}{\beta_w} \times (0.7071 \times s \times L) \text{ , for HSS-to-plate}$$
$$P_{n,w} = \frac{f_{uts,b}}{\beta_w} \times (0.7071 \times s \times L_e) \text{ , for HSS-to-HSS} \quad (4.19)$$

Similar to AISC 360 (AISC, 2010), Figure 4.25 clearly shows that Eurocode 3 also consistently under-predicted the nominal load capacity even before adding the design safety factor into consideration and the coefficient of determination is equal to 0.69 only.

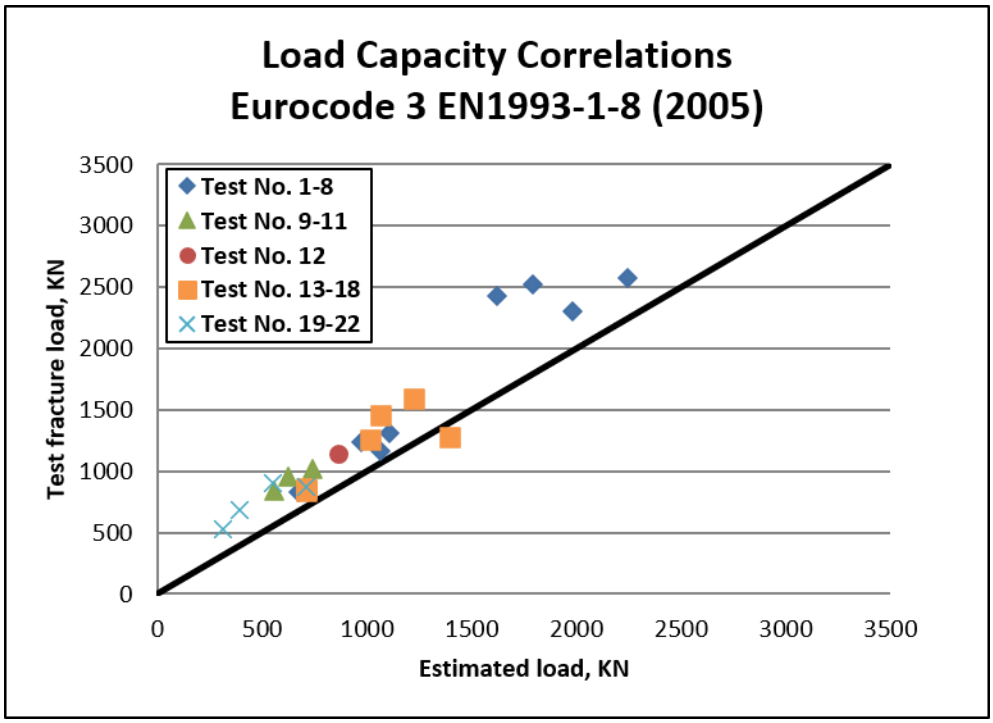

Figure 4.25: Load capacity correlations between test results and Eurocode 3

4.4.3.4 TSM Estimated Load Capacity

Above all, the traditional weld failure criteria do not provide good load capacity correlations between the estimated and test results. To improve the situation, authors in this study

follow the traction stress based weld strength criterion, take the FEA results into account, and convert the generalized weld strength equation (i.e., Eqs. (4.13) & (4.15)) to Eq. (4.20) or Eq. (4.21) for calculating HSS joints' nominal load capacity, in which the nominal weld shear strength is taken as 60% or 67% of its ultimate tensile strength (UTS) carried over from AISC 360 (AISC, 2010) or CSA S16 (CSA, 2014) respectively. Note that θ_{max} is a function of the parameter λ_1 (see Eq. (4.13)).

$$P_{n,w} = \frac{0.60 \times f_{uts,w} \times s \times L}{(0.0225 \times \lambda_2 + 1.0)} \times \frac{1}{\{\cos\theta_{max} - (-0.1089 \ln \lambda_1 + 0.5) \times \sin\theta_{max}\} \times (\cos\theta_{max} + \sin\theta_{max})}$$

$$P_{n,w} = \frac{0.60 \times f_{uts,w} \times s \times L_e}{(0.0225 \times \lambda_2 + 1.0)} \times \frac{1}{\{\cos\theta_{max} - (-0.1089 \ln \lambda_1 + 0.5) \times \sin\theta_{max}\} \times (\cos\theta_{max} + \sin\theta_{max})} \quad (4.20)$$

$$P_{n,w} = \frac{0.67 \times f_{uts,w} \times s \times L}{(0.0225 \times \lambda_2 + 1.0)} \times \frac{1}{\{\cos\theta_{max} - (-0.1089 \ln \lambda_1 + 0.5) \times \sin\theta_{max}\} \times (\cos\theta_{max} + \sin\theta_{max})}$$

$$P_{n,w} = \frac{0.67 \times f_{uts,w} \times s \times L_e}{(0.0225 \times \lambda_2 + 1.0)} \times \frac{1}{\{\cos\theta_{max} - (-0.1089 \ln \lambda_1 + 0.5) \times \sin\theta_{max}\} \times (\cos\theta_{max} + \sin\theta_{max})} \quad (4.21)$$

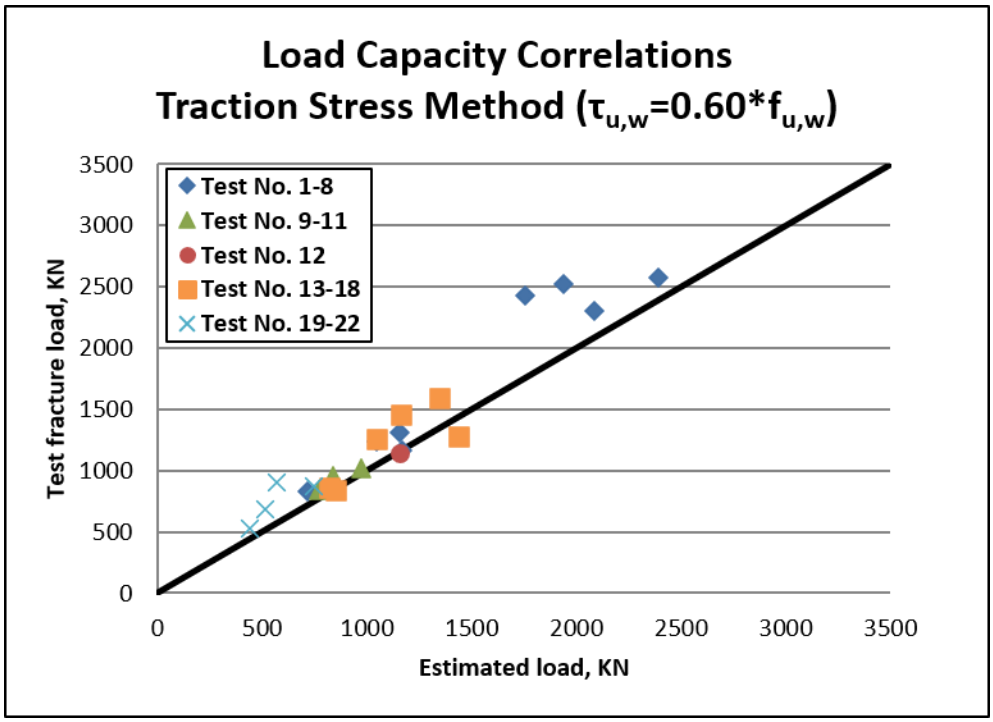

(a)

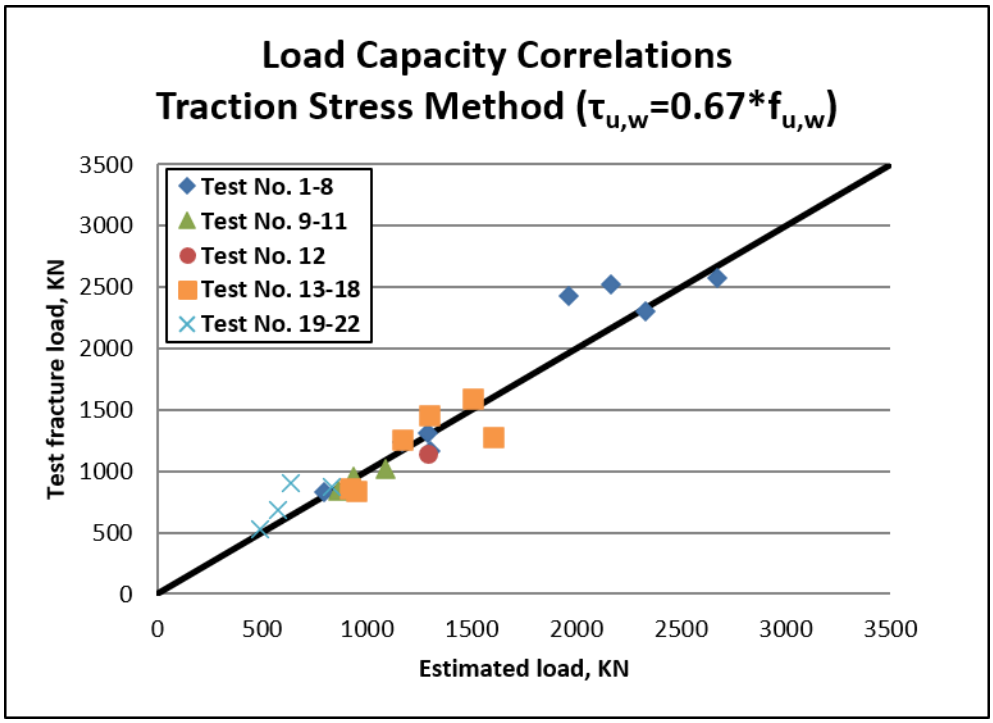

(b)

Figure 4.26: Load capacity correlations between test results and TSM: (a) Nominal weld shear strength is set to 60% of its tested ultimate tensile strength; (b) Nominal weld shear strength is set to 67% of its tested ultimate tensile strength

The load correlation results are present in Figure 4.26. By setting the nominal weld shear strength to 60% (Figure 4.26a) and 67% (Figure 4.26b) of the tested UTS, the coefficient of determination R^2 is increased from 0.58 obtained from AISC 360 to 0.87 and 0.92 obtained from Eq. (4.20) and Eq. (4.21), respectively. The load correlation improvement by TSM is as much as 60% compared to the traditional weld failure criteria, which can significantly reduce the design fillet weld size for the lightweight HSS connections.

4.4.4 Weld Sizing Criterion

The proposed weld sizing criterion for the HSS connections, as expressed in Eq. (4.22), is derived from both the traction stress method approach and the FEA study as described in the previous sections.

$$\frac{s}{t_b} = \frac{f_{uts,b}}{\tau_{u,w}} \times (0.0225 \times \lambda_2 + 1.0) \times (\cos\theta_{max} + \sin\theta_{max}) \times \{\cos\theta_{max} - (-0.1089 \ln\lambda_1 + 0.5) \times \sin\theta_{max}\} \quad (4.22)$$

The weld sizing comparison for the HSS joints tested in the studies of Frater (1986), Packer and Cassidy (1995), Oatway (2014), and Tousignant (2017) shows that Eq. (4.22) can provide a weld size reduction up to about 23% compared to Eq. (4.2), as shown in Table 4.3.

Table 4.3: Weld size reduction from Eq. (4.2) by Eq. (4.22)

No.	Type	D or B mm	D_b or B_b mm	t mm	t_b mm	$C_{b,max}$ mm	r_c mm	Weld size reduction, %
1	RHS to Plate	N/A	127.0	25.0	7.78	83.22	15.88	11%
2	RHS to Plate	N/A	177.8	25.0	12.53	111.23	35.00	15%
3	RHS to Plate	N/A	127.6	19.0	9.54	82.32	19.08	15%
4	CHS to Plate	N/A	167.9	25.0	6.70	83.95	83.95	21%
5	CHS to Plate	N/A	127.4	25.0	11.55	63.70	63.70	23%
6	CHS to Plate	N/A	101.0	25.0	7.34	50.50	50.50	23%

7	RHS to RHS	253.8	126.9	12.08	12.20	80.66	21.90	18%
8	RHS to RHS	253.8	203.0	12.08	12.05	134.13	22.72	10%

4.5 Conclusions

The major conclusions and key findings of this chapter are summarized as follows:

1. A closed-form expression (Eq. (4.13)) with a clear mechanics underpinning has been developed to relate weld throat stress to weld size and remote loading for CHS and RHS structural joints, which can be conveniently used to estimate load capacity under a given weld shear strength or perform quantitative weld sizing under a specified remote load.
2. Ultimate load capacity correlations of available CHS and RHS test data show that the proposed method provides up to about 60% improvement over existing methods in Codes and Standards.
3. With the proposed weld sizing criterion given in Eq. (4.22), the results show that a reduction of weld size can be as much as about 23% from those determined by using existing weld sizing criteria, which can be very beneficial for control of welding-induced distortions in construction of thin-wall HSS structures.

Chapter 5 Discussion

A traction stress based analytical shear strength model for load-carrying fillet-welded connections has been proposed in Chapter 2 and is further completed by incorporating nonlinear effects in Chapter 3. Its effectiveness has been proven through the great correlation of both shear strength and failure angle between the analytical and test results obtained from a comprehensive test program of standard fillet-welded longitudinal and transverse shear specimens made of steel. In Chapter 4, the structural-level application of the analytical shear strength model has been demonstrated by successfully correlating the predicted failure load and those measured from test data of large-scale steel hollow structural section connections available from literature. Note that all the theoretical developments in the previous chapters are solely dependent on joint geometry and independent of materials. Therefore, it is worth further validating the findings by test data obtained from different materials, such as aluminum alloys and titanium alloys.

In addition, some important factors observed from the test data, such as weld size and weld penetration, are showing effects on the analytical shear strength model and being discussed about how to incorporate them in this chapter.

Finally, a generalized quantitative weld sizing criterion is proposed here and proven effective for a significant weld size reduction without compromising structural safety, which is very beneficial for welding-induced distortion control in the construction of lightweight ship structures.

5.1 Aluminum Alloys

To verify the generality of the proposed theoretical developments with respect to different materials other than steel, a total of 80 standard longitudinal and transverse shear specimens made of aluminum alloys designed and fabricated according to AWS B4.0 (AWS, 2007) (refer to Figure 2.1) have been tested in this study. Major ship hull aluminum grades with matching filler materials and associated welding processes were considered. Nominal fillet weld leg size varied from 1/8" (3 mm) to 3/8" (10 mm). A summary of the tested aluminum alloys specimens used in this study is given in Table 5.1.

Table 5.1: Aluminum alloys shear specimens tested in this study

Specimen Type	Base Material	Welding Process	Filler Material	Base Plate Thickness T_1	Nominal Weld Size s	Number
Longitudinal Shear	AL 6082	GMAW	5183	1" (25 mm)	3/16" (5 mm) – 3/8" (10 mm)	16
	AL 5456	GMAW	5556	0.5" (12 mm) 1" (25 mm)	1/8" (3 mm) – 3/8" (10 mm)	24
Transverse Shear	AL 6082	GMAW	5183	1" (25 mm)	3/16" (3 mm) – 3/8" (10 mm)	16
	AL 5456	GMAW	5556	0.5" (12 mm) 1" (25 mm)	1/8" (3 mm) – 3/8" (10 mm)	24

Shear strength test data are calculated using conventional method (Eq. (1.1)), traction stress method (Eq. (2.7) & Eq. (2.13)), and traction stress method incorporating nonlinear effects (Eq. (3.7) & Eq. (3.8)), respectively, as seen in Figure 5.1 and Figure 5.2. Figure 5.1 shows that: (1) the averaged weld strength discrepancy of AL 5456 (GMAW with 5556 weld wire) is about 14 ksi, i.e., longitudinal shear strength is only about 62% of transverse shear strength when using the traditional AWS shear strength equation; (2) the weld strength correlation is much improved by traction stress method that longitudinal shear strength is about 88% of transverse shear strength; and (3) further reduction of the discrepancy, i.e., unified shear strength, can be achieved by incorporating the nonlinear effects into traction stress method. Similarly, Figure 5.2 shows that the

averaged weld strength discrepancy of AL 6082 (GMAW with 5183 weld wire) is reduced from 35% when using traditional AWS shear strength equation to 12% by traction stress method, and eventually improved down to less than 3% when nonlinear effects are considered in traction stress based shear strength equations (Eqs. (3.7) & (3.8)). The same trend can be observed in the rest of test groups given in Table 5.1 and will be demonstrated in Appendix D.

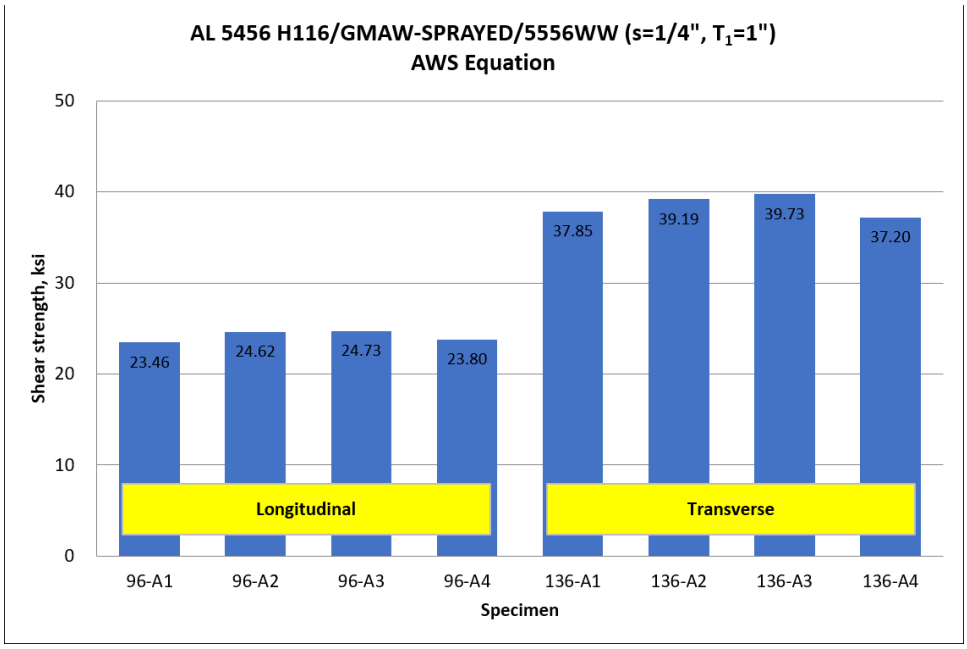

(a)

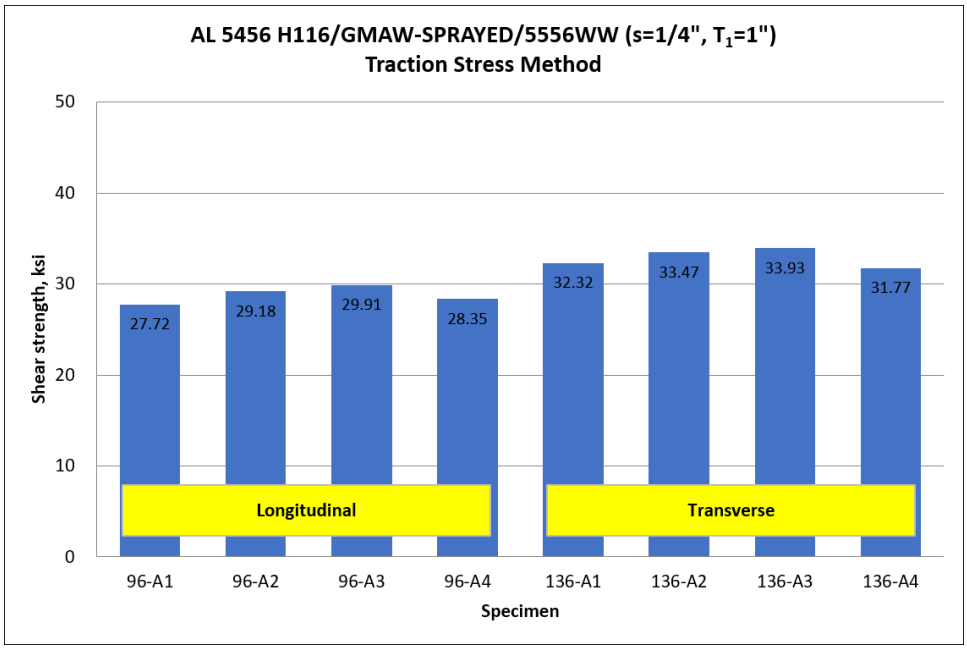

(b)

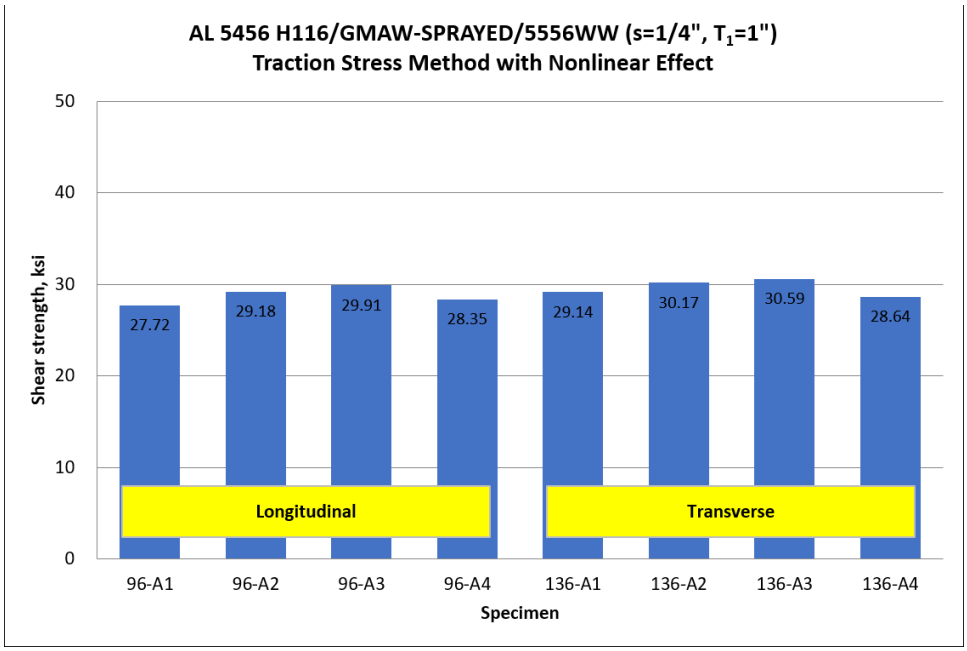

(c)

Figure 5.1: Comparison of shear strengths between longitudinal and transverse shear specimens of AL 5456 with GMAW and 5556 weld wire: (a) AWS traditional equation; (b) traction stress method; (c) traction stress method with nonlinear effects

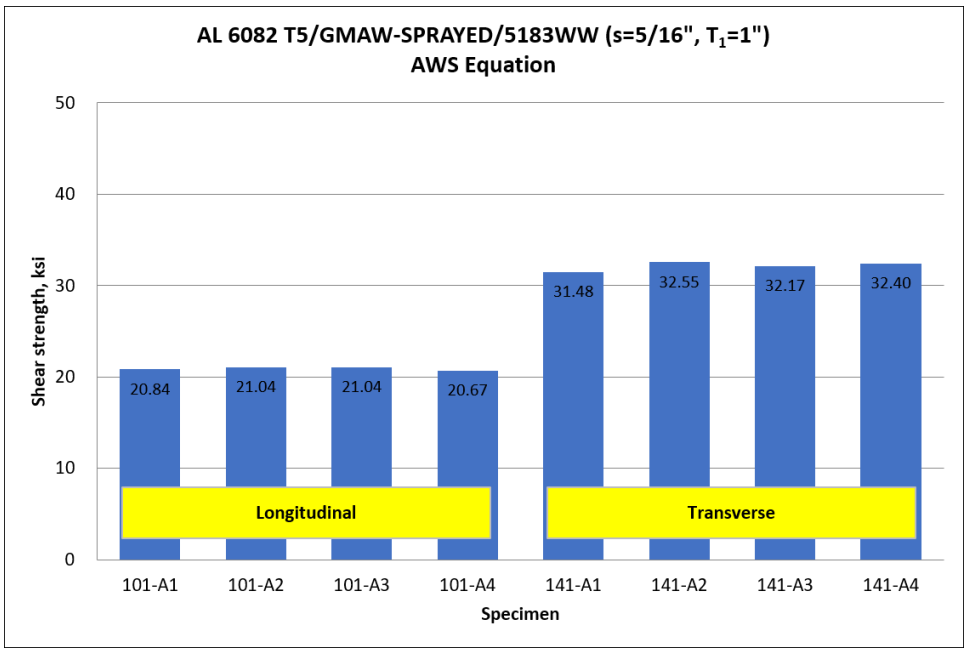

(a)

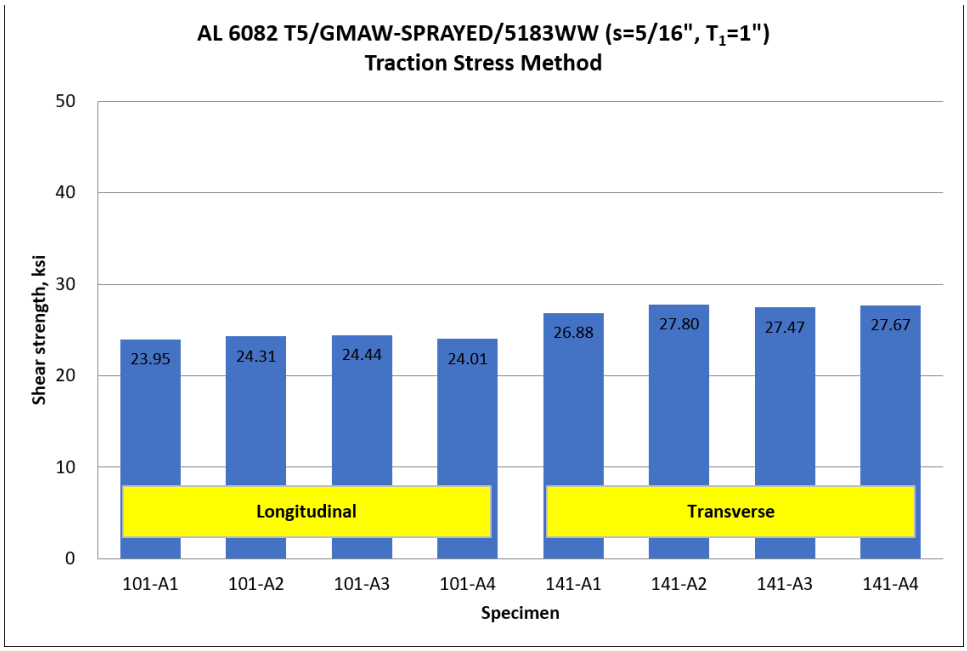

(b)

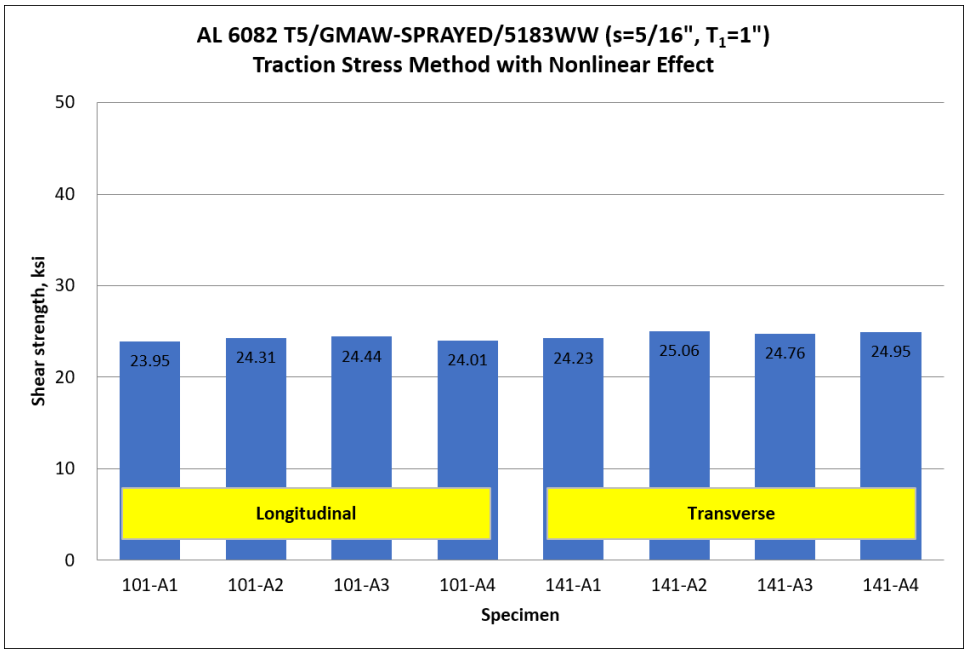

(c)

Figure 5.2: Comparison of shear strengths between longitudinal and transverse shear specimens of AL 6082 with GMAW and 5183 weld wire: (a) AWS traditional equation; (b) traction stress method; (c) traction stress method with nonlinear effects

5.2 Titanium Alloys

To complete the generality verification of the proposed theoretical developments with respect to different materials, a total of 72 standard longitudinal and transverse shear specimens

made of titanium alloys according to AWS B4.0 (AWS, 2007) (refer to Figure 2.1) have been tested in a companion program related to this study. Three major ship hull titanium grades with matching filler materials and two welding processes (GTAW and GMAW) were considered. Nominal fillet weld leg size varied from 1/8” (3 mm) to 3/16” (5 mm). A summary of the tested titanium alloys specimens used in this study is given in Table 5.2.

Table 5.2: Titanium alloys shear specimens tested in this study

Specimen Type	Base Material	Welding Process	Base Plate Thickness T_1	Nominal Weld Sizes	Number
Longitudinal Shear	Ti CP Gr-2	GMAW	0.5" (12 mm)	1/8" (3 mm) – 3/16" (5 mm)	6
		GTAW	0.5" (12 mm)	1/8" (3 mm) – 3/16" (5 mm)	6
	Ti 6-4 Gr-5	GMAW	0.5" (12 mm)	1/8" (3 mm) – 3/16" (5 mm)	6
		GTAW	0.5" (12 mm)	1/8" (3 mm) – 3/16" (5 mm)	6
	Ti 425 Gr-38	GMAW	0.5" (12 mm)	1/8" (3 mm) – 3/16" (5 mm)	6
		GTAW	0.5" (12 mm)	1/8" (3 mm) – 3/16" (5 mm)	6
Transverse Shear	Ti CP Gr-2	GMAW	0.5" (12 mm)	1/8" (3 mm) – 3/16" (5 mm)	6
		GTAW	0.5" (12 mm)	1/8" (3 mm) – 3/16" (5 mm)	6
	Ti 6-4 Gr-5	GMAW	0.5" (12 mm)	1/8" (3 mm) – 3/16" (5 mm)	6
		GTAW	0.5" (12 mm)	1/8" (3 mm) – 3/16" (5 mm)	6
	Ti 425 Gr-38	GMAW	0.5" (12 mm)	1/8" (3 mm) – 3/16" (5 mm)	6
		GTAW	0.5" (12 mm)	1/8" (3 mm) – 3/16" (5 mm)	6

Titanium shear strength test data are calculated using conventional method (Eq. (1.1)), traction stress method (Eq. (2.7) & Eq. (2.13)), and traction stress method incorporating nonlinear effects (Eq. (3.7) & Eq. (3.8)), respectively. Three examples of shear strength comparison are demonstrated in Figure 5.3, Figure 5.4, and Figure 5.5, in which significant shear strength discrepancies as much as about 40% observed in AWS equation are reduced by introducing

traction stress based shear strength definition and unified strength values can be obtained when nonlinear effects are considered for all Ti 6-4, Ti CP and Ti 425 materials. The full test data are shown in Appendix E.

Above all, through these comprehensive static strength testing programs, traction stress based shear strength definition and weld failure criterion have been proven effective among all common materials used in ship structures such as mild steel, high strength steel, aluminum alloys and titanium alloys.

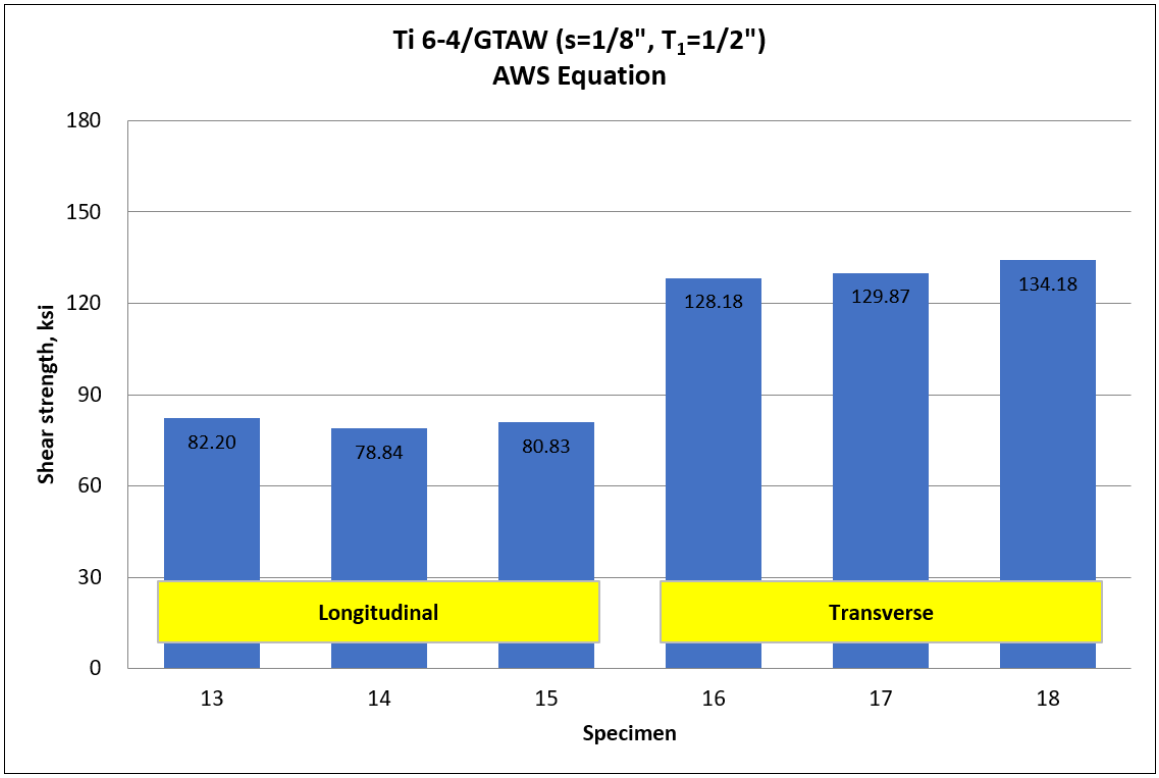

(a)

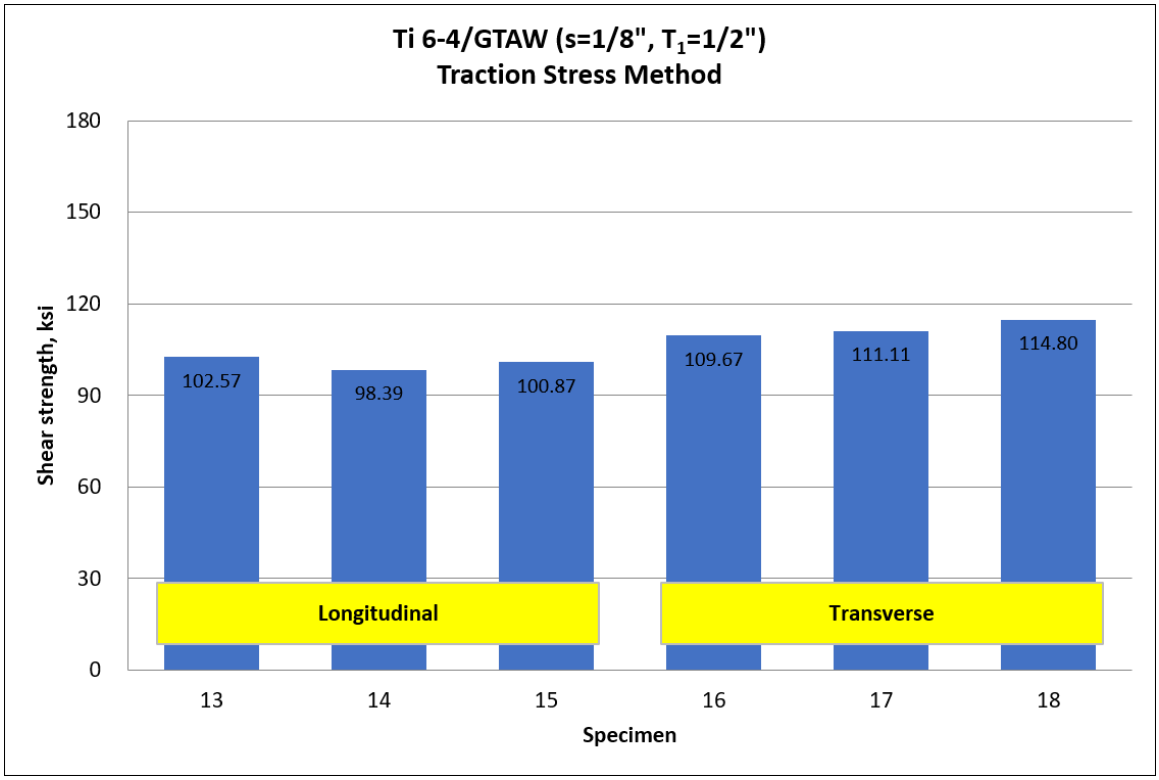

(b)

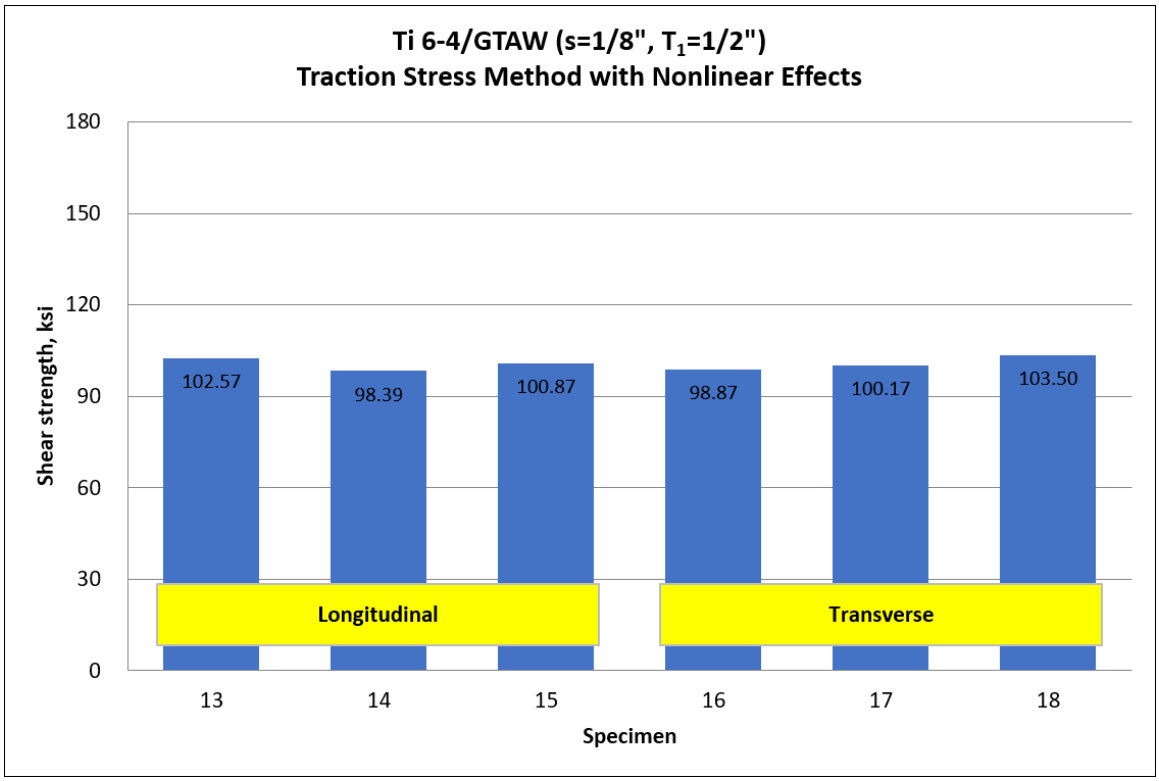

(c)

Figure 5.3: Comparison of shear strengths between longitudinal and transverse shear specimens of Ti 6-4 with GTAW: (a) AWS traditional equation; (b) traction stress method; (c) traction stress method with nonlinear effects

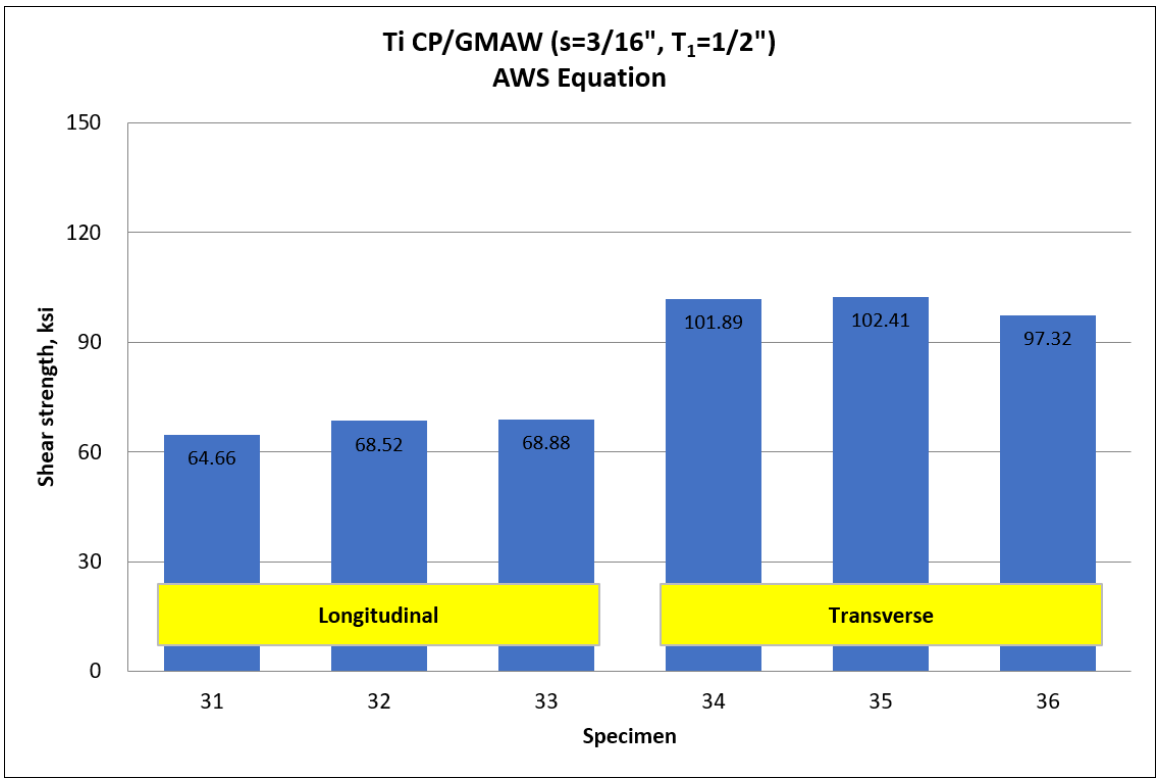
Ti CP/GMAW (s=3/16", T1=1/2")
AWS Equation
Shear strength, ksi
150
120
90
60
30
0
64.66
68.52
68.88
101.89
102.41
97.32
Longitudinal
Transverse
31
32
33
34
35
36
Specimen

(a)

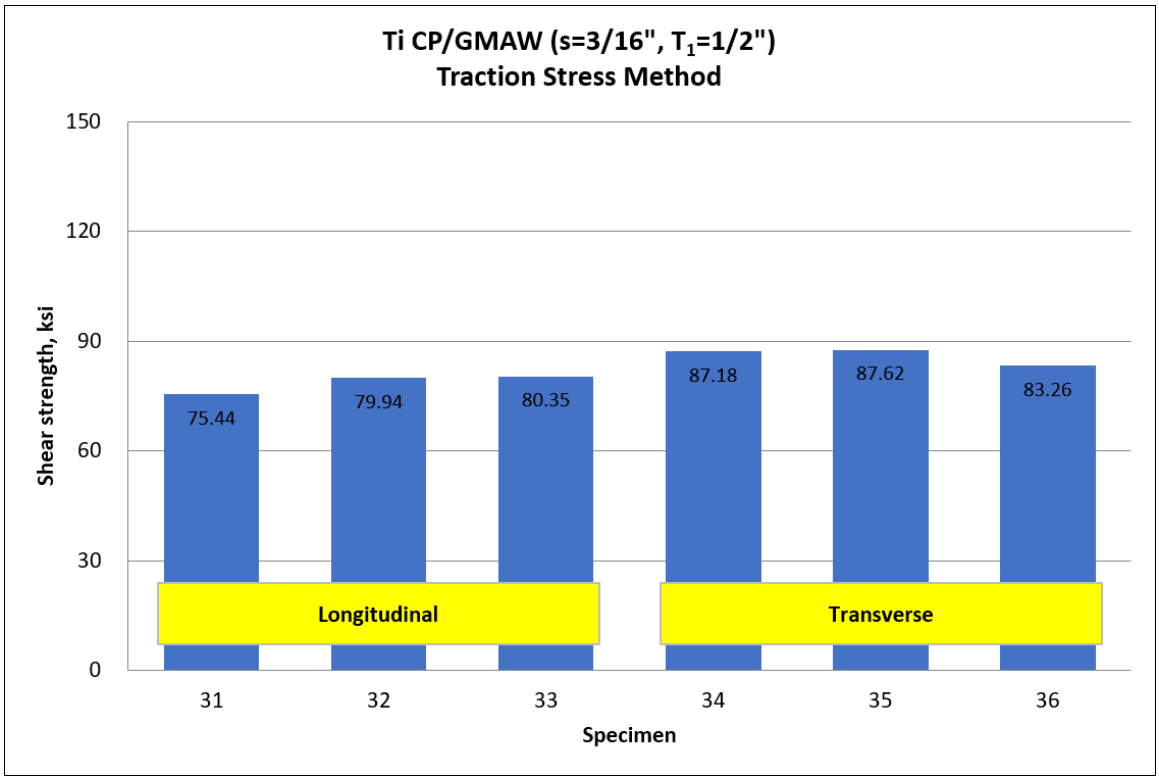
Ti CP/GMAW (s=3/16", T1=1/2")
Traction Stress Method
Shear strength, ksi
150
120
90
60
30
0
75.44
79.94
80.35
87.18
87.62
83.26
Longitudinal
Transverse
31
32
33
34
35
36
Specimen

(b)

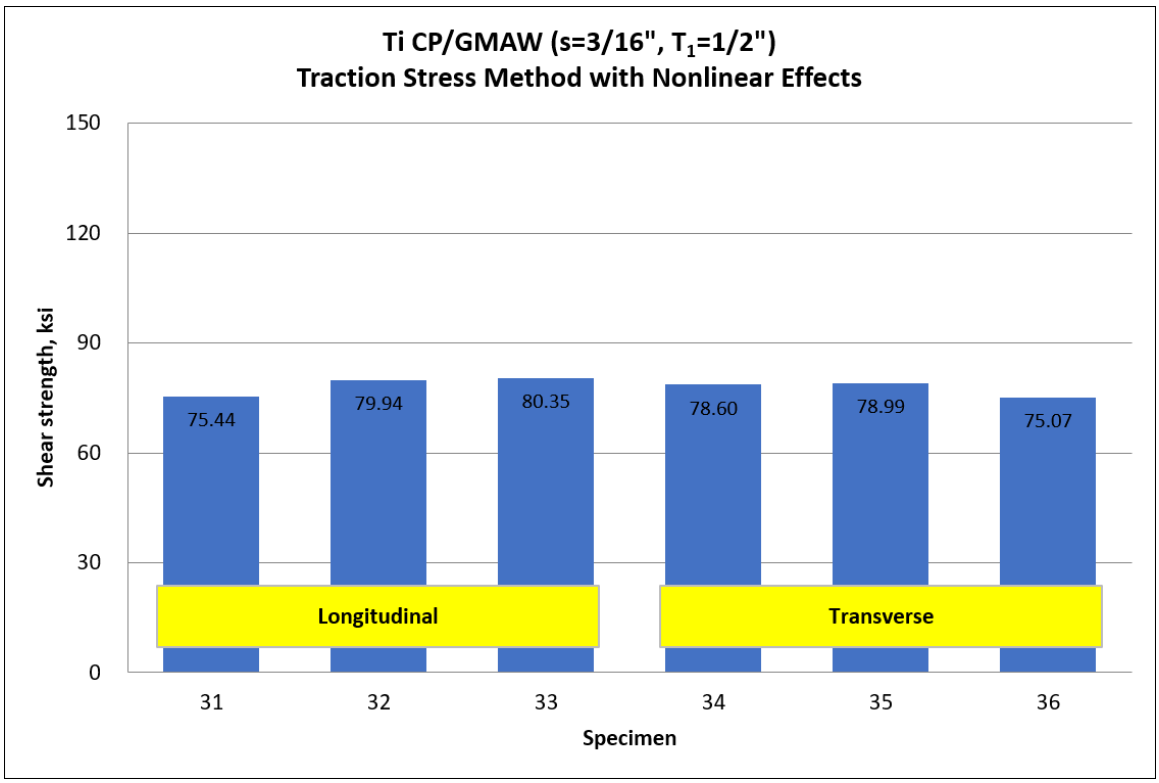

(c)

Figure 5.4: Comparison of shear strengths between longitudinal and transverse shear specimens of Ti CP with GMAW: (a) AWS traditional equation; (b) traction stress method; (c) traction stress method with nonlinear effects

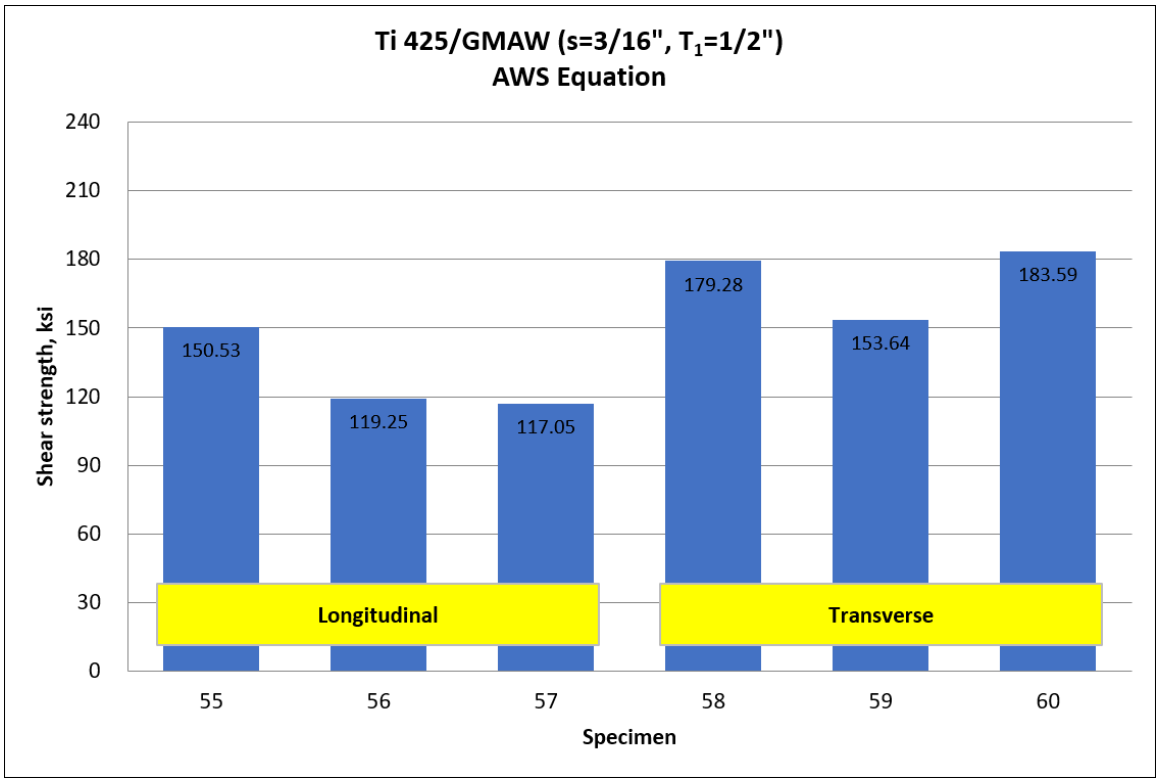

(a)

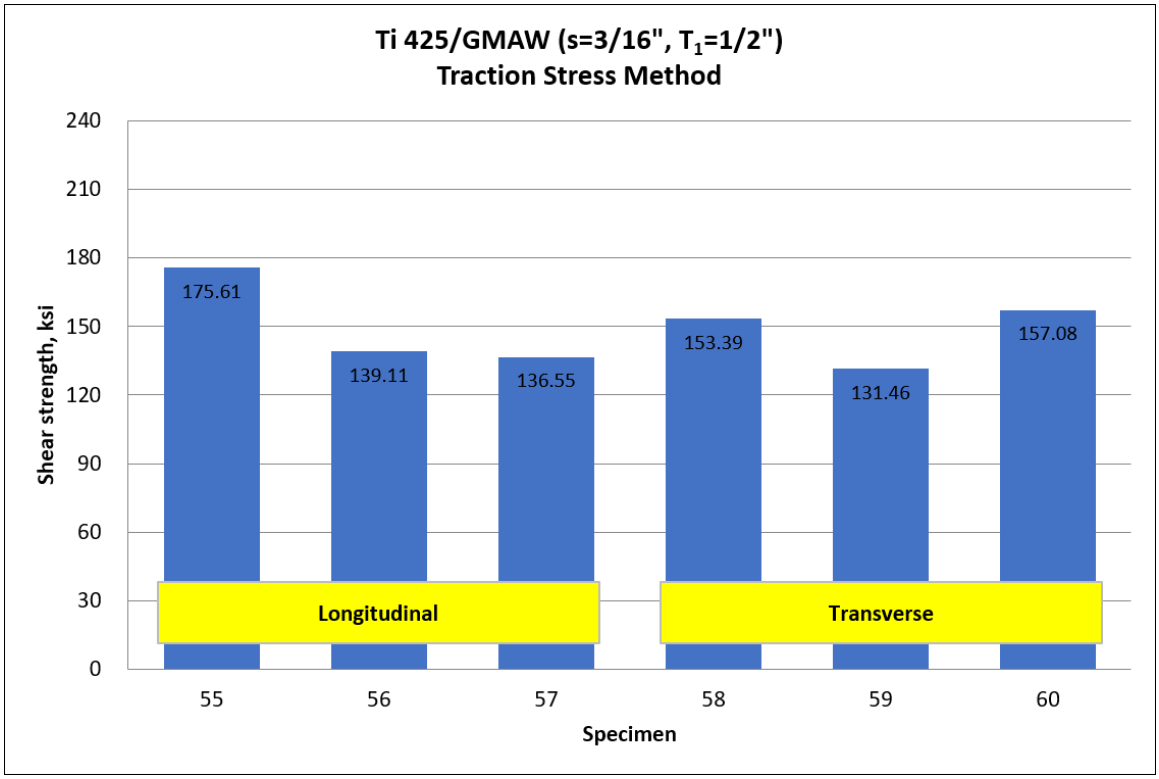

(b)

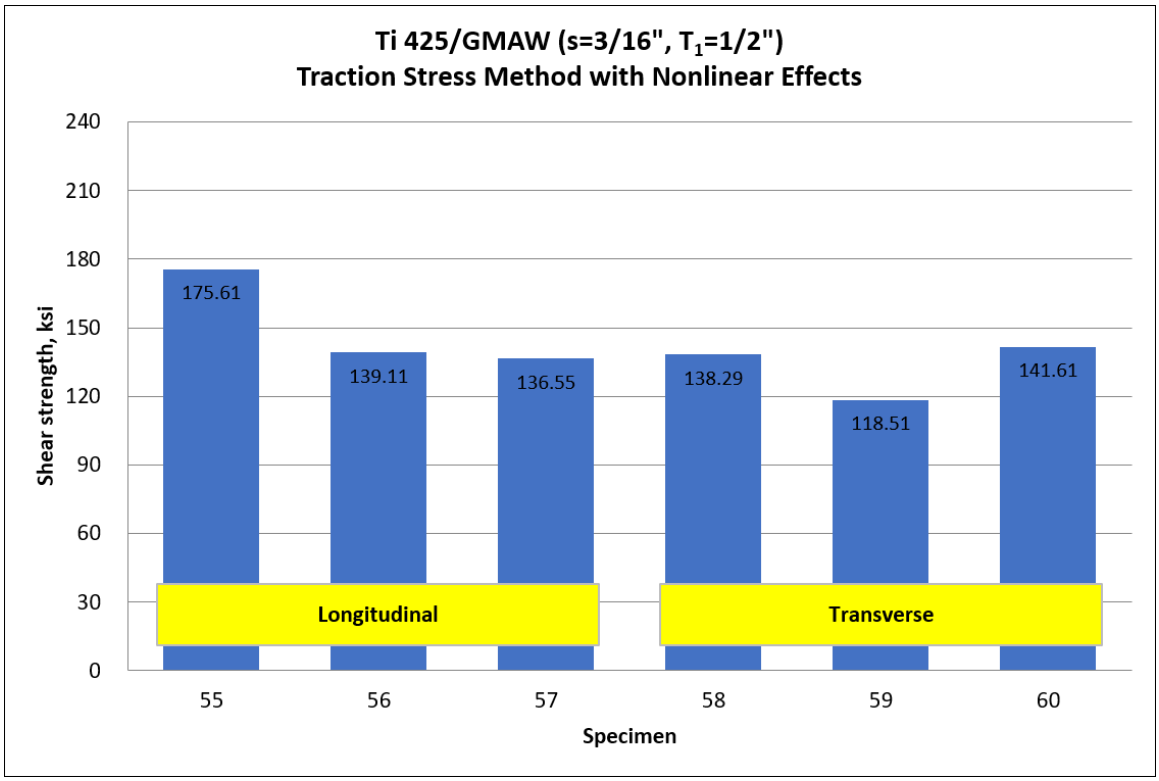

(c)

Figure 5.5: Comparison of shear strengths between longitudinal and transverse shear specimens of Ti 425 with GMAW: (a) AWS traditional equation; (b) traction stress method; (c) traction stress method with nonlinear effects

5.3 Weld Size Effects

Further examinations are done for the fractured shear specimens. Some major weld size effects are observed: (1) weld penetrations, s_p as shown in Figure 5.6, are present in the shear strength specimens tested in this study and have a clear dependency to the weld size s; (2) weld shear strengths are also affected by weld size, i.e., shear strengths have higher values in smaller weld sizes than those of larger weld sizes given the same base material and welding process.

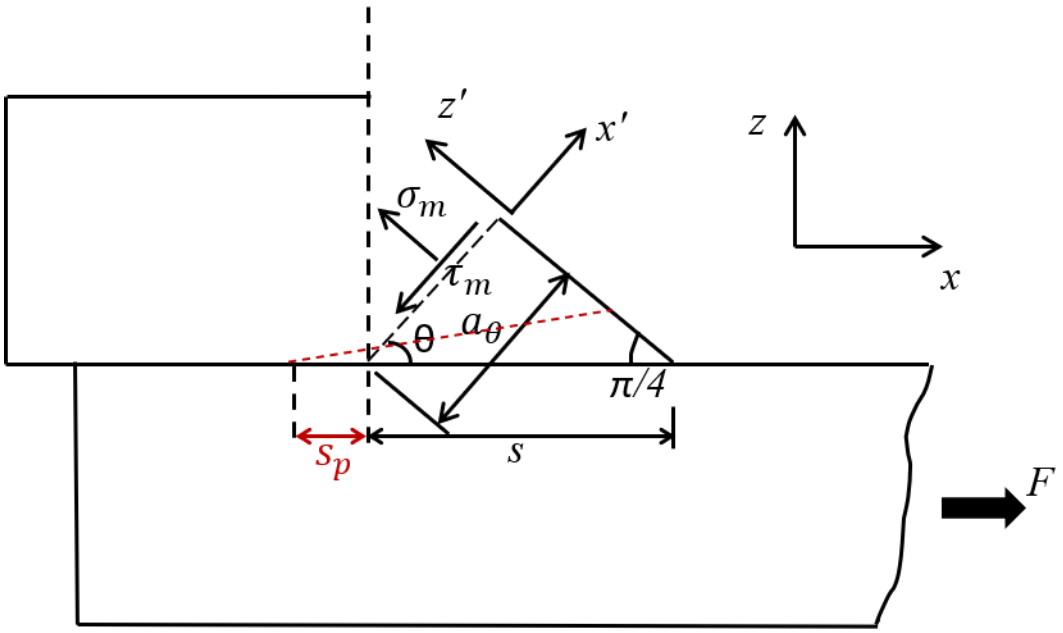

Figure 5.6: Weld penetration in load-carrying fillet weld

As seen in Figure 5.7, over 180 specimens with five combinations of base material and welding process, normalized weld penetration percent, defined as s_p/s, increases when weld size gets smaller. For quantitatively including this effect into weld sizing criterion, a linear regression equation is derived as expressed in Eq. (5.1).

$$\frac{s_p}{s} = -0.025s + 0.311 \tag{5.1}$$

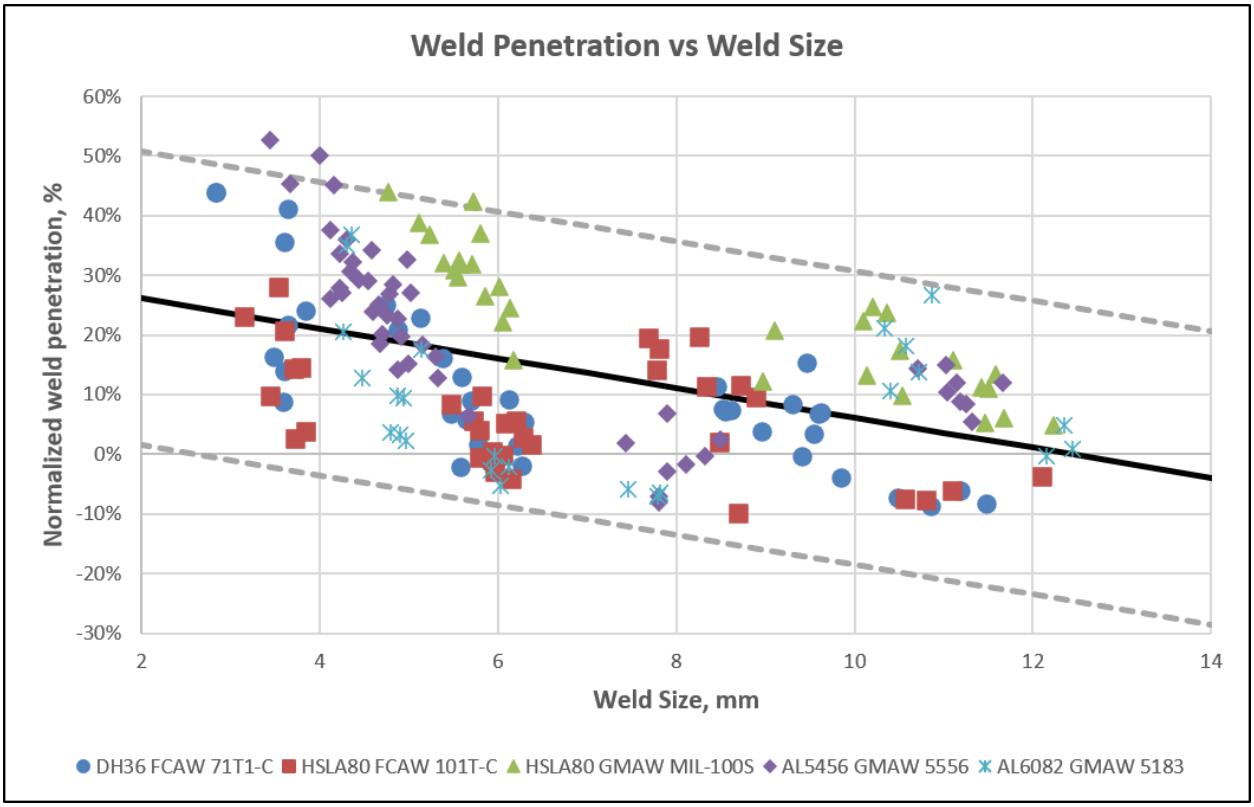

Figure 5.7: Weld penetration vs weld size

Similarly, as demonstrated in Figure 5.8, shear strengths (normalized by the averaged value of the corresponding test group) increases when weld size gets smaller. For example, for HSLA 80 with GMAW and 101T-C weld wire, shear strength is increased from 70% of the averaged value for the specimens with 11 mm weld size to 140% for the specimens with 4 mm weld size.

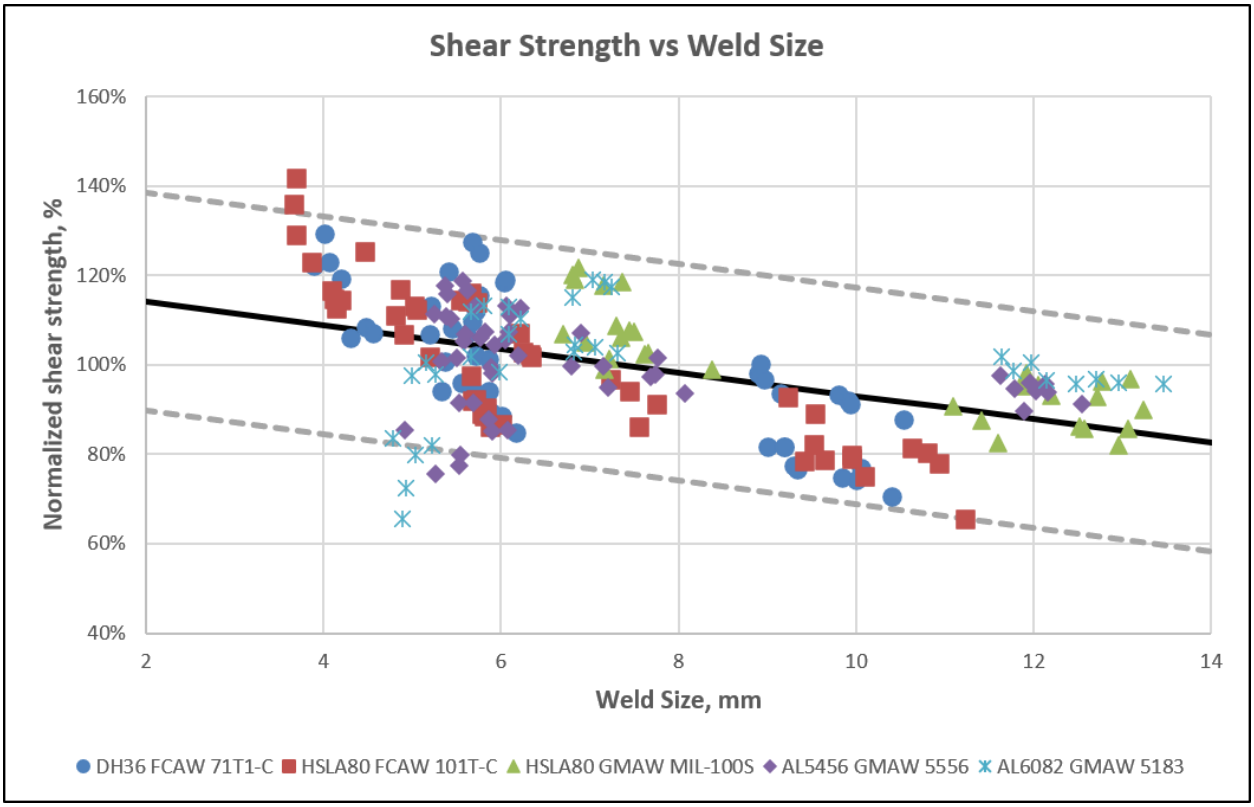

Figure 5.8: Shear strength vs weld size

A further investigation shows that the weld size effect on the shear strength is possibly caused by the material hardening and tempering process. Smaller weld leg size specimens cooled down very quickly causing hardening process, while larger weld leg size specimens were often multi-pass welded which required re-heating the specimens causing tempering process. Hardness tests have conducted for 1/8" (3 mm) and 3/8' (10 mm) welds to validate the hypothesis above, which indeed demonstrated that 1/8' weld has higher Vickers hardness number than 3/8" weld, as shown in Figure 5.9.

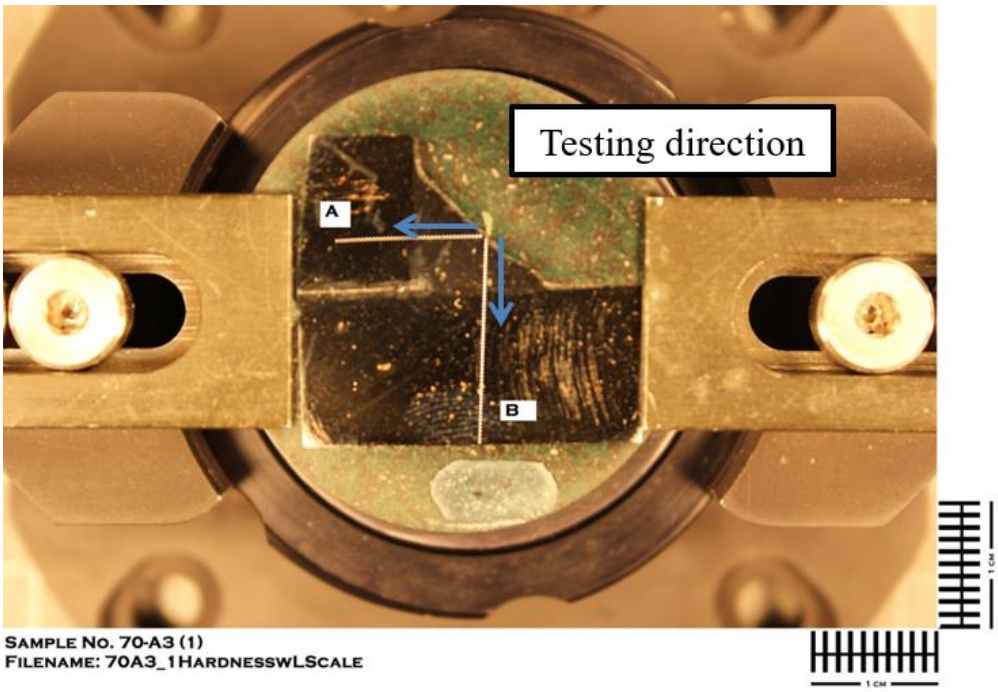
Testing direction
A
B
SAMPLE NO. 70-A3 (1)
FILENAME: 70A3_1HARDNESSWLSCALE

(a)

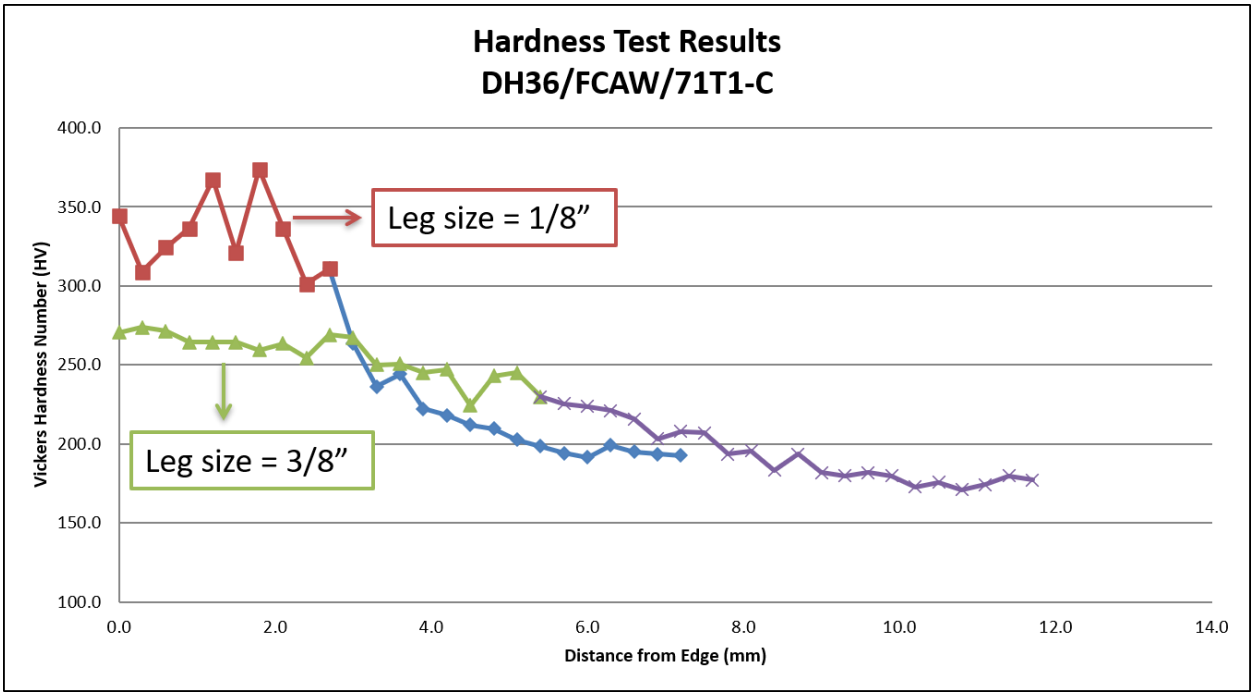
Hardness Test Results
DH36/FCAW/71T1-C
Vickers Hardness Number (HV)
400.0
350.0
300.0
250.0
200.0
150.0
100.0
0.0
2.0
4.0
6.0
8.0
10.0
12.0
14.0
Distance from Edge (mm)
Leg size = 1/8”
Leg size = 3/8”

(b)

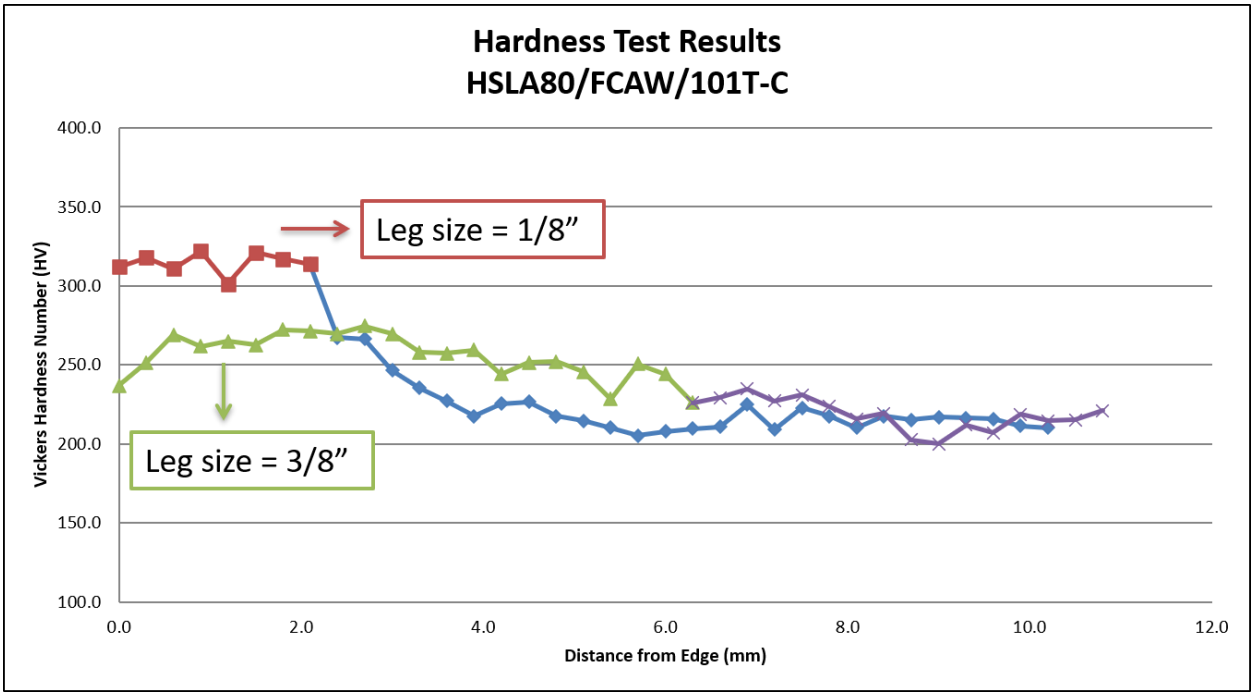

(c)

Figure 5.9: Hardness test for weld with different size: (a) hardness test procedure; (b) hardness test results for DH36 with FCAW & 71T1-C; (c) hardness test results for HSLA80 with FCAW & 101T-C

A linear regression equation is derived based over 180 specimens with five combinations of base material and welding process, as expressed in Eq. (5.2), for including this strength increase effect into weld sizing criterion.

$$\tau_{\%} = -0.0263s + 1.1935 \tag{5.2}$$

Note that both Eqs. (5.1) and (5.2) are derived based on the results of design weld size from 1/8” (3 mm) to 3/8” (10 mm) in this study , which are made strictly according to AWS D1.1 (AWS, 2015). Further investigation and more data correlation are needed to prove their effectiveness. For the time being, one should pay extra attention when implementing them into weld sizing.

5.4 Generalized Quantitative Weld Sizing Criterion

After all the theoretical developments and experimental efforts in Chapter 2, 3 and 4, a generalized quantitative weld sizing criterion can be proposed and its mechanics basis is expressed by Eq. (5.3):

$$\tau_{u,w} = \frac{P_u}{s \times L} \times (0.0225 \times \lambda_2 + 1.0) \times (\cos\theta_{max} + \sin\theta_{max}) \times \sqrt{\{\sin\alpha \times (\cos\theta_{max} - K \times \sin\theta_{max})\}^2 + (\cos\alpha)^2} \tag{5.3}$$

where θ_{max} can be calculated by Eq. (5.4):

$$\frac{\cos\theta_{max} - \sin\theta_{max}}{\cos\theta_{max} + \sin\theta_{max}} \times \sqrt{\{\sin\alpha \times (\cos\theta_{max} - K \times \sin\theta_{max})\}^2 + (\cos\alpha)^2} = \frac{2\sin\alpha^2 \times (\cos\theta_{max} - K \times \sin\theta_{max}) \times (\sin\theta_{max} + K \times \cos\theta_{max})}{\sqrt{\{\sin\alpha \times (\cos\theta_{max} - K \times \sin\theta_{max})\}^2 + (\cos\alpha)^2}} \tag{5.4}$$

Note that coefficient K in Eq. (5.3) and Eq. (5.4) is introduced as a nonlinear effect factor, and can be expressed by Eq. (5.5) related to structural dimensions, which has a special case of $K = 0.3$ for fillet weld with connected plates having contact surface parallel to loading direction, such as standard transverse shear specimen (see Figure 2.1b).

$$\begin{aligned} K &= -0.1089\ln\lambda_1 + 0.5 \quad \text{for general application} \\ K &= 0.3 \quad \text{for standard transverse shear specimen} \end{aligned} \tag{5.5}$$

In addition, ultimate load capacity P_u is treated as $\sigma_{u,b} \times t_b \times L$ and $\tau_{u,b} \times t_b \times L$ for loading angle of 90° and 0°, respectively (Krumpen, 1984). By setting shear strength of base plate is equal to 75% of ultimate tensile strength, ultimate load capacity P_u is assumed having a linear relationship with loading angle α as shown in Eq. (5.6).

$$P_u = \lambda_3 \times \sigma_{u,b} \times t_b \times L \tag{5.6}$$

$$\lambda_3 = 0.3183\alpha + 0.75$$

Finally, a generalized weld sizing criterion can be expressed by Eq. (5.7).

$$\frac{s}{t_b} = \frac{\sigma_{u,b}}{\tau_{u,w}} \times \lambda_3 \times (0.0225 \times \lambda_2 + 1.0) \times (\cos\theta_{max} + \sin\theta_{max}) \times \sqrt{\{\sin\alpha \times (\cos\theta_{max} - K \times \sin\theta_{max})\}^2 + (\cos\alpha)^2}$$

$$\frac{\cos\theta_{max} - \sin\theta_{max}}{\cos\theta_{max} + \sin\theta_{max}} \times \sqrt{\{\sin\alpha \times (\cos\theta_{max} - K \times \sin\theta_{max})\}^2 + (\cos\alpha)^2} \quad (5.7)$$

$$= \frac{2\sin\alpha^2 \times (\cos\theta_{max} - K \times \sin\theta_{max}) \times (\sin\theta_{max} + K \times \cos\theta_{max})}{\sqrt{\{\sin\alpha \times (\cos\theta_{max} - K \times \sin\theta_{max})\}^2 + (\cos\alpha)^2}}$$

$$K = -0.1089 \ln\lambda_1 + 0.5 \text{ or } K = 0.3$$

Eq. (5.7) can be simplified to special cases, such as standard longitudinal shear specimens, transverse shear specimens, and 90° loaded HSS connections, as expressed by Eq. (5.8), Eq. (5.9), and Eq. (5.10), respectively.

$$\frac{s}{t_b} = 0.530 \times \frac{\sigma_{u,b}}{\tau_{u,w}} \quad (5.8)$$

$$\frac{s}{t_b} = 0.544 \times \frac{\sigma_{u,b}}{\tau_{u,w}} \quad (5.9)$$

$$\frac{s}{t_b} = \frac{\sigma_{u,b}}{\tau_{u,w}} \times (0.0225 \times \lambda_2 + 1.0) \times (\cos\theta_{max} + \sin\theta_{max}) \times \{\cos\theta_{max} - (-0.1089 \ln\lambda_1 + 0.5) \times \sin\theta_{max}\} \quad (5.10)$$

Weld size reduction obtained from Eq. (5.7) compared to the traditional weld sizing criterion Eq. (1.2) and Krumpen's approach (1984) is summarized below in Table 5.3, Table 5.4, and Table 5.5 for longitudinal and transverse shear specimens tested in this study, and HSS fillet-welded connections test data available in literature, respectively. It can be clearly seen that significant weld size reductions provided by Eq. (5.8), Eq. (5.9), and Eq. (5.10) are as much as

about 40% for standard longitudinal and transverse shear specimens tested in this study, and about 20% for HSS fillet-welded connections test data available from literature. Note that weld size effect on weld penetration could further reduce design fillet weld size, i.e., including Eq. (5.1) to Eq. (5.7), as expressed by Eq. (5.11). Further investigation will be conduct on this area. Overall, the proposed generalized weld sizing criterion would be very beneficial for welding-induced distortion control in the construction of lightweight ship structures.

$$\frac{s+s_p}{t_b} = \frac{\sigma_{u,b}}{\tau_{u,w}} \times \lambda_3 \times (0.0225 \times \lambda_2 + 1.0) \times (\cos\theta_{max} + \sin\theta_{max}) \times \sqrt{\{\sin\alpha \times (\cos\theta_{max} - K \times \sin\theta_{max})\}^2 + (\cos\alpha)^2}$$

$$\frac{\cos\theta_{max} - \sin\theta_{max}}{\cos\theta_{max} + \sin\theta_{max}} \times \sqrt{\{\sin\alpha \times (\cos\theta_{max} - K \times \sin\theta_{max})\}^2 + (\cos\alpha)^2} \quad (5.11)$$

$$= \frac{2\sin\alpha^2 \times (\cos\theta_{max} - K \times \sin\theta_{max}) \times (\sin\theta_{max} + K \times \cos\theta_{max})}{\sqrt{\{\sin\alpha \times (\cos\theta_{max} - K \times \sin\theta_{max})\}^2 + (\cos\alpha)^2}}$$

$$K = -0.1089 \ln\lambda_1 + 0.5 \text{ or } K = 0.3$$

Table 5.3: Weld size reduction from traditional approach (Eq. (1.2))by proposed weld sizing criterion (Eq. (5.7) for longitudinal shear specimens

Specimen Type	Base Material	Base Material UTS, $\sigma_{u,b}$	Welding Process	Filler Material	Shear Strength by AWS, τ_{u,w_L}	Shear Strength by TSM, $\tau_{u,w}$	Weld Size $\frac{s}{t_b}$ by Eq. (1.2)	Weld Size $\frac{s}{t_b}$ by Krumpen	Weld Size $\frac{s}{t_b}$ by TSM Eq. (5.7)	Weld Size Reduction from Eq. (1.2)	Weld Size Reduction from Krumpen
Longitudinal	DH36	71 ksi (490 MPa)	FCAW	71T1-C	65 ksi	86 ksi	0.772	0.579	0.438	43%	24%
	HSLA80	96 ksi (660 MPa)	FCAW	101T-C	76 ksi	96 ksi	0.893	0.670	0.530	41%	21%
	HSLA80	96 ksi (660 MPa)	GMAW	MIL-100S	78 ksi	93 ksi	0.870	0.653	0.547	37%	16%
	AL 5456	51 ksi (350 MPa)	GMAW	AL 5556	23 ksi	27 ksi	1.568	1.176	1.001	36%	15%
	AL 6082	45 ksi (450 MPa)	GMAW	AL 5183	20 ksi	23 ksi	1.591	1.193	1.037	35%	13%
	Ti-64 Gr-2	138 ksi (950 MPa)	GTAW	Ti-64	94 ksi	106 ksi	1.038	0.779	0.690	34%	11%
	Ti-CP Gr-5	62 ksi (430 MPa)	GMAW	Ti-CP	61 ksi	67 ksi	0.719	0.539	0.490	32%	9%
	Ti-CP Gr-5	62 ksi (430 MPa)	GTAW	Ti-CP	54 ksi	61 ksi	0.812	0.609	0.539	34%	12%
	Ti-425 Gr-38	146 ksi (1010 MPa)	GMAW	Ti-425	115 ksi	122 ksi	0.898	0.673	0.634	29%	6%

Table 5.4: Weld size reduction from traditional approach (Eq. (1.2))by proposed weld sizing criterion Eq. (5.7) for transverse shear specimens

Specimen Type	Base Material	Base Material UTS, $\sigma_{u,b}$	Welding Process	Filler Material	Shear Strength by AWS, τ_{u,w_L}	Shear Strength by TSM, $\tau_{u,w}$	Weld Size $\frac{s}{t_b}$ by Eq. (1.2)	Weld Size $\frac{s}{t_b}$ by Krumpen	Weld Size $\frac{s}{t_b}$ by TSM Eq. (5.7)	Weld Size Reduction from Eq. (1.2)	Weld Size Reduction from Krumpen
Transverse	DH36	71 ksi (490 MPa)	FCAW	71T1-C	65 ksi	86 ksi	0.772	0.536	0.449	42%	16%
	HSLA80	96 ksi (660 MPa)	FCAW	101T-C	76 ksi	96 ksi	0.893	0.620	0.544	39%	12%
	HSLA80	96 ksi (660 MPa)	GMAW	MIL-100S	78 ksi	93 ksi	0.870	0.604	0.562	35%	7%
	AL 5456	51 ksi (350 MPa)	GMAW	AL 5556	23 ksi	27 ksi	1.568	1.089	1.028	34%	6%
	AL 6082	45 ksi (450 MPa)	GMAW	AL 5183	20 ksi	23 ksi	1.591	1.105	1.064	33%	4%
	Ti-64 Gr-2	138 ksi (950 MPa)	GTAW	Ti-64	94 ksi	106 ksi	1.038	0.721	0.708	32%	2%
	Ti-CP Gr-5	62 ksi (430 MPa)	GMAW	Ti-CP	61 ksi	67 ksi	0.719	0.499	0.503	30%	-1%
	Ti-CP Gr-5	62 ksi (430 MPa)	GTAW	Ti-CP	54 ksi	61 ksi	0.812	0.564	0.553	32%	2%
	Ti-425 Gr-38	146 ksi (1010 MPa)	GMAW	Ti-425	115 ksi	122 ksi	0.898	0.623	0.651	27%	-4%

Table 5.5: Weld size reduction from traditional approach (Eq. (1.2))by proposed weld sizing criterion Eq. (5.7) for HSS connections from literature

No.	Type	D or B mm	D_b or B_b mm	t mm	t_b mm	$C_{b,max}$ mm	r_c mm	Weld Size Reduction from Eq. (1.2) by Eq. (5.7), %
1	RHS to Plate	N/A	127.0	25.0	7.78	83.22	15.88	11%
2	RHS to Plate	N/A	177.8	25.0	12.53	111.23	35.00	15%
3	RHS to Plate	N/A	127.6	19.0	9.54	82.32	19.08	15%
4	CHS to Plate	N/A	167.9	25.0	6.70	83.95	83.95	21%
5	CHS to Plate	N/A	127.4	25.0	11.55	63.70	63.70	23%
6	CHS to Plate	N/A	101.0	25.0	7.34	50.50	50.50	23%
7	RHS to RHS	253.8	126.9	12.08	12.20	80.66	21.90	18%
8	RHS to RHS	253.8	203.0	12.08	12.05	134.13	22.72	10%

Chapter 6 Conclusions and Future Work

6.1 Major Contributions

To enable an effective connection design and construction of lightweight ship structures, a quantitative weld sizing criterion has been established through analytical and computational modeling, and detailed experimental validations. The major contributions resulted from this study can be summarized as follows:

1. A new effective traction shear stress based failure criterion has been analytically formulated for fillet-welded components without needing differentiating longitudinal versus transverse shear loading conditions. The new failure criterion not only predicts the correct weld throat failure plane, but also provides an effective means for a unified shear strength definition regardless of joint specimen types used (i.e., longitudinal versus transverse shear specimens), as proven by a large number of fillet-welded specimen tests performed within this study.
2. The developed failure criterion and its mechanics underpinning can now reconcile the discrepancies between the test results obtained from standardized longitudinal and transverse shear specimens (e.g., by AWS B4.0 used by class societies), which have puzzled researchers and engineers for decades. Furthermore, the new failure criterion can significantly simplify the existing test requirements for establishing fillet weld shear strengths through standardized fillet-welded specimen testing. As such, the standard transverse shear specimens are the only specimen type that is needed,

potentially reducing test cost by at least 60%-70% by eliminating the high fabrication and testing costs associated with the longitudinal shear specimens for joint design.

3. In addition to support the validation of various aspects of the new failure criterion developed, a comprehensive fillet weld strength database has been established through a systematic experimental testing of welded connections with a wide range of base metals (mild steel, high strength steel, aluminum alloys, and titanium alloys), welding processes (FCAW, GMAW, and GTAW), and weld wires (71T1-C, 101T-C, and MIL-100S, etc.). Furthermore, longitudinal and transverse shear specimens tested in this study considered base plate thickness varying from 0.5" (12 mm) to 1" (25 mm), and weld sizes from 1/8" (3 mm) to 3/8" (10 mm) to cover a wide range of structural lightweighting applications. In doing so, over 200 fillet-welded longitudinal and transverse shear specimens have been tested in this study.
4. A new analytical method is also developed for incorporating geometrical nonlinear effects, e.g., those due to contact between two plates, for a broader applicability of the proposed failure criterion, which have been shown important for performing test data analysis of transverse shear specimens. The effectiveness of the combined failure criterion has been validated by finite element computation incorporating nonlinear material and nonlinear geometry conditions. In addition, its effectiveness in correlating shear strengths obtained from transverse shear specimens has been proven through the experimental test data obtained in this study.
5. To further prove the broad applicability of the developed failure criterion in load capacity evaluation of full-scale complex welded components, it has been applied for analyzing a large number of well-recognized full-scale test data on hollow structural

section joint components. The traction stress based weld failure criterion has again been proven effective. The correlations obtained by the traction stress based failure criterion between the predicted and actual failure loads of various HSS fillet-welded connections show as much as 60% improvement over those predicted by existing Codes and Standards used today.

6. Finally, the proposed closed-form weld sizing criterion in the form of Eq. (5.7) has been shown to result in reducing fillet weld sizes by as much as 40% compared to the traditional empirical-based weld sizing criterion (Eq. (1.2)), as demonstrated in Chapter 5 in the context of these standard shear test specimens and full-scale HSS connections. Thus, the quantitative weld sizing criterion developed in this study should enable the elimination of the widespread weld over-sizing resulted from the existing empirical-based weld sizing rules in Codes and Standards, which has been the root cause of severe welding-induced distortions experienced today in the construction of lightweight shipboard structures.

6.2 Areas of Future Study

Based on the investigations conducted in this study, the following areas are recommended for future work to address additional fundamental issues and engineering applications:

1. The testing results obtained in this study have revealed weld quality issues for certain aluminum alloys and titanium alloys, in which noticeable welding-induced defects are present. These defects are believed to have contributed to not only lower joint strengths, but also a larger than usual data scatter. This suggests that more appropriate weld quality acceptance criteria need to be developed for supporting the use of these lightweight structural metals in future ship platforms.

2. To further reduce weld size for meeting today's lightweight requirements nowadays, equivalent weld size incorporating weld penetration which can be achieved consistently by advanced welding processes, e.g. hybrid laser-arc welding (HLAW), should be investigated for incorporation in the quantitative weld sizing criterion developed in this study. Such considerations could lead to another 10% to 20% weld size reduction based on the insights gained from available test results obtained in this study.
3. Although the proposed weld sizing criterion has yielded a very good correlation between predicted and actual failure angle of fillet welds in various joint configurations and loading conditions, joint strength test data scatter band needs to be established for defining an appropriate design safety factor for application in practice to take full advantage of the quantitative weld sizing criterion developed in this study.
4. New joint types produced by more advanced welding and joining processes, such as friction stir welding and hybrid laser-arc welding, etc., need to be considered for adapting the developed weld sizing criterion.

Appendix A Shear Strength Correlation between Longitudinal and Transverse Shear Specimens using Conventional Method

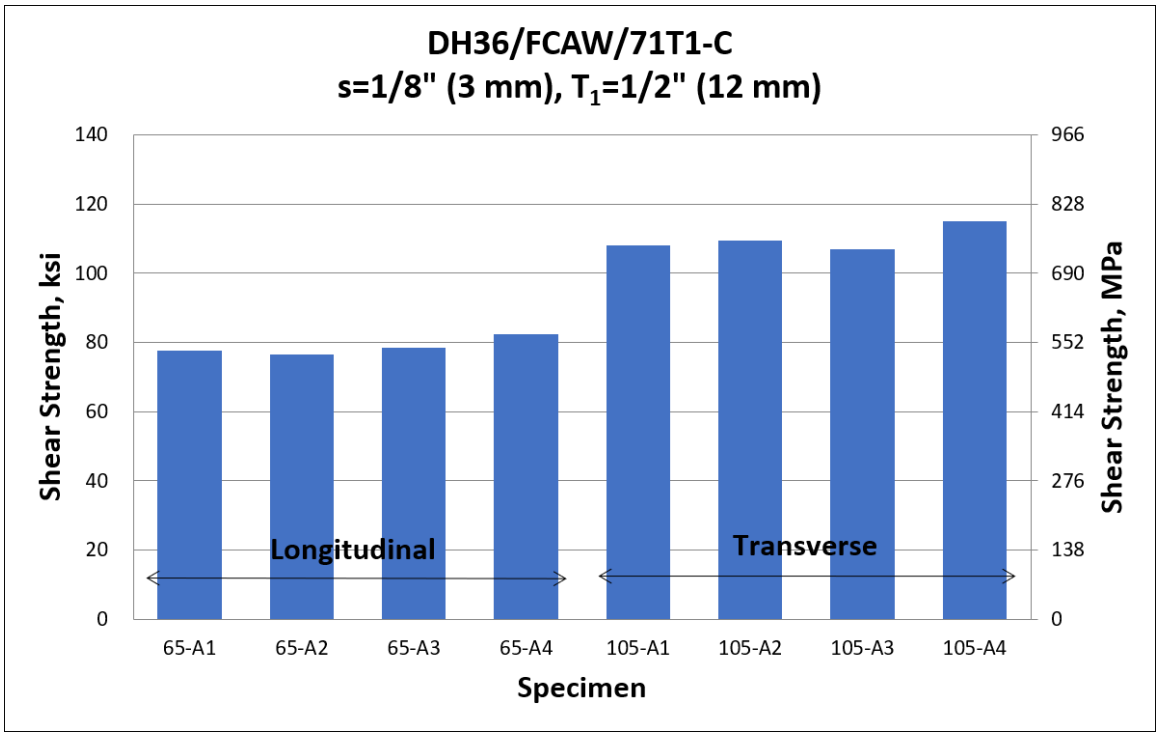

(a)

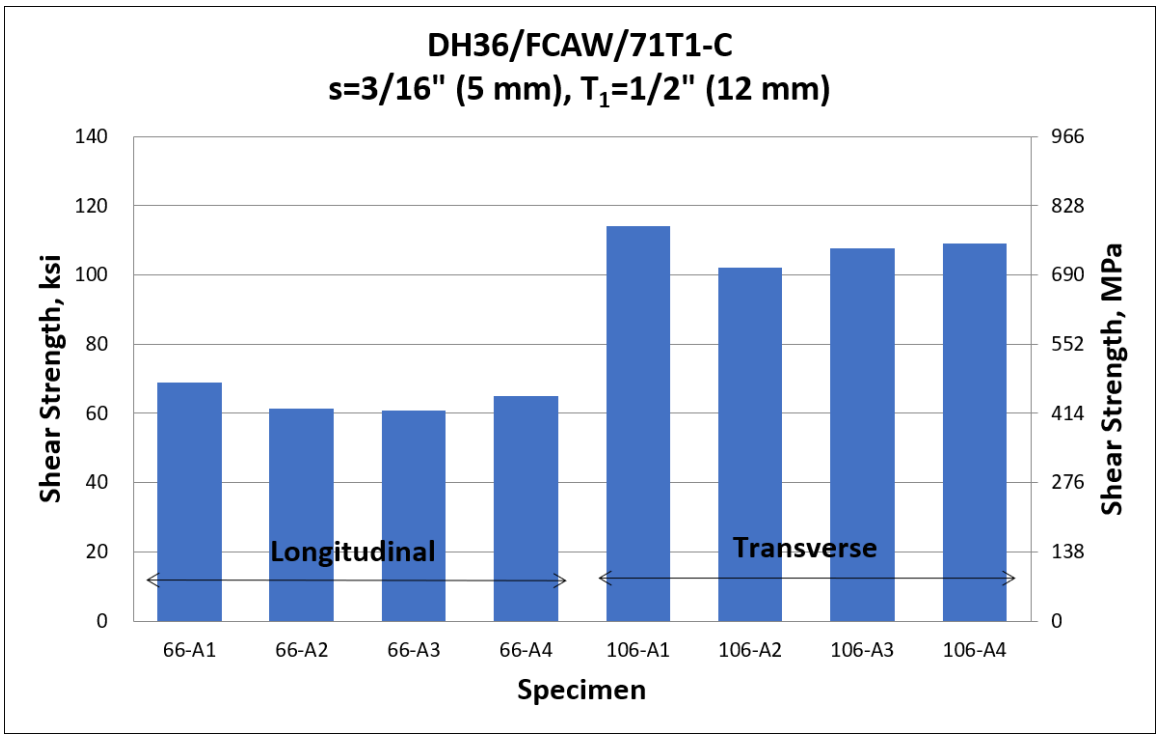
DH36/FCAW/71T1-C
s=3/16" (5 mm), T1=1/2" (12 mm)
Shear Strength, ksi
Shear Strength, MPa
140
120
100
80
60
40
20
0
966
828
690
552
414
276
138
0
Longitudinal
Transverse
66-A1
66-A2
66-A3
66-A4
106-A1
106-A2
106-A3
106-A4
Specimen

(b)

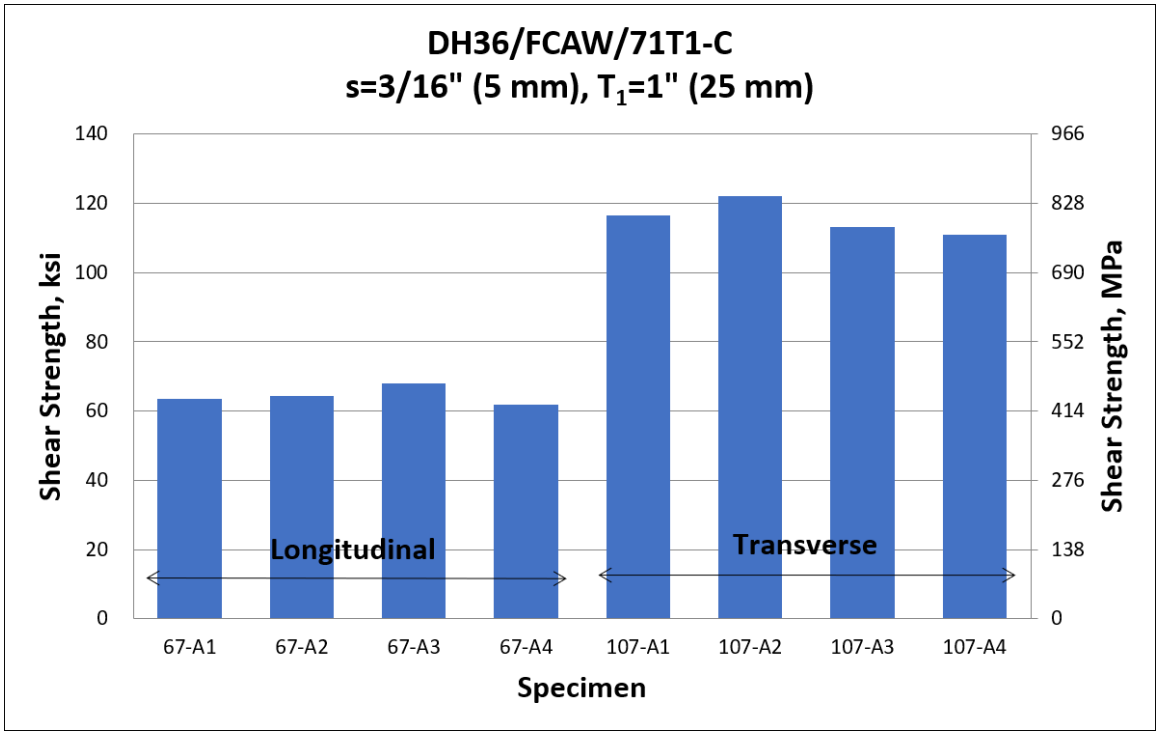
DH36/FCAW/71T1-C
s=3/16" (5 mm), T1=1" (25 mm)
Shear Strength, ksi
Shear Strength, MPa
140
120
100
80
60
40
20
0
966
828
690
552
414
276
138
0
Longitudinal
Transverse
67-A1
67-A2
67-A3
67-A4
107-A1
107-A2
107-A3
107-A4
Specimen

(c)

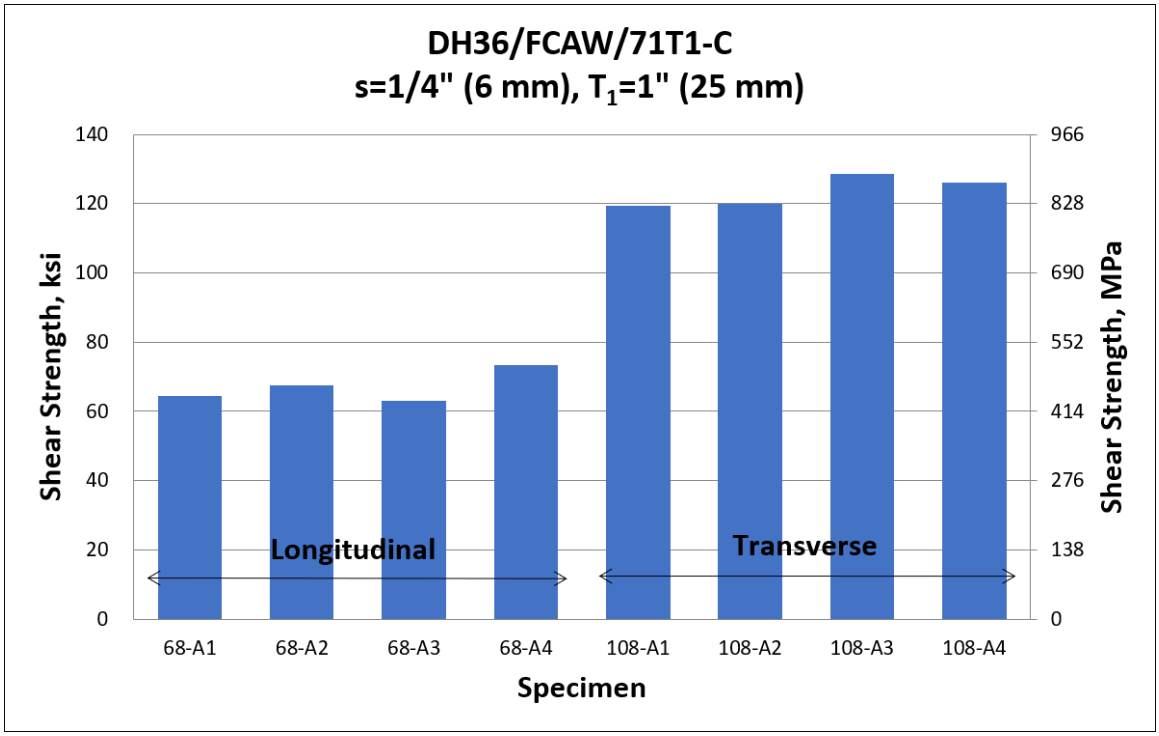
DH36/FCAW/71T1-C
s=1/4" (6 mm), T1=1" (25 mm)
Shear Strength, ksi
Shear Strength, MPa
140
120
100
80
60
40
20
0
966
828
690
552
414
276
138
0
Longitudinal
Transverse
68-A1
68-A2
68-A3
68-A4
108-A1
108-A2
108-A3
108-A4
Specimen

(d)

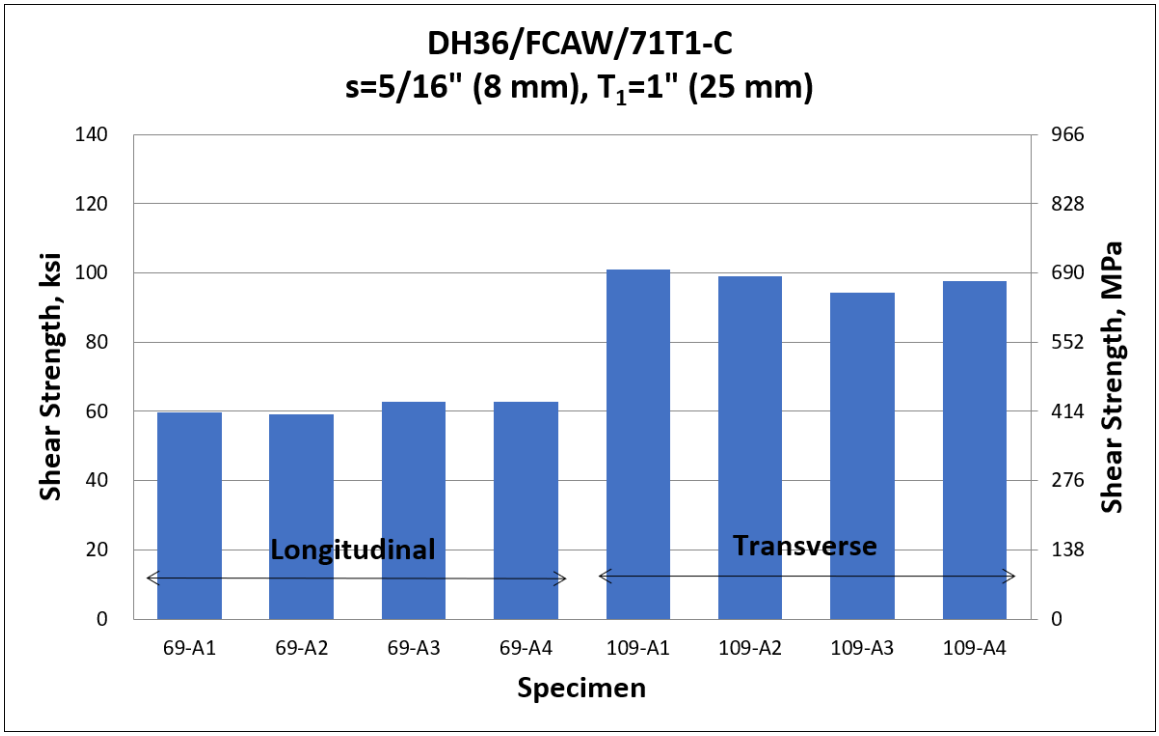
DH36/FCAW/71T1-C
s=5/16" (8 mm), T1=1" (25 mm)
Shear Strength, ksi
Shear Strength, MPa
140
120
100
80
60
40
20
0
966
828
690
552
414
276
138
0
Longitudinal
Transverse
69-A1
69-A2
69-A3
69-A4
109-A1
109-A2
109-A3
109-A4
Specimen

(e)

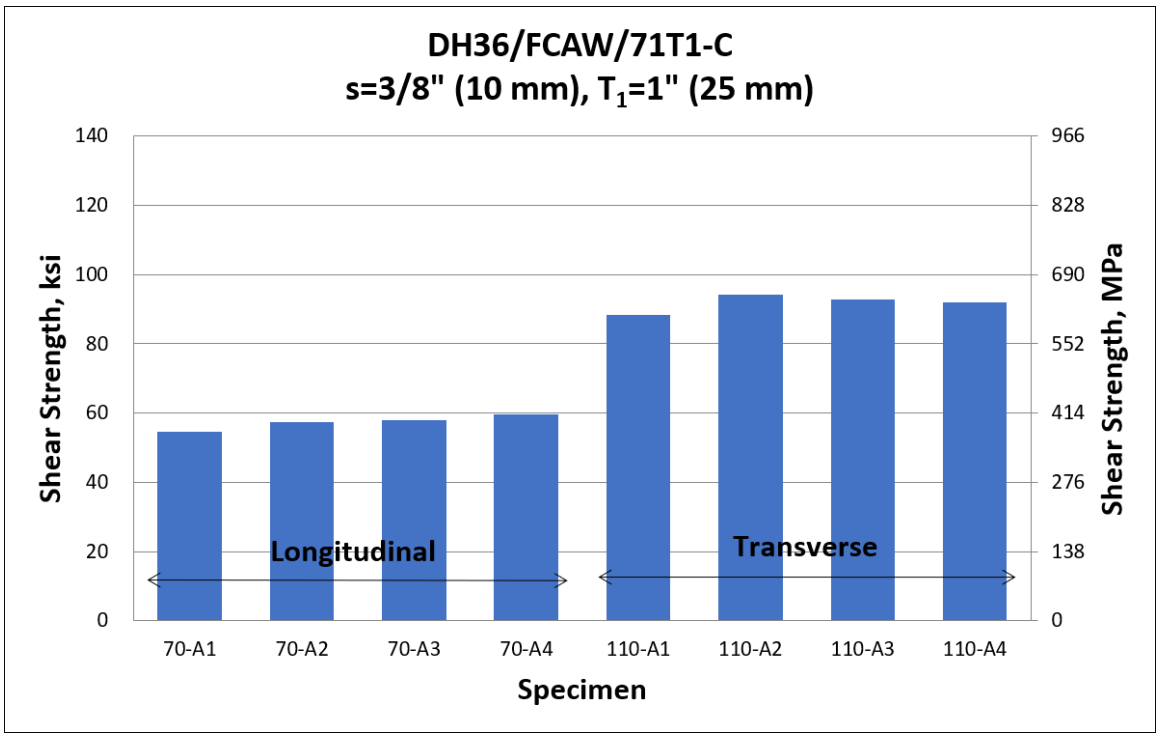

(f)

Figure A.1: Shear strength correlation between longitudinal and transverse shear specimens using conventional method for DH36 with FCAW and 71T1-C weld wire

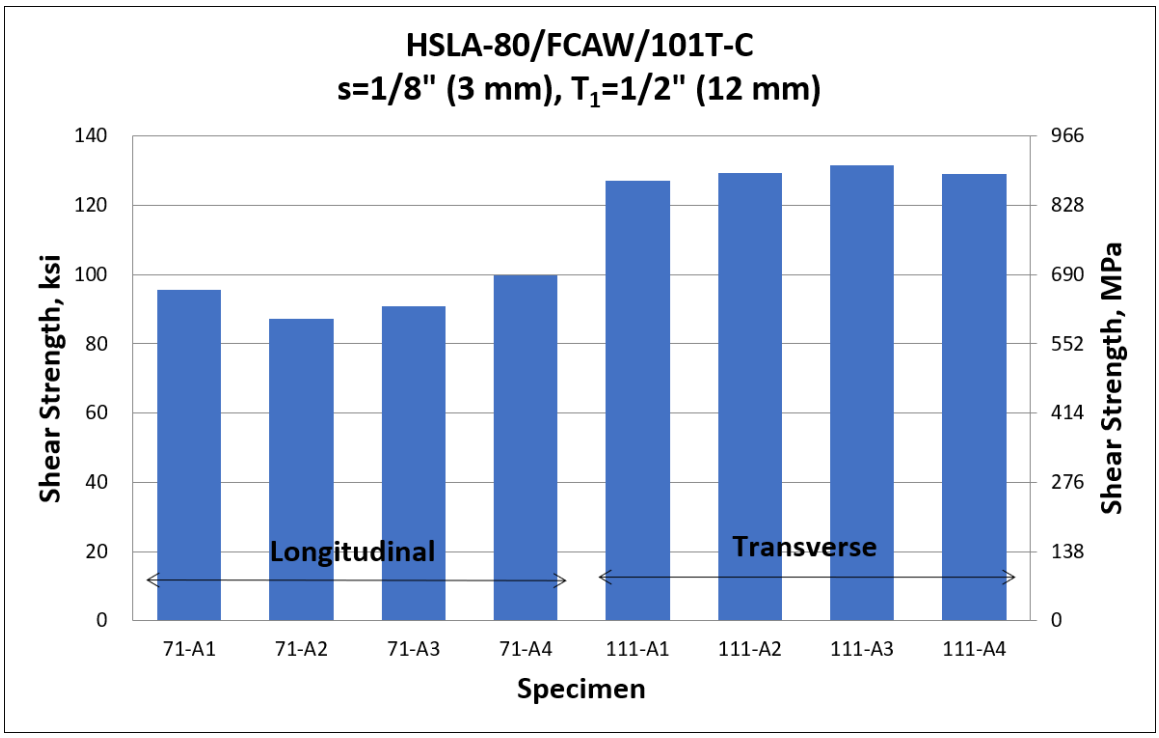

(a)

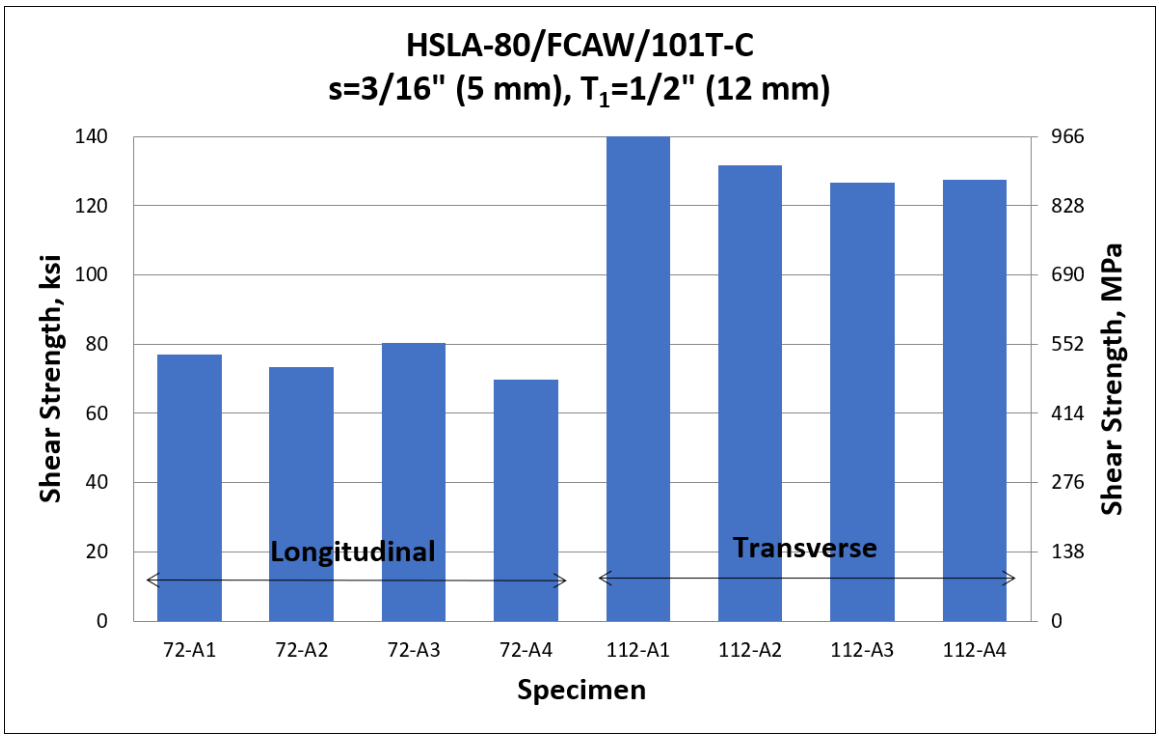
HSLA-80/FCAW/101T-C
s=3/16" (5 mm), T1=1/2" (12 mm)
Shear Strength, ksi
Shear Strength, MPa
140
120
100
80
60
40
20
0
966
828
690
552
414
276
138
0
Longitudinal
Transverse
72-A1
72-A2
72-A3
72-A4
112-A1
112-A2
112-A3
112-A4
Specimen

(b)

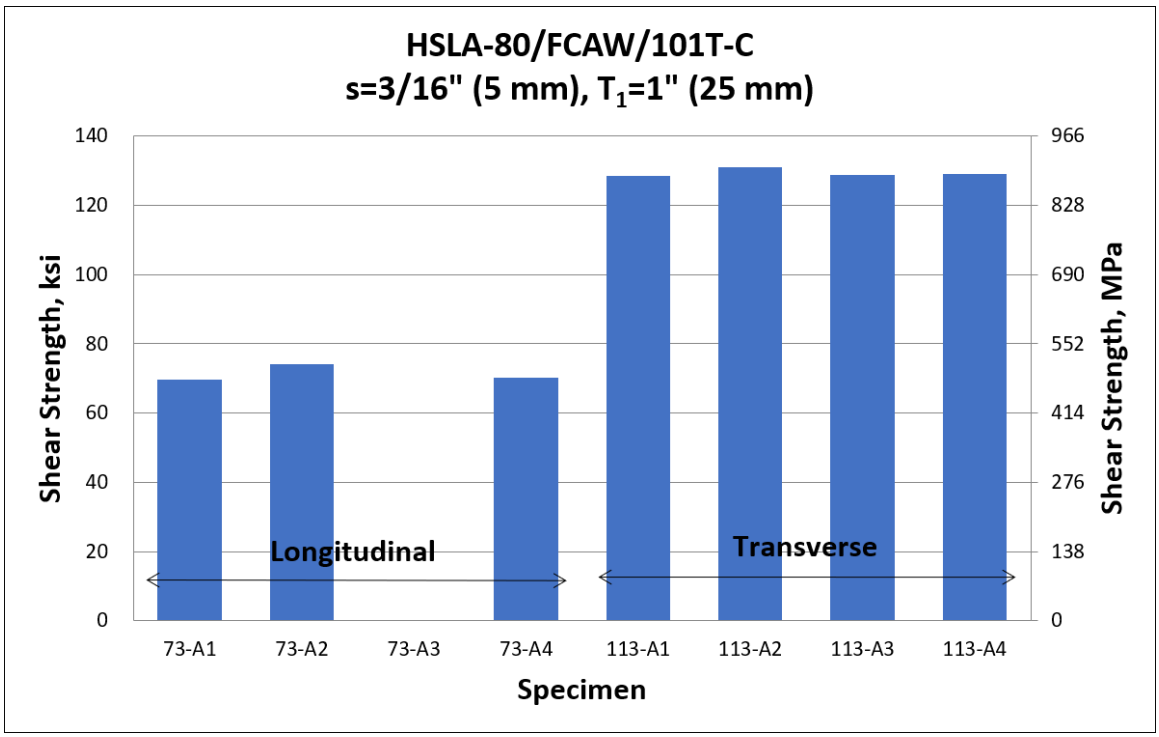
HSLA-80/FCAW/101T-C
s=3/16" (5 mm), T1=1" (25 mm)
Shear Strength, ksi
Shear Strength, MPa
140
120
100
80
60
40
20
0
966
828
690
552
414
276
138
0
Longitudinal
Transverse
73-A1
73-A2
73-A3
73-A4
113-A1
113-A2
113-A3
113-A4
Specimen

(c)

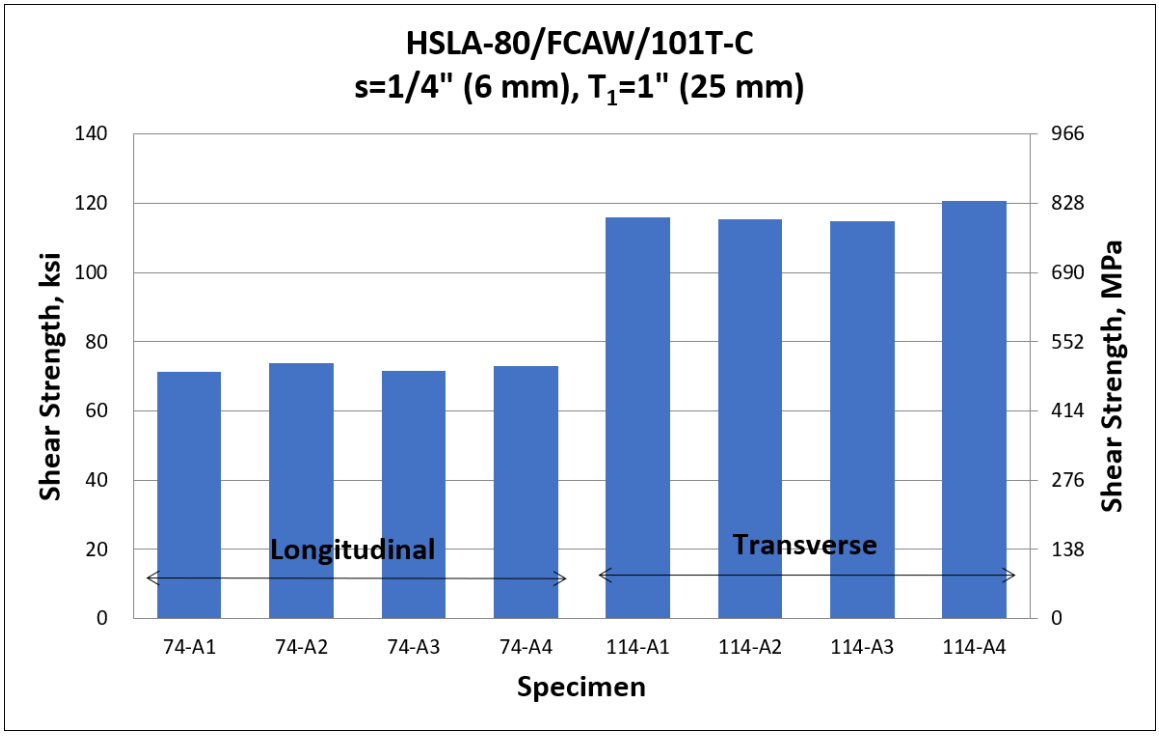
HSLA-80/FCAW/101T-C
s=1/4" (6 mm), T1=1" (25 mm)
Shear Strength, ksi
Shear Strength, MPa
140
120
100
80
60
40
20
0
966
828
690
552
414
276
138
0
Longitudinal
Transverse
74-A1
74-A2
74-A3
74-A4
114-A1
114-A2
114-A3
114-A4
Specimen

(d)

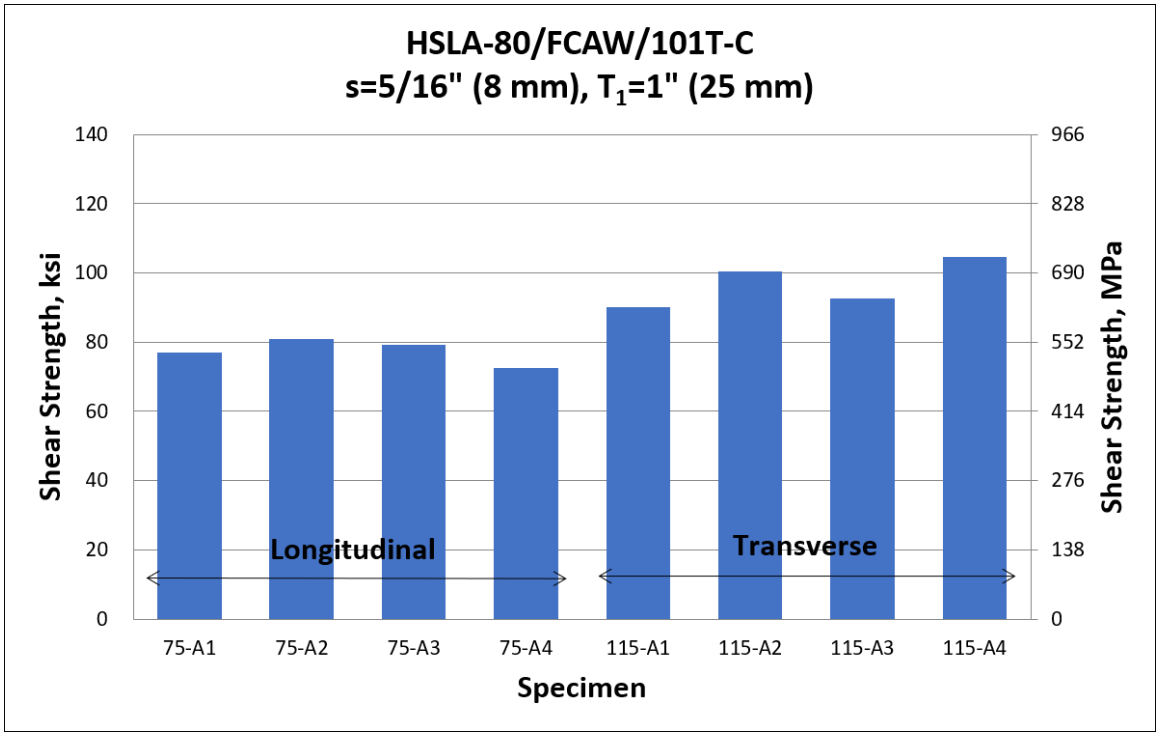
HSLA-80/FCAW/101T-C
s=5/16" (8 mm), T1=1" (25 mm)
Shear Strength, ksi
Shear Strength, MPa
140
120
100
80
60
40
20
0
966
828
690
552
414
276
138
0
Longitudinal
Transverse
75-A1
75-A2
75-A3
75-A4
115-A1
115-A2
115-A3
115-A4
Specimen

(e)

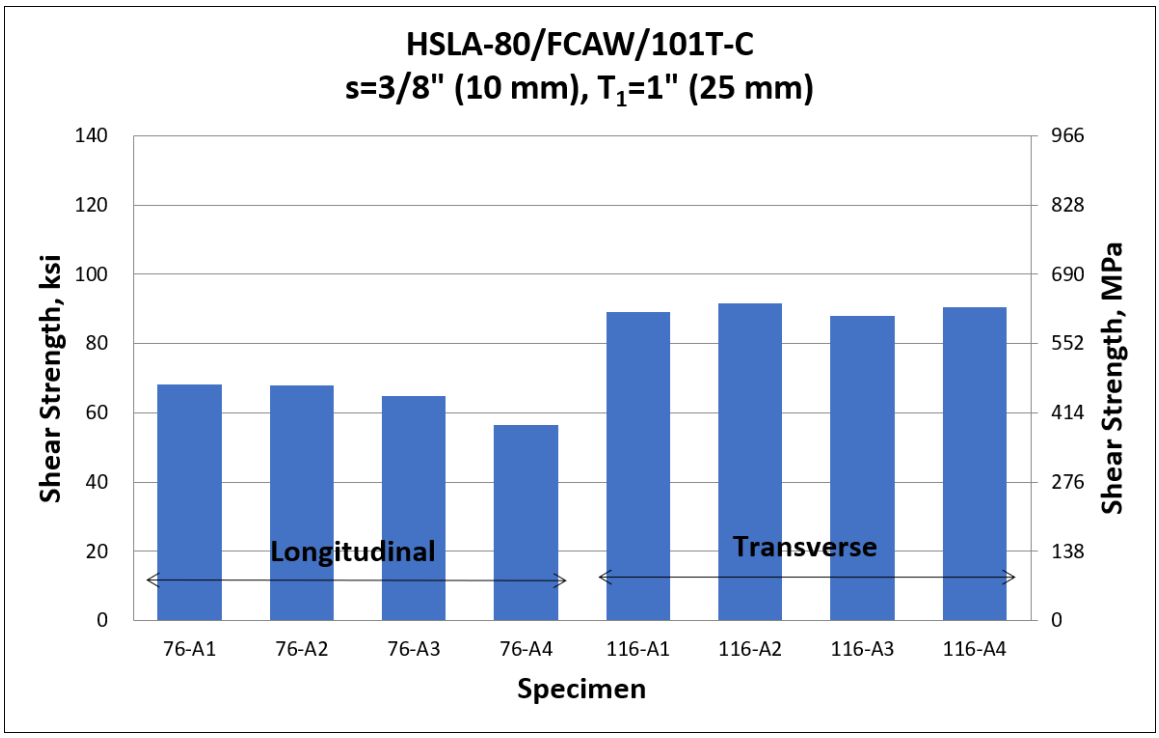

(f)

Figure A.2: Shear strength correlation between longitudinal and transverse shear specimens using conventional method for HSLA-80 with FCAW and 101T-C weld wire

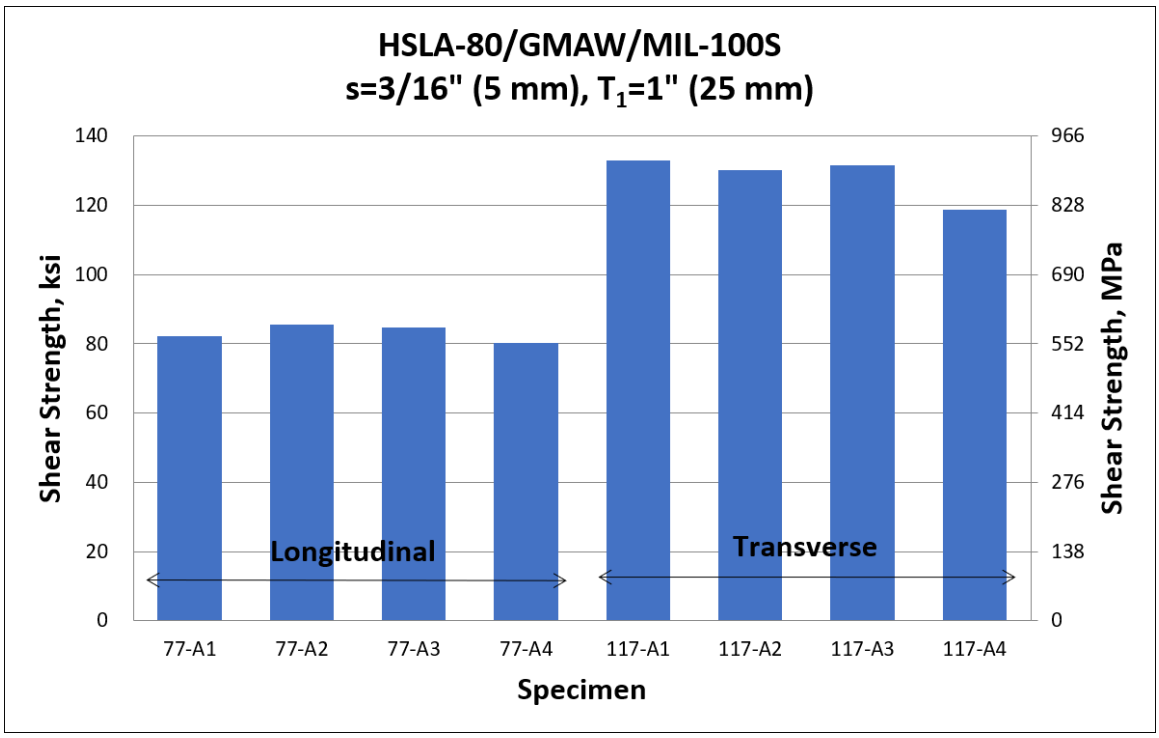

(a)

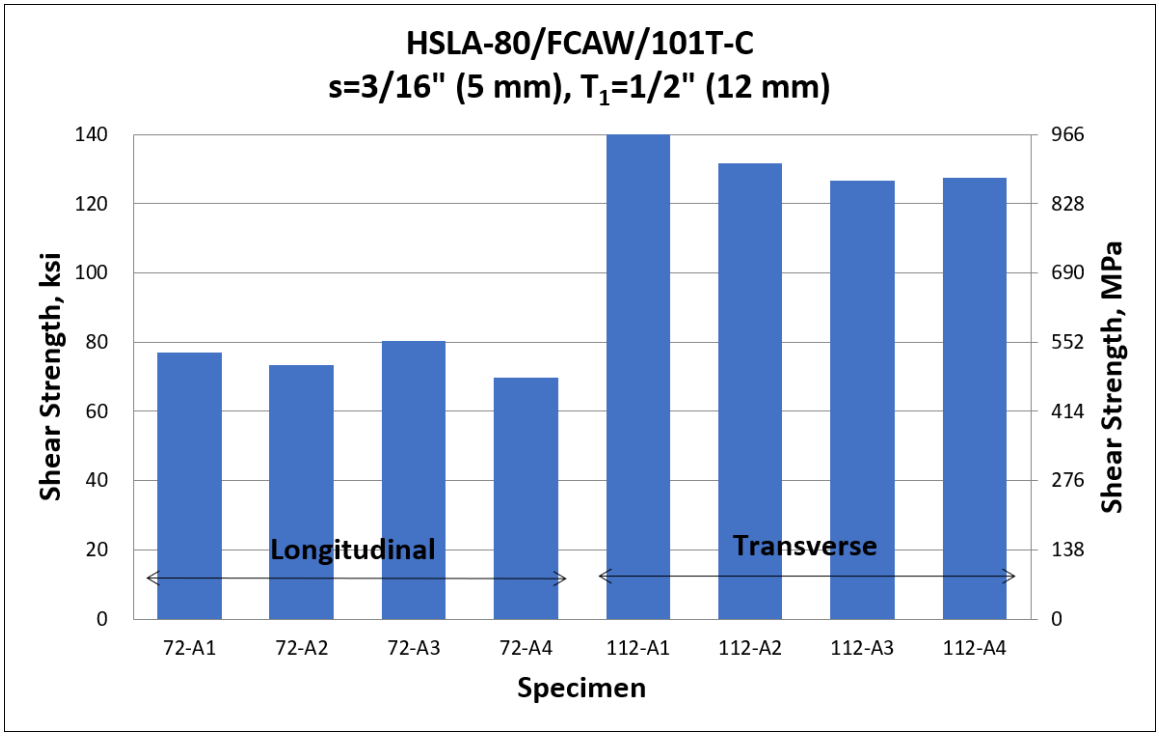
HSLA-80/FCAW/101T-C
s=3/16" (5 mm), T1=1/2" (12 mm)
Shear Strength, ksi
Shear Strength, MPa
140
120
100
80
60
40
20
0
966
828
690
552
414
276
138
0
Longitudinal
Transverse
72-A1
72-A2
72-A3
72-A4
112-A1
112-A2
112-A3
112-A4
Specimen

(b)

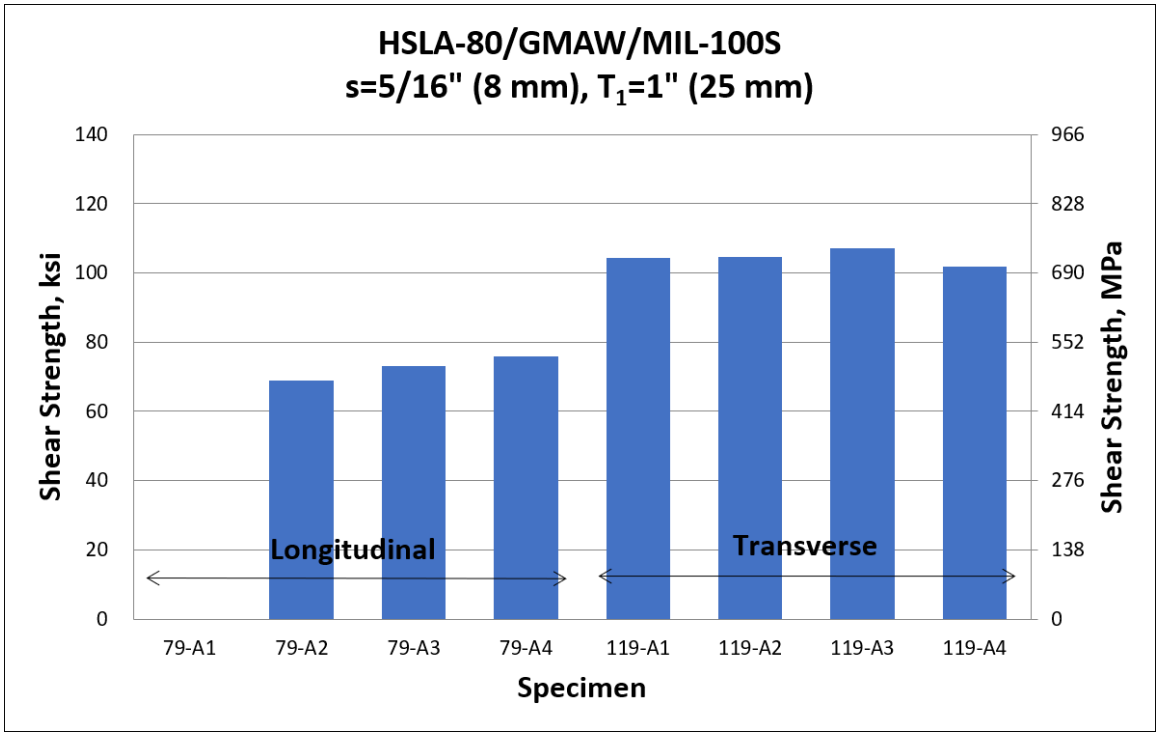
HSLA-80/GMAW/MIL-100S
s=5/16" (8 mm), T1=1" (25 mm)
Shear Strength, ksi
Shear Strength, MPa
140
120
100
80
60
40
20
0
966
828
690
552
414
276
138
0
Longitudinal
Transverse
79-A1
79-A2
79-A3
79-A4
119-A1
119-A2
119-A3
119-A4
Specimen

(c)

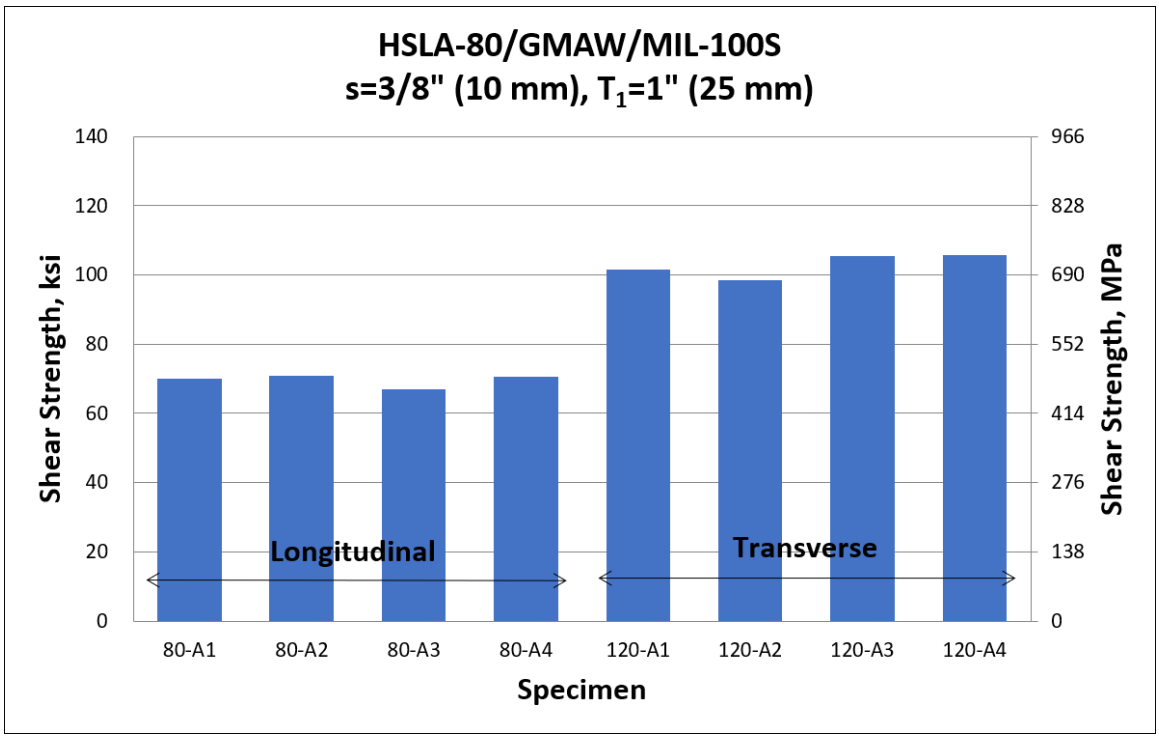

(d)

Figure A.3: Shear strength correlation between longitudinal and transverse shear specimens using conventional method for HSLA-80 with GMAW and MIL-100S weld wire

Appendix B Shear Strength Correlation between Longitudinal and Transverse Shear Specimens using Traction Stress Method

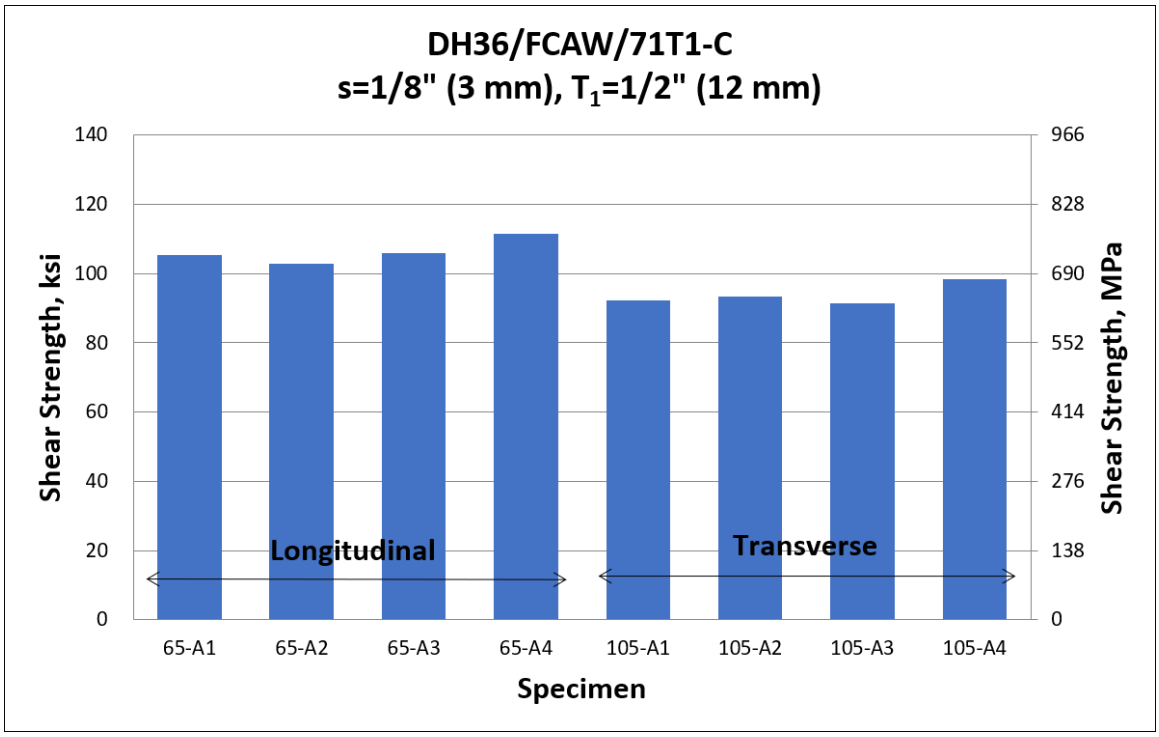

(a)

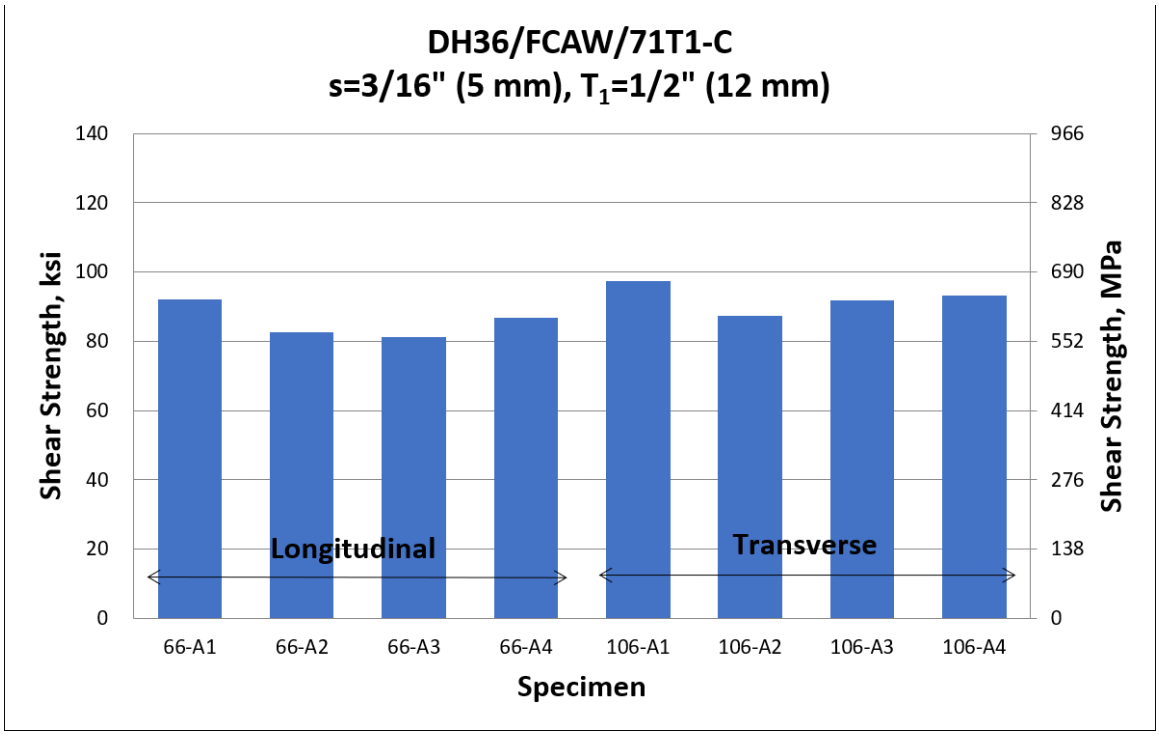
DH36/FCAW/71T1-C
s=3/16" (5 mm), T1=1/2" (12 mm)
Shear Strength, ksi
Shear Strength, MPa
140
120
100
80
60
40
20
0
966
828
690
552
414
276
138
0
Longitudinal
Transverse
66-A1
66-A2
66-A3
66-A4
106-A1
106-A2
106-A3
106-A4
Specimen

(b)

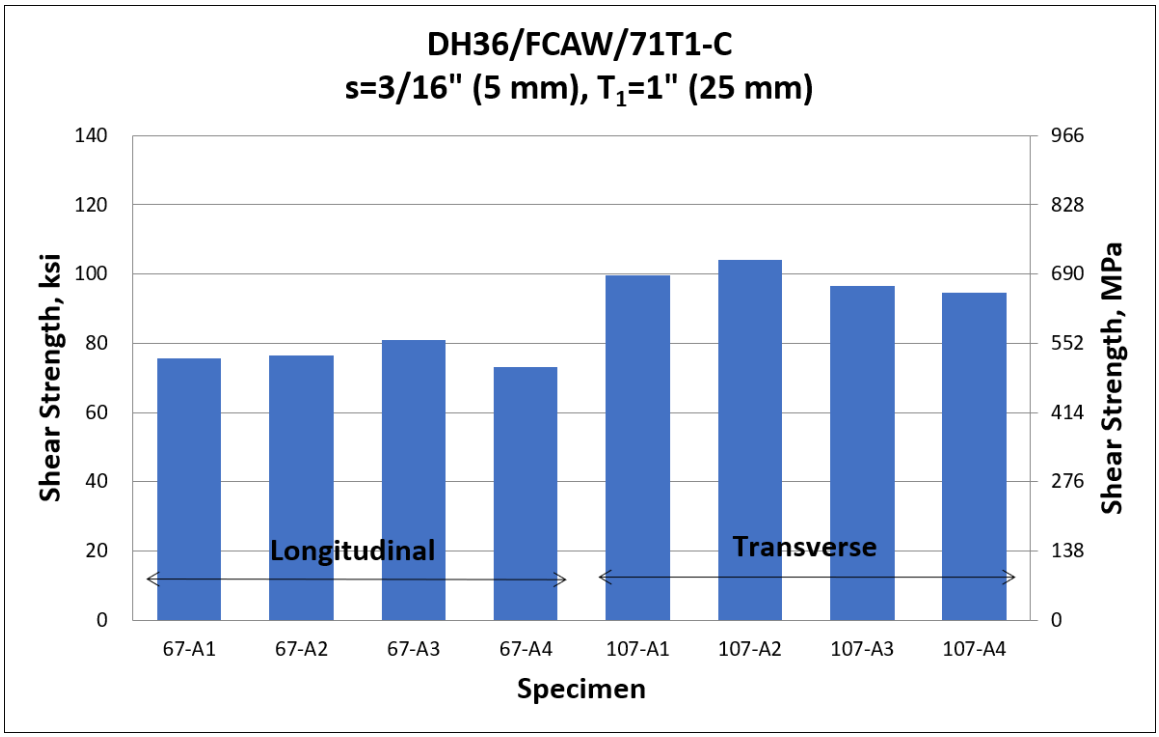
DH36/FCAW/71T1-C
s=3/16" (5 mm), T1=1" (25 mm)
Shear Strength, ksi
Shear Strength, MPa
140
120
100
80
60
40
20
0
966
828
690
552
414
276
138
0
Longitudinal
Transverse
67-A1
67-A2
67-A3
67-A4
107-A1
107-A2
107-A3
107-A4
Specimen

(c)

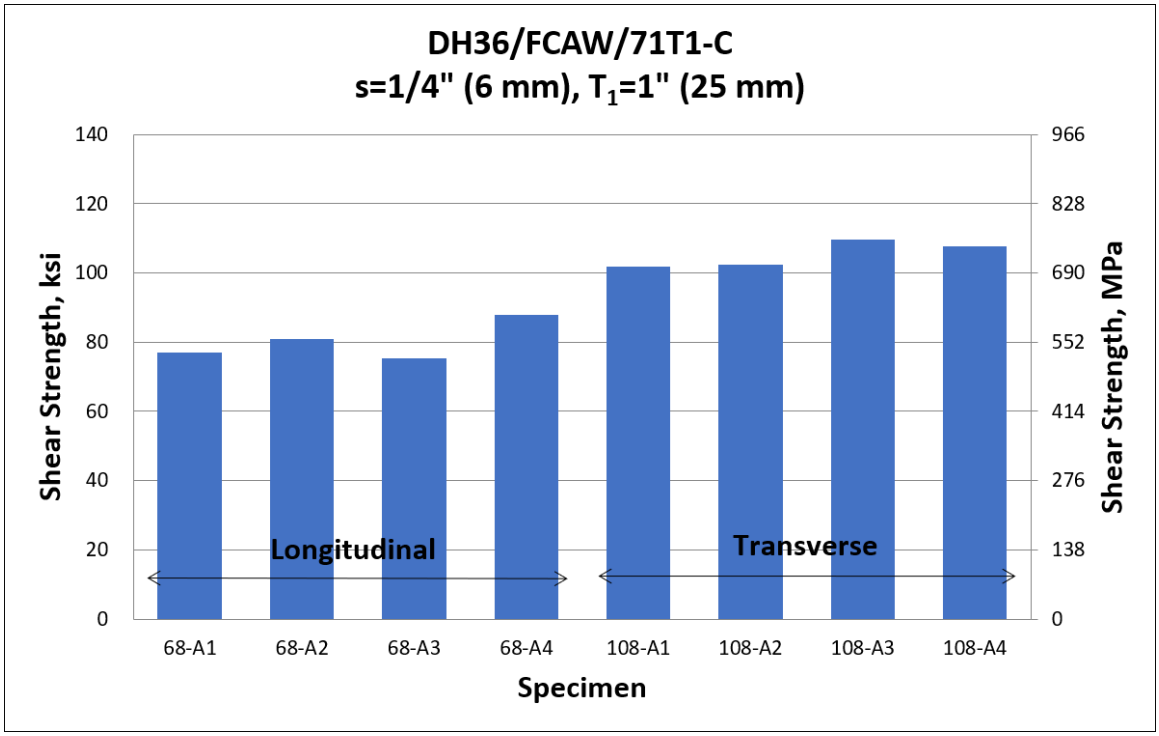
DH36/FCAW/71T1-C
s=1/4" (6 mm), T1=1" (25 mm)
Shear Strength, ksi
Shear Strength, MPa
140
120
100
80
60
40
20
0
966
828
690
552
414
276
138
0
Longitudinal
Transverse
68-A1
68-A2
68-A3
68-A4
108-A1
108-A2
108-A3
108-A4
Specimen

(d)

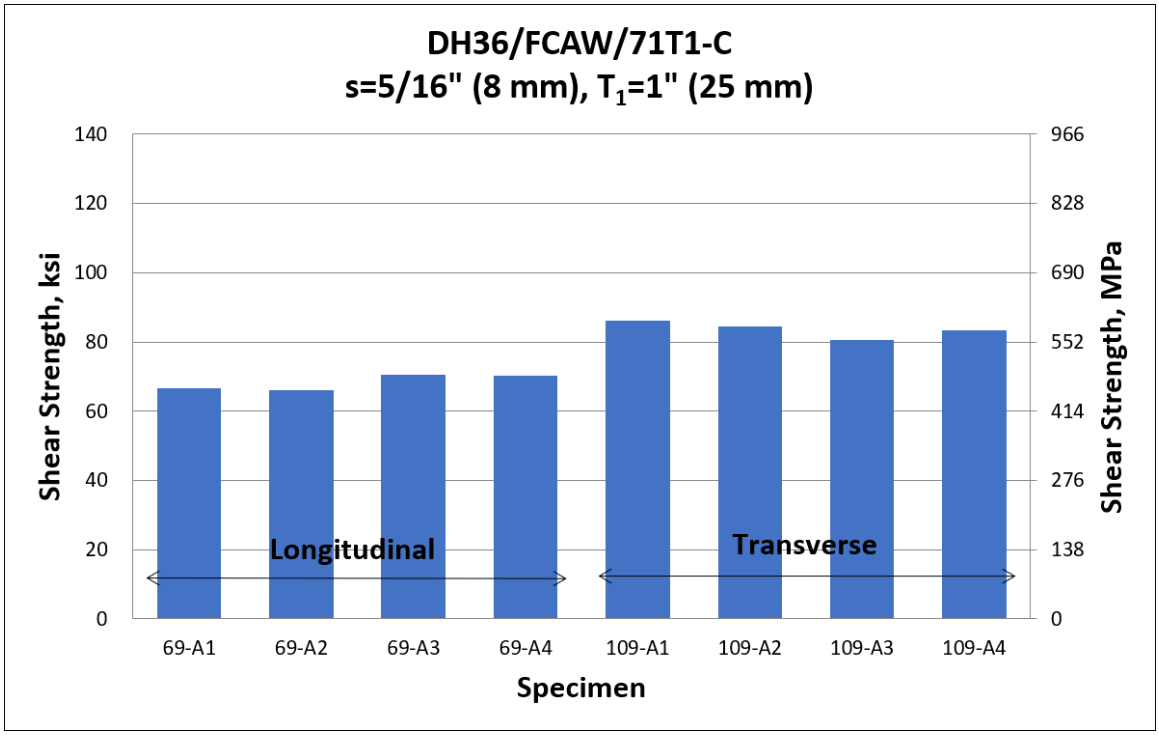
DH36/FCAW/71T1-C
s=5/16" (8 mm), T1=1" (25 mm)
Shear Strength, ksi
Shear Strength, MPa
140
120
100
80
60
40
20
0
966
828
690
552
414
276
138
0
Longitudinal
Transverse
69-A1
69-A2
69-A3
69-A4
109-A1
109-A2
109-A3
109-A4
Specimen

(e)

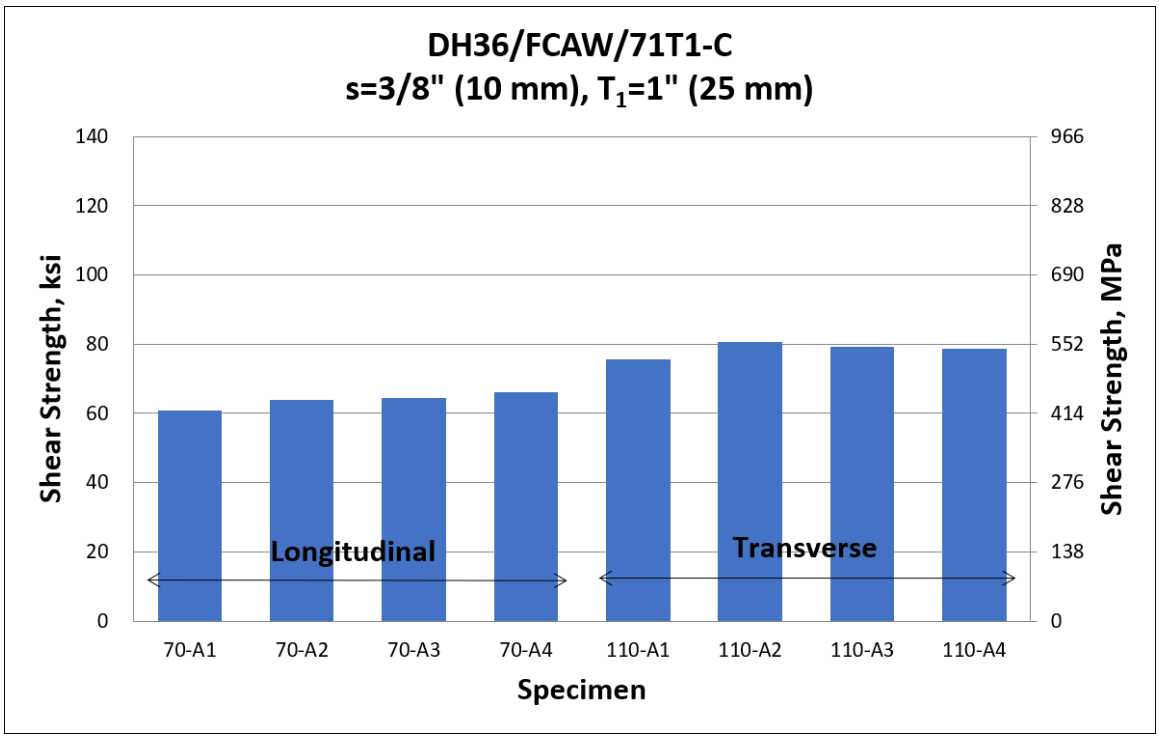

(f)

Figure B.1: Shear strength correlation between longitudinal and transverse shear specimens using traction stress method for DH36 with FCAW and 71T1-C weld wire

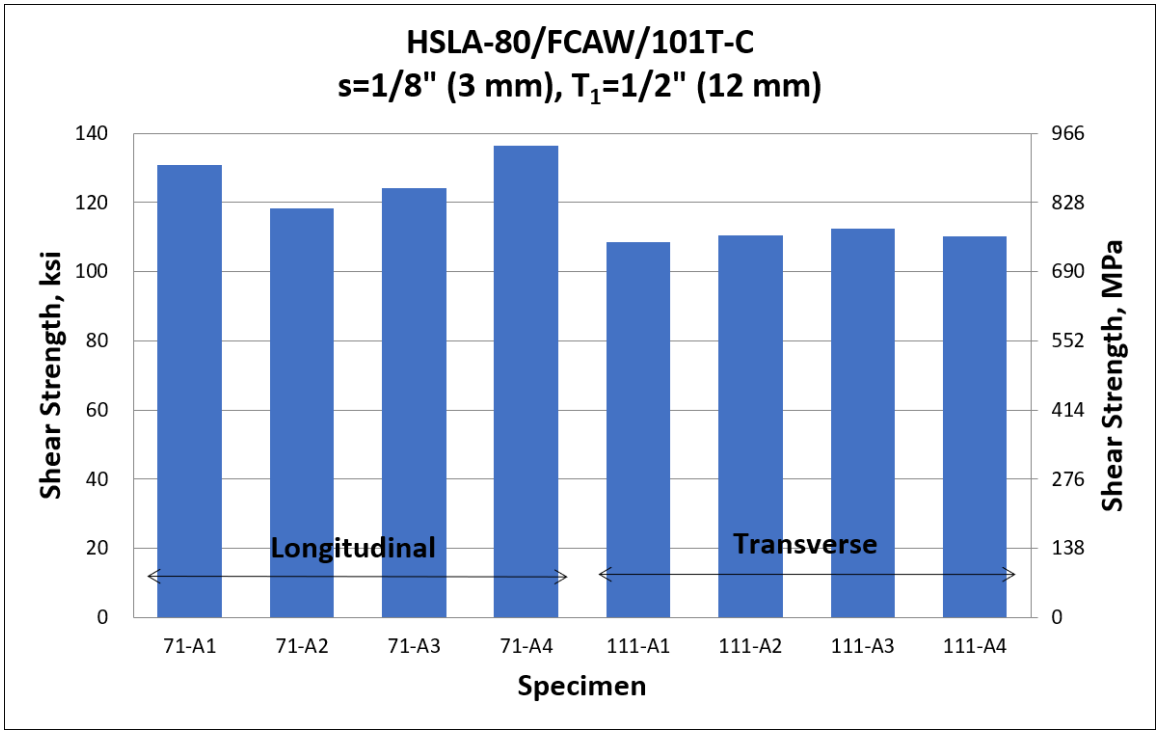

(a)

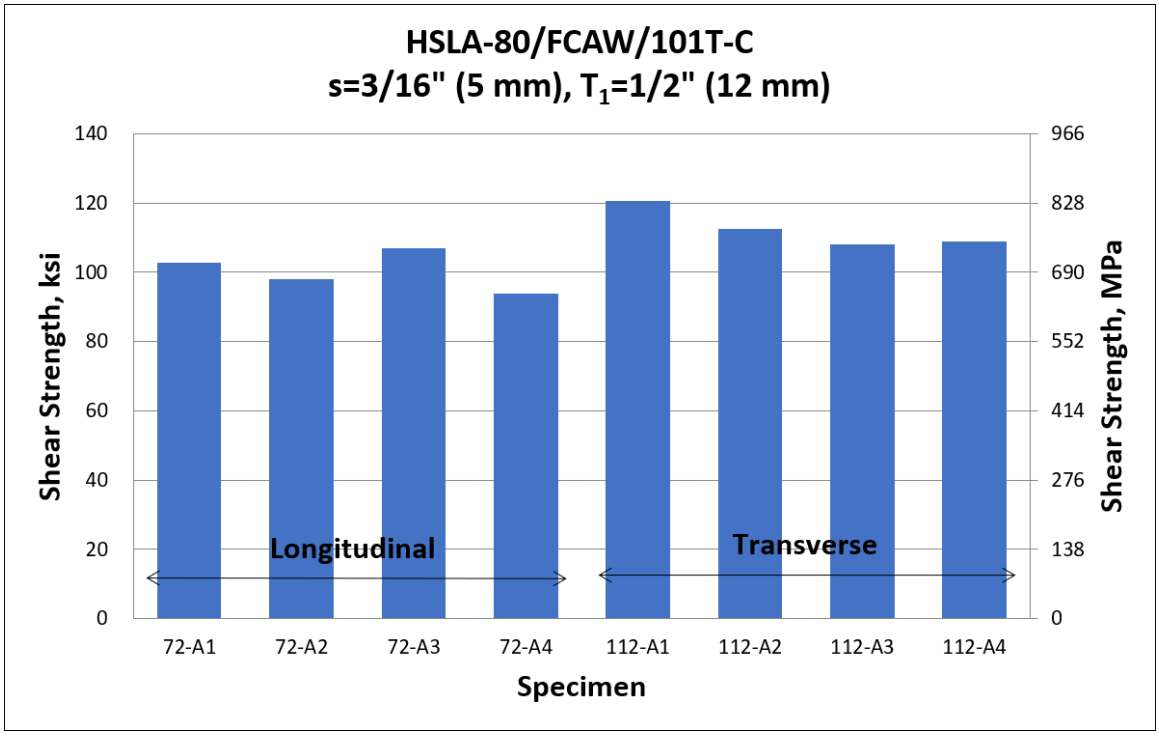
HSLA-80/FCAW/101T-C
s=3/16" (5 mm), T1=1/2" (12 mm)
Shear Strength, ksi
Shear Strength, MPa
140
120
100
80
60
40
20
0
966
828
690
552
414
276
138
0
Longitudinal
Transverse
72-A1
72-A2
72-A3
72-A4
112-A1
112-A2
112-A3
112-A4
Specimen

(b)

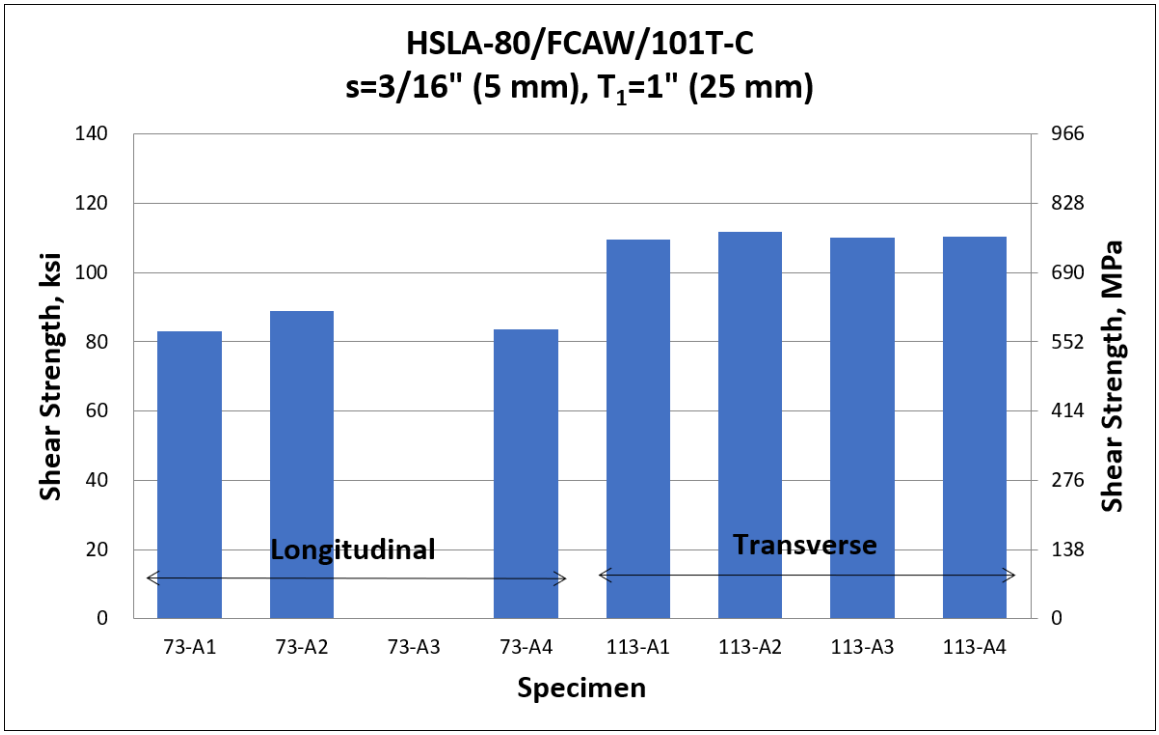
HSLA-80/FCAW/101T-C
s=3/16" (5 mm), T1=1" (25 mm)
Shear Strength, ksi
Shear Strength, MPa
140
120
100
80
60
40
20
0
966
828
690
552
414
276
138
0
Longitudinal
Transverse
73-A1
73-A2
73-A3
73-A4
113-A1
113-A2
113-A3
113-A4
Specimen

(c)

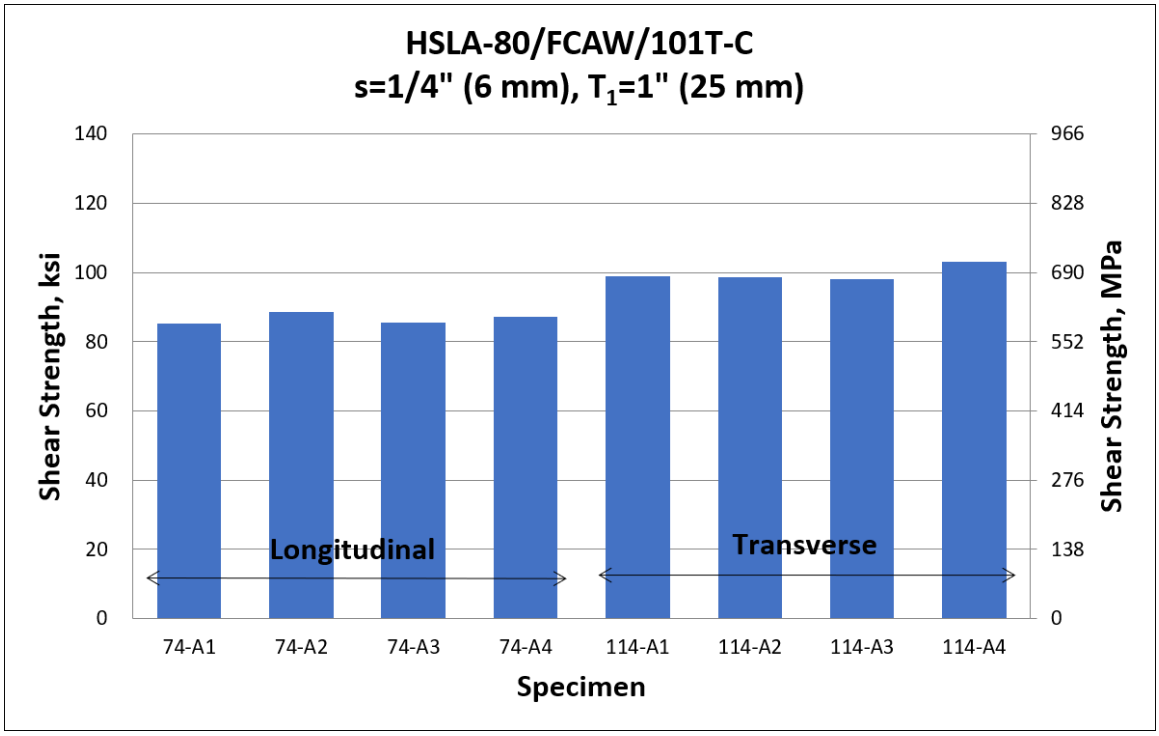
HSLA-80/FCAW/101T-C
s=1/4" (6 mm), T1=1" (25 mm)
Shear Strength, ksi
Shear Strength, MPa
140
120
100
80
60
40
20
0
966
828
690
552
414
276
138
0
Longitudinal
Transverse
74-A1
74-A2
74-A3
74-A4
114-A1
114-A2
114-A3
114-A4
Specimen

(d)

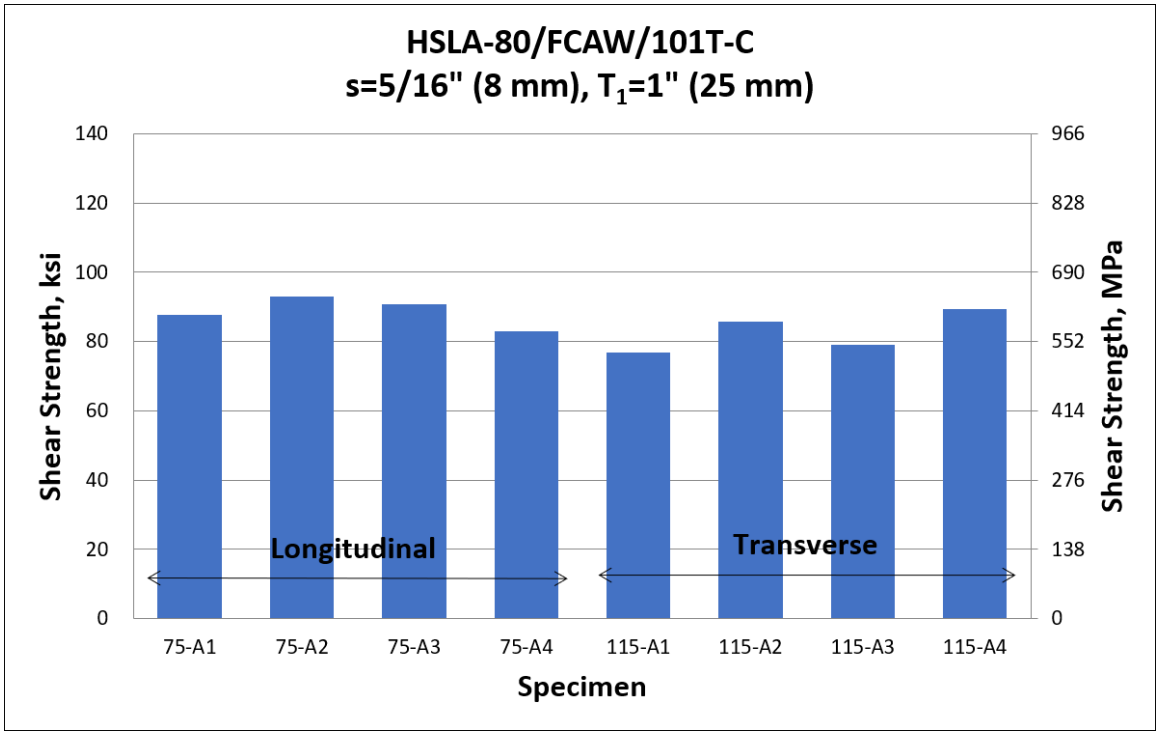
HSLA-80/FCAW/101T-C
s=5/16" (8 mm), T1=1" (25 mm)
Shear Strength, ksi
Shear Strength, MPa
140
120
100
80
60
40
20
0
966
828
690
552
414
276
138
0
Longitudinal
Transverse
75-A1
75-A2
75-A3
75-A4
115-A1
115-A2
115-A3
115-A4
Specimen

(e)

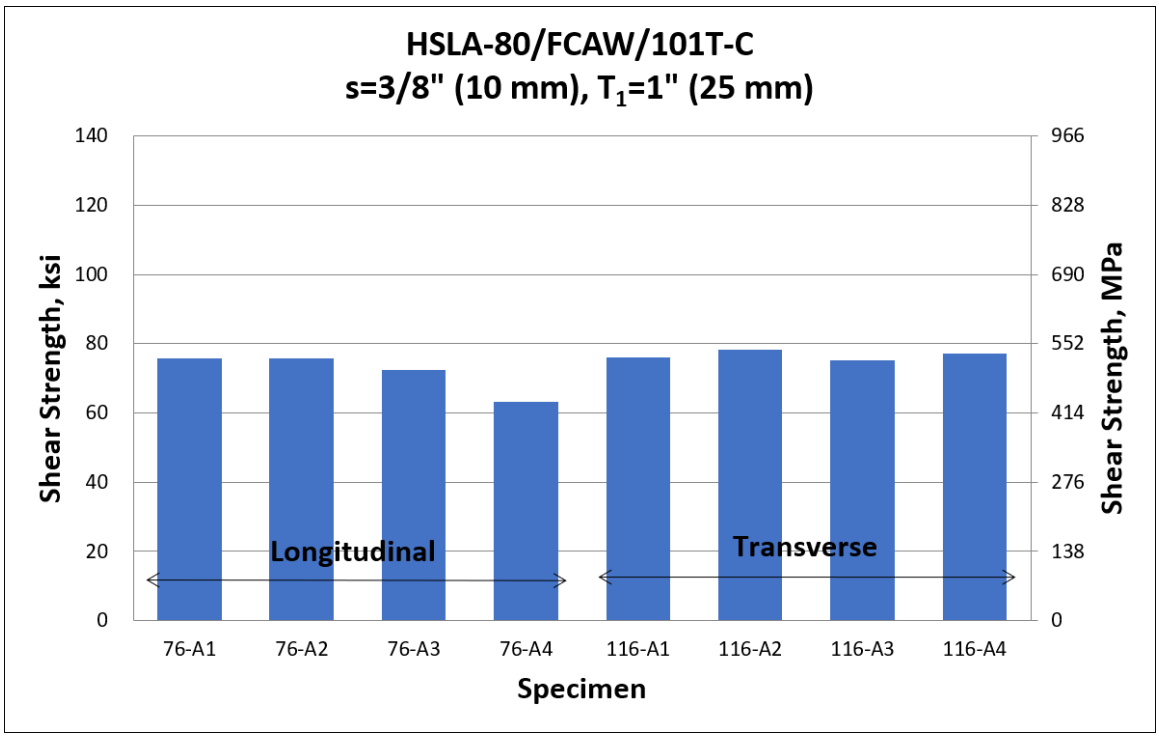

(f)

Figure B.2: Shear strength correlation between longitudinal and transverse shear specimens using traction stress method for HSLA-80 with FCAW and 101T-C weld wire

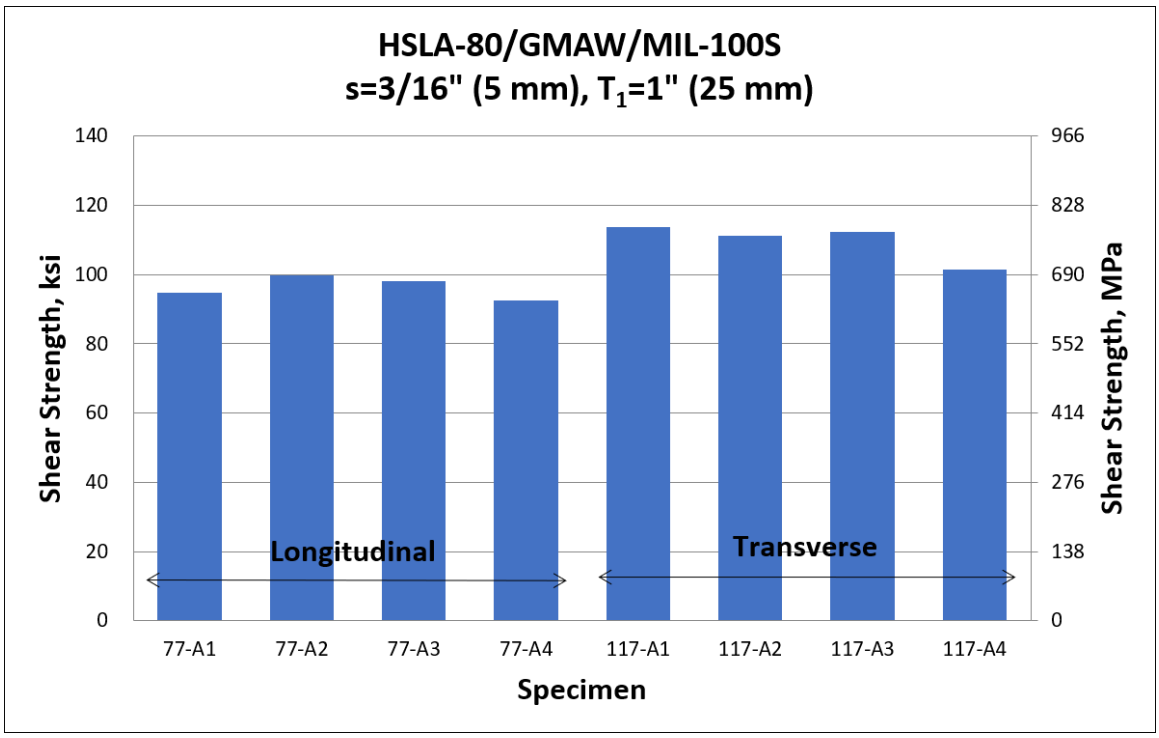

(a)

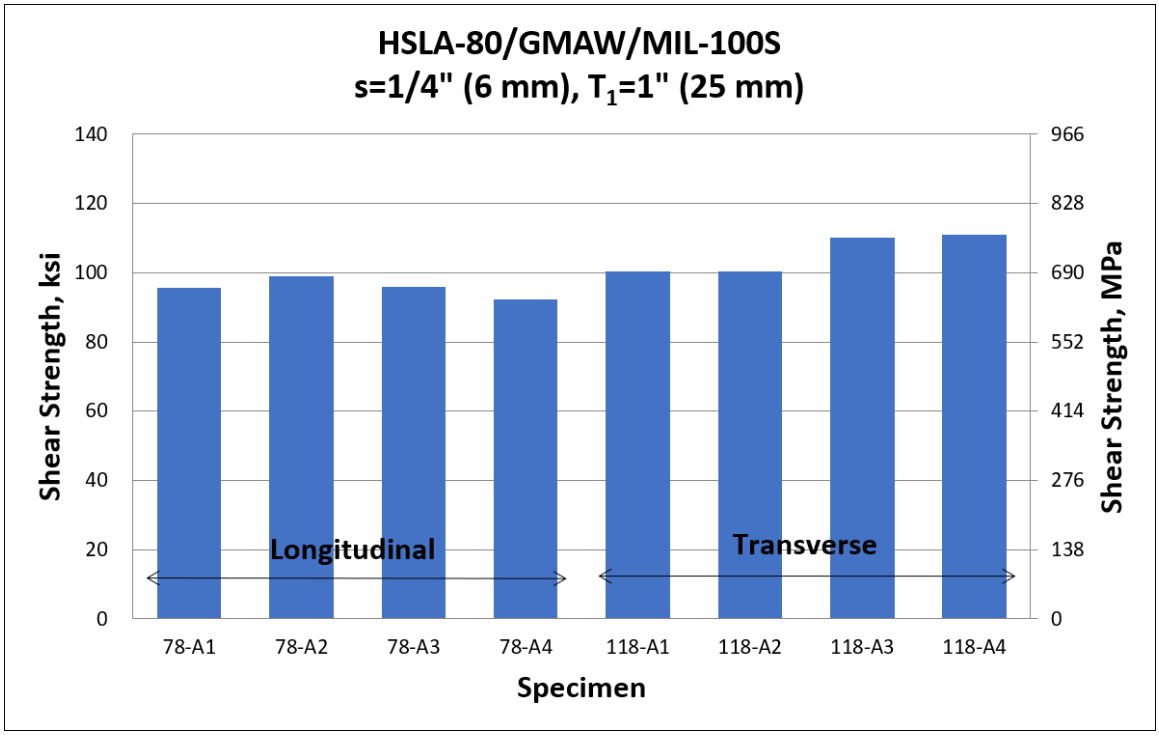
HSLA-80/GMAW/MIL-100S
s=1/4" (6 mm), T1=1" (25 mm)
Shear Strength, ksi
Shear Strength, MPa
140
120
100
80
60
40
20
0
966
828
690
552
414
276
138
0
Longitudinal
Transverse
78-A1
78-A2
78-A3
78-A4
118-A1
118-A2
118-A3
118-A4
Specimen

(b)

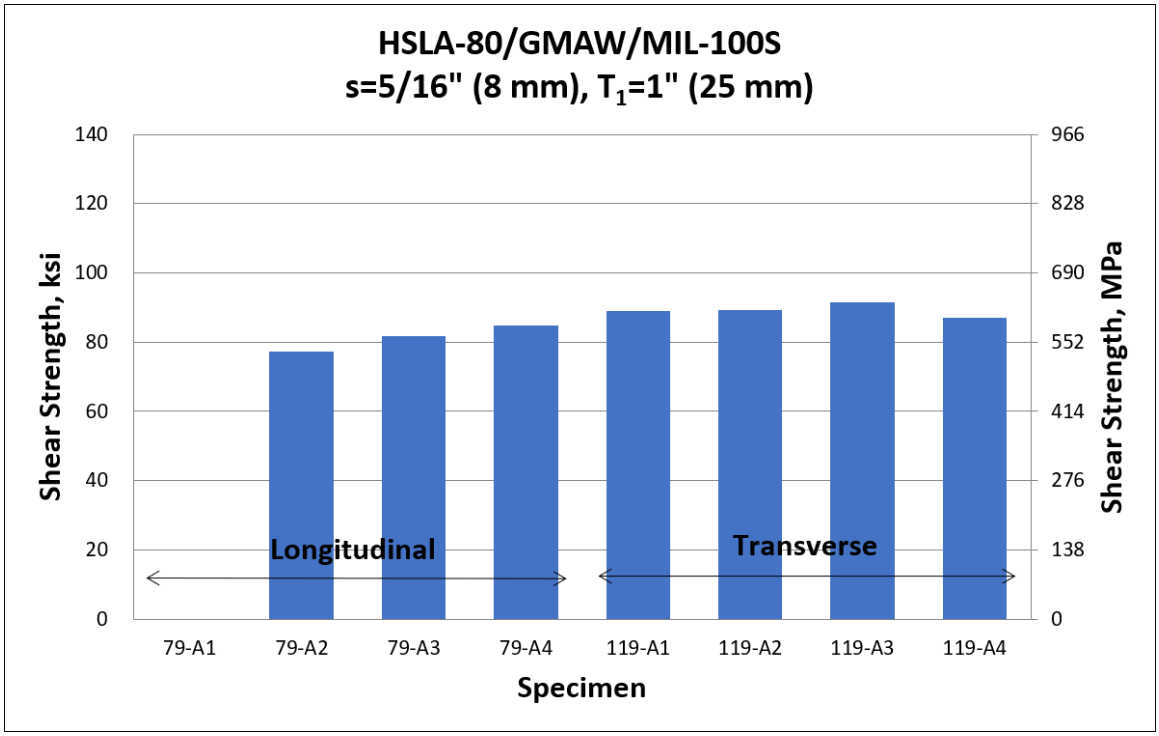
HSLA-80/GMAW/MIL-100S
s=5/16" (8 mm), T1=1" (25 mm)
Shear Strength, ksi
Shear Strength, MPa
140
120
100
80
60
40
20
0
966
828
690
552
414
276
138
0
Longitudinal
Transverse
79-A1
79-A2
79-A3
79-A4
119-A1
119-A2
119-A3
119-A4
Specimen

(c)

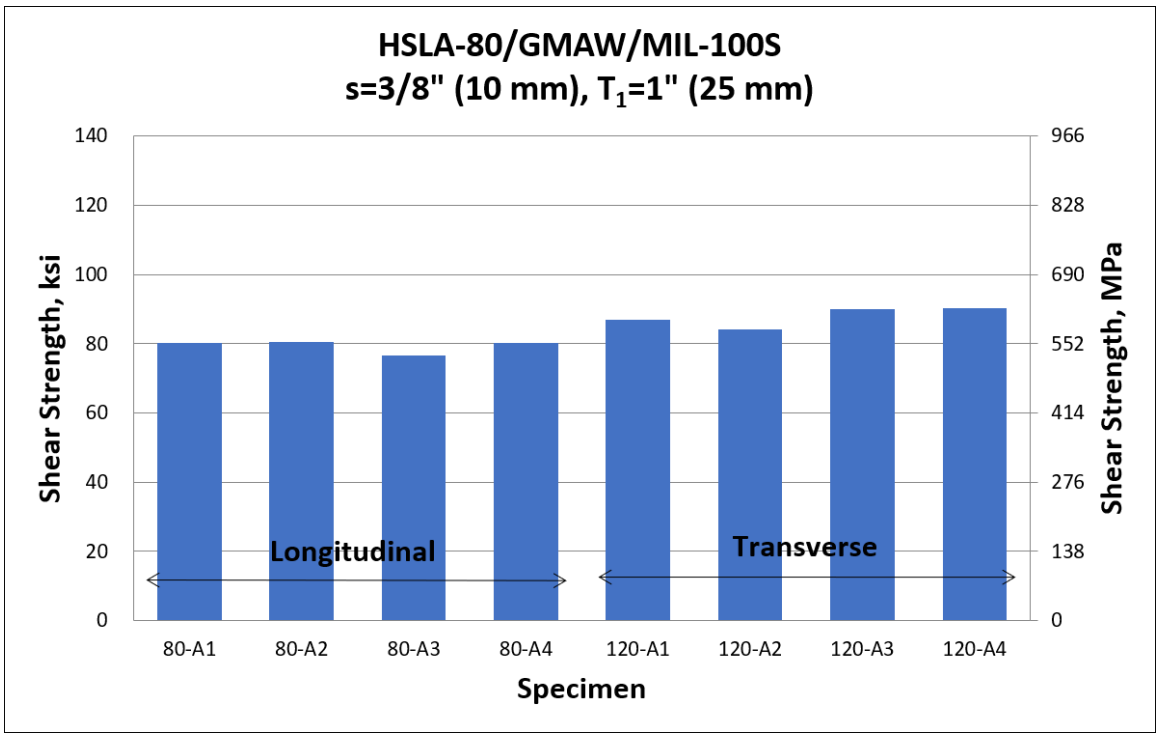

(d)

Figure B.3: Shear strength correlation between longitudinal and transverse shear specimens using traction stress method for HSLA-80 with GMAW and MIL-100S weld wire

Appendix C Shear Strength Correlations by Traction Stress Method with and without Plate Contact Effects

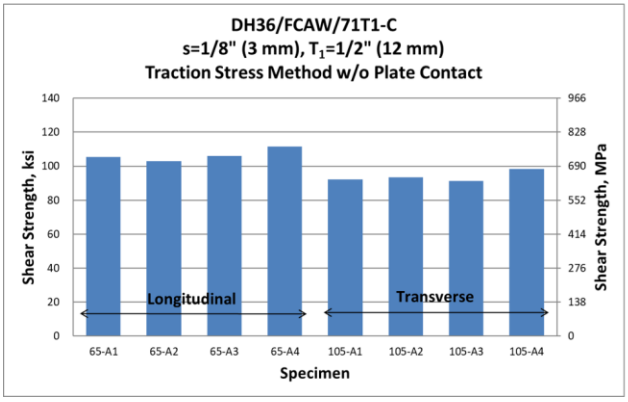

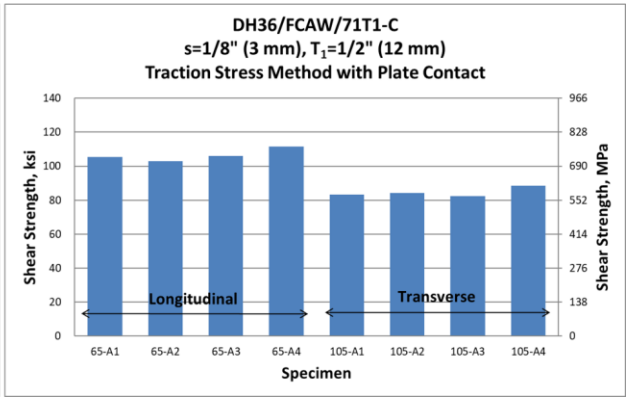

(a)

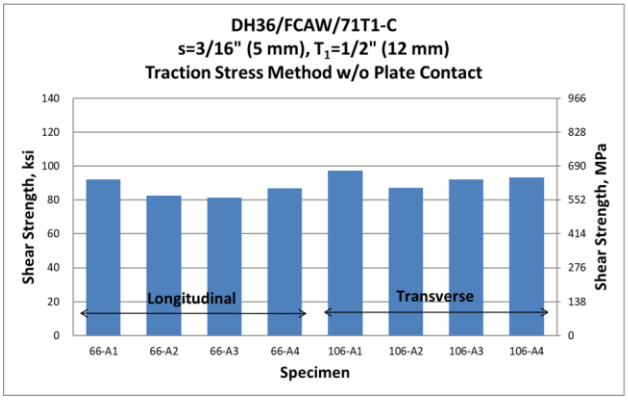

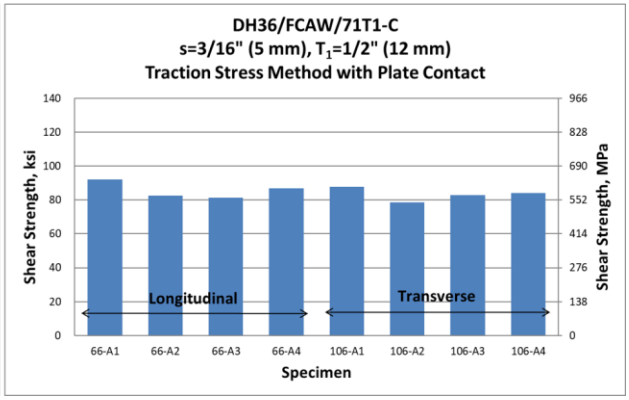

(b)

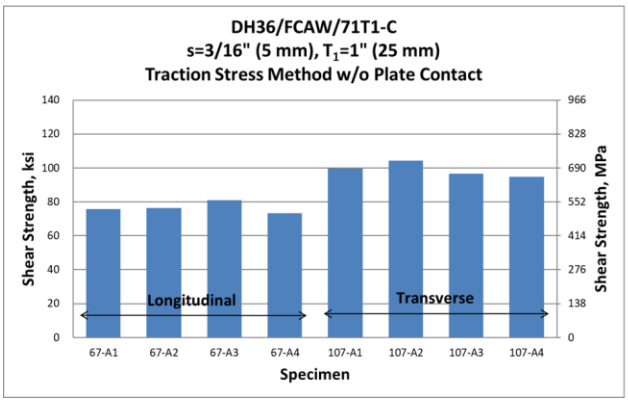

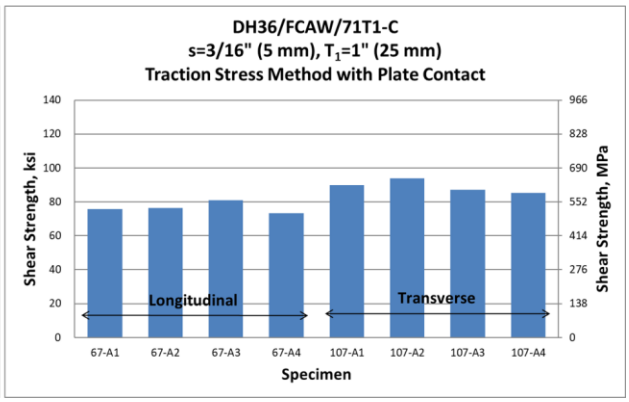

(c)

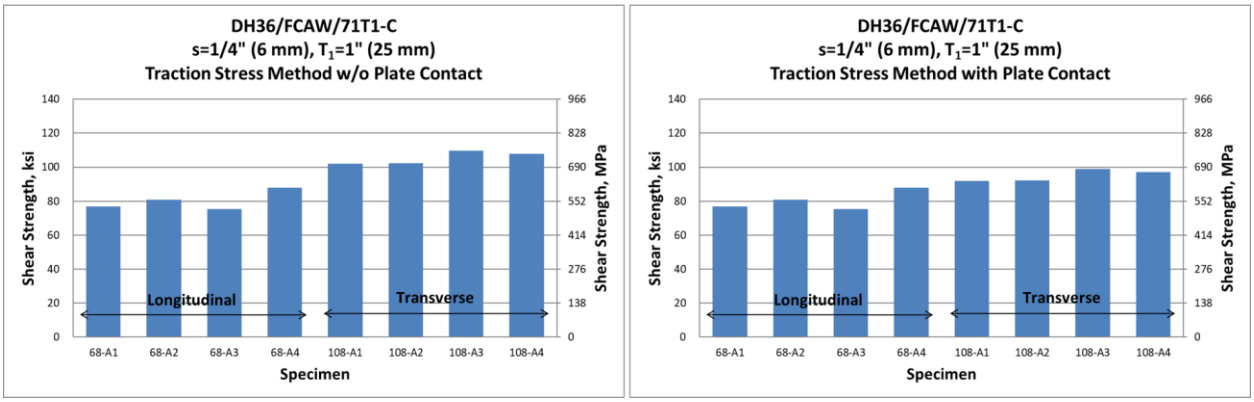

(d)

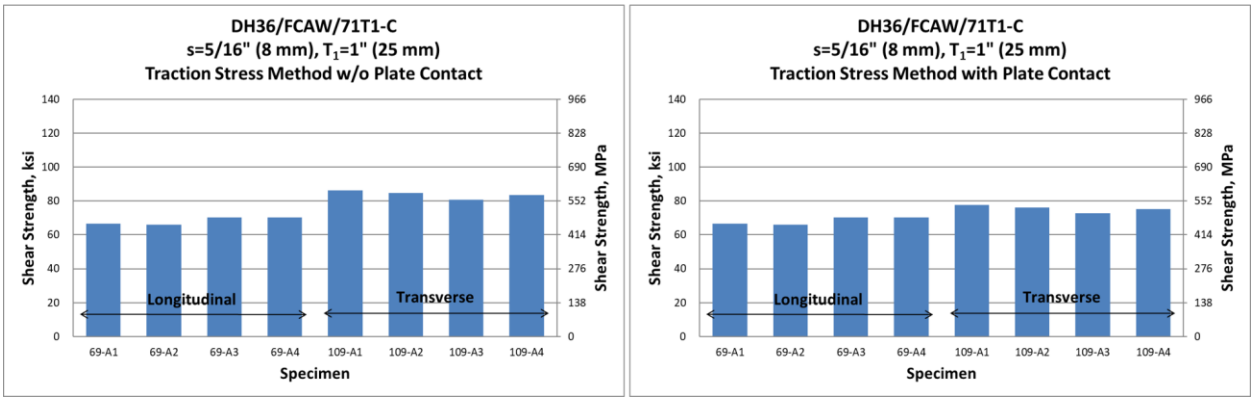

(e)

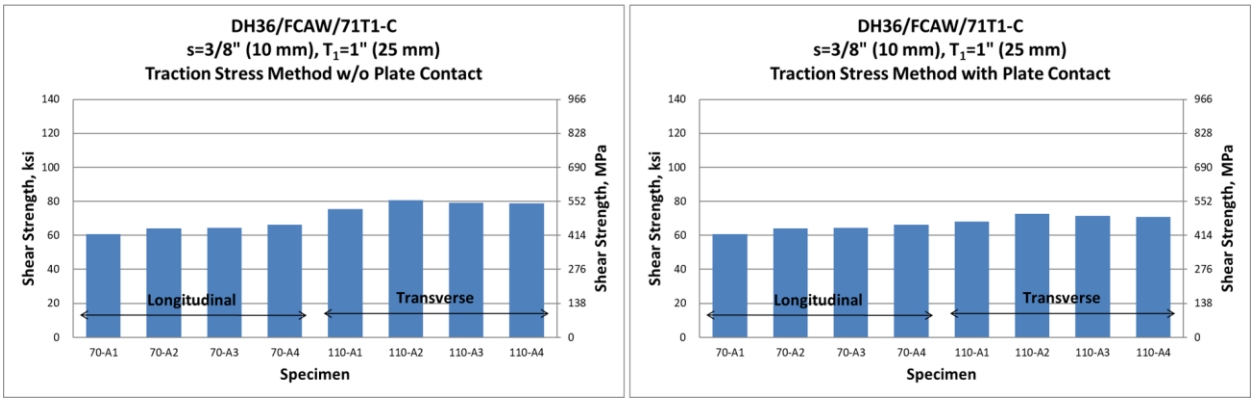

(f)

Figure C.1: Shear strength correlations by traction stress method with and without contact effects for DH36 with FCAW, and 71T1-C weld wire

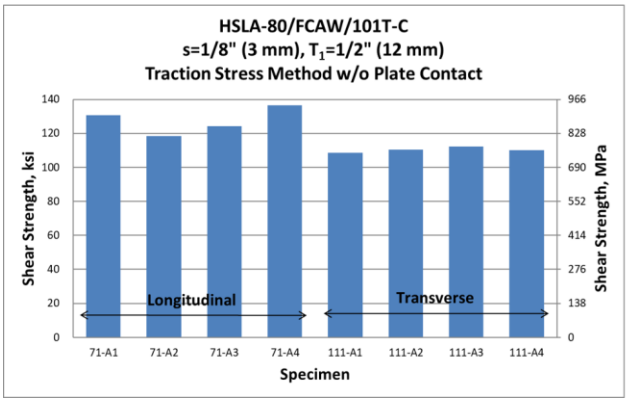
HSLA-80/FCAW/101T-C
s=1/8" (3 mm), T1=1/2" (12 mm)
Traction Stress Method w/o Plate Contact
Shear Strength, ksi
Shear Strength, MPa
Longitudinal
Transverse
71-A1 71-A2 71-A3 71-A4 111-A1 111-A2 111-A3 111-A4
Specimen

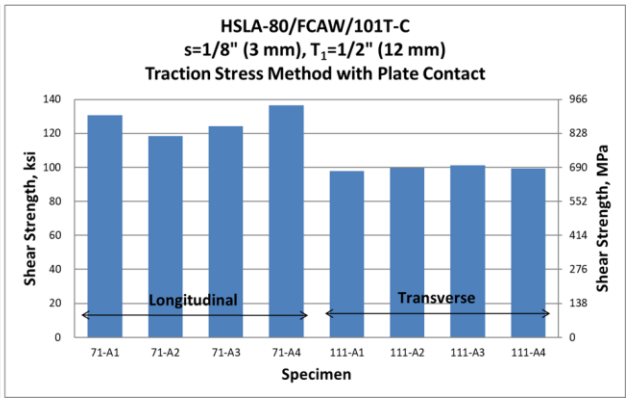
HSLA-80/FCAW/101T-C
s=1/8" (3 mm), T1=1/2" (12 mm)
Traction Stress Method with Plate Contact
Shear Strength, ksi
Shear Strength, MPa
Longitudinal
Transverse
71-A1 71-A2 71-A3 71-A4 111-A1 111-A2 111-A3 111-A4
Specimen

(a)

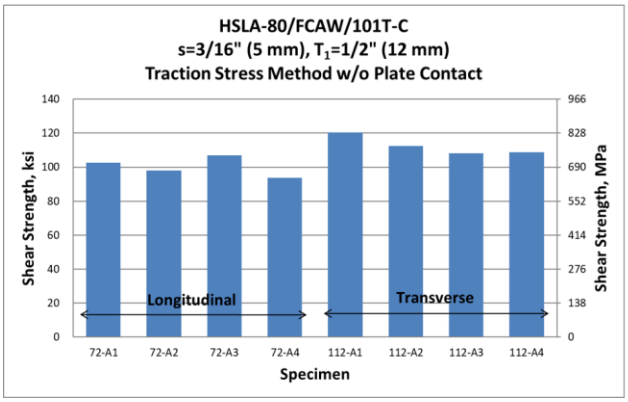
HSLA-80/FCAW/101T-C
s=3/16" (5 mm), T1=1/2" (12 mm)
Traction Stress Method w/o Plate Contact
Shear Strength, ksi
Shear Strength, MPa
Longitudinal
Transverse
72-A1 72-A2 72-A3 72-A4 112-A1 112-A2 112-A3 112-A4
Specimen

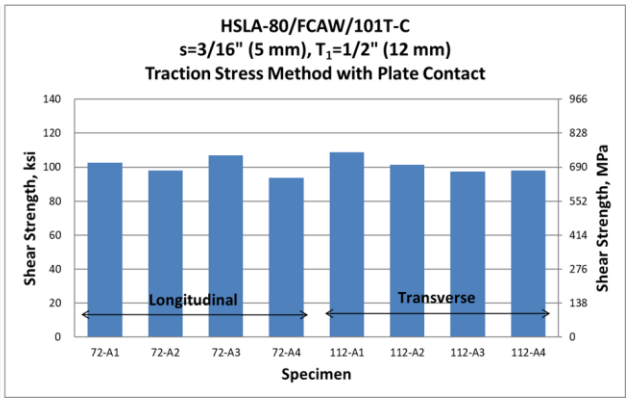
HSLA-80/FCAW/101T-C
s=3/16" (5 mm), T1=1/2" (12 mm)
Traction Stress Method with Plate Contact
Shear Strength, ksi
Shear Strength, MPa
Longitudinal
Transverse
72-A1 72-A2 72-A3 72-A4 112-A1 112-A2 112-A3 112-A4
Specimen

(b)

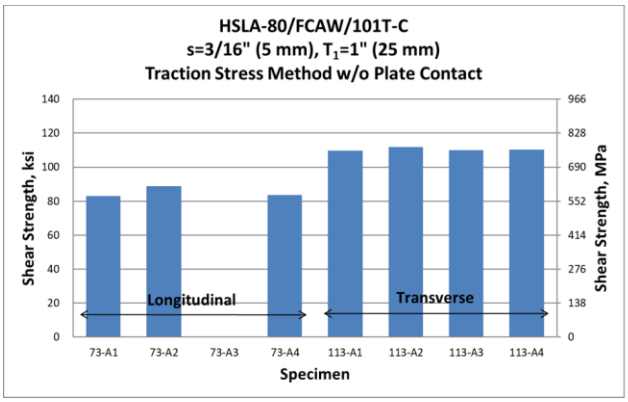
HSLA-80/FCAW/101T-C
s=3/16" (5 mm), T1=1" (25 mm)
Traction Stress Method w/o Plate Contact
Shear Strength, ksi
Shear Strength, MPa
Longitudinal
Transverse
73-A1 73-A2 73-A3 73-A4 113-A1 113-A2 113-A3 113-A4
Specimen

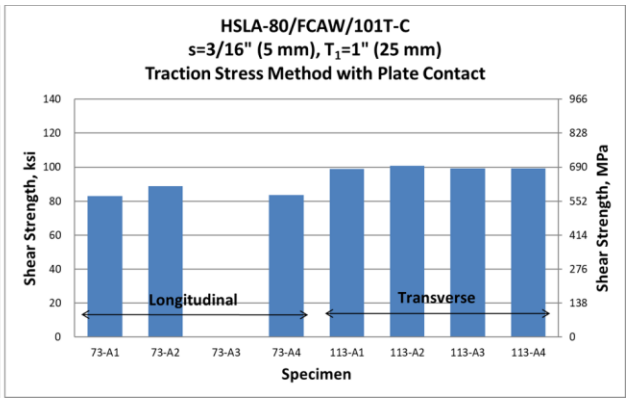
HSLA-80/FCAW/101T-C
s=3/16" (5 mm), T1=1" (25 mm)
Traction Stress Method with Plate Contact
Shear Strength, ksi
Shear Strength, MPa
Longitudinal
Transverse
73-A1 73-A2 73-A3 73-A4 113-A1 113-A2 113-A3 113-A4
Specimen

(c)

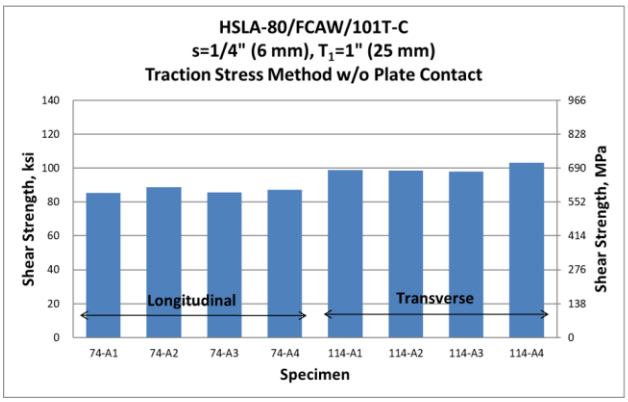
HSLA-80/FCAW/101T-C
s=1/4" (6 mm), T1=1" (25 mm)
Traction Stress Method w/o Plate Contact
Shear Strength, ksi
Shear Strength, MPa
Longitudinal
Transverse
74-A1 74-A2 74-A3 74-A4 114-A1 114-A2 114-A3 114-A4
Specimen

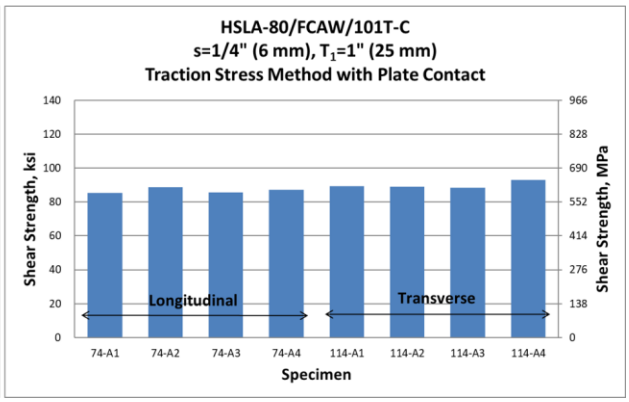
HSLA-80/FCAW/101T-C
s=1/4" (6 mm), T1=1" (25 mm)
Traction Stress Method with Plate Contact
Shear Strength, ksi
Shear Strength, MPa
Longitudinal
Transverse
74-A1 74-A2 74-A3 74-A4 114-A1 114-A2 114-A3 114-A4
Specimen

(d)

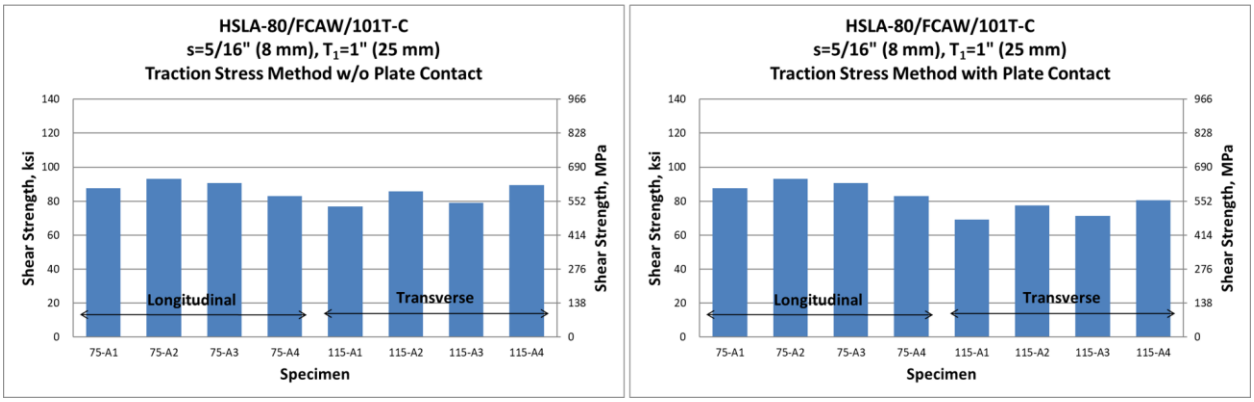

(e)

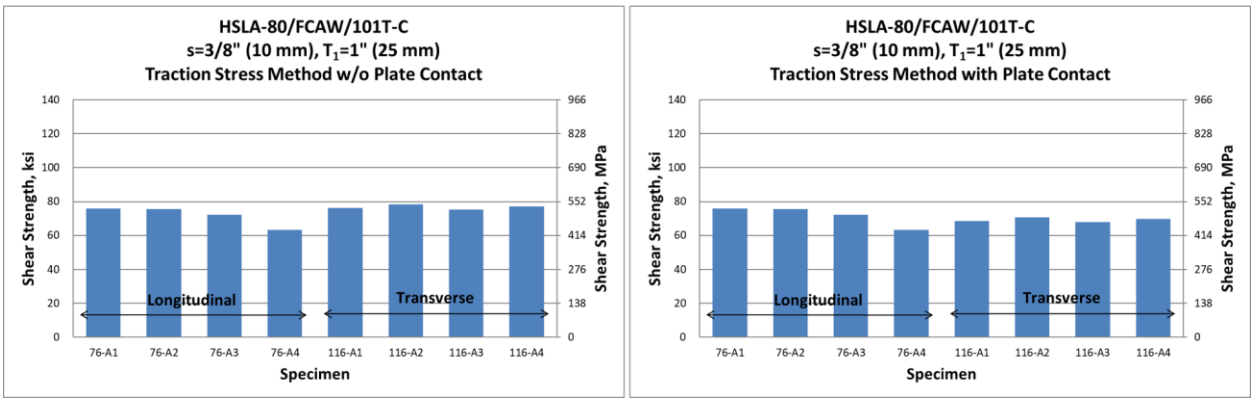

(f)

Figure C.2: Shear strength correlations by traction stress method with and without contact effects for HSLA-80 with FCAW, and 101T-C weld wire

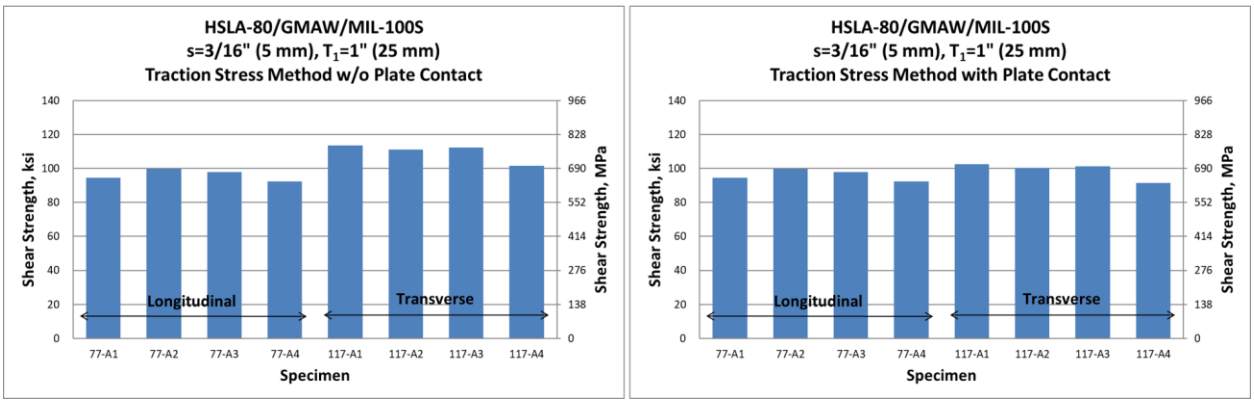

(a)

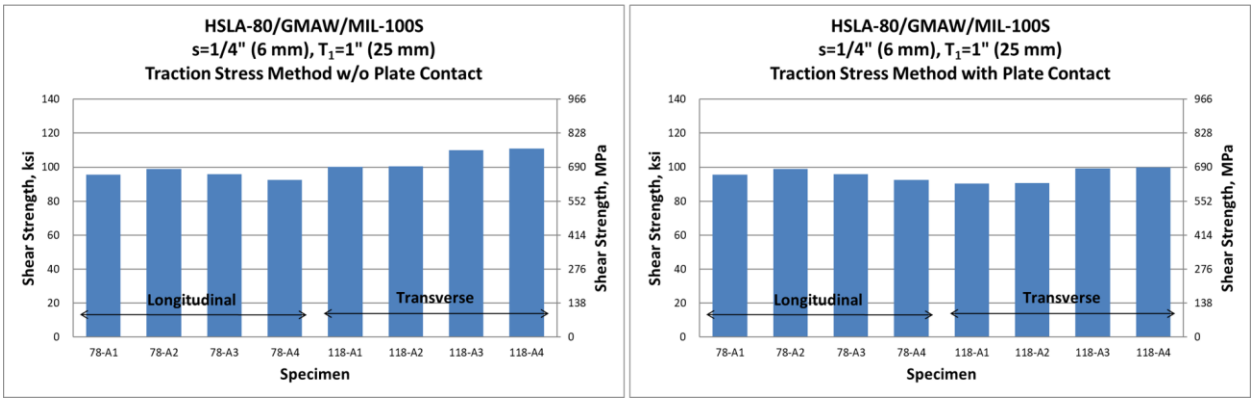

(b)

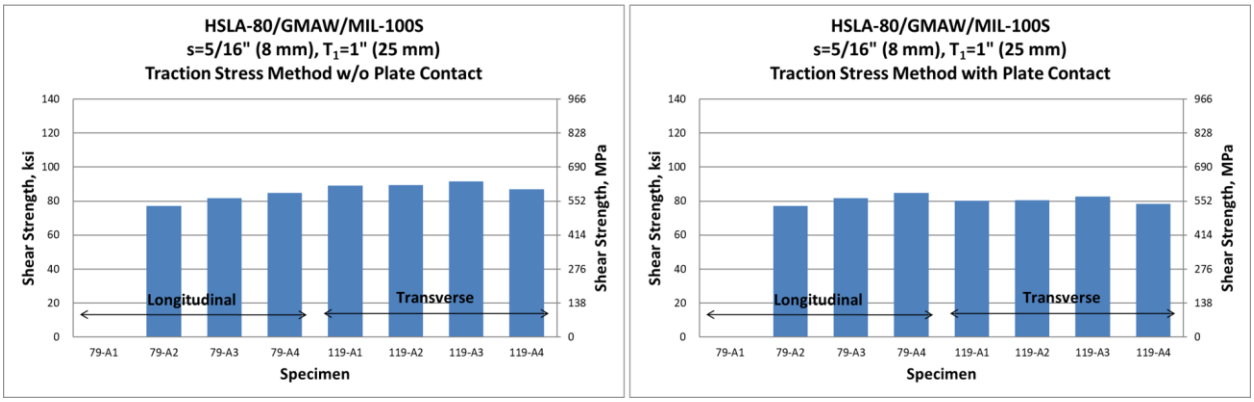

(c)

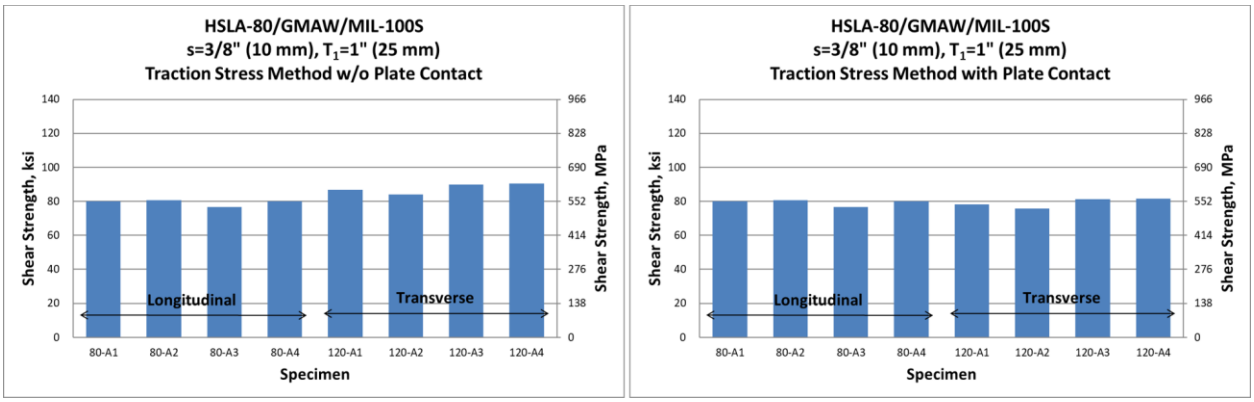

(d)

Figure C.3: Shear strength correlations by traction stress method with and without contact effects for HSLA-80 with GMAW, and MIL-100S weld wire

Appendix D Shear Strength Correlations between Longitudinal and Transverse Specimens Made of Aluminum Alloys

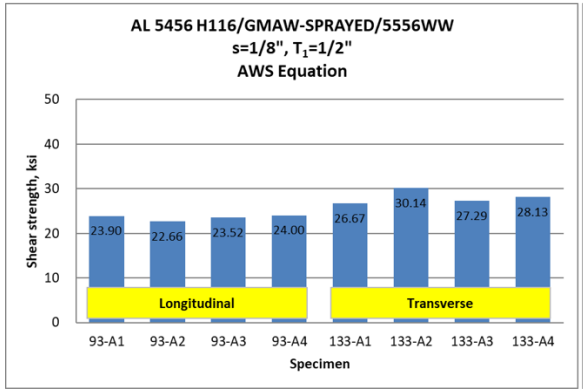

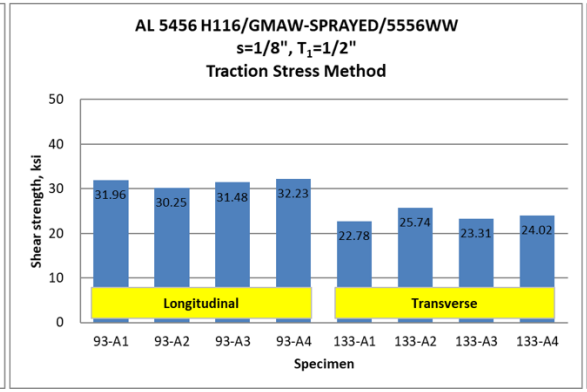

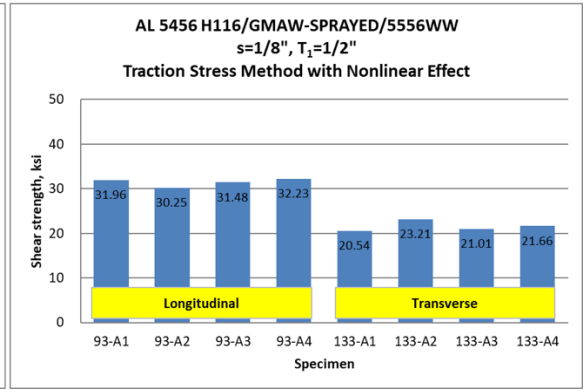

(a)

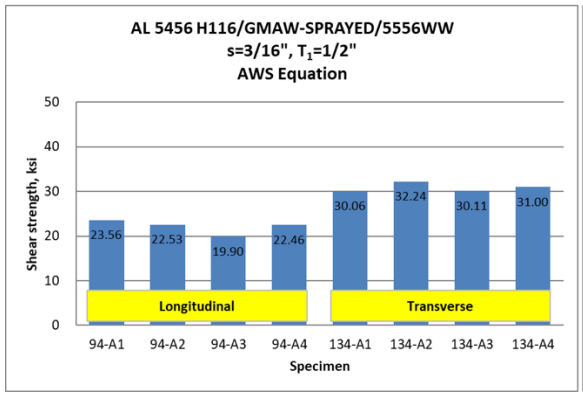

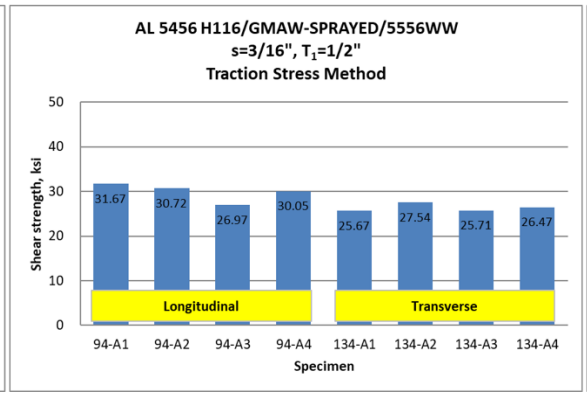

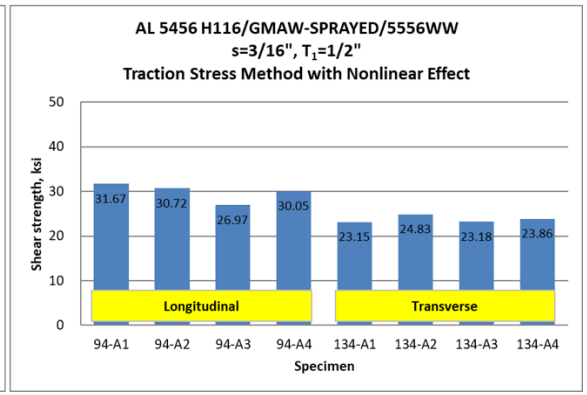

(b)

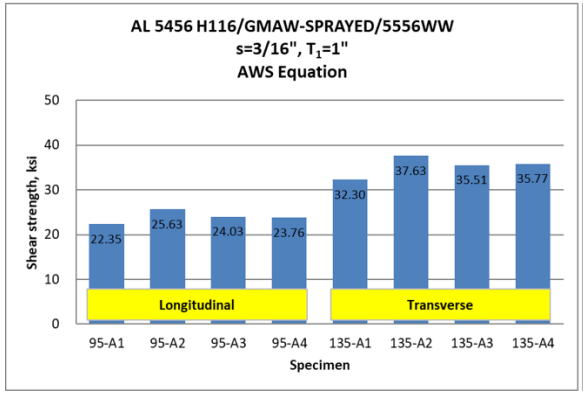
AL 5456 H116/GMAW-SPRAYED/5556WW
s=3/16", T1=1"
AWS Equation
Shear strength, ksi
50
40
30
20
10
0
22.35
25.63
24.03
23.76
32.30
37.63
35.51
35.77
Longitudinal
Transverse
95-A1
95-A2
95-A3
95-A4
135-A1
135-A2
135-A3
135-A4
Specimen

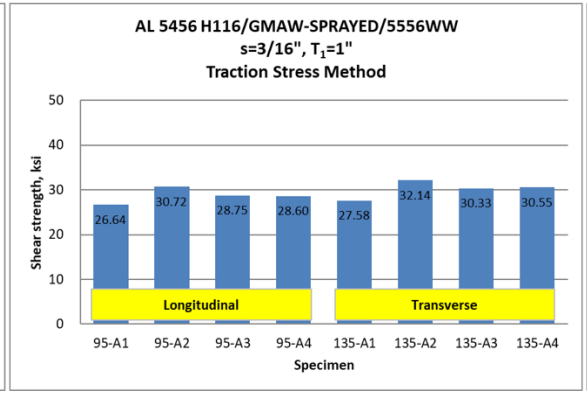
AL 5456 H116/GMAW-SPRAYED/5556WW
s=3/16", T1=1"
Traction Stress Method
Shear strength, ksi
50
40
30
20
10
0
26.64
30.72
28.75
28.60
27.58
32.14
30.33
30.55
Longitudinal
Transverse
95-A1
95-A2
95-A3
95-A4
135-A1
135-A2
135-A3
135-A4
Specimen

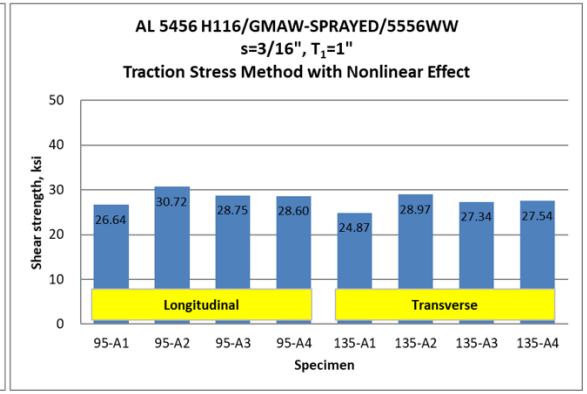
AL 5456 H116/GMAW-SPRAYED/5556WW
s=3/16", T1=1"
Traction Stress Method with Nonlinear Effect
Shear strength, ksi
50
40
30
20
10
0
26.64
30.72
28.75
28.60
24.87
28.97
27.34
27.54
Longitudinal
Transverse
95-A1
95-A2
95-A3
95-A4
135-A1
135-A2
135-A3
135-A4
Specimen

(c)

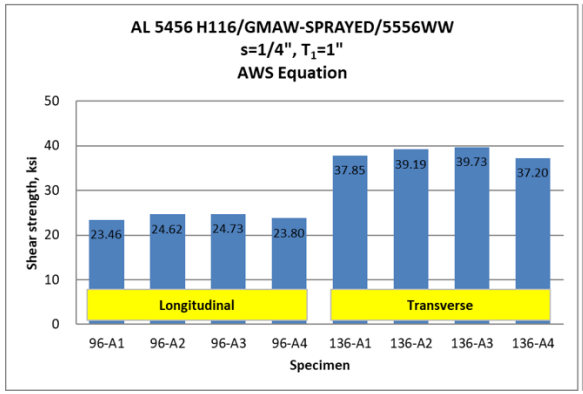
AL 5456 H116/GMAW-SPRAYED/5556WW
s=1/4", T1=1"
AWS Equation
Shear strength, ksi
50
40
30
20
10
0
23.46
24.62
24.73
23.80
37.85
39.19
39.73
37.20
Longitudinal
Transverse
96-A1
96-A2
96-A3
96-A4
136-A1
136-A2
136-A3
136-A4
Specimen

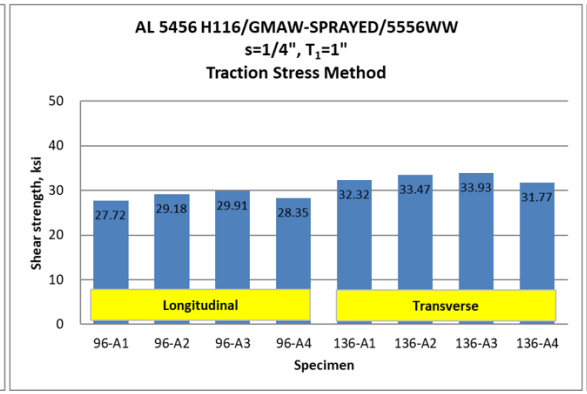
AL 5456 H116/GMAW-SPRAYED/5556WW
s=1/4", T1=1"
Traction Stress Method
Shear strength, ksi
50
40
30
20
10
0
27.72
29.18
29.91
28.35
32.32
33.47
33.93
31.77
Longitudinal
Transverse
96-A1
96-A2
96-A3
96-A4
136-A1
136-A2
136-A3
136-A4
Specimen

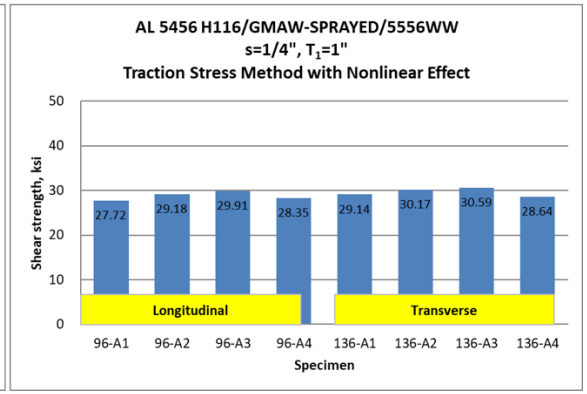
AL 5456 H116/GMAW-SPRAYED/5556WW
s=1/4", T1=1"
Traction Stress Method with Nonlinear Effect
Shear strength, ksi
50
40
30
20
10
0
27.72
29.18
29.91
28.35
29.14
30.17
30.59
28.64
Longitudinal
Transverse
96-A1
96-A2
96-A3
96-A4
136-A1
136-A2
136-A3
136-A4
Specimen

(d)

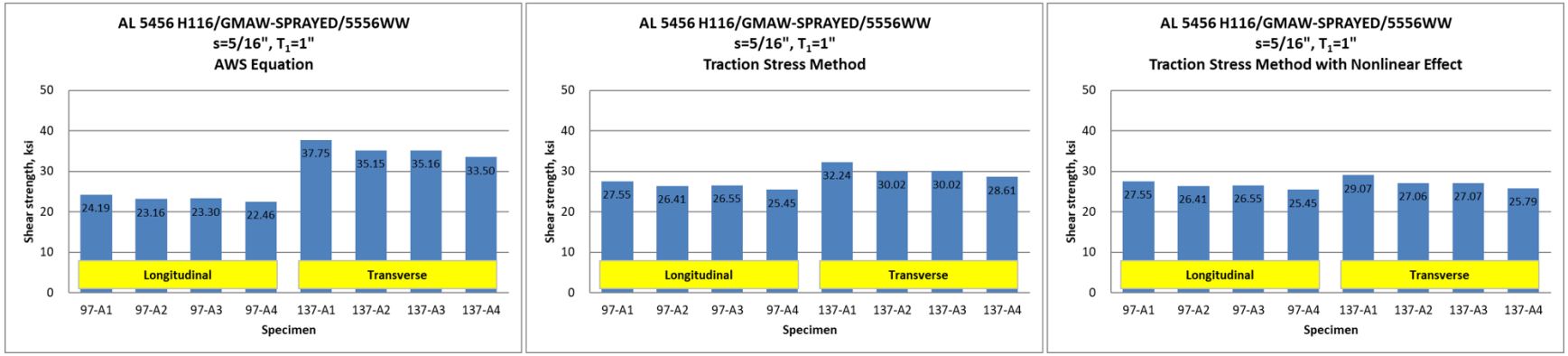

(e)

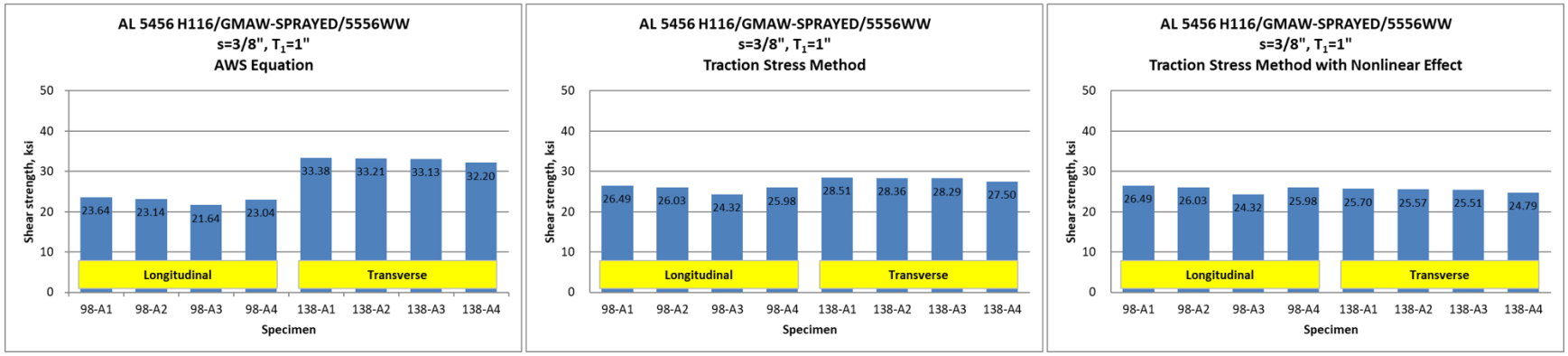

(f)

Figure D.1: Shear strength correlations between longitudinal and transverse specimens made of AL 5456 with GMAW and 5556 weld wire: a comparison between AWS traditional equation and traction stress method with/without nonlinear effects

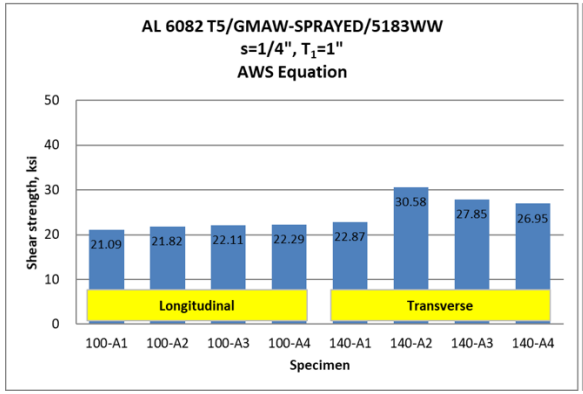
AL 6082 T5/GMAW-SPRAYED/5183WW
s=1/4", T1=1"
AWS Equation
Shear strength, ksi
50
40
30
20
10
0
21.09
21.82
22.11
22.29
22.87
30.58
27.85
26.95
Longitudinal
Transverse
100-A1
100-A2
100-A3
100-A4
140-A1
140-A2
140-A3
140-A4
Specimen

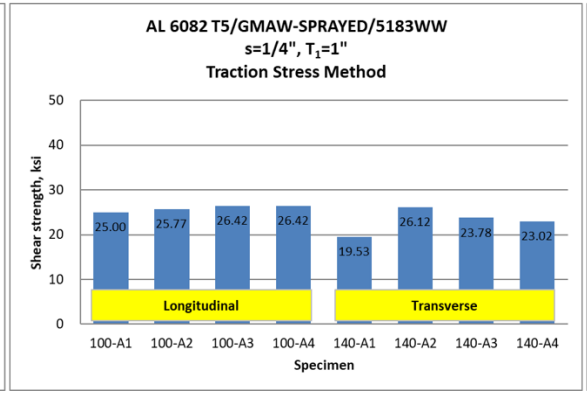
AL 6082 T5/GMAW-SPRAYED/5183WW
s=1/4", T1=1"
Traction Stress Method
Shear strength, ksi
50
40
30
20
10
0
25.00
25.77
26.42
26.42
19.53
26.12
23.78
23.02
Longitudinal
Transverse
100-A1
100-A2
100-A3
100-A4
140-A1
140-A2
140-A3
140-A4
Specimen

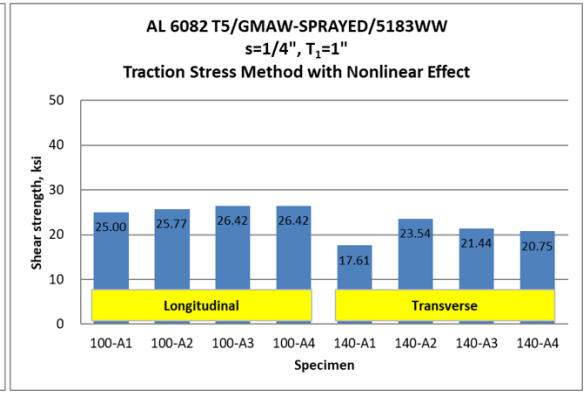
AL 6082 T5/GMAW-SPRAYED/5183WW
s=1/4", T1=1"
Traction Stress Method with Nonlinear Effect
Shear strength, ksi
50
40
30
20
10
0
25.00
25.77
26.42
26.42
17.61
23.54
21.44
20.75
Longitudinal
Transverse
100-A1
100-A2
100-A3
100-A4
140-A1
140-A2
140-A3
140-A4
Specimen

(a)

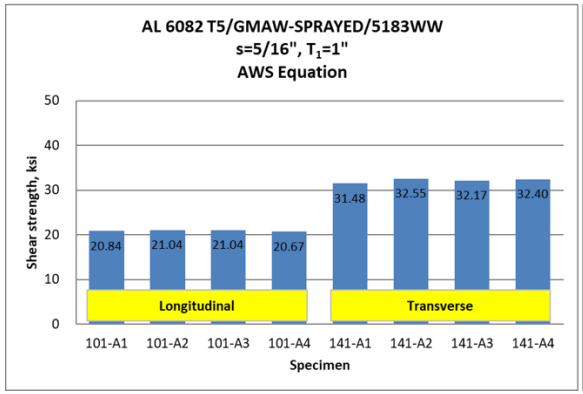
AL 6082 T5/GMAW-SPRAYED/5183WW
s=5/16", T1=1"
AWS Equation
Shear strength, ksi
50
40
30
20
10
0
20.84
21.04
21.04
20.67
31.48
32.55
32.17
32.40
Longitudinal
Transverse
101-A1
101-A2
101-A3
101-A4
141-A1
141-A2
141-A3
141-A4
Specimen

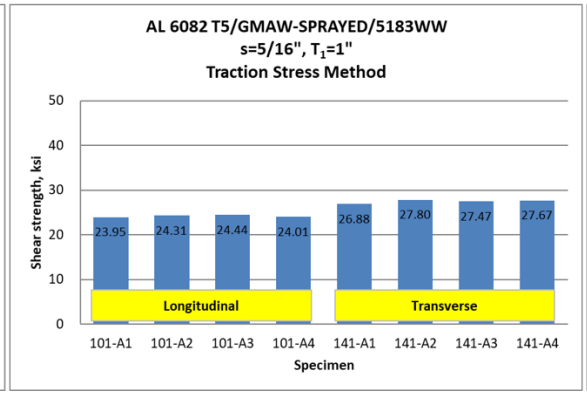
AL 6082 T5/GMAW-SPRAYED/5183WW
s=5/16", T1=1"
Traction Stress Method
Shear strength, ksi
50
40
30
20
10
0
23.95
24.31
24.44
24.01
26.88
27.80
27.47
27.67
Longitudinal
Transverse
101-A1
101-A2
101-A3
101-A4
141-A1
141-A2
141-A3
141-A4
Specimen

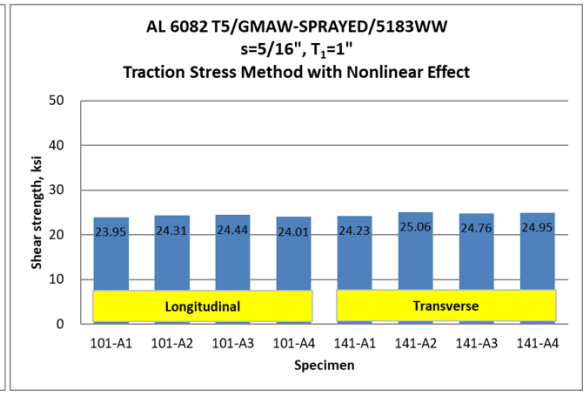
AL 6082 T5/GMAW-SPRAYED/5183WW
s=5/16", T1=1"
Traction Stress Method with Nonlinear Effect
Shear strength, ksi
50
40
30
20
10
0
23.95
24.31
24.44
24.01
24.23
25.06
24.76
24.95
Longitudinal
Transverse
101-A1
101-A2
101-A3
101-A4
141-A1
141-A2
141-A3
141-A4
Specimen

(b)

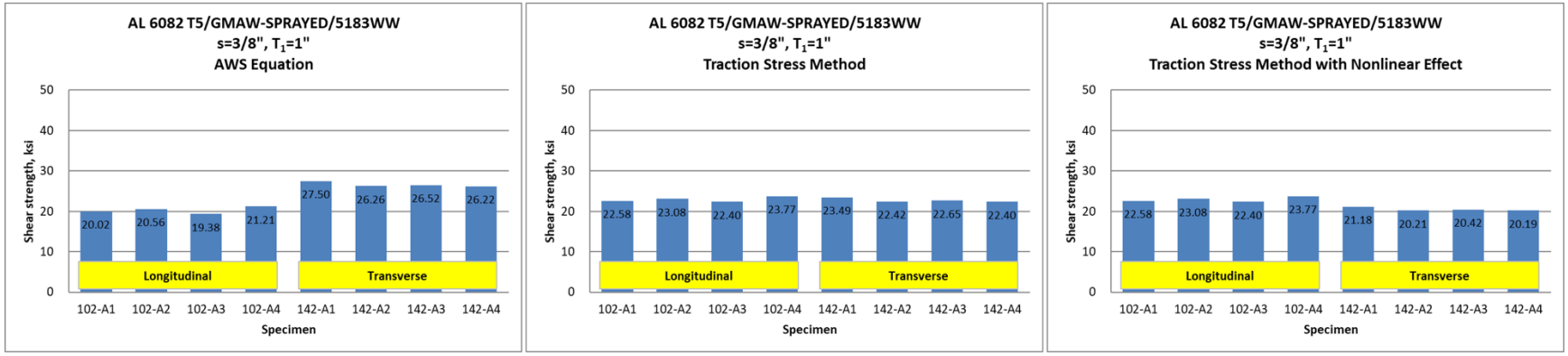

(c)

Figure D.2: Shear strength correlations between longitudinal and transverse specimens made of AL 6082 with GMAW and 5183 weld wire: a comparison between AWS traditional equation and traction stress method with/without nonlinear effects

Appendix E Shear Strength Correlations between Longitudinal and Transverse Specimens Made of Titanium Alloys

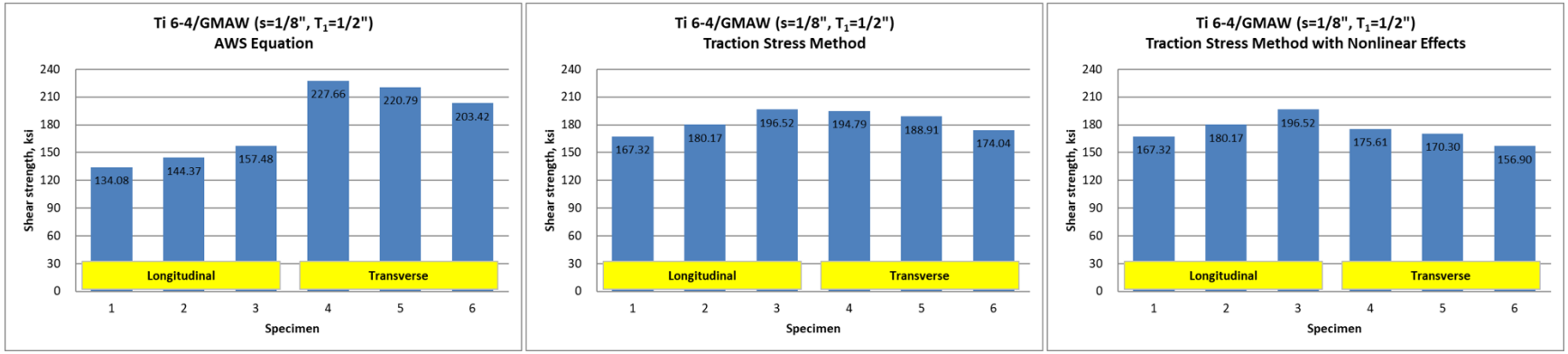

(a)

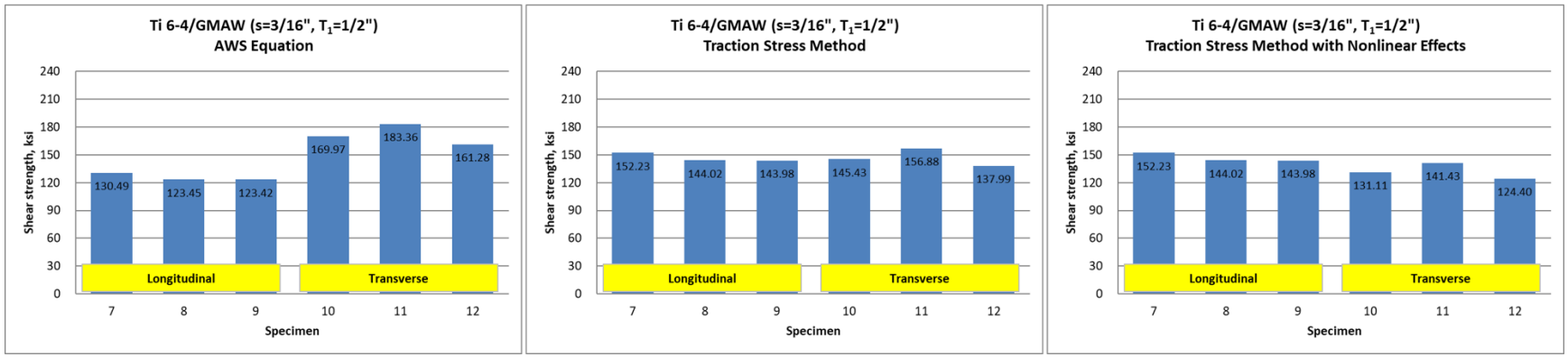

(b)

Figure E.1: Shear strength correlations between longitudinal and transverse specimens made of Ti 6-4 with GMAW: a comparison between AWS traditional equation and traction stress method with/without nonlinear effects

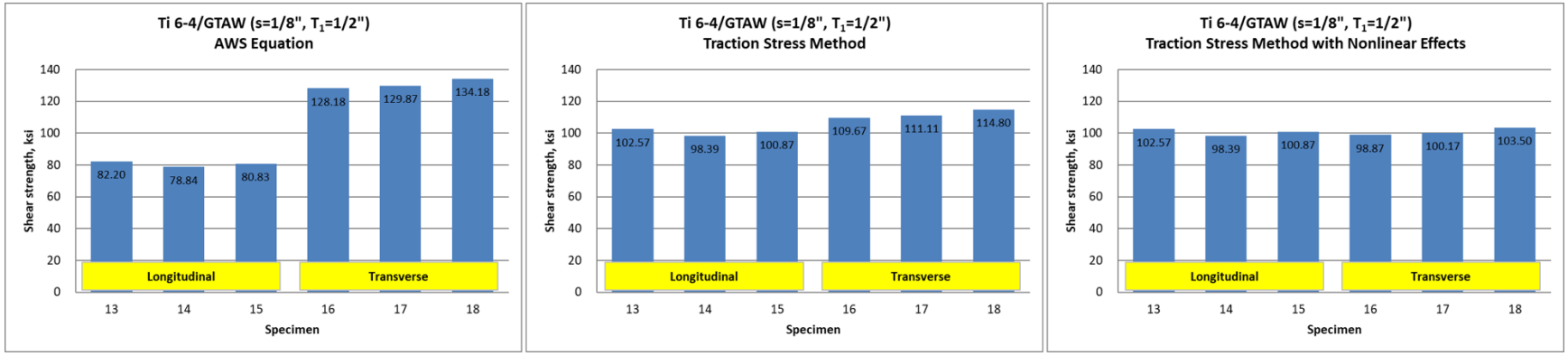

(a)

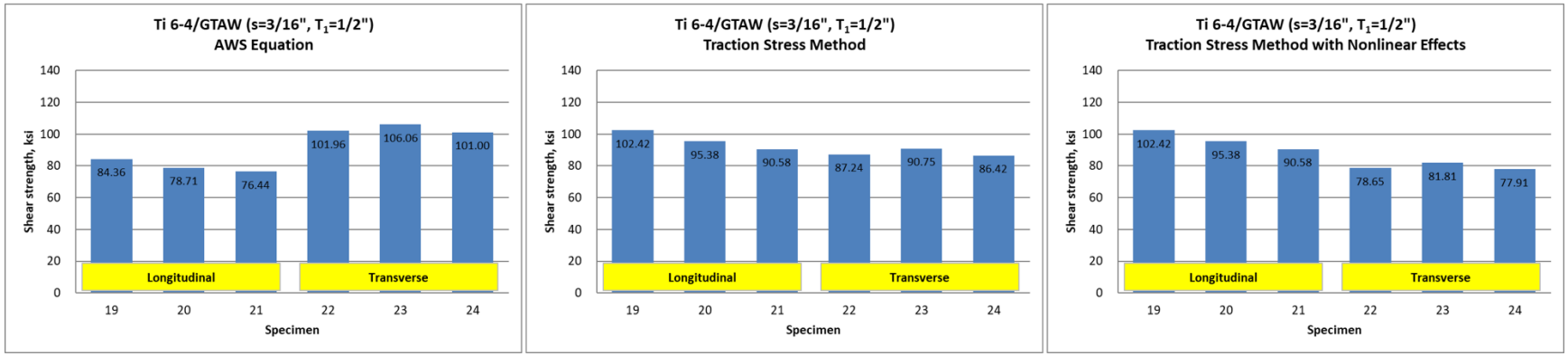

(b)

Figure E.2: Shear strength correlations between longitudinal and transverse specimens made of Ti 6-4 with GTAW: a comparison between AWS traditional equation and traction stress method with/without nonlinear effects

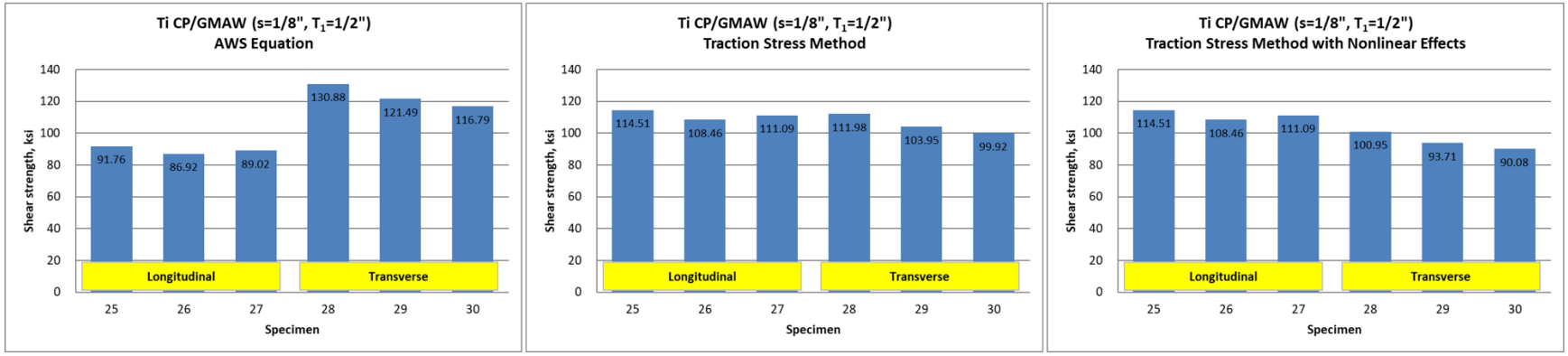

(a)

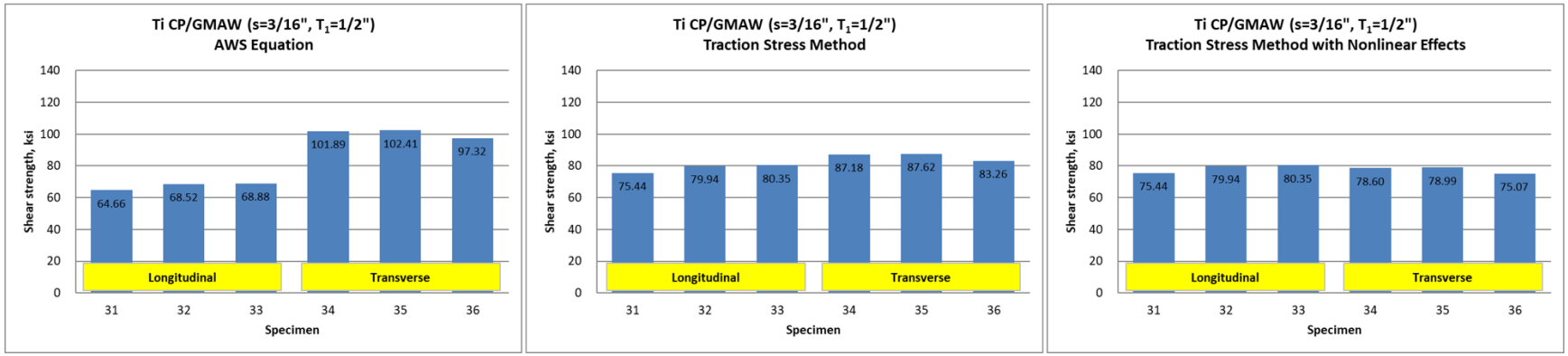

(b)

Figure E.3: Shear strength correlations between longitudinal and transverse specimens made of Ti CP with GMAW: a comparison between AWS traditional equation and traction stress method with/without nonlinear effects

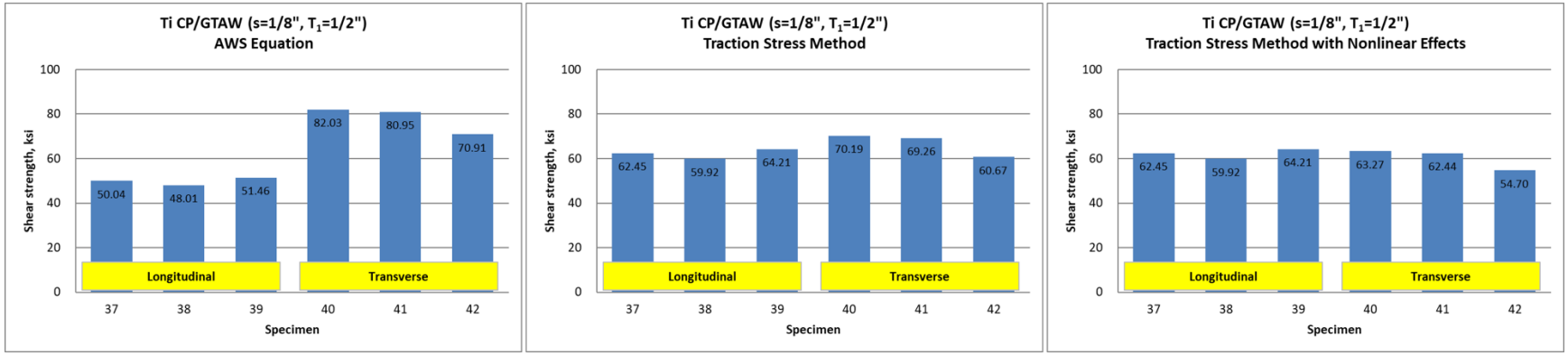

(a)

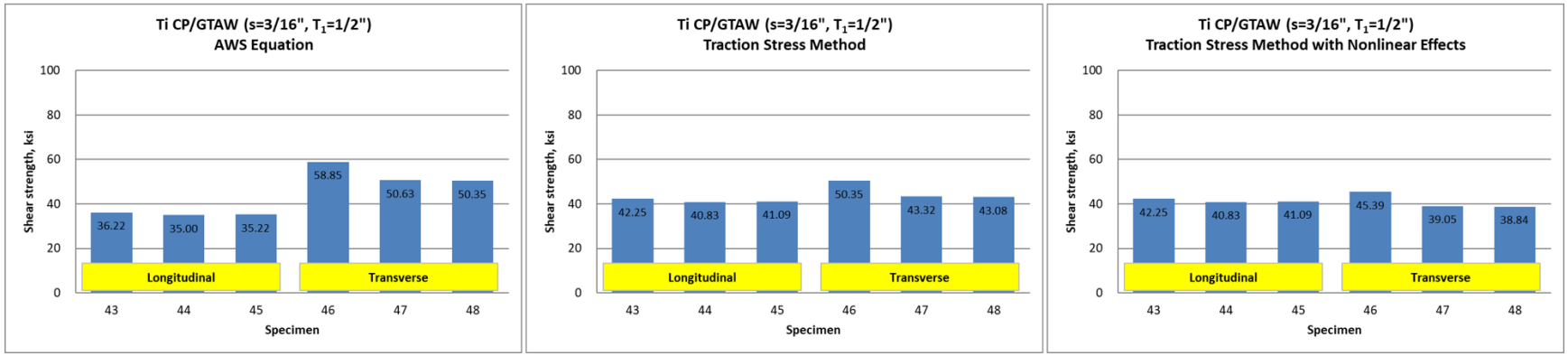

(b)

Figure E.4: Shear strength correlations between longitudinal and transverse specimens made of Ti CP with GTAW: a comparison between AWS traditional equation and traction stress method with/without nonlinear effects

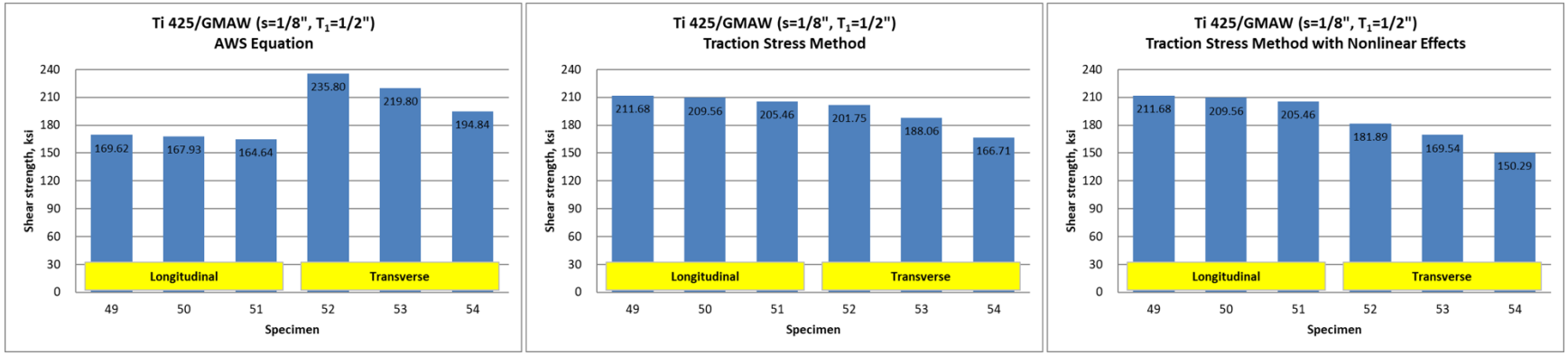

(a)

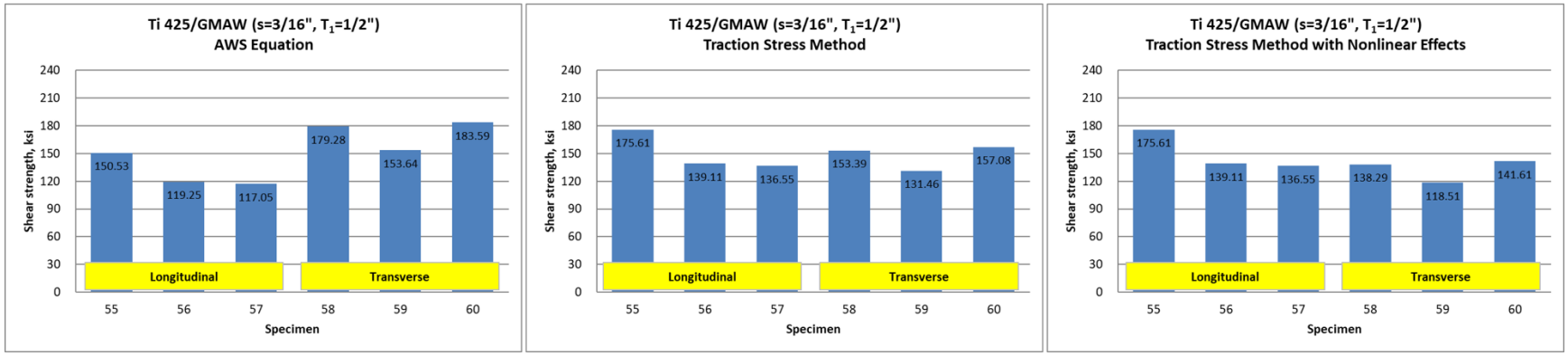

(b)

Figure E.5: Shear strength correlations between longitudinal and transverse specimens made of Ti 425 with GMAW: a comparison between AWS traditional equation and traction stress method with/without nonlinear effects

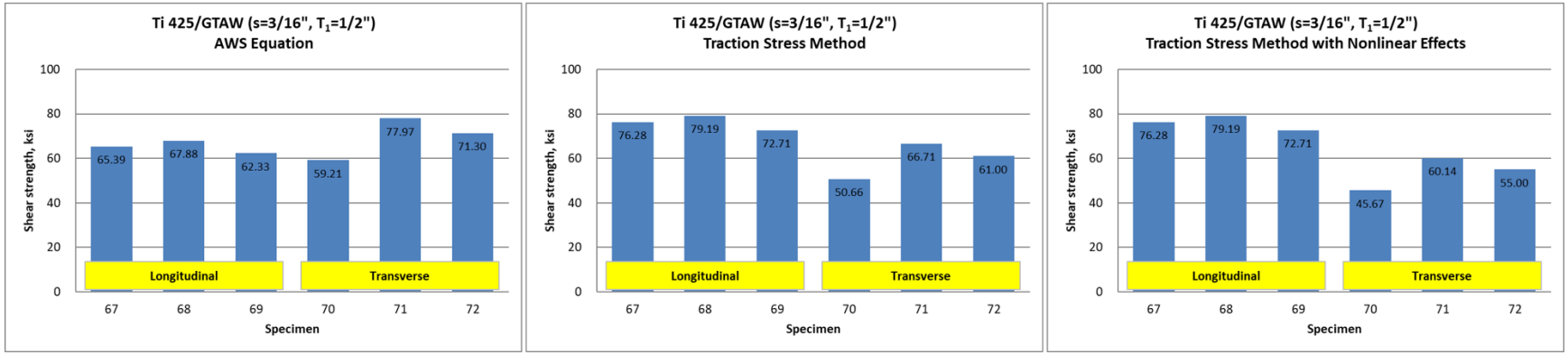

Figure E.6: Shear strength correlations between longitudinal and transverse specimens made of Ti 425 with GTAW: a comparison between AWS traditional equation and traction stress method with/without nonlinear effects

References

ABS. (2000). *Rule requirements for materials and welding – supplementary requirements for naval vessels.* ABS.

AISC. (2010). *Specification for structural steel buildings.* Chicago: AISC.

Archer, F. E., et al. (1959). Fillet welds subjected to bending and shear. *Civil Engineering and Public Works Review, 54*(634), 455-458.

AWS (American Welding Society). (2007). *AWS B4.0. Standard methods for mechanical testing of welds.* Miami: AWS.

AWS (American Welding Society). (2015). *AWS D1.1. Structural welding code - Steel.* Miami: AWS.

Björk, T., et al. (2012). Capacity of fillet welded joints made of ultra high-strength steel. *Welding in the World, 56*(3), 71-84.

Butler, L. J., & Kulak, G. L. (1971). Strength of fillet welds as a function of direction of load. *Welding Journal, 50*(5), 231-234.

Butler, L. J., et al. (1972). Eccentrically loaded welded connections. *Journal of the Structural Division, 98*(5), 989-1005.

CEN (European Committee for Standardization). (2005). *Eurocode 3: Design of steel structures - Part 1-8 Design of joints. CEN 1993-1-8.* Brussels: CEN.

CSA (Canadian Standards Association). (2014). *CSA S16. Design of steel structures.* Rexdale, ON: CSA.

Dassault Systemes SIMULIA Abaqus CAE (2018).

De Bruyne, N. A. (1944). The strength of glued joints. *Aircraft engineering and aerospace technology*.

Department of Defense. (1974). *Fillet weld size, strength and efficiency determination. MIL-STD-1628.* Arlington, VA: Department of Defense.

Department of Defense. (1990). *Fabrication, welding, and inspection of ship structure. MIL-STD-1689A.* Arlington, VA: Department of Defense.

DNV-RP-203. (2012). *Fatigue design of offshore steel structures. DNV-RP-203.* Oslo: Det Norske Veritas Germanischer Lloyd.

Dong, P. (2001). A structural stress definition and numerical implementation for fatigue analysis of welded joints. *International Journal of Fatigue, 23*(10), 865-876.

Dong, P. (2005). A robust structural stress method for fatigue analysis of offshore/marine structures. *Journal of offshore mechanics and arctic engineering, 127*(1), 68-74.

Dong, P., & Hong, J. K. (2004). The master SN curve approach to fatigue evaluation of offshore and marine structures. *In International Conference on Offshore Mechanics and Arctic Engineering, 37440*, 847-855.

Dong, P., & Hong, J. K. (2006). A robust structural stress parameter for evaluation of multiaxial fatigue of weldments. *Journal of ASTM International, 3*(7), 1-17.

Dong, P., et al. (2010a). *The master S-N curve method: an implementation for fatigue evaluation of welded components in the 2007 ASME B&PV code, section VIII, division 2 and API 579-1/ASME FFS-1. WRC Bulletin 523.* New York: Welding Research Council.

Dong, P., et al. (2010b). A path-dependent cycle counting method for variable-amplitude multi-axial loading. *International Journal of Fatigue, 32*(4), 720-734.

Dong, P., et al. (2013). A math-based design-for-produceability evaluation of titanium applications in ship hull structures. *Transactions-Society of Naval Architects and Marine Engineers, 120*(1), 299-305.

Dong, P., et al. (2014). A structural strain method for low-cycle fatigue evaluation of welded components. *International Journal of Pressure Vessels and Piping, 119*, 39-51.

Frater, G. S. (1986). *Weldment design for hollow structural section joints.* (Doctoral dissertation, Toronto, Canada: University of Toronto).

Frater, G. S., & Packer, J. A. (1992a). Weldment design for RHS truss connections. I: Applications. *Journal of Structural Engineering, 118*(10), 2784-2803.

Frater, G. S., & Packer, J. A. (1992b). Weldment design for RHS truss connections. II. Experimentation. *Journal of Structural Engineering, 118*(10), 2804-2819.

Higgins, T. R., & Preece, F. R. (1968). Proposed working stresses for fillet welds in building construction. *Welding Journal, 15*(10), 429-432.

Huang, T. D., et al. (2004). Fabrication and engineering technology for lightweight ship structures, part 1: distortions and residual stresses in panel fabrication. *Journal of Ship Production, 20*(1), 43-59.

Huang, T. D., et al. (2007). Engineering and production technology for lightweight ship structures, Part II: distortion mitigation technique and implementation. *Journal of ship production, 23*(2), 82-93.

Huang, T. D., et al. (2014). Reduction of overwelding and distortion for naval surface combatants, Part 1: Optimized weld sizing for lightweight ship structures. *Journal of Ship Production and Design, 30*(4), 184-193.

Huang, T. D., et al. (2016). Reduction of overwelding and distortion for naval surface combatants. Part 2: weld sizing effects on shear and fatigue performance. *Journal of Ship Production and Design, 32*(1), 21-36.

IIW (International Institute of Welding). (1976). *Design rules for arc welded connections in steel submitted to static loads. Doc. No. XV-358-74. Commission XV.* IIW.

IIW (International Institute of Welding). (1980). *Deformation curves of fillet welds. Doc. No. XV-467-80. Commission XV.* Paris: IIW.

Jensen, A. P. (1988). Limit analysis of welds. *Journal of Constructional Steel Research, 11*(3), 205-235.

Kamtekar, A. G. (1982). A new analysis of the strength of some simple fillet welded connections. *Journal of Constructional Steel Research, 2*(2), 33-45.

Kamtekar, A. G. (1987). The strength of inclined fillet welds. *Journal of Constructional Steel Research, 7*(1), 43-54.

Kato, B., & Morita, K. (1974). Strength of transverse fillet welded joints. *Welding journal, 53*(2), 59-64.

Kennedy, D. L., et al. (1985). The strength of fillet welds under longitudinal and transverse shear: a paradox. *Canadian Journal of Civil Engineering, 12*(1), 226-231.

Khurshid, M., et al. (2012). Ultimate strength and failure modes for fillet welds in high strength steels. *Materials & Design, 40*, 36-42.

Krumpen, R. P., & Jordan, C. R. (1984). Reduced fillet weld sizes for naval ships. *Welding journal, 63*(4), 34-41.

Lesik, D. F., & Kennedy, D. J. (1988). Ultimate strength of eccentrically loaded fillet welded connections. *Structural Engineering Report No. 159, University of Alberta*.

Lesik, D. F., & Kennedy, D. L. (1990). Ultimate strength of fillet welded connections loaded in plane. *Canadian Journal of Civil Engineering, 17*(1), 55-67.

Ligtenberg, F. K. (1968). International Test Series Final Report, IIW Doc XV-242-68. *International Institute of Welding*.

Lu, H., & Dong, P. (2020). An Analytical Shear Strength Model for Load-Carrying Fillet-Welded Connections Incorporating Nonlinear Effects. *Journal of Structural Engineering, 146*(3), 04019224.

Lu, H., et al. (2015). Strength analysis of fillet welds under longitudinal and transverse shear conditions. *Marine Structures, 43*, 87-106.

Marsh, C. (1985). Strength of aluminum fillet welds. *Welding Journal, Welding Research Supplement*, 335-338.

Marsh, C. (1988). Strength of aluminum T-joint fillet welds. *Welding Journal, Welding Research Supplement*, 171-176.

McClellan, R. W. (1990). An Evaluation of the Fillet Weld Shear Strength of Flux Cored Arc Welding Electrodes. *In National Shipbuilding Research Program (NSRP) 1990 Ship Production Symposium*.

Mei, J., & Dong, P. (2017a). An equivalent stress parameter for multi-axial fatigue evaluation of welded components including non-proportional loading effects. *International Journal of Fatigue, 101*, 297-311.

Mei, J., & Dong, P. (2017b). A new path-dependent fatigue damage model for non-proportional multi-axial loading. *International Journal of Fatigue, 90*, 210-221.

Miazga, G. S., & Kennedy, D. L. (1989). Behaviour of fillet welds as a function of the angle of loading. *Canadian Journal of Civil Engineering, 16*(4), 583-599.

Nie, C., & Dong, P. (2012). A traction stress based shear strength definition for fillet welds. *The Journal of Strain Analysis for Engineering Design, 47*(8), 562-575.

Oatway, P. (2014). *Fillet-welded end-plate connections to square and rectangular HSS.* (M Eng. thesis. Toronto, Canada: University of Toronto).

Packer, J. A., & Cassidy, C. E. (1995). Effective weld length for HSS T, Y, and X connections. *Journal of Structural Engineering, 121*(10), 1402-1408.

Packer, J. A., & Henderson, J. E. (1997). Hollow structural section connections and trusses: a design guide. Canadian Institute of Steel Construction.

Packer, J. A., et al. (2016). Experimental evaluation of design procedures for fillet welds to hollow structural sections. *Journal of Structural Engineering, 142*(5), 04016007.

Paik, J., et al. (2006). Ultimate limit state design technology for aluminum multi-hull ship structures. *Transactions-Society of Naval Architects and Marine Engineers, 113*, 270-305.

Pei, X., & Dong, P. (2019). An analytically formulated structural strain method for fatigue evaluation of welded components incorporating nonlinear hardening effects. *Fatigue & Fracture of Engineering Materials & Structures, 42*(1), 239-255.

Pei, X., et al. (2019). A structural strain parameter for a unified treatment of fatigue behaviors of welded components. *International Journal of Fatigue, 124*, 444-460.

Pei, X., et al. (2020). A simplified structural strain method for low-cycle fatigue evaluation of girth-welded pipe components. *International Journal of fatigue, 139*, 105732.

Picón, R., & Cañas, J. (2009). On strength criteria of fillet welds. *International Journal of Mechanical Sciences, 51*(8), 609-618.

Spraragen, W., & Claussen, G. E. (1942). Static tests of fillet and plug welds: a review of the literature from 1932 to January 1, 1940. *Welding Journal, 21*(4), 161-197.

Swannell, P. (1967). The load-carrying capacity of two thin lapped plates joined by an intermittent run of bond. *British Welding Journal*, 153-156.

Swannell, P. (1972). Primary stress and strain distributions in longitudinal fillet welds. *Australian Welding Journal*, 117-123.

Timoshenko, S. P. (1951). *Theory of elasticity.* New York: McGraw-Hill Book.

Tousignant, K. J. (2017). *Weld Effective Lengths for Hollow Structural Section Connections.* (Doctoral dissertation, Toronto, Canada: University of Toronto).

Wardenier, J., et al. (2002). *Hollow sections in structural applications.* The Netherlands: Bouwen met staal.

Wei, Z., & Dong, P. (2010). Multiaxial fatigue life assessment of welded structures. *Engineering Fracture Mechanics, 77*(15), 3011-3021.

Xing, S., et al. (2016). Analysis of fatigue failure mode transition in load-carrying fillet-welded connections. *Marine Structures, 46*, 102-126.

Yang, L., et al. (2019). Strength of duplex stainless steel fillet welded connections. *Journal of Constructional Steel Research, 152*, 246-260.